



Monograph-2024

Space Debris and Space Situational Awareness Research Studies in ISRO



Ram Krishan Sharma
A K Anil Kumar
Adimurthy Vipparthi

Indian Space Research Organisation



Monograph-2024

Space Debris and Space Situational Awareness Research Studies in ISRO

Ram Krishan Sharma

A K Anil Kumar

Adimurthy Vipparthi



SDSSARS IN ISRO

Space Debris and Space Situational
Awareness Research Studies



Contents

TITLE	PAGE
Foreword	xv
Preface	xvii
Acknowledgements	xix
Nomenclature	xxi
List of Figures	xxv
List of Tables	xxxix

1	An Overview of Space Debris Environment and Relevant Studies in ISRO	1
1.1	Introduction	
1.2	Fragmentation Events	
1.3	On-Orbit Collisions	
1.4	Growth of Catalogued Population	
1.5	Threats Due to Space Debris	
1.6	Space Debris Mitigation	
1.7	ISRO's Efforts	
1.8	Conjunction Assessment and Collision Avoidance for Spacecraft	
1.9	Collision Avoidance Analysis (COLA) for Launch Vehicles	
1.10	Passivation	
1.11	Minimization of GTO Lifetime	
1.12	Post Mission Disposal	
	1.12.1 Post Mission Disposal in LEO regime	
	1.12.2 Post Mission Disposal for GEO satellites	
1.13	Summary of ISRO's efforts towards Space Debris Mitigation	
1.14	Atmospheric Re-entry Analysis	



SDSSARS IN ISRO

Space Debris and Space Situational
Awareness Research Studies

1.15	Shielding	
1.16	Space Debris Observation	
1.17	Debris Environmental Modelling	
1.18	Areas of Further Research	
2	Space Debris Environment and its Sources	33
2.1	Introduction	
2.2	ASSEMBLE Model from ISRO	
	2.2.1	Life Time of Fragments
	2.2.2	Mass of the Debris Fragments and Their Imparted Delta Velocities
	2.2.3	Number Density Distribution with Respect to Eccentricity
	2.2.4	Number Density Distribution with Respect to Inclination
2.3	Stability of the Future LEO Environment	
	2.3.1	A Model used by ISRO for Long-Term Orbit Computations
	2.3.2	Solar Flux Projection Models
	2.3.3	Study Results
3	On-Orbit Breakup and Environment Modelling	53
3.1	Introduction	
3.2	Calculation of Fragment Velocity Additions of the Breakup of a Launch Vehicle Upper Stage	
3.3	A New Modeling Approach for Orbital Breakup in Space	
3.4	Simulation of Some Historical On-Orbit Breakups Using ASSEMBLE Model	
3.5	A Posterior Semi-stochastic Low Earth Debris On-orbit Breakup Simulation Model	

	3.6	A new stochastic impressionistic low Earth model of the space debris scenario	
4	Orbit Propagation		63
	4.1	Orbit Propagators for Satellites	
	4.1	Orbital Decay of RS-1 Satellite with KS Differential Equations	
	4.2.1	Equations of Motion	
	4.2.2	Computer Package 'OBLETRA' For Orbit Predictions	
	4.3	RS-1 Orbital Decay in an Oblate Diurnal Atmosphere	
	4.4	Long-term orbit computations with KS uniformly regular canonical elements with oblateness	
	4.4.1	Equations of motion	
	4.4.2	Canonical KS-Transformation	
	4.4.3	Perturbations and Numerical Results	
	4.4.4	Checks during Numerical Integration	
	4.4.5	Sun-Synchronous Orbit	
	4.5	Analytical approach using KS elements to short-term orbit predictions including J_2 , J_3 and J_4	
	4.6	Analytical short-term orbit predictions with J_2 , J_3 , J_4 in terms of K-S uniformly regular canonical elements	
	4.7	Contraction of Satellite Orbits using KS Elements with Air Drag for Low Eccentricity Orbits	
	4.8	Generation of Non-singular Analytical Theories for the Contraction of High Eccentricity Satellite Orbits under the Influence of Air Drag	
	4.9	Non-singular Analytical Theories for the Motion of Near-Earth Satellite Orbits with Air Drag in terms of Uniformly Regular KS Canonical Elements for Small Eccentricity Orbits	
	4.10	Orbit Propagation using Semi-Analytical Theory and its Applications in Space Debris Field	



5	Modelling of the Space Debris Environment		83
	5.1	Introduction	
	5.2	Satellite Breakups	
	5.3	Stochastic IMPressionistic Low Earth (SIMPLE) Engineering Model of Space Debris Scenario	
	5.4	A New Stochastic Impressionistic Low Earth Model of Space Debris Scenario	
	5.5	Regularized Luni-Solar Gravity Dynamics on Resident Space Objects	
6	Conjunction Analysis and Modeling		95
	6.1	Introduction	
	6.2	Statistical Conjunction analysis and Modeling of Low-Earth Orbit Catalogued Objects	
	6.3	Modeling spatial density in low Earth orbits using wavelets	
	6.4	Analytical methods for pre-filtering of close approaches between space objects	
	6.5	Collision Avoidance Analysis for ISRO Launch Vehicles	
	6.6	Space Object Proximity Analysis for Indian LEO Satellites	
	6.6.1	Equations of motion	
	6.6.2	Canonical KS-Transformation	
	6.6.3	Perturbations and Numerical Results	
	6.7	On-Orbit Collision Probability in LEO Using SIMPLE Model	
	6.8	A Proposed Reference Collision Probability Estimation Model of the Space Debris Scenario	
	6.8.1	Comparison of the Present Results with Other Models	
	6.9	Selection of optimal collision avoidance manoeuvre by evolutionary algorithms	
	6.9.1	Input Data Set for Space Debris Proximity Analysis	

	6.9.2	Optimal Collision Avoidance Manoeuvre Strategy	
6.10		Recent Collision Avoidance Manoeuvre Detection and Design	
6.11		Modeling of sunspot numbers	
7	Space Debris Mitigation and Risk Estimation		121
7.1		Introduction	
7.2		Overview of space debris activities in ISRO	
7.3		Passivation of upper stages	
7.4		End-of-mission re-orbiting from GSO	
7.5		Space debris proximity analysis for collision avoidance	
7.6		Minimization of GTO lifetime	
7.7		Estimation of On-Ground Risk due to Uncontrolled Re-entries from Eccentric Orbits	
	7.7.1	Application of the proposed method in long-term risk assessment	
7.8		Active Debris Removal	
	7.8.1	Identification of Space Debris from SSO for Active Debris Removal	
7.9		Requirements of Shielding from Space Debris for Human Space Missions	
8	Re-entry Prediction Studies		141
8.1		Re-entry of Space Objects	
8.2		IADC Re-entry Test Campaigns	
8.3		Orbital Lifetime of Decaying Objects	
	8.3.1	Characteristics of Decay from GTO	
	8.3.2	The Effect of Third Body Perturbations on GTO	
	8.3.3	Effect of Launch Time on Lifetime	
	8.3.4	Decay of the Spent Orbiting Stage of GSLV-D1	
	8.3.5	Re-entry time Estimation of GSLV-F01/CS and More	



SDSSARS IN ISRO

Space Debris and Space Situational
Awareness Research Studies

8.4	Studies on Material Degradation under Re-Entry Conditions	
8.5	Re-entry prediction using Kalman filter approach	
8.6	Estimation of Orbital Life Time by estimating Ballistic Coefficient using Genetic Algorithm	
8.7	Re-entry Estimation with KS Regular Elements and Genetic Algorithm	
8.8	Orbital lifetime estimation of upper stages with different inclinations	
8.9	Presence of Chaotic Motion	
8.10	Orbit life time prediction using KS elements equations and genetic algorithm	
8.11	Re-entry Prediction of Phobos-Grunt and ROSAT satellites	
8.12	Re-entry Prediction with response surface method using genetic algorithm and Lifetime optimization with STK	
8.13	STK OPTIM	
8.14	Re-entry Time Prediction of Phobos-Grunt	
8.15	STK LTOptim	
8.16	Prediction of Orbital Lifetime of Space Objects in GTO as a Function of Launch Time	
8.17	Comparison of Three Methods for Re-entry Prediction for Low Eccentricity Orbits	
8.18	Re-entry time prediction for CUS of GSLV-F09 mission	
8.19	Re-entry predictions of space objects from highly elliptical orbits using KS Elements	
8.20	Re-entry predictions of Space Objects from Low Eccentric Orbits	
8.21	Re-entry time prediction of Molniya orbit objects	
8.22	Assessment of three in-house developed re-entry prediction methods	
8.23	Regularized analytical orbit theory with solar radiation pressure	

8.24	Assessment of four in-house re-entry prediction algorithms	
8.25	Non-linear optimization algorithms on weighted least-square based method for re-entry predictions	
8.26	Assessment of in-house algorithms on re-entry time prediction of uncontrolled space objects	
8.27	Summarized Results of the IADC Re-entry Campaigns Obtained by ISRO	
8.27.1	IADC Re-entry Prediction of Campaign 2003#1 - COSMOS 389 Satellite	
8.27.2	IADC Re-entry Test Campaign 2005/1: Re-entry of Cosmos 2332 Satellite	
8.27.3	IADC Re-entry Campaign 2005/2: Re-entry of Coronas-F Satellite	
8.27.4	IADC Re-entry Campaign 2008/1: Re-entry of Early Ammonia Servicer	
8.27.5	IADC Re-entry Campaign 2009/1: Re-entry of Molniya 3-39 Satellite	
8.27.6	IADC Re-entry Campaign 2010/1: Re-entry of Vostok SL-3/A-1 Third Stage	
8.27.7	IADC Re-entry Campaign 2011/2: Re-entry Roentgen Satellite (ROSAT)	
8.27.8	IADC Re-entry Test Campaign 2012/1: Re-entry Analysis of Phobos-Grunt	
8.27.9	IADC Re-entry Test Campaign 2013/1: Re-entry of GOCE Satellite (#34602)	
8.27.10	IADC Re-entry Test Campaign 2014/1: Re-entry of Cosmos 1939 Satellite (#19045)	
8.27.11	IADC Re-entry Test Campaign 2016/1: Re-entry of CZ-2C Rocket Body (#39000)	
8.27.12	IADC Re-entry Test Campaign 2016/2: Re-entry of VEGA AVUM Rocket Body (#38086)	



	8.27.13	IADC Re-entry Test Campaign 2017/1: Re-entry of CZ-3B Rocket Body (#38253)	
	8.27.14	IADC Re-entry Test Campaign 2018/1: Re-entry of Tiangong-1 (#37820) Chinese Experimental Space Station	
	8.27.15	IADC Re-entry Test Campaign 2019/1: Re-entry of Electron Rocket Body (#43166)	
	8.27.16	IADC Re-entry Test Campaign 2021/1: Re-entry of Starlink-26 Spent Stage (#44240)	
	8.27.17	IADC Re-entry Test Campaign 2021/2: Re-entry of CZ-5B rocket body (2021-035B, #48275)	
	8.27.18	IADC Re-entry Test Campaign 2022/2: Re-entry of Starlink-24 Satellite (2019-029D, # 44238)	
	8.27.19	IADC Annual Re-entry Campaign of 2023 with Starlink-1065 as Test Object (# 44770)	
9	Future Concerns on Space Debris Environment and Best Practices for Space Sustainability		193
9.1	Introduction		
9.1	Future Concerns and Challenge		
	9.2.1	Space Object Observation	
	9.2.2	Data Processing and Analyses	
9.3	Challenges arising due to small satellites and large constellations		
	9.3.1	Lack of trackability and identifiability of small satellites	
	9.3.2	Lack of manoeuvrability of small satellites	
9.4	Lack of contact details of operators for coordination		
9.5	Lack of reliability		
9.6	Extensive coordination needs		

9.7	Increased operational complexity and penalties for collision avoidance	
9.8	Unavailability of safe lift-off timings within launch window	
9.9	Increased threat of space debris	
9.10	Impact on ground based optical observation	
9.11	Potential Debris Issue Beyond Earth	
9.12	Others	
9.13	Space weather	
9.14	Way forward	
9.15	Conclusion	
	References	205
	Author Index	223
	Subject Index	225

भारतीय अन्तरिक्ष अनुसंधान संगठन

अन्तरिक्ष विभाग
भारत सरकार
अन्तरिक्ष भवन
न्यू वी ई ब्लॉक रोड, बेंगलूर - 560 094, भारत
सूचना : +91-80-2341 5241 / 2217 2333
फैक्स : +91-80-2341 5328



Indian Space Research Organisation

Department of Space
Government of India
Antariksh Bhavan
New BEL Road, Bangalore - 560 004, India
Telephone: +91-80-2341 5241 / 2217 2333
Fax : +91-80-2341 5328
e-mail : chairman@isro.gov.in
secydas@isro.gov.in

सोमनाथ एस / SOMANATH. S

अध्यक्ष / Chairman

FOREWORD

The importance of space debris and space situational awareness research is gaining paramount attention and is only going to further enhance the interest among all space agencies, considering the fact that we have an ever-increasing population of space debris in LEO posing a considerable threat to the active satellites. With the upcoming large constellations of small satellites driven by communication requirement it is very essential to chalk out a concrete plan for space situational awareness to safeguard the active satellites against possible collisions from the space objects.



ISRO has been consistently working in this area for past three decades and very meticulously following the space debris mitigation guidelines in all its launches. One of the very interesting contributions by ISRO in the field of space debris modelling is on the study of characteristic decay time estimation of spent stage in highly eccentric GTO orbit due to the effect of third body perturbation. The study brought out clearly that due to influence of two important parameters namely right ascension of ascending node and solar longitude, both of which define the sun azimuth angle on the orbital plane, the decay time can be from few months to several decades just by shifting the launch time by only few minutes!! Another important contribution is in the development of various in-house software for Collision Avoidance (COLA) used for clearing the lift off time of satellite launch vehicle, Space Object Proximity Analysis (SOPA) Software for conjunction analysis of operational satellites and re-entry prediction methodologies like RSM-GA which is combination of response surface methodology and genetic algorithm. In the area of space debris mitigation ISRO is deorbiting LEO satellites which are nearing life time completion to the best possible extent. Yet another mitigation measure adopted for fourth stage of PSLV used for PSLV Orbital Experimental Mission (POEM), which serves as platform for microgravity experiments, is to lower its orbit to have decay time much less than 6 months. In the field of observation ISRO is going to establish a state of the art network for space object tracking and analysis. ISRO has a vision of committed space debris minimization and management through efficient tracking, modelling, protection and mitigation with fully automated collision avoidance manoeuvres and collaboration with other space agencies to make the space environment cleaner.

I am sure that this comprehensive document on the Space Debris and Space Situational Awareness research will serve as a ready reckoner for all the research activities carried out in Space debris in the past three decades in ISRO and will benefit the researchers in this area worldwide. I wish that ISRO, in collaboration with other space agencies under the ambit of Inter-Agency Space Debris Coordination Committee (IADC) and other international forums, address the future concerns and challenges posed by the ever-increasing small satellite constellations for the overall progressive scientific benefit to humanity and space environment.

Date: February 2nd, 2024

(सोमनाथ एस / Somanath S)

भारत सरकार
अंतरिक्ष विभाग
विक्रम साराभाई अंतरिक्ष केंद्र
तिरुवनंतपुरम - 695 022, भारत
दूरभाष : 0471-2565567/2704412
फैक्स : 0471-2704105
ईमेल : director@vssc.gov.in



Government of India
Department of Space
Vikram Sarabhai Space Centre
Thiruvananthapuram - 695 022, India
Phone : +91-471-2565567/2704412
Fax : +91-471-2704105
Email : director@vssc.gov.in

डॉ. उष्णिक्कृष्णन नायर एस
Dr Unnikrishnan Nair S
विशिष्ट वैज्ञानिक व
Distinguished Scientist &
निदेशक/Director



PREFACE

March 6, 2024

The space around planet Earth is having tens of thousands of objects that pose a potential threat to satellites and launch vehicles. Space Situational Awareness (SSA) plays a pivotal role in ensuring the safety, security and sustainability of space vehicles. The Inter Agency Space Debris Coordination Committee (IADC) is an international governmental forum, established in 1993, to facilitate coordination and cooperation among space agencies on matters related to space debris research, mitigation and remediation. ISRO has become a member of IADC in 1996 and played an important role to formulate the first set of Space Debris Mitigation Guidelines. ISRO has been actively participating in all IADC meetings since 1996 especially in the working groups dealing with space debris modelling and space debris mitigation.

As a responsible space faring nation, India has taken many proactive steps to deal the menace of space debris. The controlled reentry of Megha-Tropiques-1 satellite from its orbit by executing two de-boost burns with 11 N thrusters on 7th March 2023 was one example in that direction. Another exemplary effort to minimise the space debris from launch vehicle, ISRO has converted the final stage of PSLV, PS4, into an orbiting microgravity platform, christened as POEM, and made it open to industries, academia and start-ups to do experiments in space. The orbit is so chosen in a such a way that after doing the microgravity experiments, the orbit of POEM will naturally decay and will get destroyed during the re-entry into Earth's atmosphere through the natural decay of orbit.

One of the major issues still persisting is the prediction of the impact point of reentry bodies within a few kilometers of accuracy at least days before the reentry event. Presently only the track of the body is possible to be estimated. However, this does not pose a major problem as 70% of earth is sea and most of the material burns in atmosphere during the reentry, though there were some rare exceptions. To enable reasonable good estimation of the impact point with a low CEP, accurate estimation

of ballistic coefficient from TLEs is needed along with a good estimate of atmospheric density from 120 to 300 km altitude.

With increased launch rate and more and more countries entering into the fray of launching satellites, the menace of space debris has already become a daunting task before the space faring nations. With the deployment of more and more large constellation of satellites in LEO by many countries including the private firms, total automation of Space Object Proximity Analysis (SOPA) is very essential to avoid untoward incidences in space. Presently, debris with size of 10 cm and above in LEO are detected and catalogued. However, debris within 3 to 10 cm size also can pose significant threats despite with the presence of debris shield. Hence efforts shall continue to detect and catalogue smaller sized objects too like the NASA space fence project.

The monograph brought out by the authors has comprehensively compiled the efforts put in by generations of scientists and engineers in VSSC in the last few decades in the area of space situational awareness. I appreciate the authors for the nice compilation and editing of the monogram and look forward to an undergraduate level textbook emerging from this for the posterity.



(Unnikrishnan Nair S)
Director, VSSC and IIST

Acknowledgements

An understanding of the space environment and the potential operational hazards is essential and is critical for safe and sustainable operations in outer space. The most serious threats are posed by space debris which are non-functional and human-made objects in Earth's orbit. They no longer serve any useful purpose. These objects can vary in size, from tiny paint flecks to large defunct satellites and spent rocket stages. Space debris are not spread uniformly through space, but they are concentrated near the regions that are used by active satellites. This monograph deals with various aspects of space debris and space situational awareness studies.

The authors believe that the monograph will be a knowledge addition for all those who work-in the area of space debris and space situational awareness.

The authors express their deep gratitude to Dr. S. Somanath, Chairman, Indian Space Research Organisation, for his encouragement in this endeavour. The authors express their gratitude to Dr. S. Unnikrishnan Nair, Director, Vikram Sarabhai Space Centre (VSSC) for his constant encouragement during the preparation of this document and for getting the monograph reviewed by experts. The technical review by Dr. V. Ashok, Associate Director (R & D), VSSC and Dr. M. M. Patil, Deputy Director, Aeronautics Entity, VSSC has helped to improve the quality of the monograph and their contributions are gratefully acknowledged.

In the pursuit of the research problems and technical contributions reported in this monograph, the authors acknowledge the association of their colleagues: Shri A. Agarwal, Prof. M. R. Ananthasayanam, Shri S. Arun Kumar, Dr. V. Ashok, Shri Priyankar Bandyopadhyay, Smt. G.P. Beena, Smt. P. Bhanumathy, Shri Deepak Negi, Dr. B. Deependran, Shri D. A. Deniel, Shri R. Devasia, Dr. Pooja Dutt, Shri J. Fletcher, Shri A. S. Ganeshan, Shri N. S. Gopinath, Smt. Shraddha Gupta, Shri A. Kandari, Shri A. Kumar, Smt. T. R. Saritha Kumari, Ms. C. S. Lawrence, Smt. Leelamma Mani, Shri S. P. Mathew, Smt. Bulbul Mukherjee, Dr. M. Mutyalarao, Dr. Lila S. Nair, Shri S. Nandhu Raj, Smt. S. Nirmala, Shri P. Padmanabhan, Shri A. Painuly, Shri S. Parameswaran, Dr. M.Y.S. Prasad, Dr. M. Xavier James Raj, Shri J. Raja, Shri S. C. Rathnakara, Dr. D. Sudheer Reddy, Shri N. G. Reddy, Shri A. Sabarinath, Dr. Himani Saini, Ms. Sharon S. Saji, Dr. Harishkumar Sellamuthu, Shri A. Selvam, Shri S. Shajahan, Shri M. S. Siva, Ms. M. J. Smibi, Shri K. J. Sreejith, Dr. P. V. Subba Rao, Shri V. V. Vijay and Shri S. Xavier.

Ram Krishan Sharma
A K Anil Kumar
Adimurthy Vipparthi



SDSSARS IN ISRO

Space Debris and Space Situational
Awareness Research Studies



Nomenclature

a	: Semi-major axis
a	: Area parameter in the modified Laplace distribution
A_c	: Casualty area
ADR	: Active Debris Removal
A_{eff}	: Effective area
ASAT	: Anti-Satellite Test
B	: Ballistic coefficient
B^*	: $(\rho_0/2) B$
C_A	: Total casualty expectancy
C_d	: Drag coefficient
CAM	: Collision Avoidance Maneuver
CM	: Crew Modules
COLA	: Collision Avoidance Analysis
d	: Diameter
e	: Eccentricity
ESA	: European Space Agency
f	: True anomaly
$f(n, h/h_p, i, e, B, t)$ – Joint probability density function (pdf); n is number density, h is altitude or the perigee altitude h_p , i is inclination, e is eccentricity, B is ballistic coefficient, t is time.	
GA	: Genetic algorithm
GEO	: Geosynchronous Equatorial Orbit
GMT	: Greenwich Mean Time
GSO	: Geo-synchronous orbit
GTO	: Geostationary Transfer Orbit
h_p	: Perigee altitude



SDSSARS IN ISRO

Space Debris and Space Situational
Awareness Research Studies

HST	: Hubble Space Telescope
i	: Inclination
IADC	: Inter-Agency Space Debris Coordination Committee
ICBM	: Intercontinental ballistic missile
ISTRAC	: ISRO Telemetry Tracking and Command Network
J_2, J_3 and J_4	: Earth's zonal harmonic terms
JSpOC	: Joint Space Operation Centre
K-S	: Kustaanheimo-Stiefel
LCOLA	: Launch COLLision Avoidance
LDEF	: Long Duration Exposure Facility
LEO	: Low Earth Orbit
LEGEND	: LEO-to-GEO Environment Debris Model
m	: Location parameter in the modified Laplace distribution
m/s	: Meters/second
MC	: Monte-Carlo
MMH	: Mono-methyl hydrazine
MMOD	: Micro-meteoroid and orbital debris
n	: Density number
NASA	: National Aeronautics and Space Administration
NETRA	: Network for space objects TRacking and Analysis
NORAD	: North American Aerospace Defense Command
NPOE	: Numerical Prediction of Orbital Events
OLT	: Orbital Life Time
p	: Weight parameter of the distribution
$P_0 h$: Negative of total energy
P	: Remaining perturbing forces

$P_i(\Phi_1, \Phi_2)$: Impact probability between two latitudes Φ_1 and Φ_2
PMD	: Post Mission Disposal
$P_{\infty 1}$: Maximum collision probability for a single close conjunction event
r	: Radial distance
R_{\min}	: Minimum approach distance
RSM	: Response surface method
R_s	: Effective collision radius
RSO	: Resident Space Object
s	: Scale parameter in the modified Laplace distribution
S/C	: Spacecraft
SIMPLE	: Stochastic IMPressionistic Low Earth
SM	: Service Modules
SOPA	: Space Object Proximity Analysis
SP	: Special Perturbation
SSO	: Sun Synchronous Orbit
STK	: Systems Tool Kit (formerly Satellite Tool Kit)
STM	: Space Traffic Management
TCA	: Time of closest approach
TLE	: Two-Line Elements
TPS	: Thermal protection system
USSAPCECOM	: U.S. Space Command
UTC	: Coordinated Universal Time
V	: Velocity
V	: Perturbing potential
VLEO	: Very low Earth orbit



SDSSARS IN ISRO

Space Debris and Space Situational
Awareness Research Studies

VSSC	: Vikram Sarabhai Space Centre
x	: Position vector of the particle
$\Delta V_t, \Delta V_n, \Delta V_r$	– Incremental velocity in the transverse, normal and radial directions, respectively, with respect to the orbital plane (m/s)
θ	: True anomaly
λ	: Longitude measured with respect to the line of nodes
λ	: Sun declination angle on spacecraft orbital plane
λ	: Scale parameter of the distribution
Λ	: Sun azimuth angle on spacecraft orbital plane
μ	: Location parameter of the distribution
ρ_0	: Density
$\rho_p(\Phi)$: Population density in terms of latitude bins
Φ	: Latitude
ω	: Argument of perigee

List of Figures

Figure 1.1	Sources and sinks of space debris
Figure 1.2	Spread of fragments created by Cosmos-Iridium collision (image credit: Celestrack, AGI)
Figure 1.3	LEO and GEO region (Image credit: CNES)
Figure 1.4	Growth of Catalogued Population (Source: ODQN March 2023 [1])
Figure 1.5	Mass of catalogued objects in Earth orbit as on 03 Feb 2023 by U.S. Space Surveillance Network. (Source: ODQN March 2023)
Figure 1.6	The near Earth (up to 2000 km) altitude population. Population growth is evident at all altitudes between the 15th edition (04 July 2018) and 16th edition (01 May 2022). ODQN March 2023
Figure 1.7	Number of CAMs (till September 2023)
Figure 1.8	Black out zones within launch window
Figure 1.9	Oppositely oriented nozzle configuration ensures equal thrust in opposite direction and no orbital change
Figure 1.10	Cartosat-2 de-orbiting at end-of-life
Figure 1.11	Re-entry Manoeuvres of Megha-Tropiques-1
Figure 1.12	PMD of a typical GEO satellite
Figure 2.1	The Gabbard Diagram from the TLEs of PSLV-TES Spent Upper Stage Breakup Fragments after 31 Days of Breakup
Figure 2.2	The Distribution of Apogee, Inclination, Eccentricity and B* from the TLEs of PSLV-TES Spent Upper Stage Breakup Fragments after 31 Days of Breakup
Figure 2.3	Histograms of the Semi-major Axis of the Catalogued GEO
Figure 2.4	The distribution fit for the semi-major axis of the non-functional GEO objects using the tertiary mixture of the Laplace distributions for the year 2004



Figure 2.5	The distribution fit for the semi-major axis of the non-functional GEO objects using the tertiary mixture of the Laplace distributions for the Laplace distributions for the year 2002
Figure 2.6	Comparison of SIMPLE model with observations for the year 2000 to 2004
Figure 2.7	Histograms of the Eccentricity of the catalogued GEO objects
Figure 2.8	The binary mixture of normal distribution fit for Eccentricity of the non-functional objects
Figure 2.9	Histograms of the Inclinations of the catalogued GEO objects
Figure 2.10	Solar flux projections used by participating agencies. Only the period from 2010 through 2060 is shown for clarity
Figure 2.11	Effective numbers of objects 10 cm and larger in LEO predicted by the six different models. All models assumed no future explosion and 90% compliance of the commonly adopted
Figure 2.11	Effective numbers of objects 10 cm and larger in LEO predicted by the six different models. All models assumed no future explosion and 90% compliance of the commonly adopted
Figure 2.12	Cumulative numbers of catastrophic collisions predicted by the six models mitigation measures
Figure 3.1	Predicted evolution of the Iridium and Cosmos debris planes 30 days and six months after the collision
Figure 3.2	Cosmos 2251 debris (red) are more numerous and spread across a greater altitude regime than that of Iridium 33 (blue)
Figure 3.3	The relationship between changes in inclination and right ascension of ascending node
Figure 3.4	The scatter plot for velocity changes in PSLV-C3/PS4 fragmentation
Figure 3.5	The histograms for velocity changes in PSLV-C3/PS4 fragmentation
Figure 2.11	Effective numbers of objects 10 cm and larger in LEO predicted by the six different models. All models assumed no future explosion and 90% compliance of the commonly adopted

Figure 2.12	Cumulative numbers of catastrophic collisions predicted by the six models mitigation measures
Figure 3.1	Predicted evolution of the Iridium and Cosmos debris planes 30 days and six months after the collision
Figure 3.2	Cosmos 2251 debris (red) are more numerous and spread across a greater altitude regime than that of Iridium 33 (blue)
Figure 3.3	The relationship between changes in inclination and right ascension of ascending node
Figure 3.4	The scatter plot for velocity changes in PSLV-C3/PS4 fragmentation
Figure 3.5	The histograms for velocity changes in PSLV-C3/PS4 fragmentation
Figure 5.1	Number of breakups by year since 1961. Breakups after 18 July 2018 are shown in red. (Anz-Meador et al., 2022)
Figure 5.2	Variation of Location Parameter for Eccentricity in Individual Altitude bins
Figure 5.3	Comparison of model values of Location Parameter for Eccentricity in moving window Altitude bins and individual Altitude bins
Figure 5.4	(a) Number density distributions in altitude and perigee for the year 2002 and (b) eccentricity and B distributions of the debris objects for the year 2002
Figure 5.5	Comparison of number density of debris from measurements and model distributions in inclination band (610, 730)
Figure 5.6	Comparison between observed and predicted osculating perigee altitude for Transtage 10 of Titan III C launch vehicle (Case A-NORAD ID: 2770)
Figure 5.7	Comparison between observed and predicted osculating perigee altitude for H-2A Rocket Body (NORAD ID: 41037)
Figure 6.1	Fit of binary mixture of the modified Laplace distribution for the Spatial density for the August 2007 data for inclinations from 0 -180 degrees
Figure 6.2	Fit of binary mixture of the modified Laplace distribution for the Spatial density for the August 2007 data for inclinations of 98-99 degrees



Figure 6.3	Fit of binary mixture of the modified Laplace distribution for the Spatial density for the August 2007 data for inclinations of 95-105 degrees
Figure 6.4	Fit of binary mixture of the modified Laplace distribution for the Spatial density for the December 2006 data for inclinations of 95-105 degrees
Figure 6.5	Fit of tertiary mixture of the modified Laplace distribution for the Spatial density for the April 2010 data for inclinations from 0–180 degrees
Figure 6.6	Fit of tertiary mixture of the modified Laplace distribution for the Spatial density for the April 2010 data for inclinations from 95–105 degrees
Figure 6.7	Fit of tertiary mixture of the modified Laplace distribution for the Spatial density for the April 2010 data for inclinations from 98–99 degrees
Figure 6.8	COLA analysis for a typical LEO mission on the launch day
Figure 6.9	SOPA flow chart
Figure 6.10	Distribution of Resident Space Objects (RSO)
Figure 6.11	The Strategy for Optimal Collision Avoidance Maneuver
Figure 6.12	Variation of Cumulative Collision Probability with the Time of Application of Impulse
Figure 6.13	Convergence of Genetic Algorithm in Case 1 and Case 2
Figure 6.14	Relation between Minimum $(\Delta V)^2$ and Cumulative Maximum Collision Probability
Figure 7.1	Cumulative decay of PSLV-C3 debris fragments
Figure 7.2	Firing pulse durations for INSAT-2C relocation
Figure 7.3	Changes in INSAT-2C position during relocation operation
Figure 7.4	Orbital evolution of GSLV-D1 rocket body
Figure 7.5	The Impact Probability and Casualty Expectancy Variations for Circular and Elliptic Orbits

Figure 7.6	The Casualty Expectancy Variations with Latitude
Figure 7.7	BC Estimation and RCS History of some of the Identified Objects
Figure 8.1	Sat25947 re-entry prediction: Observed and estimated values of Apogee and Perigee heights with the constant gain approach
Figure 8.2	Perigee altitude variation during a day for different apogee altitudes with the variation of Sun azimuth angle on spacecraft orbital plane. Nominal perigee altitude is taken as 150 km
Figure 8.3	Typical dependence of orbital lifetime on the time of launch during a day
Figure 8.4	Illustration of a bifurcation in neighboring orbital evolution patterns
Figure 8.5	Variation of Λ -dot with apogee altitude at various inclinations. The bifurcation at a given apogee altitude can occur in neighboring orbital evolution patterns when the Λ -dot is very small, as indicated with the shaded area (Perigee altitude of 150 km is assumed)
Figure 8.6	Orbital evolution of the spent orbiting stage of GSLV-D1
Figure 8.7	Comparison between the observed and predicted mean apogee altitudes using Least Square method
Figure 8.8	Comparison between the observed and predicted mean apogee altitudes using RSM with GA method
Figure 8.9	Variation of mean apogee altitude of GSLV-F04/CS (NORAD No. 32051) with each zone label mentioned
Figure 8.10	Variation of observed mean apogee altitude of GSLV R/B
Figure 8.11	SCOSS-C2 re-entry times using BALEST- Online predictions
Figure 8.12	Re-entry prediction methodology
Figure 8.13	Five zones for finding ballistic coefficient and eccentricity (Case 2)
Figure 8.14	Optimal and non-optimal apogee altitude solution compared with TLE data for Case 4
Figure 8.15	Re-entry time estimation for Starlink-26 using four methods
Figure 8.16	Re-entry time estimation for CZ-5B using four methods
Figure 8.17	Re-entry predictions by ISRO (COIW: Centre of Impact Window)



SDSSARS IN ISRO

Space Debris and Space Situational
Awareness Research Studies



List of Tables

Table 1.1	Top ten worst historical break-up (source: NASA, ODPO)
Table 1.2	A Summary of on-orbit collisions
Table 1.3	Details of lift-off time change based on COLA recommendations
Table 2.1	Model parameters for number density of GEO objects in Semi-major axis μ -Location parameter, λ -Scale parameter, p -Weight parameter
Table 2.2	Model parameters for number density of GEO objects in Eccentricity. μ -Location parameter, λ -Scale parameter, p -Weight parameter
Table 2.3	Number of Monte Carlo (MC) simulations performed by participating models
Table 2.4	Summary of the projected LEO population increase based on regular launches and a 90% compliance of the commonly-adopted mitigation measures
Table: 4.1	Orbital Parameters of RS-1 (20 July 1980 Epoch)
Table 4.2	Orbital parameters of Sun-synchronous Orbit
Table 4.3	BC Estimation of Phobos-Grunt with different TLE sets and re-entry prediction (Re-entry epoch: 15th Jan 2012 17:45 UTC)
Table 4.4	BC Estimation of SFERA with different TLE sets and re-entry prediction (Re-entry epoch date: 24th Nov 2012)
Table 5.1	On-orbit or decayed-and-beyond-Earth-Orbit of Space objects Distribution
Table 5.2	Parameters of the lognormal distribution for the eccentricity of catalogued debris objects
Table 6.1	Close conjunction objects within launch window (only 2 piggy-back satellites are included for brevity)
Table 6.2	Details of Force Model
Table 6.3	Details of Collision Avoidance Maneuvers for LEO spacecraft carried out in 2022
Table 6.4	Comparison of collision probability prediction between SIMPLE and DAS



Table 6.5	Comparisons of Collision Probabilities at different Target Altitudes by various Approaches
Table 6.6	Close Conjunction Events with Resident Space Objects without Any Collision Avoidance Manoeuvre
Table 6.7	Collision Avoidance Manoeuvre to Achieve Minimum Cumulative Collision Probability (Case 1)
Table 6.8	Collision Avoidance Manoeuvre to Achieve Specified Cumulative Collision Probability (Case 2)
Table 6.9	Details of Collision Avoidance Maneuvers Carried out during fourth quarter of 2017
Table 6.10	Maneuver Strategy for Resourcesat-2 on 23 September 2017
Table 7.1	Top debris creation events
Table 7.2	List of Candidates from SSO selected on the basis of RCS
Table 8.1	Predicted reentry time in zones A to H
Table 8.2	Comparison between actual and predicted reentry times of some decayed objects
Table 8.3	Computed values of initial osculating eccentricity and ballistic coefficient and re-entry time for each zone using RSM and GA
Table 8.4	Computed values of parameters with predicted re-entry time of GSLV-D5/CUS (Re-entry epoch: 8 June 2014 01:31 UTC a)
Table 8.5	Prediction of Re-entry of COSMOS 2332 Satellite
Table 8.6	Computed values of initial ballistic coefficients (B) (Match TLE 28-May-2002, 10:51:54 (UTC))
Table 8.7	Comparison between observed and estimated parameters of ARIANE-V
Table 8.8	Re-entry prediction results for SROSS satellite
Table 8.9	Re-entry prediction results of SL3-rocket body
Table 8.10	Re-entry prediction GSLV-D5/CUS
Table 8.11	Computed values of parameters with predicted re-entry time of Phobos-Grunt satellite (Re-entry epoch: 15 Jan 2012 17:45:00 UTCA)

Table 8.12	Computed values of parameters with predicted re-entry time of ROSAT satellite (Re-entry epoch: 23 Oct 2011 01:57:00 UTC)
Table 8.13	Re-entry predictions of Phobos-Grunt
Table 8.14	Re-entry predictions for ROSAT
Table 8.15	Re-entry predictions for GOCE made using STK LTOptim
Table 8.16	Prediction of re-entry time of CZ-2C rocket with RSM-GA method
Table 8.17	Re-entry predictions with STKOptim method
Table 8.18	Re-entry predictions for CZ-2C using STK LTOptim method
Table 8.19	Re-entry prediction time computed for GSLV-F09/CUS rocket using RSM with GA in each time interval
Table 8.20	Eccentricity and ballistic coefficient (BC) used for 5 intervals
Table 8.21	Predicted re-entry decay and percentage errors for 5 predictions
Table 8.22	Launch log of selected Molniya satellites
Table 8.23	Optimal solutions for Molniya satellites re-entry time prediction
Table 8.24	Re-entry estimation of the three PSLV R/Bs (LEO objects) during different time zones
Table 8.25	Comparison of optimization methods for EBP estimation using STKOptim method
Table 8.26	Average percentage error during campaign for Starlink-26 and CZ-5B using four methods
Table 8.27	COSMOS 389 satellite re-entry predictions made using 'KSGEN' (Actual re-entry time \approx 24th November 2003, 22:36 hrs. UTC)
Table 8.28	Percentage errors on re-entry predictions made by VSSC (Actual re-entry time \approx 24th November 2003, 22:36 hrs. UTC)
Table 8.29	Percentage errors on re-entry predictions made by Different Agencies (Actual re-entry time \approx 24th November 2003, 22:36 hrs. UTC)
Table 8.30	Re-entry Prediction of CZ-5B Rocket Body
Table 8.31	Final predictions by various agencies



SDSSARS IN ISRO

Space Debris and Space Situational
Awareness Research Studies



CHAPTER 1

An Overview of Space Debris Environment and Relevant Studies in ISRO

1.1 Introduction

An understanding of the space environment and the potential operational hazards is essential and critical for safe and sustainable operations in outer space. The most serious threats are posed by space debris which are as non-functional, human-made objects in Earth's orbit that no longer serve any useful purpose. These are also called orbital debris and are distinguished from naturally occurring objects like meteoroids. These objects can vary in size, from tiny paint flecks to large defunct satellites and spent rocket stages. Space debris are not spread uniformly through space, but they are concentrated near the regions that are heavily used by satellites.

Space debris are created in space by the accumulation of defunct satellites, spent rocket stages, and various fragments, which now pose a significant threat to both current and future space missions (Klinkrad, 2006).

- **Defunct Satellites:** Satellites have limited life spans and eventually become inoperable or reach the end of their missions. However, they remain in orbit, posing a risk of collision and further debris creation.
- **Mission operations related:** Materials released during spacecraft mission operations such as cameras, lens caps, solid fuel, items like gloves, toolboxes, solid motor exhausts, payload adaptor etc., contribute to the debris related to mission operations.
- **Rocket Stages:** Launching satellites into space involves multi-stage rockets. After the final stage burn out, they are often discarded and left to orbit as space debris.
- **Fragmentation/Break-ups and Collisions:** Break up events may be high energy separation from the parent body or a low energy separation for which the fragmentation root cause is mostly not known. Intentional activities like the anti-satellite tests and self-destruct mission such as the Cosmos self-destruct at end of life, Anti-Satellite Test (ASAT) on Fengyun 1C and Russian Cosmos spacecraft

also resulted in the creation of large number of fragments. Accidental collision of satellites such as the infamous collision between the Cosmos 2251 and Iridium 33 also created a large number of space debris (Anz Meador et al., 2023)

- Micro-debris, or small particles less than a centimetre in size, are generated when larger objects break apart due to mechanical stresses, impact with other objects, or natural causes like micrometeoroid impacts. Breakup of smaller substances from larger surface due to reasons like thermal flexing, atomic erosion and small particulate impact also produce such small-sized space debris.

The orbits of space debris evolve due to various perturbations and may naturally decay over time to eventually re-enter the atmosphere. This natural cleansing mechanism is mostly applicable to Low Earth orbits. The debris can be also removed from the space through active means by direct retrieval or relocation. Figure 1.1 shows the sources of space debris and the mechanisms of removal from outer space.

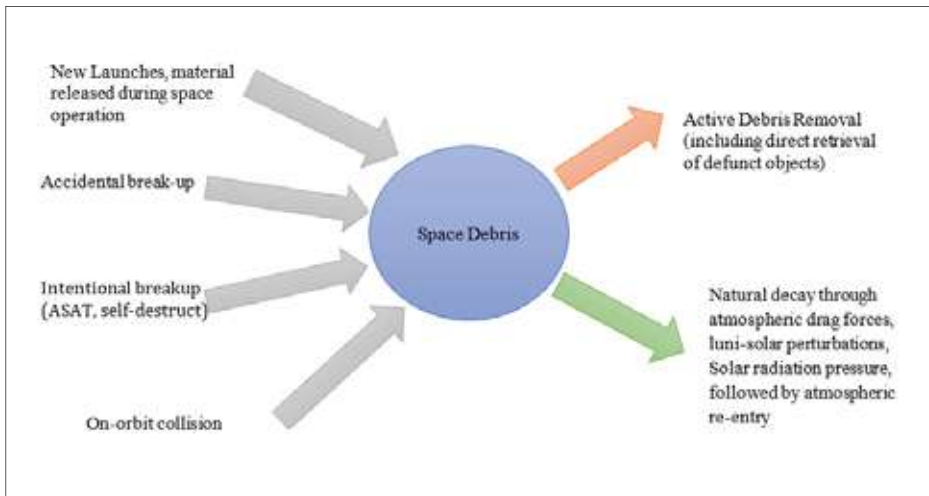


Figure 1.1: Sources and sinks of space debris

1.2 Fragmentation Events

Historically, fragmentation or break-up events have been the most significant contributor to the space debris population.

Table 1.1: Top ten worst historical break-up (source: NASA, ODPO)

Rank	International Designator	Common Name	Year	Apogee Alt.(km)	Perigee Alt.(km)	No of Debris	Assessed Cause of Breakup
1	1999-025A	Fengyun-1C	2007	865	845	3532	Anti-satellite (ASAT) test
2	1982-092A	Cosmos 1408	2021	490	465	1785	ASAT test
3	1993-036A	Cosmos 2251	2009	800	775	1715	Accidental collision (Iridium 33)
4	1994-029B	STEP1 upper stage	1996	820	585	754	Accidental explosion
5	1997-051C	Iridium 33	2009	780	775	657	Accidental collision (with Cosmos 251)
6	2022-151B	CZ-6A upper stage	2022	847	813	533	Accidental explosion
7	2006-026A	Cosmos 2421	2008	420	400	509	Unknown
8	1986-019C	SPOT 1 upper stage	1986	835	805	498	Accidental explosion
9	1981-053A	Cosmos 1275	1981	1015	960	479	Accidental explosion
10	1965-082DM	Tita 3C-4 transtage	1965	790	710	473	Accidental explosion

1.3 On-Orbit Collisions

The table below summarises a few known on-orbit collisions.

Table 1.2 A Summary of on-orbit collisions

Object#1 (Satellite/ Rocket body)	Object #2 (Threat object)	Event Date	Consequence	Orbital character- istics at the time of collision
COSMOS 1934	COSMOS 926	23-Dec- 1991	N/A (non-func- tional)	Both in 980 km, 83 deg inclination
Cerise	Fragment from third stage of Ariane 1 LV	24-Jul- 1996	Gravity-gradient stabilising boom severed, change in moments of inertia and alti- tude of satellite, loss of mission	656x652 km, 98.5 deg inclined
Thor Burner 2A upper stage (which launched DMSP 5B F5)	Fragmentation debris from CZ-4 R/B	17 Jan 2005	7 catalogued debris	885 km, both ob- jects in retrograde orbits
Iridium-33	COSMOS-2251 (Defunct Rus- sian satellite)	10-Feb- 2009	Catastrophic collision, 2370 catalogued debris	Iridium-33: 800 km, 98.4 deg inclina- tion; COSMOS-2251: 800 km, 74 deg inclination
BLITS	Fengyun 1C (Chinese ASAT) debris	22-Jan- 2013	Altitude lower- ing and spin rate change	BLITS: 829 x823 km, 98.55 deg
GOES 13	Small meteor- oid or orbital debris particle impact	22-May- 2013	Attitude distur- bance causing 2 deg/hr drift off nadir pointing, no permanent damage	GEO

Object#1 (Satellite/ Rocket body)	Object #2 (Threat object)	Event Date	Consequence	Orbital character- istics at the time of collision
NEE-01 Pegaso	believed to have suffered a "glancing blow" af- ter passing through a debris cloud around the 1985 Tsyklon-3 stage	23-May- 2013	spinning wildly in two axes, lost communica- tion to ground station, declared lost though later recovered signals indicat- ed the satellite survived the glancing blow	640x 600 km orbit, 98 deg inclination
Sentinel 1A	Impact by a small (maxi- mum of 1cm) manmade debris object	23-Aug- 2016	Sudden and permanent power reduction in a solar array, impact dent captured by on- board camera	697x695 km, 98.1 deg inclina- tion
YunHai 1-02	Mission-relat- ed debris from SL-6 (Russian) Launch Vehicle	18 Mar 2021	37 catalogued fragments	780 km (sun-syn- chronous orbit), 98.53 deg inclina- tion

The debris generated due to fragmentation (accidental or intentional break-up, or collision) spread over time as shown in Figure 1.2.

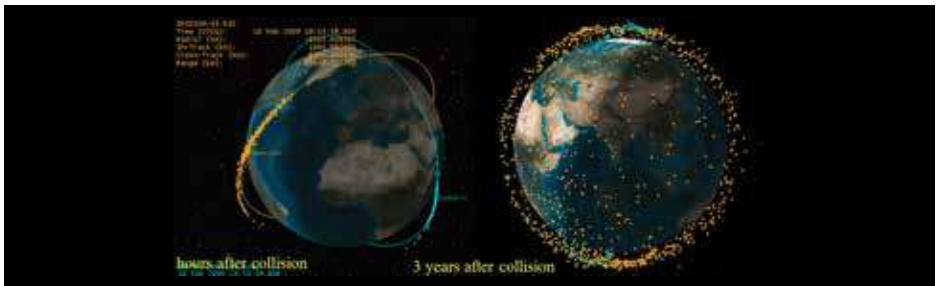


Figure 1.2: Spread of fragments created by Cosmos-Iridium collision (image credit: Celestrack, AGI)

1.4 Growth of Catalogued Population

Low Earth Orbit (LEO) region extends up to an altitude of 2000 km. This is the most densely populated region in space. Geosynchronous (GEO) region is a toroid shaped zone at the +/-200 km altitude band around the Geostationary altitude of 35786 km (i.e. from 35586 to 35986 km altitude) and +/-15 deg. latitude about the equator. These two regions are called protected regions because they are highly utilised and any space debris creation will have potentially severe impact on the space environment. Figure 1.3 shows pictorially orbital regimes around Earth (IADC, 2021).

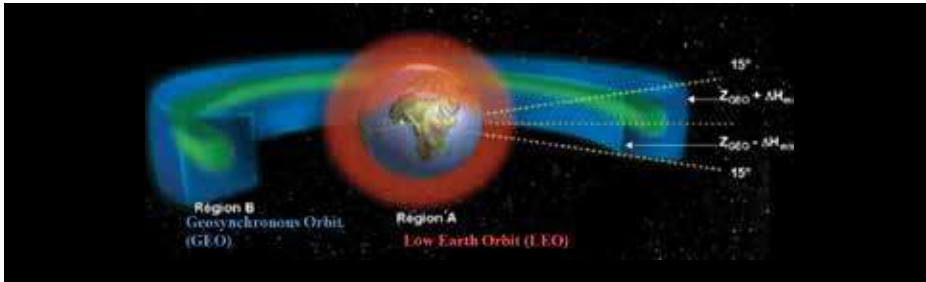


Figure 1.3: LEO and GEO region (Image credit: CNES)

Low Earth Orbit (LEO) region extends up to an altitude of 2000 km. This is the most densely populated region in space. Geosynchronous (GEO) region is a toroid shaped zone at the +/-200 km altitude band around the Geostationary altitude of 35786 km (i.e. from 35586 to 35986 km altitude) and +/-15 deg. latitude about the equator. These two regions are called protected regions because they are highly utilised and any space debris creation will have potentially severe impact on the space environment. Figure 1.3 shows pictorially orbital regimes around Earth (IADC, 2021).

The U.S. Space Command (USSAPCECOM) tracks the space debris and has catalogued objects sized typically 10 cm or more in LEO and 0.3 m or more in GEO. These measurements are made through the ground based (generally radars and optical telescopes) and space-based sensors. The non-catalogued objects less than 10 cm in size are measured through detection of samples by ground based sensors, examination of returned spacecraft and through active measurements in orbit. The knowledge of the smaller debris is based on the extrapolation of the incomplete data.

According to the latest figures provided by ESA's Space Debris Office, as on 06 June 2023, there are about 36500 space debris objects greater than 10 cm, 1000000 space debris objects greater than 1 cm to 10 cm and 130 million space debris objects greater than 1 mm to 1 cm (ESA, 2023).

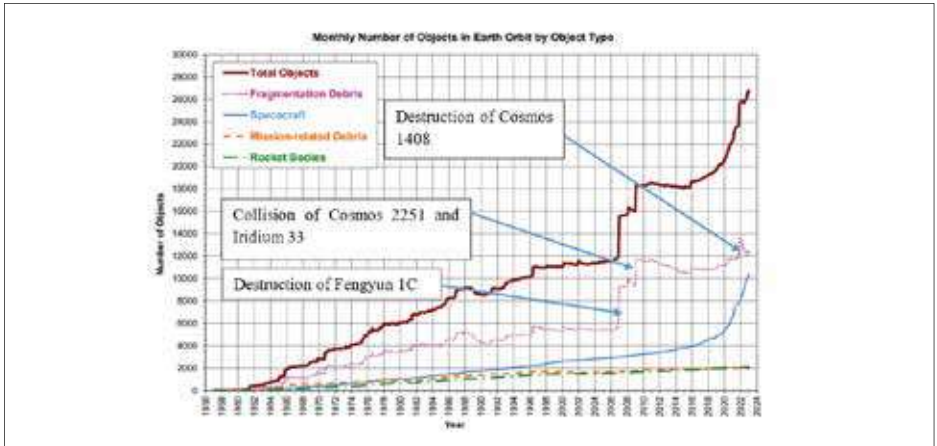


Figure 1.4: Growth of Catalogued Population (Source: ODQN March 2023 [1])

Figure 1.4 shows total number of catalogued space objects as a function of time (Cowardin and Johnson, 2023). The four curves represent the population break down. The curves show that fragmentations have dominated the population. Three major chunks have been created by the ASAT tests on Fengyun 1C satellite by China in 2007 which has created more than 3000 debris. Accidental collision of Russia’s defunct Cosmos 2551 satellite generated more than 2000 pieces of debris, and the recent ASAT test on Cosmos 1408 by Russian Federation in 2001 resulted in around 2000 debris. The Figure 1.4 shows that there are about 3000 retired spacecraft and around 7100 operational spacecraft.

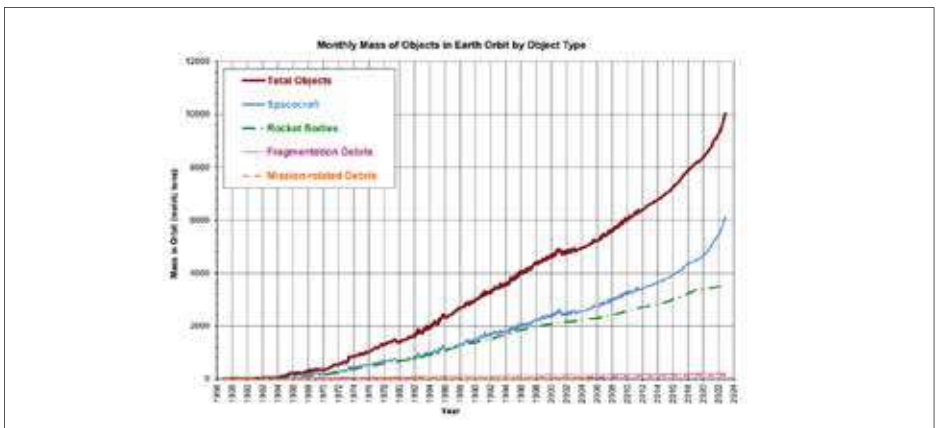


Figure 1.5: Mass of catalogued objects in Earth orbit as on 03 Feb 2023 by U.S. Space Surveillance Network. (Source: ODQN March 2023)

Figure 1.5 shows that the mass of objects in space also shows continuous increasing trend and there is no sign of slowing down. The mass of spacecraft is the major contributor and the total mass has exceeded 9000 metric tonnes. In LEO (up to 2000 km altitude region) orbit alone, the total mass has exceeded more than 4000 metric tonnes. It is to be noted that the history of mass increase is different from the distribution of mass.

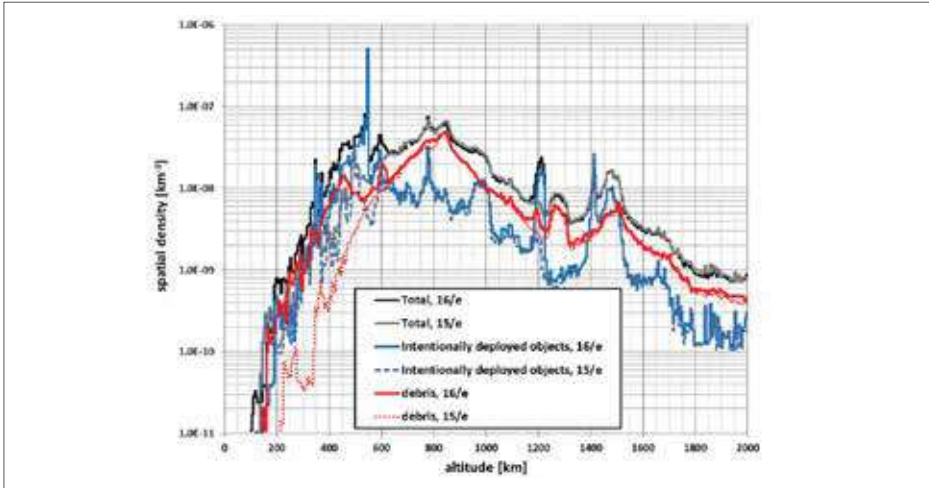


Figure 1.6: The near Earth (up to 2000 km) altitude population. Population growth is evident at all altitudes between the 15th edition (04 July 2018) and 16th edition (01 May 2022). ODQN March 2023

The distribution of objects at a given orbital regime is represented by spatial density, which is defined as the number of objects per unit volume. Figure 1.6 shows the spatial density of objects as a function of altitude in LEO. Proliferation of CubeSats and the deployment of large constellations were primarily responsible for the increase below 600 km. It is to be noted that collision rates will vary not only with the spatial density, but also with the inclination-dependent relative velocity.

1.5 Threats Due to Space Debris

Space debris poses a serious threat to operational satellites which might be damaged or even catastrophically destroyed due to collision. The debris have very high orbital velocity. In LEO, it is in the order of 7-8 km/s which gives high momentum approximately ten times the speed of a bullet. The general rule is that the space debris follows a power law distribution i.e. there are more small sized debris than large debris. With such high speed, even millimetre sized debris can create serious problem for mission operations including the human space flight and robotic missions. It may be noted that debris of size 0.4 mm can penetrate the space suit of astronauts during spacewalk and threaten the safety of astronauts. The big tracked objects represent only the tip of the iceberg but most of the mission ending catastrophes are dominated by small (mm to cm sized) debris impacts. There can be a risk of debris collision for launch vehicles as well. Even though no satellite launch vehicle was reported to have been hit by debris so far, the third stage of a Minuteman ICBM was reportedly destroyed in collision with uncatalogued space debris during a flight on January 15, 1998 (Sundahl, 2000).

Major perturbing forces such as atmospheric drag, luni-solar attraction, solar radiation pressure may result in the re-entry of space debris in to Earth's atmosphere (Vallado, 2001). An object experiences very high aerodynamic load that may cause its structure to break-up during the re-entry. The intense aerothermal heating further causes most of the fragments to ablate, except for those having very high melting point. Such surviving objects poses risk to human life, property and environment on surface of the Earth.

From the previous discussions, it is evident that space debris poses a serious risk to space activities. As we continue to add more and more material to the near-Earth environment, we only increase the potential of more collisions, as more and more fragments are generated. Finally, this may lead to a cascading effect creating a self-sustaining cloud of debris around the Earth. This scenario is known the Kessler Syndrome, after its proponent Kessler, a NASA scientist. In his 1978 seminal paper (Kessler and Cour Palais, 1978), he showed that even without any new launches, such a cascading event can be triggered due to collision among the orbiting objects themselves, the resultant artificial debris belt would severely hinder any future space-based activities. Therefore, various analysis, mitigation and remediation techniques are in place to address the space debris problems.

1.6 Space Debris Mitigation

It has long been unanimously agreed at an international level that space-based activities need to be properly managed to minimise the generation of space debris. Space Debris Mitigation involves measures to reduce the generation of new orbital debris, ensure the safety of operation of operational assets, and thereby, contribute to long-term the sustainability of outer space activities.

Many organisations involved in space operations have become aware of the potential threats of space debris, and have initiated efforts to mitigate debris generation and to share the results of these efforts with the international community. The foundational guidelines (IADC-2021) for space debris mitigation were developed by Inter-Agency Space Debris Coordination Committee (IADC-home). IADC was formally founded in 1993 to exchange information on space debris research activities between member space agencies, to facilitate opportunities for cooperation in space debris research, to review the progress of ongoing cooperation activities and to identify and evaluate debris mitigation options. The IADC comprises of a Steering Group and four specialised Working Groups: Working Group 1, on Measurement; Working Group 2, on Environment and Data Base; Working Group 3, on Protection, and Working Group 4, on Mitigation. The objectives of the WG on Measurements is to review space debris research efforts in the area of measurement techniques, to identify, evaluate and recommend new opportunities for cooperation, and to serve as means for exchanging information and plans concerning research activities in the area of measurements of orbital debris. The objectives of the WG on Environment and Data Base is to review research efforts in environment modelling and related data base, to identify, evaluate and recommend new opportunities for cooperation, and to serve as means for exchanging information and plans concerning research activities in the area of environment modelling and related data base. The scope of the activities of WG on Protection comprises design and technology of shielding against space debris and the associated test methods which include Test Facility and Procedure. Hypervelocity Impact Data, Simulation Software (Hydro code, Damage Probability Analysis Code). Design and Test Commonality, etc. The scope of Working Group on Mitigation is to study of all measures to reduce or avoid the creation of space debris, or reduce the hazards created by space debris. This includes identification of space debris sources, design and operations of space system to avoid or reduce the creation of space debris, removal of man-made objects, measures to prevent the creation of space debris, measures to reduce the collision hazard, and guidelines for debris mitigation. With its activities over the years, IADC has gained the recognition as the competent and prime international forum for the technical studies devoted to various issues of space debris.

United Nations Committee on the Peaceful Uses of Outer Space (COPUOS) was established in 1959 to govern the exploration and use of outer Space for the benefit of humanity. A set of high-level qualitative guidelines for space debris mitigation, having wider acceptance among the global space community was adopted by UN-COPUOS in 2007 (UNOOSA, 2007) based on the technical content of IADC space debris mitigation guidelines and in consideration of the United Nations treaties and principles on outer space. The item on space debris was included on the agenda of the Scientific and Technical Subcommittee since 1994, agreeing that the consideration of space debris was important and that international cooperation was needed to evolve appropriate and affordable strategies to minimize the potential impact of space debris on future space missions.

Guidelines for debris mitigation can be summarised as:

(a) Limiting of debris released during normal operations

- Space systems should be designed not to release debris during normal operations
- Where this is not feasible, any release of debris should be limited in number, area, and orbital lifetime
- Any release of objects in orbit should not be planned unless adequate assessment can verify effect on orbital environment and population
- Potential hazard of both intact and severed tethers should be analysed

(b) Minimisation of the potential for on-orbit break-ups

- Residual propellants and other fluids should be depleted
- Batteries should be designed to prevent break-ups, charging lines should be de-activated at the end of operations
- High pressure vessels should be vented to ensure no break-ups can occur
- Self-destruct systems should be designed not to cause unintentional activation
- Power to flywheels and momentum wheels should be terminated during disposal phase
- Other forms of stored energy should be assessed and adequate mitigation measures applied
- Using failure analyses, programs should demonstrate that there is no failure mode leading to accidental break-ups or, if cannot be excluded, probability minimised

- During operational phases, system should be periodically monitored to detect malfunctions which could lead to break-up or loss of control. If recovery measures cannot be conducted, disposal and passivation measures should be applied

(c) Post-mission disposal

- Space systems that have terminated their mission should be manoeuvred far enough away from geostationary orbit to avoid interference with GEO systems
- Systems terminating operational phases in orbits passing through low Earth orbit region should be de-orbited or, where appropriate, manoeuvred to orbit with reduced lifetime. The most preferred option is controlled re-entry into the atmosphere, direct retrieval is also an option. Otherwise, systems should be left in an orbit where drag will limit lifetime to about 25 years after completion of operations. This 25-year rule for LEO objects recommended by IADC prescribes is an effective and achievable way to limit the long-term presence of spent upper stage or defunct satellite in LEO.
- For re-entering objects, ground casualty risk should be minimised.

(d) Prevention of on-orbit collisions

- Analysis should be done to limit probability of accidental collision with known objects
- Avoidance of collisions and redefinition of launch windows may be considered
- Spacecraft design should limit probability of collision with small debris, which could cause loss of control, preventing post-mission disposal.

1.7 ISRO's Efforts

Over the years ISRO has developed substantial capabilities for space debris related analyses and have made significant contribution to protect operational Indian assets and mitigate space debris (Anil Kumar, 2022). The current activities are focussed on

- Establishing a robust, indigenous observational capability of space objects, including space debris, through a network of tracking facilities
- Evolving a reliable, end-to-end operational mechanism to process tracking observations
- Continual assessments of space situations to enable safe mission operations
- Dissemination of Space Situational Awareness (SSA) information in a timely manner

- Capacity building for space weather prediction, natural threat detection and monitoring
- Active participation in global efforts of SSA information exchange by sharing observational data on Resident Space Objects (RSO)

ISRO follows UN COPUOS/IADC guidelines for space debris mitigation (Adimurthy, 2006). The implemented measures include passivation of Launch Vehicles upper stages, collision avoidance for launch vehicles and spacecraft, re-orbiting of GEO satellites into higher orbits and passivation at end-of-life, post-mission disposal for LEO missions (India, 2023). As a further initiative towards the preservation of the space environment for the future, ISRO has also formulated India's requirements for space debris mitigation and management. Prasad (2005) briefly presents the historical perspective of ISRO and India, to the growing problem of space debris. Establishment of the ISRO System for Safe and Sustainable Space Operations Management (IS4OM) marks another major milestone, for the establishment of dedicated observational facilities (RADARS, Telescopes, space-based platforms) to obtain more accurate orbital information of space objects, extensive coordination with national and international bodies to avoid on-orbit collisions, collaboration with academia and research institutes for the assessment of the orbital space debris environment, engagement with emerging Indian space sectors to raise the awareness on the importance of space debris mitigation for the long-term sustainability of space activities.

1.8

Conjunction Assessment and Collision Avoidance for Spacecraft

Space Object Proximity Analysis (SOPA) is the fundamental process behind the detection and prevention of collision between ISRO's space assets and other resident space objects (Bandyopadhyay et al., 2004a) (Gupta et al., 2014). The process has evolved over the years. Initially, the screening was performed once daily and was limited to deriving and using the orbital information of the threat bodies from the publicly available TLE data. The orbits of all the primary satellites were propagated from initial state-vectors. As a result, any orbit manoeuvre was treated as an impulsive manoeuvre and screened in parts as pre-manoeuve and post-manoeuve trajectory. It may be noted that impulsive manoeuvre assumption is normally valid for routine orbit manoeuvres that are of short duration. The present conjunction analysis process supports all the legacy formats and has been augmented to include orbital information in various other formats and coordinate frames for both primary and secondary objects. Conjunction assessment screening is done for a period of 7 days using TLE data and for the ephemeris availability duration using more accurate SP (Special Perturbation) data. In addition, the orbits of primary satellites can be ingested as state-vector or ephemeris files. The primary satellite orbits are acquired from their

dedicated satellite control centres. This update allows seamless screening of satellite trajectories even in the presence of multiple manoeuvres within a trajectory. It also adds the capability to screen finite burn manoeuvres without needing to simulate the burn.

In case a close approach is detected that might result in a collision risk (quantified as maximum probability of collision), necessary actions are initiated. If the threat object is a piece of debris or a defunct object it cannot change its trajectory. The most straightforward evasive action to mitigate a collision risk in such a case would be performing a propulsive manoeuvre to change the orbit of the primary satellite. However, risk mitigation manoeuvres always need careful consideration before execution. Every manoeuvre consumes on-board fuel and fuel usage results in a reduction of the satellite's operational life. Collision avoidance manoeuvres, depending on their magnitude and direction can sometimes result in a "safe" orbit which deviates from the nominal mission orbit. This not only causes loss of payload tasking opportunities but also needs additional fuel to perform a restitution manoeuvre to return to the nominal mission orbit required for providing the satellite services. Therefore, in case of a conjunction, whenever possible, collision avoidance manoeuvres are designed not only to avoid conjunction but also to favourably impact orbit maintenance. These manoeuvres are designed to be fuel efficient and do not cause undue breaks in satellite services.

CAM design like any other manoeuvre design depends on both the spacecraft and ground station constraints. The target of an evasive manoeuvre is to reduce the probability of collision at the time of closest approach. The main parameters of a CAM plan are the magnitude; direction and time of burn that induces the velocity change. Each CAM plan goes through a screening against all space objects to ensure that the CAM execution does not give rise to fresh conjunctions.

When there are conjunctions between two active satellites the owner/operators of both the satellites normally exchange ephemerides. Conjunction analysis with operator ephemeris gives the most accurate conjunction assessment. If the operator ephemeris-based conjunction assessment indicates the necessity of avoidance manoeuvre only one of the satellites performs an orbit manoeuvre based on mutual consent of the satellite operators. It is also customary for the other party to keep a backup plan ready in case the planned CAM cannot be performed due to unforeseen circumstances.

The conjunction assessment process screens the orbits of all ISRO satellites against the orbits of all other resident space objects. Presently, it relies on the Space-Track database and the available operator ephemeris for the screening of conjunctions. The screening runs once per day. Provision is built to allow for need-based screening. The results of screening are provided to all the stakeholders along with recommendations for collision avoidance manoeuvre when required. The screening results are stored in

a database for easy retrieval on a need basis.

Figure 1.7 shows the collision avoidance manoeuvres executed by Earth-orbiting ISRO spacecraft since 2010 to till August 2023.

Since 2020, ISRO has evolved a methodology for conjunction assessment of its Mars

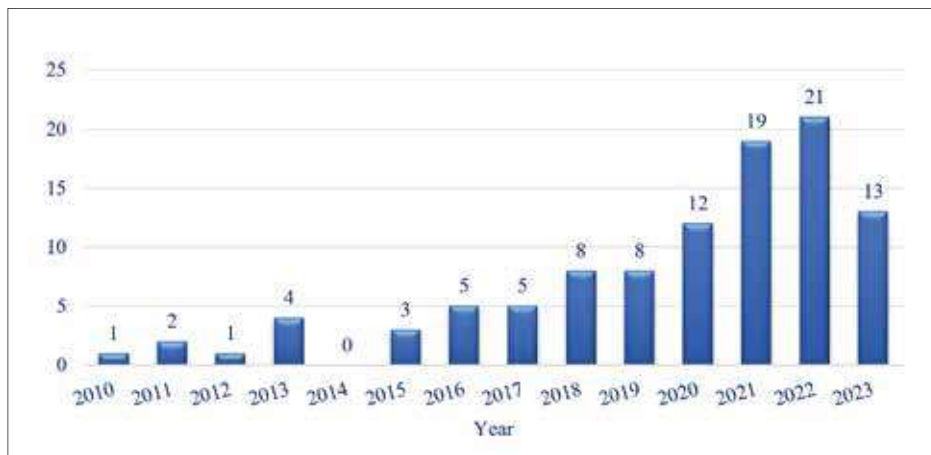


Figure 1.7: Number of CAMs (till September 2023)

and Moon orbiting spacecraft, namely BEARCAT (Beyond EarthOrbit Conjunction Assessment). The methodology considers the special characteristics of deep-space missions:

1. The orbit determination is poorer by roughly an order compared to Earth bound missions
2. The uncertainty in defunct satellites' orbit is very large because they are not tracked, some of them are often considered as "lost"
3. The update in ephemeris is infrequent, of the order of weeks compared to the update frequency of hours/days for earth bound satellites
4. The 'small-force' due to momentum dumping by thrusters non-negligibly impact the orbit

Therefore, the conjunction assessments are limited to mostly active secondary objects and CAM decisions have a higher lead time, typically a few days. During this lead time, additional measurements can be scheduled to have a better estimate of satellite orbit and re-assess the situation. International cooperation plays a crucial role as the latest and most accurate operator ephemerides, inclusive of any

forthcoming manoeuvre effects, must be shared for more accurate assessment and arriving at a common operational picture to mitigate risks. Any collision avoidance strategy must be devised based on mutual understanding and consent through proper coordination.

All manoeuvre plans for Chandrayaan missions (Chandrayaan-2 Orbiter/CH2O, Chandrayaan-3 composite and its propulsion and lander module) are screened to avoid any post manoeuvre potential conjunction with other neighbouring orbiters. Till Oct 2023, ISRO has performed three CAMs for CH2O. 7 manoeuvre plans including the first CAM plan on 18 Oct 2021 were modified based on spaceflight safety considerations.

1.9

Collision Avoidance Analysis (COLA) for Launch Vehicles

Pre-launch conjunction assessment is carried out to identify potential collision threats from space objects during the ascent phase of launch vehicles (LV) and the initial orbital phase of the injected satellites. Basic inputs are the orbital elements of space objects from USSPACECOM, operator-shared ephemerides (wherever available), nominal injection parameters of the injected S/C, LV trajectory, and the launch window. Launch COLLision Avoidance (LCOLA) analysis is performed to identify the safe lift-off timings within the entire launch window. In ISRO, the analysis is initiated about a week before the launch and repeated every day with the updated LV trajectories. The time instances within the launch window where a lift-off would result in critically close approaches to other space objects are marked as blackout zones. For a given lift-off time, a conjunction is flagged as critical if a pre-defined threshold on the probability of collision is exceeded. The corresponding lift-off timing is not recommended within these time zones (usually a +/-10 sec window centred around the blocked lift-off timing).

The analysis specifically addresses any close approach with the crewed missions like the International Space Station and Tiangong with a wider close approach distance screening threshold. Any close approach with an active satellite is notified to the concerned Owner/Operator with a request to avoid manoeuvring their satellite till the end of the predicted close approaches. The necessary coordination is also carried out to acquire more accurate operator-provided ephemerides for improving the accuracy of collision risk assessment.

COLA analyses for lift-off clearance of launch vehicles are carried out as part of the mandatory Launch Clearance Protocol of ISRO launch vehicles. The table below lists the occasions where the lift-off was delayed for ISRO launch vehicles (till September 2023).

Table 1.3: Details of lift-off time change based on COLA recommendations

Mission	Nominal liftoff time (IST)	Delayed by	Actual liftoff time (IST)
PSLV-C18/ Megatropiques-1	12 Oct 2011, 11:00:00	1 min	12 Oct 2011, 11:01:00
PSLV-C21/SPOT-6	06 Sep 2012, 09:00:00	2 min	06 Sep 2012, 09:02:00
PSLV-C20/SARAL	25 Feb 2013, 18:00:00	5 min	25 Feb 2013, 18:05:00
PSLV-C23/SPOT-7	30 Jun 2014, 09:49:00	3 min	30 Jun 2014, 09:52:00
PSLV-C32/ IRNSS-1F	10 Mar 2016, 16:00:00	1 min	10 Mar 2016, 16:01:00
PSLV-C36/ Resourcesat-2A	07 Dec 2016, 10:24:00	1 min	07 Dec 2016, 10:25:00
PSLV-C39/ IRNSS-1H	31 Aug 2017, 18:59:00	1 min	31 Aug 2017, 19:00:00
PSLV-C40/ Cartosat-2F	12 Jan 2018, 09:28:00	1 min	12 Jan 2018, 09:29:00
PSLV-C42/ Novasar S1-4	16 Sep 2018, 22:07:00	1 min	16 Sep 2018, 22:08:00
PSLV-C43/Hysis	29 Nov 2018, 09:47:00	30 sec	29 Nov 2018, 09:47:30
PSLV-C53/DS-EO	30 Jun 2022, 18:00:00	2 min	30 Jun 2022, 18:02:00
PSLV-C55/ TelEOS-2	22 Apr 2023, 14:19:00	1 min	22 Apr 2023, 14:20:00
LVM3-M4/ Chandrayaan-3	14 Jul 2023, 14:35:13	4 sec	14 Jul 2023, 14:35:17
PSLV-C56/ DS-SAR	30 Jul 2023, 06:30:00	1 min	30 Jul 2023, 06:31:00

A typical case of lift-off time modification for PSLV-C53/DS-EO is explained below.

The nominal lift-off of PSLV-C53 was delayed by 2 minutes based on the COLA analysis due to potentially close conjunctions within 5 km with COSMOS 2251 debris (NORAD id 35891), ICEYE-X6 satellite (NORAD id 46497) and a few Starlink satellites (namely Starlink-3787 with NORAD id 52277, Starlink-2701 with NORAD id 48656, and Starlink-2090 with NORAD id 47677) during the ascent phase of the launch vehicle and the initial orbital phase of the passenger satellites. The requisite coordination was also carried out with the operators of the operational satellites for the safety of spaceflight.

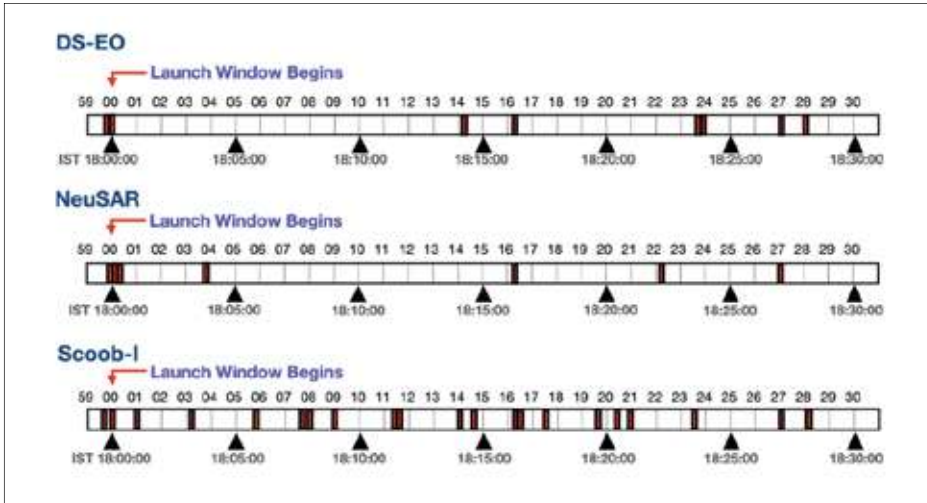


Figure 1.8: Black out zones within launch window

The figure shows the “black-out” zones within the launch window, over which the lift-off timings were prohibited for the PSLV-C53 launch to avoid close approach risk with other space objects.

1.10 Passivation

Passivation or removal of active energy sources is carried out at end-of-life for a spacecraft or launch vehicle to prevent post-mission break-up. Some of the effective passivation measures include the expulsion of residual propellants by burning or venting, the discharge of batteries, the release of pressurized fluids, safing of unused destruct devices, etc.

Subsequent to the breakup of PSLV-C3 upper stage on 19th December 2001, passivation has been a standard practice for all ISRO launch vehicles since 2002 (Prasad, 2005). PSLV’s final stage with Earth-storable liquid propellants and the cryogenic upper stage of GSLV with LH2 and LOX as propellants are passivated. Methods for safe depletion of all residual energy sources in the spent stage are studied in detail and force-time profiles with bounds considering dispersion in all the relevant parameters are defined for carrying out separation dynamics.



Figure 1.9: Oppositely oriented nozzle configuration ensures equal thrust in opposite direction and no orbital change

For spacecraft, strategy is implemented on a case-by-case basis based on the energy sources but techniques like the discharge of batteries, the release of pressurized fluids, the safing of unused destruct devices, etc. are usually implemented. Usually, any residual propellant is depleted to lower the orbit for LEO satellites to reduce its orbital life. ISRO's communication satellites in Geo-synchronous orbit (GSO) are designed with adequate propellant margins for re-orbiting to a higher orbit at the end of their useful life. After re-orbiting the residual propellant is passivated through depletion (by inclination change manoeuvre) and venting.

Electrical passivation includes the discharge of batteries and their disconnection from the solar array (for GEO), placing solar arrays in orthogonal configuration to minimise projected area (and hence, power generation and solar radiation pressure induced perturbations), momentum/reaction wheel spin down and switch off, turning off magnetic torquers and gyros, and other electronics. Finally, all RF transmitters are turned off to avoid any interference.

1.11 Minimization of GTO Lifetime

The geostationary transfer orbit (GTO) is a highly eccentric orbit with the perigee normally at low altitudes (170 to 800 km) and the apogee near the geostationary altitude of around 36000 km. The evolution of objects in GTO orbits is determined by a complex interplay of atmospheric drag and luni-solar gravity and such orbits are characterized by periodic changes in perigee altitudes. The initial orientation of

the orbit just after the launch with respect to the Sun and the Moon predominantly determines the subsequent orbital evolution. As a result, the lifetime of a GTO object can vary from a few months to several decades, depending on the time of its launch. Unfortunately, one cannot always use this natural phenomenon to limit the orbital lifetime, as the launch time of a geostationary satellite is dictated by many other factors like thermal aspects and eclipse time related to the spacecraft design. Nevertheless, the lifetime in GTO can be significantly reduced (Adimurthy, 2001) through appropriate choice of the initial perigee altitude and launch time.

1.12 Post Mission Disposal

PMD is one of the most important mitigation measures to limit the growth of space debris as it plays a vital role in decongesting operational orbits, critical for sustainable space operations. LEO satellites are required to be de-orbited after completion of their mission to comply with the 25-year rule. A direct re-entry from LEO orbit is an ideal but fuel-intensive disposal strategy. In case of a controlled re-entry, the air traffic and maritime traffic authorities are informed about the re-entry time, trajectory and the associated ground area. IADC recommends that the satellites in GEO orbits are manoeuvred away from the GEO belt to ensure that they do not interfere with other satellites in the geostationary orbit. The spacecraft is placed in an orbit that remains above the GEO protected region for at least 100 years. The fuel is completely depleted and all energy sources are “passivated” after de-orbiting/re-orbiting to minimise the possibility of post-mission breakup.

1.12.1 Post Mission Disposal in LEO regime

In order to limit post-mission long-term presence in the LEO regime, ISRO's LEO satellites are de-orbited at their end-of-life satisfying the UN/IADC guideline to the maximum possible extent. ISTRAC is responsible for operating and maintaining the mission defined orbits for LEO satellites. The technical requirements can be summarised as below:

- a. Controlled re-entry to uninhabited regions is preferred. If not possible, the satellite must be removed from the LEO region no more than 25 years after the end of mission operations. This is done by lowering the altitude. An increased drag in the lower orbit causes faster decay in the orbit's altitude and results in natural uncontrolled re-entry of the satellite.
- b. Fluidic passivation is done by expending fuel usually by executing orbit manoeuvres. Electrical passivation is done by switching off systems like reaction wheels and telemetry transmitters followed by disconnecting batteries.

Cartosat-2 post mission disposal

Cartosat-2 was launched on 10th January 2007 by PSLV-C7 into a sun-synchronous orbit of 635 km altitude and 09:30 AM local time. The planned life of the satellite was 5 years, but the payloads were operated till August 2019. The post-mission lifetime at the 630 km altitude of Cartosat-2 was estimated to be about 30 years, which was not compliant with the 25-year limit on post-mission lifetime of LEO objects, as prescribed by IADC. The satellite had about 25 kg of leftover fuel (monopropellant – hydrazine). This along with the internal energy sources like batteries added to the potential of accidental explosion and breakup.

It was decided to de-orbit Cartosat-2 to be compliant with the IADC guidelines on post-mission disposal of LEO satellites. Although de-orbiting the perigee to 600 km altitude would have been sufficient to meet the IADC post-mission 25-year rule, de-orbiting till fuel depletion was recommended to minimise the chances of accidental breakup due to left-over propellant.

Two options were considered. The first option was to expend the entire fuel for perigee reduction. Assuming no contingency, this option would result in an orbit of 630 x 380 km; this orbit would have a lifetime of less than 5 years. The second option was to de-boost to a lower circular orbit of altitude 505 km, this option was not selected because the satellite could end up orbiting near an operational constellation like Starlink if an unforeseen unrecoverable anomaly occurred during the de-boost stage. A lower circular orbit also had a longer orbital lifetime compared to the first option.

The de-boost delta-v was planned to be delivered over multiple orbit manoeuvres because there was a limitation on the maximum burn duration. Each manoeuvre was screened for post-manoevrue conjunctions for the next 7 days. Post-manoevrue orbit determination was performed at the earliest opportunity using the on-board GPS measurements. The post-OM orbit was used to evaluate the performance of each manoeuvre. The predicted trajectory was used for satellite look-angle generation till the GPS measurement-based orbit was available.

The 1st manoeuvre was executed on March 6th, 2020. Till March 20th, 2020 five manoeuvres were carried out. The next 21 de-orbit manoeuvres were done during the period from May 19th 2020 to September 3rd, 2020. The perigee by this time was about 390 km and about 3 kg of fuel was left. The satellite at this stage was used for a few exercises related to spacecraft automation. Then it was decided to lower the perigee by expending all remaining fuel, this was done to rule out the possibility of frequent conjunctions with ISS. In all 30 de-orbit manoeuvres, 23 kg of fuel was expended to deliver a cumulative delta-v of 69 m/s. The final orbit achieved was

621 km x 380 m (Agarwal, 2022). The satellite is expected to re-enter the atmosphere around January 2024.

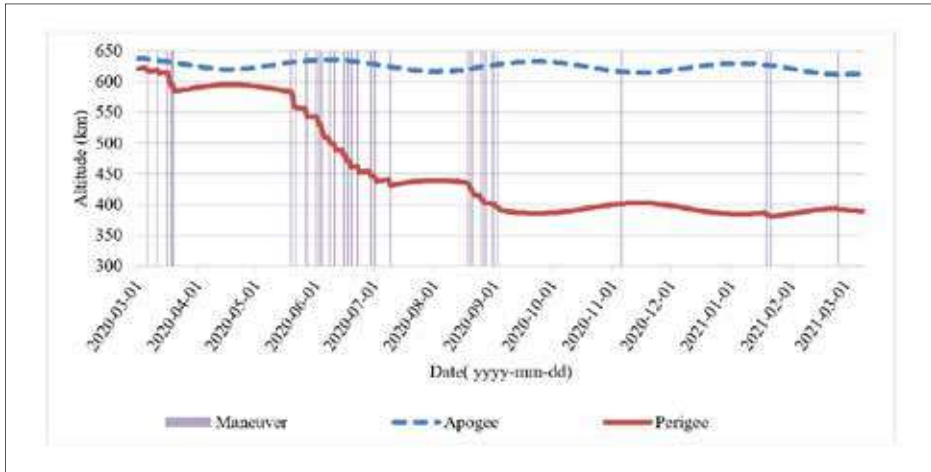


Figure 1.10: Cartosat-2 de-orbiting at end-of-life

Controlled re-entry: Post Mission Disposal of Megha-Tropiques-1

Megha-Tropiques was an Indo-French joint satellite mission launched by PSLV-C18 on October 12, 2011, in a 20° inclined orbit at 867 km altitude. The lift-off mass of the satellite was 1000 kg which included 120 kg fuel. The mission design life was 3 years, the satellite continued to provide valuable services for more than a decade. The post-mission orbital lifetime of Megha-Tropiques would be more than 100 years in its 867 km orbit. Also, the satellite had about 120 kg of propellant left which could lead to accidental breakup. UN/IADC guidelines for post-mission disposal of LEO spacecraft prefer a direct re-entry. The on-board fuel was sufficient for reducing the orbit by a series of manoeuvres causing it to re-enter in dense atmosphere and then de-busting it in the Pacific Ocean. The controlled re-entry experiment of Megha-Tropiques-1 (CREEM) began on August 10th, 2022 as a series of 19 perigee reduction manoeuvres. All manoeuvres were screened to ensure that there would be no post-manoeuvre close approaches with other space objects. The first 16 manoeuvres were completed by mid-November 2022. These resulted in perigee height reduction from 856 km to 269 km, and the apogee height reduced from 874 km to 846 km in this period. The last 3 manoeuvres were conducted from January 30, 2023, to February 25th, 2023. These short-duration manoeuvres were intended for compensating orbit decay and thrust re-calibration for the final de-boost. To ensure impact within the designated zone, the perigee needed to be over the Southern hemisphere which

imposed a constraint on the Argument of Perigee (AOP). A perigee raising manoeuvre (OM#17) was conducted to ensure that the satellite does not decay too fast before the favourable AOP conditions are met through orbital evolution. The final de-boost was planned on March 7th, 2023 and required about 30 kg of fuel and was split into two manoeuvres. After de-boost-1 execution at 11:02 UTC, the satellite's perigee altitude was reduced to 161 km. Deboost-2 was planned at 12:51 UTC and was designed to reduce the perigee altitude to below 80 km ensuring that the satellite enters into the deep atmosphere. During the 2nd de-boost manoeuvre telemetry from spacecraft was received till the perigee altitude of 116 km and indicated that the de-boost progressed nominally. From telemetry data analysis it was inferred that the satellite had re-entered over the deep Pacific Ocean as planned. Observations from USSPACECOM also confirmed the same (ISRO press release, 2023).

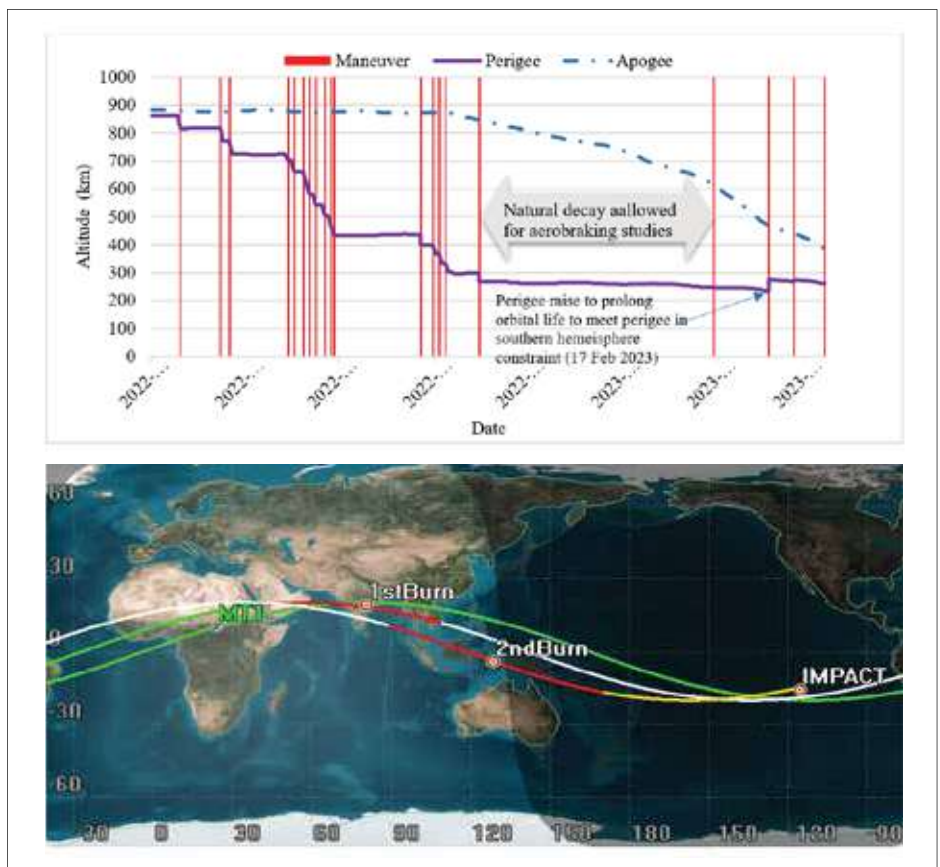


Figure 1.11: Re-entry Manoeuvres of Megha-Tropiques-1

1.12.2 Post Mission Disposal for GEO satellites

In order to limit post-mission long-term presence in the GEO regime, ISRO's GEO satellites are re-orbited to super-synchronous orbits at their end-of-life satisfying the IADC guideline to the maximum possible extent. Master Control Facility (MCF) is responsible for maintaining the in-orbit GEO satellites and also performs the post-mission disposal of GEO satellites. The execution involves close coordination with the neighbouring satellite operators and extensive planning for the migration of satellite services to other replacement satellites. In one of the earliest re-orbiting operations, INSAT-2C was re-orbited during June–July 2003, using only left-over vapour and the deorbiting operation was continued for 44 days. The first successful re-orbiting which was fully compliant with IADC guidelines was of INSAT-2DT during August 2004. In general, the first manoeuvre is planned to exit the collocated constellation (if applicable). Then alternating burns at apogee and perigee are executed to ensure that the intermediate orbits are circular. The manoeuvres are continued till the super GEO orbit is reached in compliance with IADC guidelines. After re-orbiting to disposal orbit, the final passivation burn to depletion is carried out by performing inclination change, instead of changing the semi-major axis by an in-plane manoeuvre to avoid any possible increase in eccentricity.

Post Mission Disposal of GSAT-12

GSAT-12 was launched on July 15, 2011. It carried 12 extended C band transponders and was located at 83° E longitude till March 2021. The satellite served for more than a decade before being replaced by CMS-01. Compliance with IADC guidelines required the perigee of GSAT-12 to be raised by at least 261 km. A series of 7 manoeuvres were conducted to raise the satellite's orbit to a super-synchronous orbit about 400 km above the GEO belt. The first burn was executed on March 16, 2023, to circularise the orbit. The next 6 manoeuvres were conducted 12 hours apart, alternately at the perigee and the apogee. Each burn increased the altitude by 116 km alternately at apogee and perigee as shown in Figure 1.12. The orbit raising was completed by March 19, 2023. Four inclination correction manoeuvres were then conducted to deplete the fuel without disturbing the eccentricity. The final passivation manoeuvre was aimed at venting the remaining fuel by firing the oppositely mounted thrusters, this strategy ensured that the achieved near-circular orbit was not disturbed. Finally, on March 23, 2023, all sources of energy were "passivated" and the transmitter was switched off to avoid RF interface with other active missions.

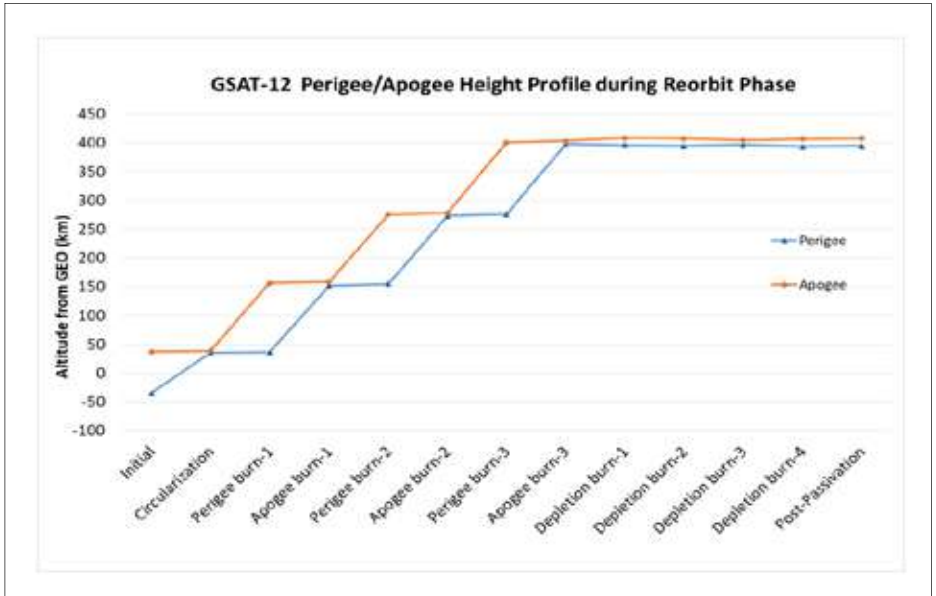


Figure 1.12: PMD of a typical GEO satellite

1.13

Summary of ISRO's efforts towards Space Debris Mitigation

Limit release of mission related objects	No operational debris during ascent phase, satellite orbital injection phase or satellite commissioning phase.
Minimize potential for break-ups during operational phases	All failure modes of systems are analysed to avoid any malfunctioning of propulsion systems and pyro systems during the operational phase
Collision avoidance	Regular conjunction analysis to avoid collision with LV and satellites
Minimize post mission break-up risk	Passivation of LV upper stages, GEO satellites at EOL
Avoid intentional destruction	None carried out by ISRO
Limit post mission life of GEO objects	For the last two decades, all GEO satellites undergo post mission disposal.

Limit post mission life of LEO objects	<ul style="list-style-type: none"> • All the GSLV rocket bodies lifetime < 25 years. • Cartosat-2 and Microsat-1 deorbited to minimize their post mission lifetime with passivation of fuel • Controlled re-entry of Meghatropiques-1 • Better compliance with PS4 re-start capability, de-orbited stages of PSLV-C38, PSLV-C40 re-entry within 1 year, PSLV-C56 de-boosted to 300 km, re-entry within 1 month
--	---

1.14 Atmospheric Re-entry Analysis

Accurate prediction of the re-entry time for uncontrolled space objects is challenging due to various factors influencing the atmospheric re-entry process. A numerical method is typically employed for the re-entry time prediction; it involves gathering data in terms of two-line element sets (TLEs) or state vectors (SV) from multiple sources and combining them using sophisticated algorithms, such as the Kalman filter, to improve the object's orbit estimation accuracy. Once an estimate of orbit is made, a high-fidelity orbit propagator which solves the governing differential equation of orbital motion in the presence of various perturbations is used to estimate the re-entry time and location. The ballistic coefficient, representing the ratio of the object's mass to its drag characteristics, is a crucial parameter in re-entry prediction. Estimating the ballistic coefficient for uncontrolled space objects is challenging due to their irregular shapes, unknown masses, and uncertain aerodynamic properties. Atmospheric models accounting for various factors such as solar activity and seasonal variations play a crucial role in orbit propagation as the drag experienced by an object depends on the density of the surrounding air.

Over the past couple of decades, ISRO developed several methodologies for re-entry time and impact location prediction of space objects making uncontrolled atmospheric re-entry. All these methods approach the re-entry prediction problem as an optimal initial parameter estimation problem, such as Constant Gain Kalman Filter Approach, KS Elements with Genetic Algorithm (KSGEN), Response Surface Methodology with Genetic Algorithm (RSMGA), STKOptim (Optimization using System Tool Kit), STKLTOptim(Life time optimization with System Tool Kit), ABPRO (Automated Back Propagation) (Dutt et al., 2023).

Recognizing the potential hazards posed by the uncontrolled re-entry of certain space objects, e.g., the Soviet Cosmos 954 spacecraft (January 1978), the U.S. Skylab space station (July 1979), and the Soviet Salyut 7- Cosmos 1686 space station (February 1991), some members of the IADC participated in an exchange of information during the final days of the orbital life of the Soviet Cosmos 398 spacecraft in December 1995. The success of this exercise led to the adoption by IADC to conduct at least one test campaign annually. The re-entry object for each test campaign is selected based on a common agreement of IADC members. Potential re-entry objects should be of sufficient size (> 1 sq. m.) and typically of sufficient inclination to be tracked by all IADC members. ISRO actively participated in these IADC re-entry exercises by developing prediction techniques and providing estimates of time of re-entry of the risk objects.

During re-entry into the Earth's atmosphere space debris may/may not completely burn and may pose ground casualty risk. Hence it is very essential to estimate the survival status of re-entering objects/spent stages and risk assessment. ISRO has also developed in-house methodologies for aerothermal break-up and survivability analysis. The basic inputs are the object's re-entry trajectory, structural components, and atmospheric model. These are used in the computation of the heat flux, evaluation of thermal response and finding break-up altitudes of various components for determining debris footprint.

1.15 Shielding

A collision is called catastrophic when an object completely disintegrates due to the collision. When a 1 mm debris hits an operational spacecraft, the impact may not be catastrophic but the impact can perforate the fuel tanks, and cause problems to batteries or other critical components which may lead to a premature termination of the mission life. In such a case we need to properly protect the asset from such small debris. We need to employ techniques like active and passive protection. Active protection uses sensors to provide a warning of impact and then protect its critical components or flag a signal to move the spacecraft to avoid the potential impact. A passive protection schemes like shielding of a spacecraft or its critical components can help safeguard a space asset against small uncatalogued objects.

ISRO has also undertaken activities related to shielding to protect against micrometeoroids and orbital debris risk. For the upcoming missions like Gaganyaan and NISAR, Probability of No Penetration (PNP) estimation and debris shield design for all regions to meet PNP specifications. Ballistic Limit Equations (BLE) available in literature are used for shield design and validated through Hydrocode simulations. Further validation through Hypervelocity impact tests is also planned.

1.16 Space Debris Observation

Measurements of space objects include the identification and characterization of the space object. Measurements are done with the help of ground-based radars and telescopes. Ground-based radars are well suited to observe space objects in LEO because of all-weather day-night observation capability. Radar power budget and operating wavelength are the limiting factors for the detection of small objects at long ranges. Optical facilities can detect debris when it is sunlit and the background sky is dark. For objects in geosynchronous orbit, optical observations can be continued during the entire night except during dawn and dusk. Debris tracking capabilities of optical telescopes in the LEO region are limited to one to two hours a day during the twilight due to availability of sunlight for illuminating the object. Higher angular rate of LEO objects results in faster transit of objects which also limits the duration of observation.

ISRO has undertaken project NETRA (NEtwork for space objects TRacking and Analysis) to establish independent end-to-end capability to detect, identify, track, and catalogue space objects, including spaced debris to safeguard national space assets. The main three elements of the project are: one phased-array, multi-object tracking Radar to be located at Chandrapur, Assam; one optical telescope capable of tracking a 40 cm object in geostationary orbit, being established at Hanle, Ladakh; and a Control Centre, which is operational at Bengaluru, Karnataka to function as a hub of all SSA related activities, including observational data processing, object identification and cataloguing. The expansion of the observational network is also envisaged by adding more telescopes and radars.

1.17 Debris Environmental Modelling

Objects less than 10 cm are difficult to track individually; hence a statistical estimation is made of the population density based on measurements. These density models are generated over the years with cumulative measurements. The centimetre sized objects are derived from the dedicated radar campaign. The encountered sub-millimetre debris population are inferred from the analysis of retrieved surfaces and in-situ impact sensors. The population is also characterized based on the ground-based simulations of hypervelocity collisions with satellite and rocket bodies, and ground-based simulations of explosive fragmentations. These data generated from experiments and campaigns are used for validation and improvement of the debris flux models which can be deterministic or statistical in type or a combination. Such models are useful in risk and damage assessment, prediction of debris detection rates for measurements, collision avoidance measures, and in the analysis of the

effectiveness of debris mitigation measures. A number of source mechanisms are considered, which include launches, break-ups produced by explosions and collisions, material separation due to aging, solid motor firing manoeuvres etc. Sink mechanisms include orbital decay due to atmospheric drag and other perturbations, retrieval from orbits and deorbiting etc. The episodic variations of the dynamic small debris population are captured through short-term and long-term models. A short-term model is an engineering model that enables the mission to assess the operational risks to be faced. NASA's Orbital Debris Environment Model (ORDEM)[4] and ESA's Meteoroid and Space Debris Terrestrial Environment Reference (MASTER) are examples of the short-term debris environment model. The long-term models are evolutionary models which are used to get better insight into future evolution, and thereby devise effective remediation measures. NASA's LEO-to-GEO Environment Debris Model (LEGEND), and JAXA-Kyushu University's LEO Near Earth Orbital Debris Environment Evolution Model (NEODEEM) are examples of long-term debris environment models. Other models like IDES from United Kingdom, NAZARENKO developed in Russia, Equivalent break-up model SIMPLE (Stochastic IMPressionistic Low Earth) developed in ISRO/India (Anilkumar, 2006) are also used.

1.18 Areas of Further Research

The area of space debris provides an ample scope for further technical research in the areas of shielding, active collision avoidance, debris removal, LEO end-of-life disposition, passivation, re-entry disposal etc. In shielding, experimental studies on hypervelocity impact, materials research for bumper design, theoretical and numerical studies of the impact are the important topics for investigation. Theoretical models and engineering analyses for cost-effective passivation methods is of great technological significance. Statistical risk analysis models for fragmentation and re-entry risks need to be improved. Studies on thermal degradation of spacecraft and material survival during re-entry are needed to make more precise prediction and evaluation of re-entry risk. Active debris removal methods are to be further investigated. Space debris removal with tethers is an interesting concept that needs further engineering feasibility studies. Destruction by laser or use of laser to accelerate the orbital decay may be useful, but must be performed so that it does not create additional objects. Debris catchers or sweepers may be feasible if discrimination or avoidance between debris and useful spacecraft can be realized. The aerospace community is working to illustrate the effectiveness and cost of typical mitigation scenarios. Long-term environment models are useful in such work. Focussed efforts are also required to devise methods for measuring and estimating existing space debris particularly in the sub-centimetre sizes. Finally, the proliferation of multiple large constellations of satellites, each comprising more than hundreds and thousands of satellites will pose serious challenges due to the sheer number of

objects and the consequent congestion. Novel technological solutions need to be sought in order to make space-based activities sustainable.

The organisation of the rest of the book is as follows:

Chapter 2 deals with space debris environment and its sources. It includes modelling of orbital breakup in space and an IADC comparison study on stability of the future LEO environment.

Chapter 3 deals with simulations of some on-orbit explosions and orbital break-ups. Simulation of some historical on-orbit breakups using new models is studied.

Chapter 4 deals with orbit propagation numerically, semi-analytically and analytically for short- and long-term orbits using different perturbing forces. KS (Kushaanheimo and Stiefel) and uniformly regularly KS elements are used in some of the studies. Orbital evolution studies of some catalogued fragments are also done.

In Chapter 5, modelling of the space debris environment is discussed. It includes a new Stochastic Impressionistic Low Earth (SIMPLE) model of the space debris scenario. A characterisation of eccentricity and ballistic coefficient of space debris in altitude and perigee bins is made.

Chapter 6 concerns with conjunction analysis and modelling. Space debris proximity analysis in powered and orbital phases during satellite launch is discussed. Statistical conjunction analysis and modelling of low-earth orbit catalogued objects is studied. Wavelets are also used for doing this analysis. Modelling of Sunspot cycle is done with different techniques.

Chapter 7 deals with space debris mitigation and risk estimation in India. Estimation of on-ground risk due to uncontrolled re-entries from eccentric orbits is studied.

Re-entry prediction studies of IADC re-entry test campaigns and other risk objects in GTO are presented in Chapter 8. Different techniques including genetic algorithm, response surface technique and Kalman filter are used.

Chapter 9 presents the challenges and future directions to cope with the space debris issues.



SDSSARS IN ISRO

Space Debris and Space Situational
Awareness Research Studies



CHAPTER 2

Space Debris Environment and its Sources

2.1 Debris Environmental Modelling

Space debris is any object orbiting Earth but is no longer functional. This can be as large as a discarded rocket stage or as small as a microscopic chip of paint. Much of the debris is in low Earth orbit (LEO) within 2,000 km of Earth's surface, some are in medium Earth orbit (MEO) between 2000 and 35786 km, and some debris are found around the geostationary orbit 35786 km (https://en.wikipedia.org/wiki/Main_Page).

As of 2023, the United States Space Surveillance Network was tracking more than 26,000 pieces of space debris larger than 10 cm sized. According to the United States Space Surveillance Network, there are about 200,000 pieces of space debris between 1 and 10 cm sized. There are also millions of pieces smaller than 1 cm. Objects below 600 km orbit take around 25 years or less before re-entering Earth's atmosphere. Objects above 1,000 km will orbit for centuries. Because of the high speeds at which objects orbit Earth (up to 7.5 km per second), a collision with even a small piece of space debris can damage a spacecraft depending on the direction of velocity vector with relative velocity more than 10 km per second. For example, space shuttle windows often had to be replaced because of damage from collisions with debris smaller than 1 mm (<https://www.britannica.com/explore/space/space-debris/>).

The amount of debris in space threatens both crewed and uncrewed spaceflight. The risk of a catastrophic collision of a space shuttle with a piece of space debris was 1 in 300. (For missions to the Hubble Space Telescope, with its higher and more debris-filled orbit, the risk was 1 in 185.) If there is a greater than 1-in-100,000 chance of a known piece of debris colliding with the International Space Station (ISS), the astronauts perform a debris avoidance manoeuvre in which the ISS's orbit is manoeuvred to avoid collision. On particularly dangerous occasions, such as in November 2021, when the ISS passed through the debris cloud from a Russian anti-satellite test, astronauts closed the station's hatches and shelter in their spacecraft.

In the first reported collision between an operational satellite and a piece of space debris on July 24, 1996, a fragment from the upper stage of a European Ariane rocket collided with Cerise, a French microsatellite. Cerise was damaged but continued to function.

The first collision that destroyed an operational satellite happened on February 10, 2009, when Iridium 33 S/C, a communications satellite owned by the American company Motorola, collided with Cosmos 2251, an inactive Russian military communications satellite, about 760 km above northern Siberia, shattering both satellites. (Gregersen, Erik. "space debris". Encyclopedia Britannica, 23 Sep. 2023, <https://www.britannica.com/technology/space-debris>. Accessed 23 October 2023.).

A very significant space-debris event happened on January 11, 2007 at an altitude of 865 km, when the Chinese military destroyed the Fengyun-1C weather satellite in a test of an anti-satellite system, creating more than 3,000 fragments at that altitude. Within two years those fragments had spread out from Fengyun-1C's original orbit to form a cloud of debris that completely encircled Earth and that would not re-enter the atmosphere for decades.

On January 22, 2013, the Russian laser-ranging satellite BLITS (Ball Lens in the Space) experienced a sudden change in its orbit and its spin, which caused scientists to abandon the mission. The culprit was believed to have been a collision with a piece of Fengyun-1C debris. Fragments from Fengyun-1C, Iridium 33, and Cosmos 2251 account for about one-half of all debris below 1,000 km at that time.

With the increasing amount of space debris and the advent of mega-constellations of thousands of satellites, there are fears that collisions such as that between Iridium 33 and Cosmos 2251 could set off a chain reaction (called the Kessler syndrome after American scientist Donald Kessler) in which the resulting space debris would destroy other satellites and so on, with low Earth orbit eventually becoming unusable. To forestall such a debris buildup, space agencies have begun taking steps to mitigate the problem, such as burning up all the fuel in a rocket stage so it does not explode later or saving enough fuel to deorbit a satellite at the end of its mission.

The British satellite RemoveDEBRIS, which was launched in 2018 and deployed from the ISS, tested two different technologies for removing space debris: capture with a net and capture with a harpoon. RemoveDEBRIS also attempted to test a dragsail to slow down the satellite so that it could reenter the atmosphere, but the sail failed to deploy. Satellites in geostationary orbit that are near the end of their missions are sometimes moved to a "graveyard" orbit 300 km higher, and in January 2022 the Chinese Shijian-21 satellite pulled the defunct Beidou-2 G2 far past the usual graveyard orbit to a new orbit 3,000 km higher than the belt of geostationary satellites (Gregersen, 2023).

2.2 Assemble Model from ISRO

Anil Kumar et al (2002) and Anil Kumar (2004) obtained the basic structure of the 'ASSEMBLE' model based on an analysis of the characteristics of the parameters of the fragments of the PSLV-TES Mission spent upper stage breakup on 19 December 2001 as given by the TLE set of the USSPACECOM catalogue. If one is able to utilize, as is done in this study, the orbital characteristics soon after the breakup, the velocity distribution of the fragments can be obtained more accurately and later derive their physical properties from the available empirical relations.

The INDIAN PSLV-TES Mission was launched on 22 October 2001, from the Sriharikota Range, presently the Satish Dhawan Space Centre (SDSC) of the Indian Space Research Organization (https://www.isro.gov.in/mission_PSLV_C3.html?timeline=timeline). After the successful completion of the satellite mission, the spent upper stage of PSLV was inserted in an orbit of nearly 675 km x 550 km at an inclination of 97.9 deg. The rocket body exploded on 19 December 2001 after which the fragments were tracked and catalogued in USSPACECOM TLE sets. The details of the breakup event were reported in Portman (2002).

International Designation	: 2001049
D USSPACECOM Number	: 26960
Name	: PSLV-TES R/B
Mass	: ~ 885 Kg
Breakup epoch and Location	: ~ 1140 UTC, 19 December 2001, ~ 250 S, 3400 E
Altitude	: ~ 670 km
Pre-event Orbit of PS4	: ~ 550 km x 675 km, 97.9 deg. (Incl.) (a = 6990.5 km, e = 0.0089)
Number of Large	: > 300 Catalogued Debris

The USSPACECOM catalogued TLEs for the 301 fragments of the explosion, were available on 20th January 2002. Based on the TLE data, it was possible to infer the kinematic orbital characteristics of the catalogued fragments. However, the other desirable fragmentation properties such as the mass and the characteristic area were not possible to obtain from the TLE data. The orbital decay of the debris fragments depended strongly on the ballistic coefficient. The damage from a collision depended on the mass 'm' of the fragments. The observable radar cross section of a fragment depended on its characteristic area A_{eff} or the diameter 'd'. These were strongly related to the actual physical mechanism and the intensity of the explosion or collision. The detailed breakup being unknown and random in order to estimate the above, use of one of the available empirical relations in the literature was required (Bandyopadhyay et al., 2004b; Anil Kumar et al., 2005a).

The Figure 2.1 provided the Gabbard diagram of the 301 fragments after nearly 30 days of breakup. The slight growth in the left arm of the Gabbard diagram was due to the decay of the orbits of the fragments during the 30 days. Utilizing suitable probability or cumulative distribution functions, the Figure 2.2 showed the Laplace distribution fit for apogee height, and lognormal fits for eccentricity and the ballistic parameter B values and Laplace fit for the inclination of the orbital fragments. The figure clearly brought out the validity of the basic structure of the above quantities proposed in evolving the 'ASSEMBLE' model by Anil Kumar et al. (2005b).

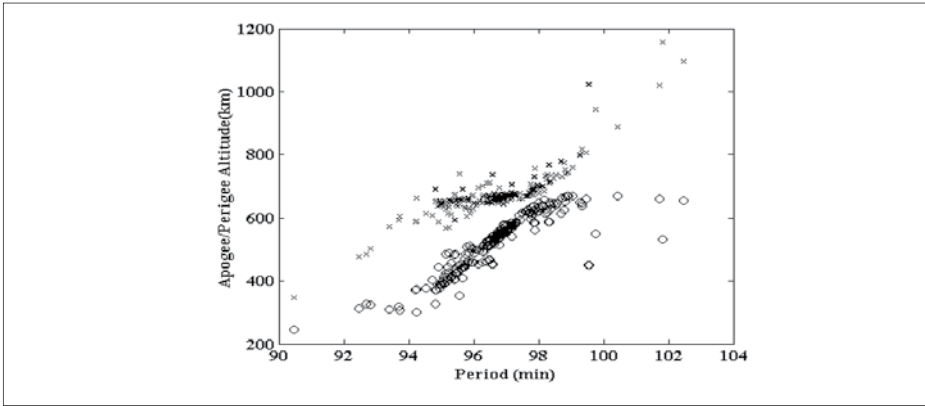


Figure 2.1: The Gabbard Diagram from the TLEs of PSLV-TES Spent Upper Stage Breakup Fragments after 31 Days of Breakup

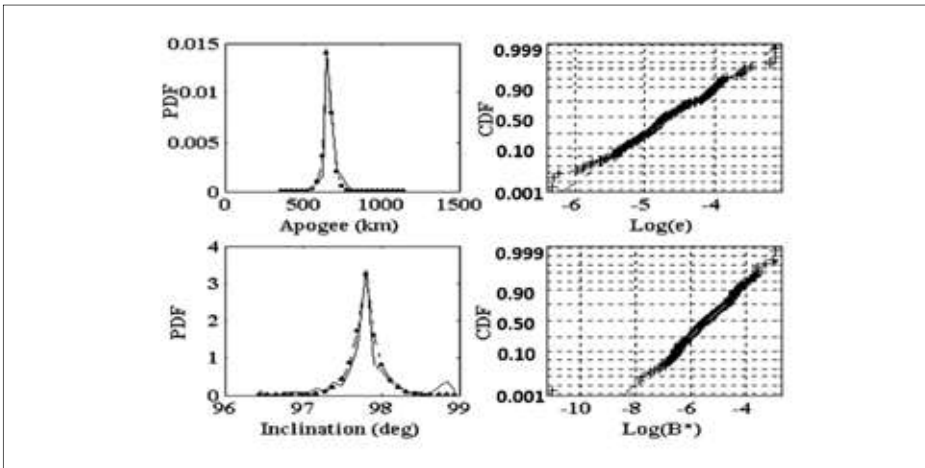


Figure 2.2: The Distribution of Apogee, Inclination, Eccentricity and B* from the TLEs of PSLV-TES Spent Upper Stage Breakup Fragments after 31 Days of Breakup

The delta velocities imparted to the fragments at the time of explosion were obtained from the relations taken from Culp and McKnight (1985):

$$\Delta V_i = [V_0^2 + V_i^2 - 2V_0V_i \cos(\theta_i) \cos(d_i)]^{1/2},$$

with the suffix 0 stands for the parent body and the suffix 'i' for the ith fragment,

V = the velocity, i = inclination and

f = true anomaly, $d_i = |i_0 - i_i|$

$\cos(\theta_i) = \sin(\phi_0) \sin(\phi_i) + \cos(\phi_0) \cos(\phi_i)$

$\phi_i = \tan^{-1}(e_i \tan(f_i) / \{1 + e_i \cos(f_i)\})$,

As the altitude of the parent body and the fragments at the instant of breakup is same, the true anomalies of the fragments and the parent body could be calculated utilizing the equation for radial distance

$$r = a(1 - e^2) / [1 + e \cos(f)],$$

where r is radius vector at the break up, valid for the fragments and parent body, a is semi major axis and e is eccentricity of the parent body or the fragments as the case might be.

The delta velocities estimated for each of these fragments ranged from 0.2 m/s to 400 m/s with an average of 52.5 m/s. The calculated components of the delta velocities, radial V_r , transversal V_t , and normal V_n , imparted to the fragments both in plane and out of plane were useful to obtain further knowledge about the process of explosion.

Since there was no data, it was very difficult to infer the mass of the debris fragments. It was compelling to depend on some empirical relations to arrive at the distribution of the mass of the fragments. The literature provides a large number of relations, which could be utilized for explosions (high intensity or low intensity) and collisions based on the explosion or collision experiments. The number and the mass distribution depend on the density and shape of the parent mass, the directionality, and the intensity of explosion or collision. Anil Kumar et al. (2002) utilized the rescaled relations given by Reynolds (1991) if the satellite mass differs considerably from 1000 kg:

$$171 \times \exp(-0.02056 m^{1/2} / fm), \quad \text{for } m > 1936 \text{ g} / fm$$

$$Nm = \{$$

$$869 \times \exp(-0.05756 m^{1/2} / fm), \quad \text{for } m < 1936 \text{ g} / fm$$

where

m = the mass of the fragments in grams,

M_t = the mass of the breakup object in grams,

N = cumulative number of fragments with mass m or greater,

f_m = the ratio of the reference mass of 1000 kg to the satellite mass M_t .

The above expression estimates the number of fragments created by the explosion of PSLV-TEJ as 868 with the mass ranging from nearly 56 kg to 2 grams, which accounts for a mass of about 840 kg. This means that for the largest 301 objects the cumulative sum of mass is 840 kg. These mass values have been scaled up to conserve the total initial object mass of 885 kg.

2.2.1 Life Time of Fragments

The approximate lifetimes of fragments was estimated by Anil Kumar et al. (2002) using the TLE data with the software "SatEvo". The study indicated that 204 objects decayed by the end of 2002 and about 25 will remain in orbit even after 1000 days.

Determination of the area to mass ratio Jehn (1996) provided a relation

$$m = 52.67 A_{\text{eff}}^{1.42},$$

where the coefficient and the exponent are related to the density of the breakup body material. In the present study the values are obtained from the B^* and a modified maximum likelihood estimation of the coefficient and the exponent in the above relation as

$$m = 46.62 A_{\text{eff}}^{1.22}.$$

2.2.2 Mass of the Debris Fragments and Their Imparted Delta Velocities

Associating mass to the debris objects is a difficult task. It is generally accepted that the mass of the object will have some kind of inverse relation to the size of the object, assuming uniform density of the material of the parent body. The debris sizes are related to the imparted delta velocities. A detailed literature survey brings out different forms involving diameter and delta velocities. It is reported in the literature that the delta velocities imparted to the fragment follow a triangular distribution (Jehn, 1996; Reynolds, 1990). In Anil Kumar et al. (2002), the delta velocities are associated with the size of the debris by using the relation given by Reynolds (1990):

$$\log(\Delta V) = -0.0676(\log d)^2 - 0.804(\log d) - 1.514,$$

where d is the size of the fragment in meters and ΔV in km/sec describes the peak in the velocity distribution curve. In order to provide the dispersion in ΔV , the velocity is picked randomly from a triangular distribution whose minimum is 0.1 times and maximum is 1.3 times, respectively, of the peak of ΔV . The intensity of explosion is calculated using the conservation of momentum:

$$M_t(V_0 + \Delta V_0) = \sum m_i(V_0 + \Delta V_i), \quad M_t = \sum m_i,$$

where M_t is the mass of the parent body, m_i is the mass of the i th fragment, V_0 is the velocity of the parent body just before explosion, ΔV_0 is the incremental velocity required for the parent body for such an explosion and ΔV_i the delta velocities to the i th fragment.

This new approach for the modelling of the breakup in low Earth orbits will be useful for any a priori assessment of intentional or unintentional breakups.

Anil Kumar et al. (2005) brought out the statistical nature of the characteristics of the tracked non-functional GEO (Geo-stationary Earth Orbit) debris objects and proposed a distribution model of the GEO environment by utilizing the approach of SIMPLE (Stochastic IMPressionistic Low Earth) Model used for LEO (Low Earth Orbits). It was noted that the catalogued objects around 800 across the years 1998 to 2004, had the same semi-major axis mode (highest number density) around 35750 km above the Earth. Just by properly excluding the objects in the small bin of operational region, say (35700, 35800) km containing about 40 percent of objects, the rest of the objects had a number density distribution of single Laplace distribution with two parameters, namely location and scale. It was further noticed that the percentage of objects in the bin around mode was nearly same across the years. The Laplace

parameters observed across the years could be modelled mathematically, in fact the location parameters did not vary and the scale parameters showed a definite trend. Those observations were successfully utilized in providing a statistical model for the GEO debris environment.

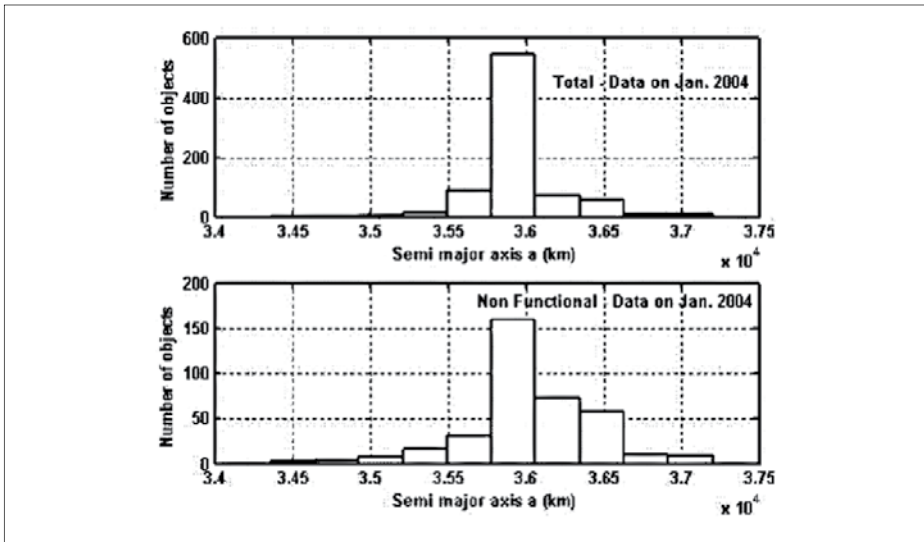


Figure 2.3: Histograms of the Semi-major Axis of the Catalogued GEO

Figure 2.3 provides the histograms of the semi-major axis of the catalogued objects for one set in the 2004. It may be noted that the first plot shows a very high peak at its modal value, in which the objects can be considered as those of the functional satellites. Second plot in Figure 2.3 is the frequency distribution of the non-functional objects after removing about 40 % of the functional objects. Studies indicated that the semi-major axis of these non-functional objects could be best fitted with the Tertiary mixture of Laplace distributions as used for the SIMPLE model for LEO (Ananthasayanam et al., 2002).

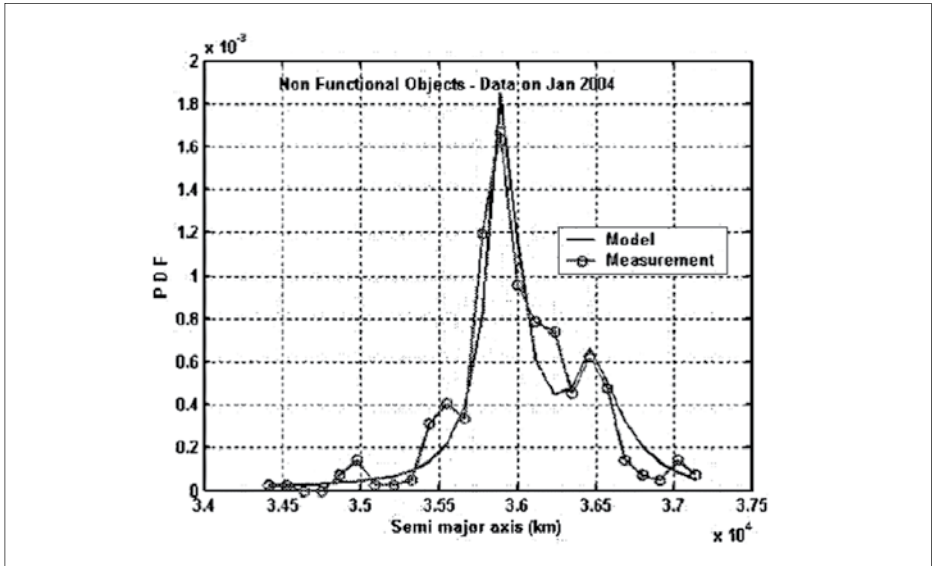


Figure 2.4: The distribution fit for the semi-major axis of the non-functional GEO objects using the tertiary mixture of the Laplace distributions for the year 2004

Figure 2.4 and Figure 2.5 provide the distribution fit for the semi-major axis of the non-functional GEO objects using the tertiary mixture of the Laplace distributions for the year 2004 and 2002. Table 2.1 provides the estimated distribution parameters for the semi-major axis for the years 2000 to 2004, quoted each for set of TLEs in January. It may be that these parameters do not vary significantly across the years, except for the first scale parameter. The weight parameters are selected as 0.3 and 0.5 after some sensitivity studies as they do not vary much across the TLE sets considered. It is seen that this parameter is not sensitive in the distribution fit. A model is proposed by estimating the parameters across the five years based on a least square technique, which is close to the average of the parameters across the years. Hence the values can be taken as $(\mu_1 \lambda_1 \mu_2 \lambda_2 \mu_3 \lambda_3 p_1 p_2) = (35500, 800, 36500, 250, 25900, 0.3, 0.5)$.

Table 2.1: Model parameters for number density of GEO objects in Semi-major axis μ -Location parameter, λ -Scale parameter, p -Weight parameter

Parameters of the Tertiary mixture of Laplace Distributions								
year	μ_1	λ_1	μ_2	λ_2	μ_3	λ_3	p_1	p_2
2000	35490	700	36450	244	35875	150	0.3	0.5
2001	35490	900	36400	242	35865	142	0.3	0.5
2002	35500	710	36420	253	35890	154	0.3	0.5
2003	35510	760	36510	247	35870	145	0.3	0.5
2004	35500	825	36500	255	35900	140	0.3	0.5

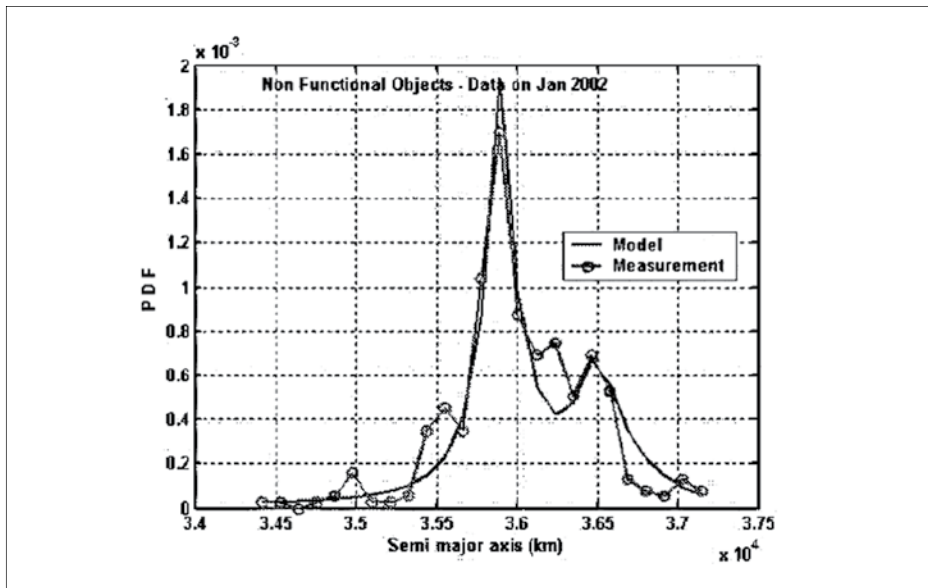


Figure 2.5: The distribution fit for the semi-major axis of the non-functional GEO objects using the tertiary mixture of the Laplace distributions for the Laplace distributions for the year 2002

Figure 2.6 provides a comparison between the model prediction and the measurement frequencies for all the five years from 2000 to 2004. It may be noted that the matching is quite good.

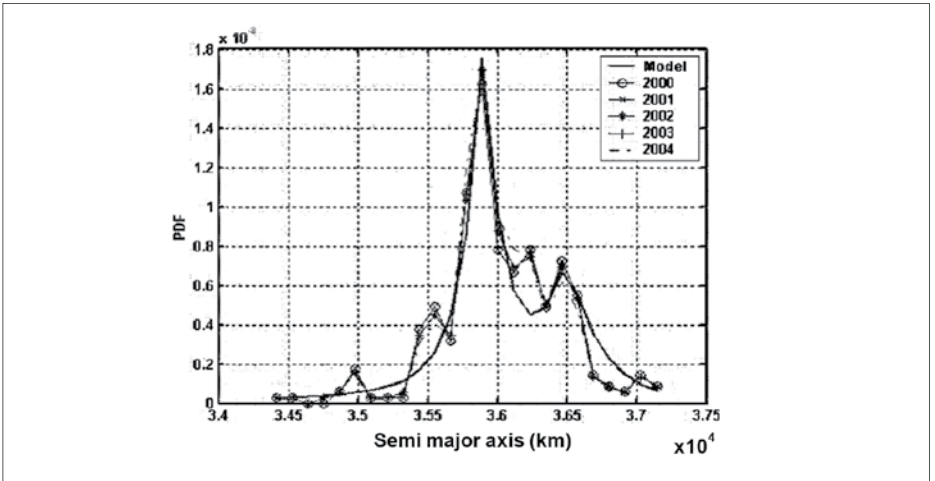


Figure 2.6: Comparison of SIMPLE model with observations for the year 2000 to 2004

2.2.3 Number Density Distribution with Respect to Eccentricity Delta Velocities

Figure 2.7 shows the eccentricity distributions of the total objects. The first of the two plots shows the eccentricity histogram and the second graph depicts the histogram of the logarithm of eccentricities. The second plot clearly shows that the log (eccentricity) can be best modeled with binary mixture of normal distributions and the same is shown in Fig. 2.8.

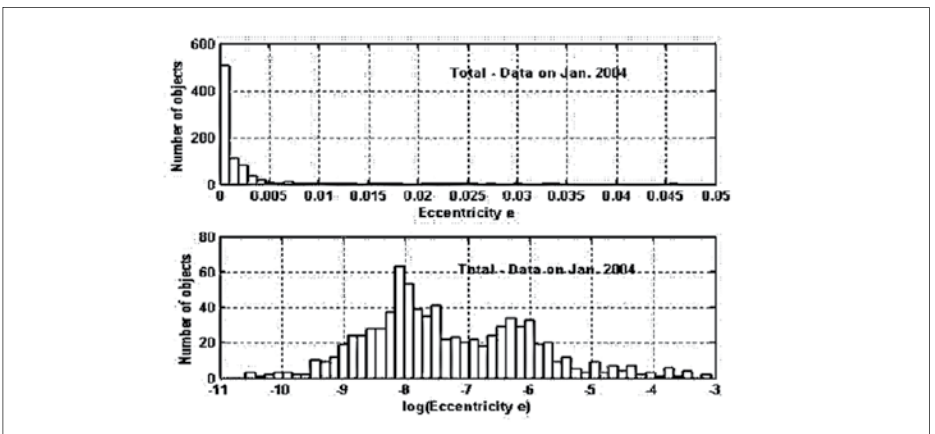


Figure 2.7: Histograms of the Eccentricity of the catalogued GEO Objects

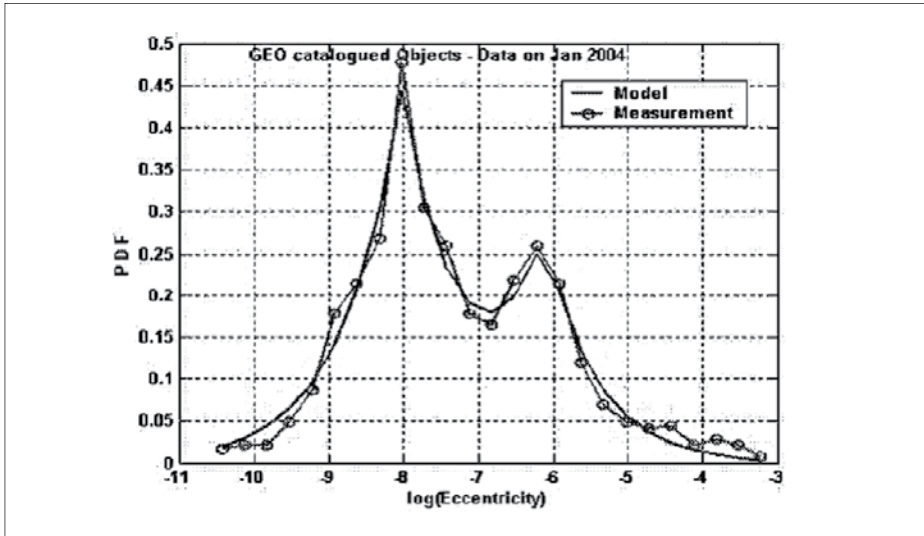


Figure 2.8: The binary mixture of normal distribution fit for Eccentricity of the non-functional objects

The distribution parameters for the eccentricity are provided in Table 2.2.

Table 2.2: Model parameters for number density of GEO objects in Eccentricity. μ -Location parameter, λ -Scale parameter, p -Weight parameter

Parameters of the Binary mixture of log Normal Distribution					
Year	μ_1	λ_1	μ_2	λ_2	p_1
2000	-7.89	0.93	-6.18	0.71	0.68
2001	-7.86	0.96	-6.23	0.72	0.66
2002	-7.95	0.95	-6.33	0.81	0.60
2003	7.94	0.92	-6.20	0.69	0.67
2004	8.01	0.89	-6.13	0.69	0.67

The parameters are not found varying much across the years. Based on the results of Table 2.2, the suggested model parameters are: $(\mu_1 \lambda_1 \mu_2 \lambda_2 p_1) = (-7.95 \ 0.95 \ -6.23 \ 0.75 \ 0.65)$.

2.2.4 Number Density Distribution with Respect to Inclination

It may be noted that the inclination of the functional satellites are nearly 0 deg. And the distribution of the inclination of the non-functional objects is shown in Figure 2.9. This shows the pattern of inclination distribution for a typical set of GEO debris objects for the year 2004. Similar pattern is observed in all other years. Uniform distribution is proposed for inclination as generalized assumption.

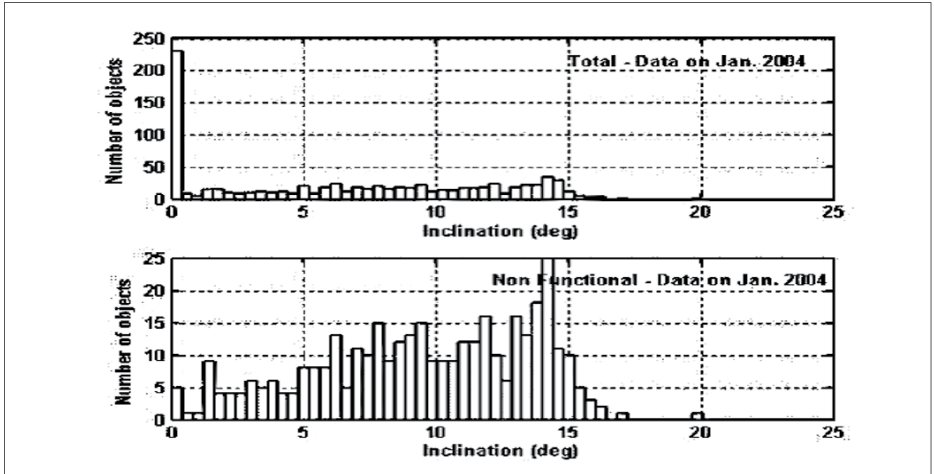


Figure 2.9: Histograms of the Inclinations of the catalogued GEO objects

2.3 Stability of the Future LEO Environment

Modeling studies of the orbital debris population in low Earth orbit had suggested that the environment has already reached the level of instability. Mitigation measures commonly adopted by the international space community, including those of the Inter-Agency Space Debris Coordination Committee (IADC) and the United Nations, might be insufficient to stop the future population growth. An official IADC modeling study was conducted to assess the stability of the current LEO debris population. Results from six different models were consistent - even with a 90% compliance of the commonly-adopted mitigation measures and no future explosion, the simulated LEO debris population increased by an average of approximately 30% in the next

200 years (Liou, Anil Kumar et al., 2013). Catastrophic collisions are expected to occur every 5 to 9 years. Remediation measures, such as active debris removal, should be considered to stabilize the future LEO environment.

2.3.1 A Model used by ISRO for Long-Term Orbit Computations

Long-term orbit computation with the in-house generated software “KSCPROP” was carried out for 200 years duration, revolution by revolution, using the non-singular, fourth-order analytical theory for the motion of near-Earth satellite orbits (Raj and Sharma, 2009). The air drag effects were computed in terms of uniformly regular Kustaanheimo and Stiefel (KS) canonical elements (Stiefel and Scheifele, 1971). A diurnally-varying oblate atmosphere with variation in density scale height dependent on altitude was considered. The theory was valid for orbits with eccentricities less than 0.2. Monthly predicted averaged values of F10.7 for 200 years were utilized. The secular effects of the Earth’s oblateness (J_2) in argument of perigee (ω), right ascension of ascending node (Ω), and long-term perturbations due to J_2 , J_3 , J_4 in eccentricity (e), were added after every revolution. Jacchia (1977) atmospheric density model was utilized to compute the values of the density and density scale height at perigee after every revolution.

Conjunction assessments were carried out by incorporating the apogee-perigee filter, geometric filter, and time filter, based on Hoots et al. (1984). The collisions between any two objects are simulated. The NASA Standard Breakup Model was used to find out the orbital characteristics of the collision fragments. Results of 17074 objects for 200 years were analyzed. Monte Carlo simulations were carried out by considering various parameter perturbations and also collision probability variations. The parameters considered in MC simulations were ballistic coefficient, F10.7 and A_p with three sigma dispersion = 10%, assuming Gaussian distribution. Other important parameters considered in MC were uncertainties in distribution parameters in breakup model, variations in size, mass, delta velocity of fragments. 40 MC runs were made using ISRO parallel computing facility available in Vikram Sarabhai Space Centre. The outputs monitored and analyzed through MC simulations were (1) number of objects decayed at the end of the each year and (2) the orbital parameters of the objects.

2.3.2 Solar Flux Projection Models

The solar flux projections used by participating agencies for the period from 2010 through 2060 are shown in Figure 2.10. There is reasonable correlation in terms of the magnitude and phase. The UK model was adopted by JAXA/KU's LEODEEM for the simulations.

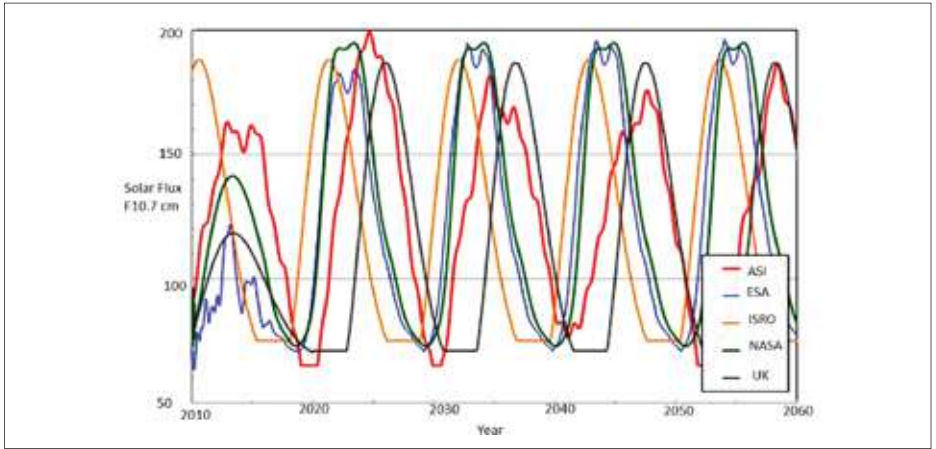


Figure 2.10: Solar flux projections used by participating agencies. Only the period from 2010 through 2060 is shown for clarity

2.3.3 Study Results

The study results are presented below. The number of MC simulations employed by each model to generate these results is shown in Tab. 2.3. The total MC runs of the six models is 725.

Table 2.3: Number of Monte Carlo (MC) simulations performed by participating models						
Agency	ASI	ESA	ISRO	JAXA	NASA	UKSA
Model	SDM	DELTA	KSCPROP	LEODEEM	LEGEND	DAMAGE
MC Runs	275	100	40	60	150	100
Runs	275	100	40	60	150	100

The projections of the total LEO population through the year 2209, assuming no future explosion and a 90% compliance of the commonly adopted mitigation measures, from the six models are summarized in Figure 2.11.

In all cases, the models predict a population growth. The average increase is 30% in 200 years. The short-term fluctuation, occurring on a timescale of approximately 11 years, is due to the solar flux cycle.

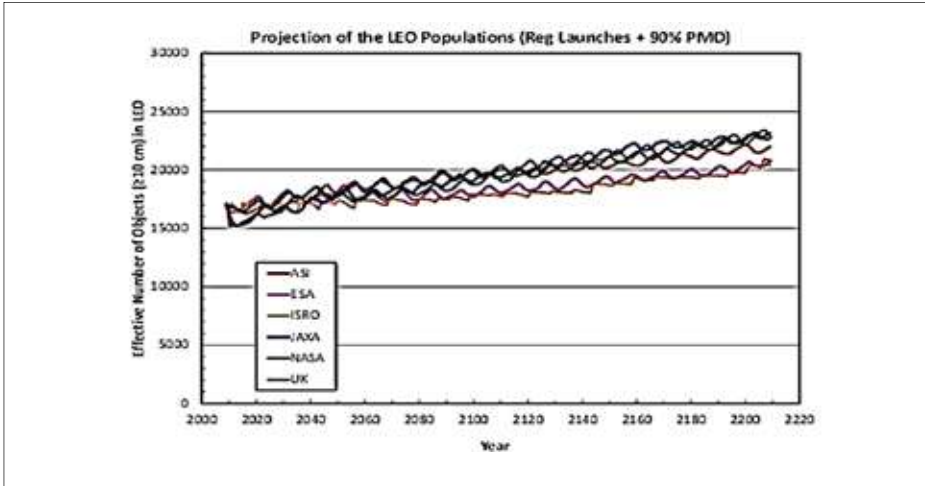


Figure 2.11: Effective numbers of objects 10 cm and larger in LEO predicted by the six different models. All models assumed no future explosion and 90% compliance of the commonly adopted mitigation measures

Figure 2.12 shows the cumulative number of catastrophic collisions occurring within the 200-year projection period. Catastrophic collisions, such as the one between Iridium 33 and Cosmos 2251 in 2009, result in the complete fragmentation of the objects involved and generate a significant amount of debris. They are the main driver for future population increase. The steepest curve (UKSA) represents a catastrophic collision frequency of one event every 5 years, whereas the shallowest curve (ISRO) represents a frequency of one event every 9 years. All model predictions for catastrophic collisions show a good fit with a straight line for the next 200 years (average correlation coefficient = 0.99). Catastrophic collisions occur primarily at altitudes of 700-800 km, 900-1000 km.

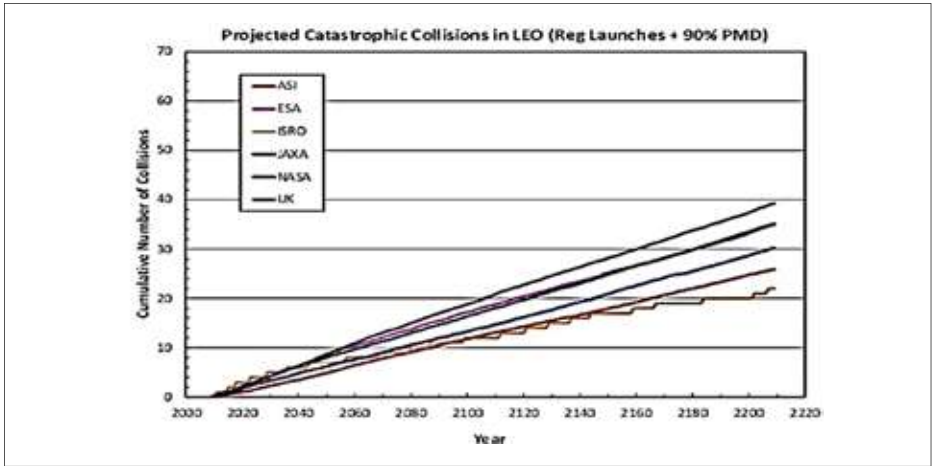


Figure 2.12: Cumulative numbers of catastrophic collisions predicted by the six models

The population increase at the end of the 200-year projection (the year 2209) predicted by the six models are shown in Figure 2.13. The initial environment (year 2009) is also included for comparison. The number of objects at any altitude, at a given point in time, is a balance between sources and sink. The former includes new launches, fragments generated from new collisions, and fragments decayed from higher altitudes (due to atmospheric drag) while the latter includes objects decayed toward lower altitudes (due to atmospheric drag). Overall, there is a general population increase above 800 km.

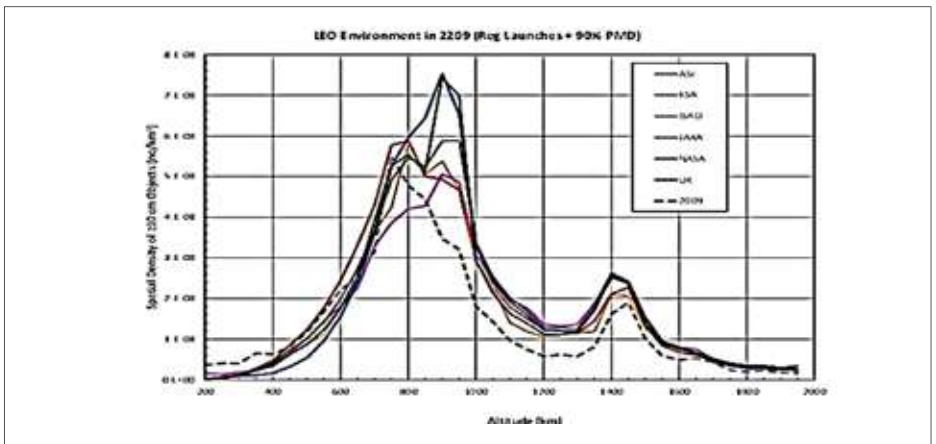


Figure 2.13: The initial (dashed curve) and projected LEO environment in year 2209

Table 2.4 provides additional details of the model predictions. Of the 725 MC simulations, 633 (87%) resulted in a net population increase in 200 years. The overall MC average is a 30% increase in 200 years.

Table 2.4: Summary of the projected LEO population increase based on regular launches and a 90% compliance of the commonly-adopted mitigation measures

Agency	ASI	ESA	ISRO	JAXA	NASA	UKSA	All
Model	SDM	DELTA	KSCPROP	LEODEEM	LEGEND	DAMAGE	–
MC Runs	275	100	40	60	150	100	725
% of MC runs with N2209>N2009	88% (242/ 275)	75% (75/ 100)	90% (36/ 40)	88% (53/ 60)	89% (133/ 150)	94% (94/ 100)	87% (633/ 725)
Average Change in Population by 2209	+29%	+22%	+19%	+36%	+33%	+33%	+30%

From the study it is shown that catastrophic collisions are expected to occur every 5 to 9 years. Remediation measures, such as active debris removal, should be considered to stabilize the future LEO environment.



SDSSARS IN ISRO

Space Debris and Space Situational
Awareness Research Studies



CHAPTER 3

On-Orbit Breakup and Environment Modelling

3.1 Introduction

Since the launch of first satellite in 1957, more than 560 spacecraft breakup events have occurred by 2021 (Ren et al. 2023). Two breakups occurred in 2022 (Cowardin and Johnson, March 2023). Three minor breakups occurred in first quarter of 2023. The debris from spacecraft breakup has accounted for more than 35% of all the catalogued debris (Cowardin and Johnson, June 2023). A satellite breakup is usually destructive disassociation of an orbital payload, rocket body, or structure with a wide range of ejecta velocities. A non-catastrophic collision only results in minor physical damage to the target. The impact can be the result of an intentional intercept with kinetic energy weapon or the result of a random collision with space debris. The explosion may be caused by abnormal residual propellant and battery, and the impact may also cause incidental internal explosion, which is essentially the combination of impact and explosion.

The impact of millimetre sized space debris can cause perforation on the satellite surface and cause some functions to fail, but the satellite may still retain its remaining functions and continue to work in orbit. Due to the low detectability of cm. sized space debris, it is difficult for satellites to manoeuvre in orbit to avoid its impact. Once the cm. sized space debris collides with the satellite, the huge kinetic energy can lead to the satellite breakup. In February 2009, the operational communication satellite Iridium 33 of the United States and the decommissioned communication satellite Cosmos 2251 of Russia collided at an altitude of 790 km with a relative velocity of more than 11 km/s, resulting in the breakup of both satellites. This event produced 1715 catalogued objects and countless small fragments that could not be catalogued and identified. 1021 are still in orbit till early 2023 (Cowardin and Johnson, March 2023).

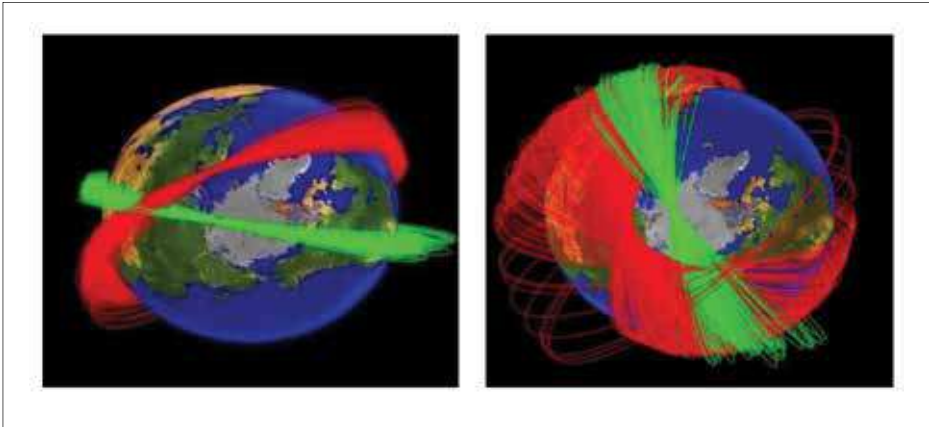


Figure 3.1: Predicted evolution of the Iridium and Cosmos debris planes 30 days and six months after the collision

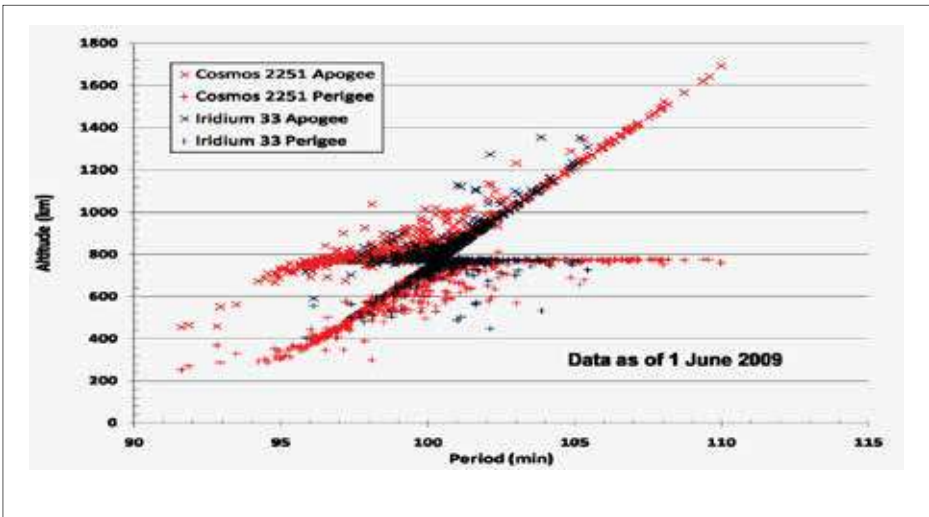


Figure 3.2: Cosmos 2251 debris (red) are more numerous and spread across a greater altitude regime than that of Iridium 33 (blue)

Due to the differential orbital periods of the debris, their orbital planes gradually separated and form a shell about the Earth. Figure 3.1 illustrates the predicted orbital planes 30 days and six months after the collision (Johnson, 2009). The debris from the Iridium 33 spacecraft spread more slowly than those from Cosmos 2251 due to their higher inclination. It may be noted from the same study, from Figure 3.2 that Cosmos 2251 debris (red) are more numerous and spread across a greater altitude regime

than that of Iridium 33 (blue). From preliminary assessments, the orbital lifetimes of many of the debris are likely to be in decades, posing future collision hazards to other satellites in LEO. The collision of Iridium 33 and Cosmos 2251 occurred in a region of relatively high spatial density, i.e., where collisions would be statistically more likely to occur. At the beginning of February 2009, the Iridium constellation itself consisted of 70 satellites in the operational altitude regime. The main body of each satellite is about 1 m x 4 m, plus two large solar arrays (1.3 m wide by 3.3 m long) and three communications antenna plates. Approximately 3300 additional catalogue objects were passing through the Iridium constellation operational band. Close approaches between these objects and Iridium spacecrafts were common occurrences.

On 11 January 2007, China conducted an anti-satellite missile test. A Chinese weather satellite in polar orbit satellite, at an altitude of 865 kilometres, with a mass of 750 kilograms was destroyed by a kinetic kill vehicle travelling with a speed of 8 km/s in the opposite direction. As of October 2016, a total of 3,438 pieces of debris had been detected, with 571 decayed and 2,867 still in orbit nine years after the incident (Kelso, 2016). On 27 March 2019, Defence Research and Development Organisation (DRDO), neutralised an Indian low Earth satellite in space with its anti-satellite (ASAT) missile. To minimize the creation of debris, the interception was done against an object moving at an altitude below 300 km. As of 26 September 2019, there were 50 tracked pieces of debris in orbit. By March 2022, only one catalogued piece of debris remained in orbit: COSPAR 2019-006DE, SATCAT 44383. This final piece also decayed on 14 June 2022 (<https://www.drdo.gov.in,mission-shakti>). Russia tested a direct-ascent anti-satellite missile on Nov. 15, 2021, that struck a Russian satellite. As of August 2022, there were 1,783 tracked objects. Of the tracked objects, 1,122 had decayed and were no longer in orbit, leaving 661 still in orbit (Foust, September 29, 2022).

Breakup can be caused by accidental explosion due to residual fuel and battery or deliberate explosion for the purpose of satellite self-destruction. On February 10, 2009, an active commercial satellite Iridium 33 and the deactivated Russian satellite Cosmos 2251 accidentally collided with a speed of 11.7 km/s at an altitude of 789 kilometres. It was the first time a hypervelocity collision occurred between two satellites. On February 3rd 2015, a Defence Meteorological Satellite of United States experienced a single breakup event resulting in the creation of a new debris cloud. The satellite was in a nearly circular orbit at an altitude of about 840 km and an inclination of 98.75° (Anz-Meador and Shoots, April 2015).

The debris generated by the breakup events have accounted for more than 35% of the total catalogued debris, which poses a serious threat to other spacecrafts. The studies for satellite breakup can evaluate the risk severity caused by the breakup event, input to the space environment model, provide impact early warning for spacecraft, and can be used as the basis for design of spacecraft protective structure.

3.2 Calculation of Fragment Velocity Additions of the Breakup of a Launch Vehicle Upper Stage

Bandyopadhyay et al. (2004b) used the method of estimating velocity-additions approach to analyse the breakup of the orbiting spent PS4 stage of PSLV-C3 which took place on 19th December 2001. Following this event, the Two Line Element (TLE) sets of more than 300 debris pieces from the upper stage were available in public domain by January 2002. These TLE sets were the major input used in the study. A lot of uncertainties were present in identifying the breakup location on the parent body. Parent true anomaly is not known accurately at the time of breakup. The TLEs of the fragments were not available for several days after the breakup. Hence, corrections were applied to the data for the change in the orbital elements during that time. By knowing the changes in the inclination and the right ascension of the ascending node, an estimate of the location of the breakup point on the parent orbit could be estimated. However, in reality, owing to inaccuracies inherent in the TLE sets of the fragments, the best way to utilize the relationship between them was to through a least square fit. For the PSLV-C3 breakup, the changes in the right ascension of the ascending node are plotted against the changes in the inclination to find out the slope through a least squares fit. The slope of the straight line is used to obtain the true anomaly of the parent at the point of breakup. The changes in inclination (Δi) and right ascension of ascending node ($\Delta \Omega$) are plotted in Figure 3.3 to obtain the slope.

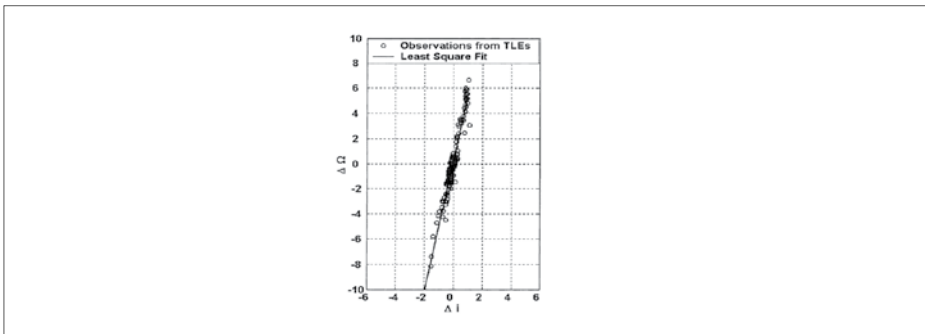


Figure 3.3: The relationship between changes in inclination and right ascension of ascending node

Once the true anomaly of the parent at the breakup is known, the method was applied to the orbital elements of the fragments. The scatter plots and histograms were shown in Figures 3.4 and 3.5, respectively. It was seen that the velocity changes were in general symmetric about zero. The method performed exceedingly well in estimating the velocity changes in the PSLV breakup event.

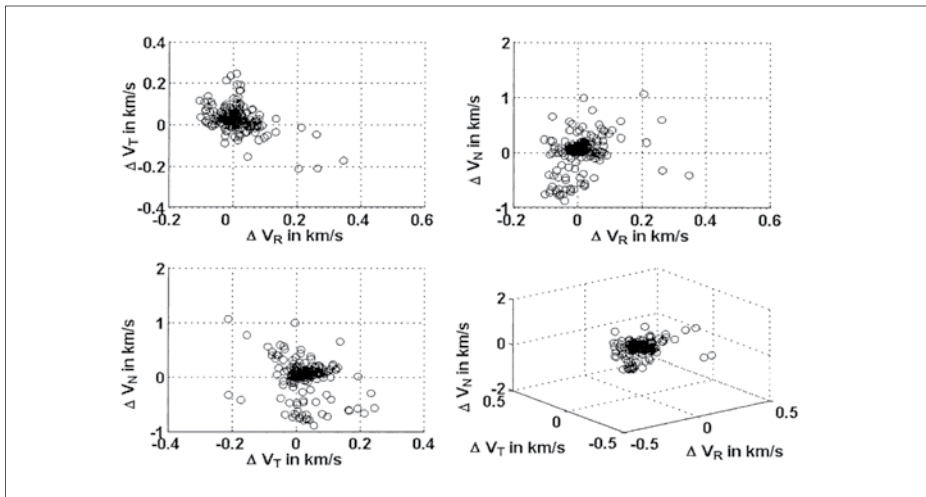


Figure 3.4: The scatter plot for velocity changes in PSLV-C3/PS4 fragmentation

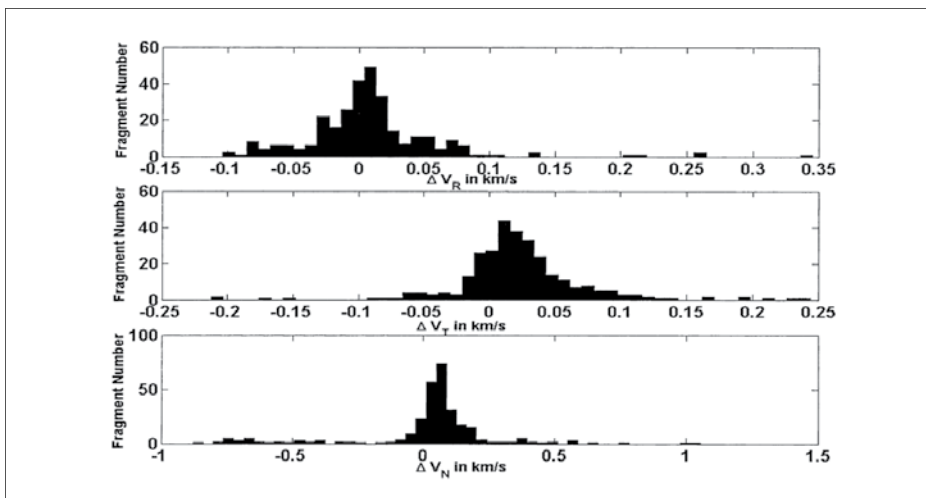


Figure 3.5: The histograms for velocity changes in PSLV-C3/PS4 fragmentation

A New Modeling Approach for Orbital Breakup in Space

Anil Kumar et al. (2002a) utilized the TLE data of the fragments of a breakup to obtain the orbital parameters consisting of apogee or perigee height, eccentricity and inclination in terms of suitable statistical distributions. These were found to be Laplace distributions for apogee or perigee height (bounded by breakup altitude) and inclination, and lognormal distribution for the eccentricity. The area-to-mass ratio corresponding to the ballistic coefficient could also be represented by a lognormal distribution. Further, in order to simulate the characteristics of any typical breakup, it could be modelled in terms of the probability distributions for orbital parameters namely apogee or perigee height, eccentricity and inclination. In order to specify the mass and effective area of the fragments, some of the available deterministic empirical relations could be utilized. The detailed procedure recommended in that approach called ASSEMBLE (A Semi Stochastic Environment Modeling of Breakup in LEO), was presented. The new approach for the modelling of the breakup in low earth orbits was useful for any a priori assessment of intentional or unintentional breakups. The model had been applied to simulate the Indian PSLV- TES Mission spent upper stage breakup on December 19, 2001. The analysis was carried out based on the TLE data of the debris fragments generated by the explosion as given by the web sites with epochs around January 20, 2002. The intensity of explosion, in terms of additional velocity requirement for such an explosion and the lifetime of the generated fragments were estimated.

Simulation of Some Historical On-Orbit Breakups Using ASSEMBLE Model

Anil Kumar et al. (2003a) utilized a new modelling approach for on-orbit breakup, named ASSEMBLE (A Semi Stochastic Environment Modeling of Breakup In LEO). Its genesis was on the hypothesis that the orbital parameters at the time of breakup were based on an analysis of the TLE data of some of the fragmentation events, obeyed certain statistical distributions. The apogee or perigee height and inclination could be described in terms of Laplace distributions and eccentricity by lognormal distribution. In order to expand the fragmentation scenario to mass, the effective area and the ballistic coefficient, some empirical relations available in the literature were utilized in ASSEMBLE. ASSEMBLE is described briefly followed by its application in simulating some of the historical breakups. In particular, the results of the simulations with respect to four major breakups, namely (1) SPOT 1 rocket body on 13 November 1986, (2) COSMOS 1813 on January 29 1987, (3) STEP II rocket body on June 3, 1996 and (4) CBERs I/ SAC I on March 11, 2000 were presented. All the simulated results with the studied breakups compared quite well with observations both at the time of breakup and at a later epoch.

Anil Kumar et al. (2005a) utilized a posterior modeling approach for on-orbit breakup, named ASSEMBLE (A Semi-Stochastic Environment Modeling of Breakup in LEO). This approach dealt with the on-orbit breakup of an object in space and was based on an analysis of the available catalogued data provided by US Space Surveillance Network (US SSN), of the fragments soon after the breakup. On-orbit breakups created many fragments and each had its orbital characteristics such as the semi-major axis, eccentricity, inclination, and other parameters such as size, shape, the ballistic coefficient, and so on. The catalogued data provided only the orbital characteristics of fragments besides a B^* term related to ballistic coefficient B with $B^* = (\rho/2) B$. The size and shape cannot be easily estimated on the basis of these characteristics and hence needed to be obtained from empirical relations based on some laboratory experiments. These relations provide estimates based on samples only and not those of the population. But all these variables characterizing the fragments are in some way connected due to the underlying physical process in an explosion and one cannot assign arbitrary random values for their various properties. The apogee and the eccentricity are related to radial and transverse components of the velocity, while the inclination and the right ascension of the ascending node are related to the normal component.

The basic procedure of ASSEMBLE can be summarized as:

1. The location parameters for apogee/perigee altitudes and inclination distributions, both of which follow generally a Laplace distribution, and the eccentricity which obeys a Lognormal distribution can be obtained from the breakup point details of the parent body. Next, based on the ranges of apogee/perigee heights and available maximum ΔP and Δi , one can obtain scale parameters related to Laplace and lognormal distributions. The number of fragments generated, namely N , and the mass of individual fragments can be obtained by using the number versus mass relationship or any other appropriate updates of relations for an explosion.
2. Generate N random sets of the apogee or perigee height, inclination and eccentricity combinations from the respective Laplace and Lognormal distributions, by restricting the apogee height or perigee height bounded by breakup altitude.
3. Using the above sampled values of the apogee/ perigee heights and eccentricity, calculate the true anomalies of each of the fragments at the breakup point.

- Obtain the velocity imparted to each of the fragments and assign the additional delta velocities to the masses (or area to mass ratio), based on triangular distribution constraint or any other method that was found suitable.

It was pointed out that the orbital parameters in Step 2 followed a joint distribution. Hence, while simulating them, the cross-coupling between the parameters could be taken into account. But the multiple correlations between those parameters are mostly unknown. However, the assumption of zero correlation if assumed, and each of the parameters independently simulated from the marginal distributions and randomly coupled, did not significantly alter the fit characteristics as an ensemble.

ASSEMBLE model was used to carry out the simulation of the breakups of PSLV-TES upper stage rocket body, STEP II rocket body, CBERS-I/SACI-1, COSMOS 1813 and SPOT I rocket body.

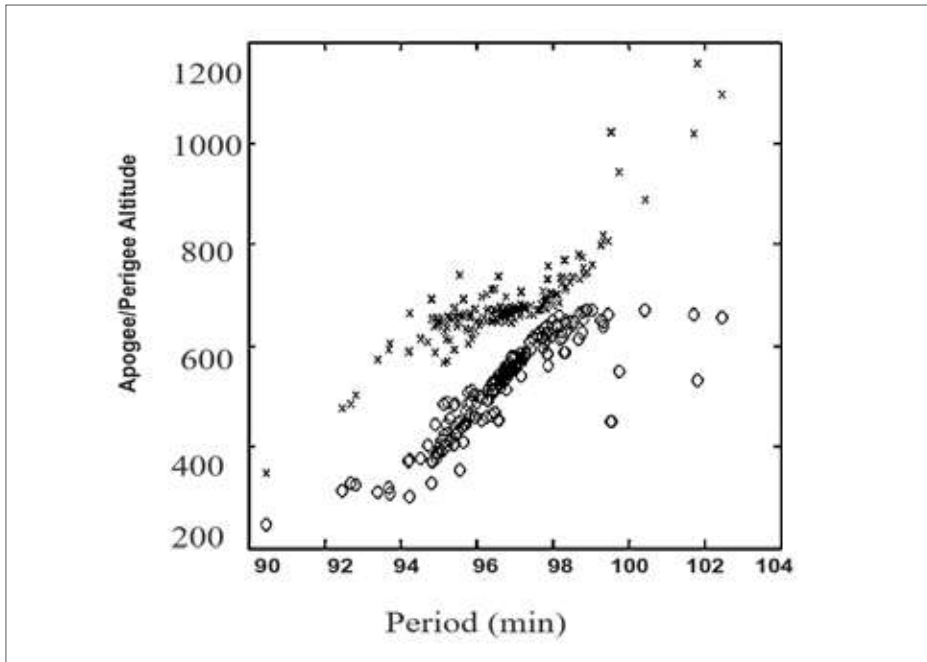


Figure 3.6: The Gabbard diagram from the TLEs of PSLV-TES spent upper stage breakup fragments after 31 days of breakup

Figure 3.6 provides the Gabbard diagram of the 301 fragments after nearly 30 days of breakup. The slight coalescence in the left arm of the Gabbard diagram is due to the decay of the orbits of the fragments in 30 days.

It is demonstrated that ASSEMBLE simulates the ensemble of fragment characteristics quite well and the incremental velocity distribution of the fragments is a consequence rather than imposed through empirical relations and the clouds remain around and much closer to the parent body than in earlier models.

3.6

A new stochastic impressionistic low Earth model of the space debris scenario

Ananthasayanam et al. (2006b) developed a new Stochastic IMPressionistic Low Earth (SIMPLE) model of the space debris environment using a stochastic approach. The approach and philosophy were similar to that utilized for evolving the international standard or other reference atmospheres. The model described the debris scenario up to an altitude of 2000 km and with eccentricity less than 0.2, covering about 75% of the large space debris objects catalogued in USSPACECOM two line elements (TLE) sets. Two types of models one called 'gross' provided insight into the physical process by characterizing the distribution of the number density 'n', eccentricity 'e', and the ballistic coefficient 'B' of objects over the whole of the LEO region for all inclinations put together as also separately. The other called 'local' model characterized the distribution of 'e' and 'B' of the debris across suitable local altitude and perigee bins useful for mission analysis and risk assessment for spacecraft designers interested in specific altitude or perigee height bins and inclination bands. The number density 'n' in all the gross models could be represented in terms of a mixture of Laplace distributions. The SIMPLE model with much less parameters captures closely all the peak fragment densities without loss of accuracy at other altitudes. The distribution of 'e' and the 'B' in each and every gross and local model could be represented by suitable lognormal distributions. Qualitatively the parameters of the 'n' and 'e' distributions in the gross and the local models exhibited statistically quasi-equilibrium state (though quantitatively the fragment density varied all over) across the time period from 1999 to 2002 and hence an average was recommended as the model value. Since, the parameters of 'B' showed large variations or trend in their values derived from the TLE data sets, the latest year 2002 value was suggested as a reference in the model. Lastly some application areas of the SIMPLE model were provided along with possible approaches to estimate the spatial density of debris objects and their flux in each altitude bin of interest.



SDSSARS IN ISRO

Space Debris and Space Situational
Awareness Research Studies



CHAPTER 4

Orbit Propagation

4.1 Orbit Propagators for Satellites

Orbit propagation is an essential component of space debris evolutionary studies. Propagation concerns the determination of the motion of a body over time. According to Newton's laws, the motion of a body depends on its initial state (i.e., its position and orientation at some known time) and the forces that act upon it over time. High fidelity propagators attempt to include all significant force models acting on the body; low fidelity propagators approximate the effects of some forces while completely disregarding others. High fidelity propagators solve Newton's laws using numerical methods; low fidelity propagators tend to be analytic (i.e., formula-based); medium fidelity models are a hybrid (i.e., semi-analytical) which combines a simple numerical technique with formulas.

Low fidelity propagators are the fastest to use and thus are appropriate for design and for planning; high fidelity propagators are the slowest to use but most appropriate when accuracy is needed, like in operations. One should use a propagation model appropriate for the type of analysis needed. Analytic propagators use a closed-form solution of the time-dependent motion of a satellite to produce ephemeris or to provide directly the position and velocity of a satellite at a particular time. Semi-analytic propagators incorporate some numerical techniques instead of using only approximations. Numerical propagators numerically integrate the equations of motion for the satellite.

4.2 Orbital Decay of RS-1 Satellite with KS Differential Equations

It is well known that the solutions of the classical Newtonian equations of motion are unstable and these equations are not suitable for long-term orbit computations numerically. Many transformations emerged in the literature to stabilize the equations of motion either to reduce the accumulation of local numerical errors

or allowing the use of larger integration step sizes in the transformed space or both. Examples of such transformations include the use of a new independent variable – time transformation, transformation to orbital parameter space which tend to decouple fast and slow variables, and the use of integrals as control terms. One such transformation, known as the KS transformation, is due to Stiefel and Kustaanheimo (1965), who regularized the non-linear Kepler motion and reduced it to linear differential equations of a harmonic oscillator of constant frequency. Stiefel and Scheifele (1971) further developed the application of the KS transformation to problems of perturbed motion, producing a perturbational equations version.

4.2.1 Equations of Motion

The KS element equations of motion are (Stiefel and Scheifele, 1971):

$$\frac{d\omega}{dE} = -\frac{r}{8\omega^2} \frac{\partial V}{\partial t} - \frac{1}{2\omega} \left(\frac{d\mathbf{u}}{dE}, L^T \mathbf{P} \right), \quad (4.1)$$

$$\begin{aligned} \frac{d\tau}{dE} = & \frac{1}{8\omega^3} (K^2 - 2rV) - \frac{r}{16\omega^3} \left(\mathbf{u}, \frac{\partial V}{\partial \mathbf{u}} - 2L^T \mathbf{P} \right) \\ & - \frac{2}{\omega^2} \frac{d\omega}{dE} \left(\mathbf{u}, \frac{d\mathbf{u}}{dE} \right), \end{aligned} \quad (4.2)$$

$$\begin{aligned} \frac{d\alpha}{dE} = & \left\{ \frac{1}{2\omega^2} \left[\frac{V}{2} \mathbf{u} + \frac{r}{4} \left(\frac{\partial V}{\partial \mathbf{u}} - 2L^T \mathbf{P} \right) \right] + \frac{2}{\omega} \frac{d\omega}{dE} \frac{d\mathbf{u}}{dE} \right\} \sin \frac{E}{2}, \\ \frac{d\beta}{dE} = & - \left\{ \frac{1}{2\omega^2} \left[\frac{V}{2} \mathbf{u} + \frac{r}{4} \left(\frac{\partial V}{\partial \mathbf{u}} - 2L^T \mathbf{P} \right) \right] + \frac{2}{\omega} \frac{d\omega}{dE} \frac{d\mathbf{u}}{dE} \right\} \cos \frac{E}{2}. \end{aligned} \quad (4.3)$$

$$\mathbf{u} = \alpha(E) \cos \frac{E}{2} + \beta(E) \sin \frac{E}{2}, \quad (4.4)$$

$$\frac{d\mathbf{u}}{dE} = -\frac{1}{2} \alpha \sin \frac{E}{2} + \frac{1}{2} \beta \cos \frac{E}{2}. \quad (4.5)$$

$$t = \tau - (\mathbf{u}, d\mathbf{u}/dE), \quad (4.6)$$

$$\mathbf{x} = (x_1, x_2, x_3) = L(\mathbf{u})\mathbf{u}, \quad (4.7)$$

$$\mathbf{r} = (x_1^2 + x_2^2 + x_3^2)^{1/2} = u_1^2 + u_2^2 + u_3^2 + u_4^2, \quad (4.8)$$

$$\dot{\mathbf{x}} = 4wL(\mathbf{u}) (d\mathbf{u}/dE)/r, \quad (4.9)$$

$$w = \left[\frac{1}{2} \left((K^2/r) - \frac{1}{2} |\dot{\mathbf{x}}|^2 - V \right) \right]^{1/2}, \quad (4.10)$$

$$L(\mathbf{u}) = \begin{pmatrix} u_1 & -u_2 & -u_3 & u_4 \\ u_2 & u_1 & -u_4 & -u_3 \\ u_3 & u_4 & u_1 & u_2 \\ u_4 & -u_3 & u_2 & -u_1 \end{pmatrix}, \quad (4.11)$$

$$V = \frac{K^2}{r} \sum_{n=2}^{\infty} J_n \left(\frac{R}{r} \right)^n P_n(\cos v), \quad (4.12)$$

$$\cos v = x_3/r, \quad (4.13)$$

$$\mathbf{P} = -\frac{1}{2}\rho\delta|\mathbf{v}| \mathbf{v}, \quad (4.14)$$

$$\begin{aligned} \rho = k \exp \{ -a\beta(1 - e \cos E) [1 + c \cos 2(\omega + E) - 2ce \sin 2(\omega + E) \sin E \\ + \frac{1}{4}c^2(1 + \cos 4(\omega + E)) - \frac{1}{2}ce^2(\cos 2\omega + 2 \cos 2(\omega + E) - 3 \cos 2(\omega + E) \cos 2E) \\ - c^2 e \sin 4(\omega + E) \sin E + O(cc, ce^2, c^2 e^2)] \}, \end{aligned} \quad (4.15)$$

$$\delta = FAC_D/m, \quad F = [1 - r_{p_0}/v_{p_0} A \cos i_0]^2, \quad (4.16)$$

$$\begin{aligned} k &= \rho_{p_0} \exp(\bar{\beta} r_{p_0} - c \cos 2\omega_0), \\ c &= \frac{1}{2} \epsilon \bar{\beta} r_{p_0} \sin^2 i, \end{aligned} \quad (4.17)$$

The energy equation given in (4.10) can be alternatively written as

$$[1/2w^2 - \{r + 4 (du/dE)^2\}/(K^2 - rV)] = 0. \quad (4.18)$$

We write equation (4.18) as

$$\Delta h \text{ (energy variation error)} = 0. \quad (4.19)$$

4.2.2 Computer Package 'OBLETRA' For Orbit Predictions

Computer software 'OBLETRA' (Sharma and Mani, 1985) was developed for orbit computation using the KS element equations of motion (4.1) to (4.4). Earth's oblateness terms J2 to J6 given in (4.13) were included along with an oblate atmospheric model

given in (4.15). If ρ_p , the density is known, then ρ at any other point with eccentric anomaly E can be computed by the oblate atmospheric model (4.15).

Orbit computation of the first satellite RS-1, launched by ISRO by its own rocket SLV-3 from Sriharikota Range (SHAR) on 18th July 1980, was done for about 400 days. Numerical integration of the equations of motion was carried out with the fourth-order fixed step size Runge-Kutta-Gill method with reference to 20 July 1980 epoch given in Table 4.1. The osculating and mean orbital parameters of RS-1 for this epoch along with satellite mass and effective area are also provided in Table-4.1 (Sharma and Mani, 1985). Constant value of the drag coefficient 2.2 is used. Constant rotational rate of atmosphere (Λ) with respect to Earth's rotation is used as 1.2.

Parameter	Mean	Osculating
Semi-major axis (km)	6989.2057	6993.1885
Eccentricity	0.04367712	0.044326
Inclination (deg.)	44.67198	44.68679
Right ascension of ascending node (deg.)	239.3378	239.3537
Argument of perigee (deg.)	174.1602	174.8279
Mean anomaly (deg.)	25.63974	25.00514
Satellite mass (kg)	35.443	-
Effective area of the satellite (m ²)	0.319019	-
Drag coefficient	2.2	-
Λ	1.2	-

ϵ is the ellipticity of the Earth, H is the density scale height, a , e and ω are orbital parameters: semi-major axis, eccentricity and argument of perigee, respectively. Bhatnagar-Taqvi's (1977) short-periodic expressions due to Earth's second harmonic (J_2) and Gooding's (1981) iteration scheme was used for mean and osculating elements conversion (Sharma, 1990). ρ_p , the density at the osculating perigee, was computed with CIRA 1972 Mean Reference Atmosphere. However, the effects due to the variations in daily 10.7 cm solar flux ($F_{10.7}$), averaged 10.7 cm solar flux, daily averaged geomagnetic index (A_p) and semi-annual variations were computed and implemented on ρ_p . The density scale height (H) during each revolution was computed with the $\frac{3}{4} H$ theory of King-Hele and Scott (1969). After some numerical

experimentation, 36 steps/revolution was chosen for numerical integration for 400 days duration. It may be seen a linear growth of error for 400 days in Δh in Figure 4.1.

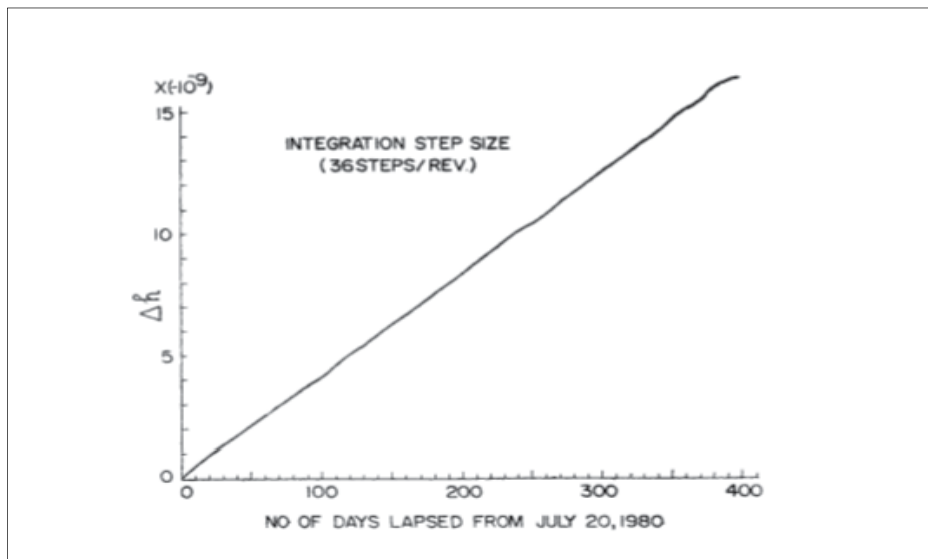


Figure 4.1: Energy variation error (Δh) versus time for RS-1

Figs. 4.2 and 4.3 depict the computed and the observed values of semi-major axis and eccentricity of RS-1 for the total computed orbital life (399.4 days) with integration step size of 36 steps/rev. It was noticed that there was good agreement for

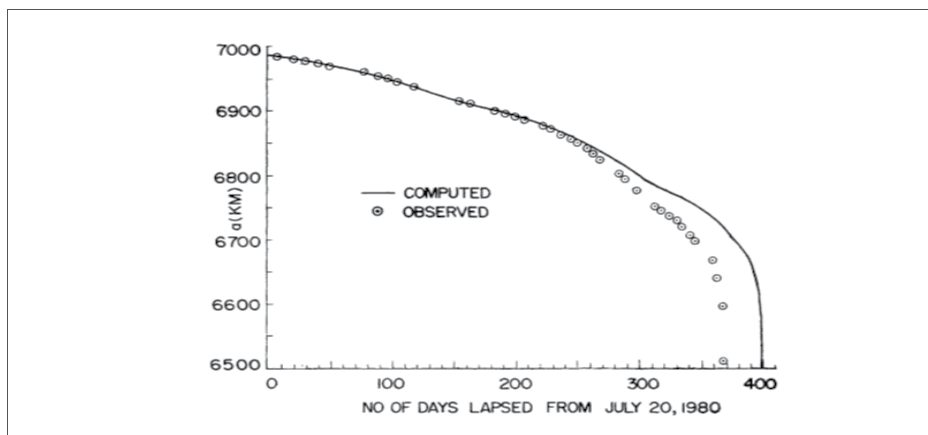


Figure 4.2: Semi-major axis decay of RS-1

first 260 days in the case of semi-major axis and for 300 days in the case of eccentricity. This study provided us the important information that due to decay, the eccentricity decreases and the effect of diurnal bulge of the atmosphere becomes important as the orbit becomes near circular, which was absent in this study. Once the effect of diurnal bulge was included in the modeling by Sharma (1993a), both the orbital parameters semi-major axis “a” and eccentricity “e” matched very well till the end of the life of RS-1.

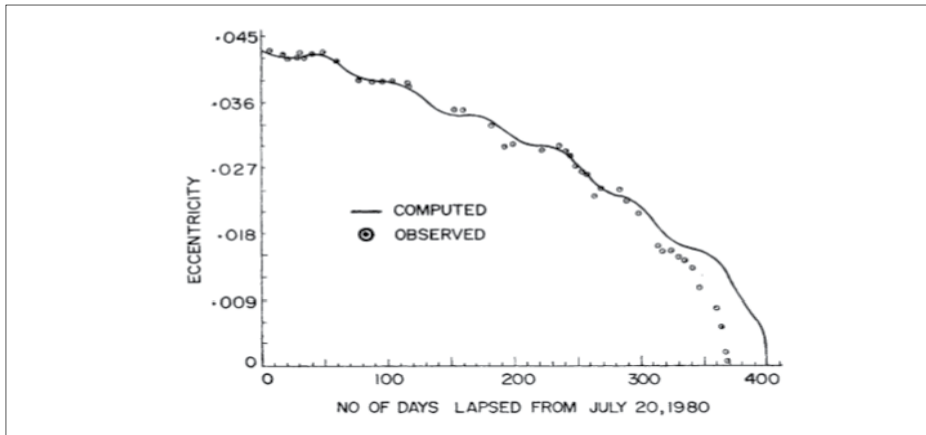


Figure 4.3: Eccentricity decay of RS-1

4.3 RS-1 Orbital Decay in an Oblate Diurnal Atmosphere

An orbit prediction package ‘SATODA’ for near-Earth satellite orbits was developed by Sharma (1993a), utilizing the analytical expressions of Swinerd and Boulton (1982) for secular changes of the semi-major axis and eccentricity per revolution in an oblate diurnal atmosphere. The data for 10.7 cm solar flux (F10.7) and averaged geomagnetic index (A_p) values was obtained from Solar Geophysical Data Prompt Reports (Lincoln, 1980-1981). The package was utilized to study the orbital decay of RS-1 satellite. A comparison between the predicted (post-facto) and observed values of the orbital decay parameters semi-major axis ‘a’ and eccentricity ‘e’ with Jacchia (1977) density model was found to be quite satisfactory as seen in Figures 4.4 and 4.5, respectively, showing the utility of the package and the importance of the oblate diurnal atmospheric modeling for near-circular orbits.

It may be noticed that the orbital parameters 'a' and 'e' are very much closer with the observed values during the whole life of RS-1 satellite with respect to the oblate diurnal atmospheric model using Jacchia (1977) density model (J1977). With respect to the epoch of 20th July 1980, RS-1 remained in the orbit for 371 days. The life predicted with oblate diurnal atmospheric model using J1977 was 377.4 days, an error of 1.72%, showing the utility of the developed package "SATODA" for accurate orbital lifetime computation.

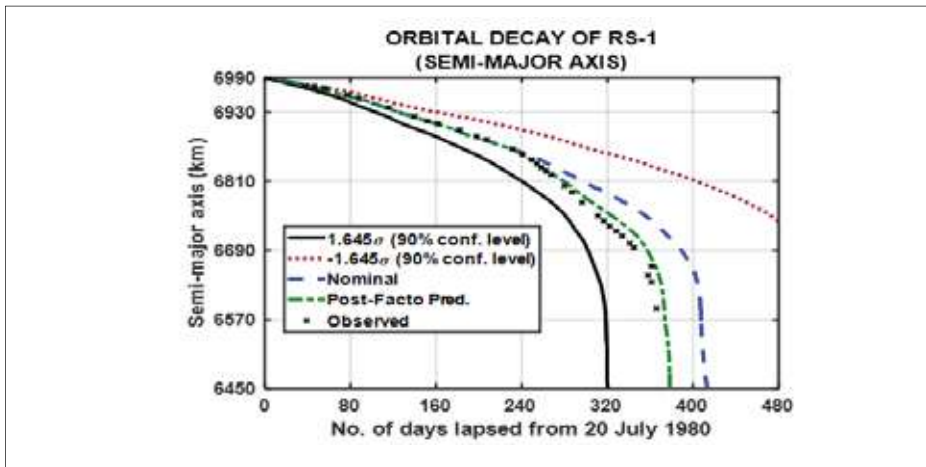


Figure 4.4: Decay of Semi-major Axis of RS-1

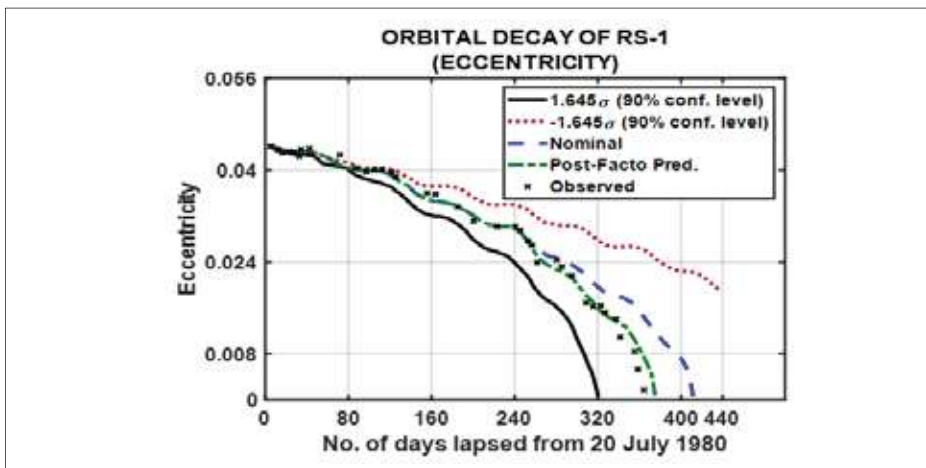


Figure 4.5: Decay of Eccentricity of RS-1

Since the canonical approach to a given mechanical system converts the system into a simpler form through transformations, in Sharma and Raj (1988) a detailed numerical study was carried out of a canonical form of the KS theory with respect to a complex force model. The derivation of canonical differential systems describing the perturbed motion, is by no means trivial, since, for instance, the adopted law of the time-transformation must be incorporated in the canonical set. The satisfaction of this requirement implies the knowledge of more refined instruments of general canonical theory as, for instance the enlargement of the phase space and the appropriate restrictions on the initial conditions.

For detailed numerical study, we have chosen the uniformly regular KS canonical elements (Stiefel and Scheifele, 1971; p 251) where all the elements α_j, β_j ($j=1$ to 5) are constant in the Keplerian motion. We developed an orbit computation package by including the effect of Earth's oblateness. The recursion formulas of Legendre polynomials were utilized to include up to any number of Earth's zonal harmonic terms J_n . However, the numerical computations were done with terms up to J_{36} . The integration of KS uniform canonical equations of motion was carried out with fixed step size fourth-order Runge-Kutta-Gill method. Bilinear relations and energy equation were used for checking the accuracies of numerical integration. It was concluded from the study that a larger integration step size (say, 36 steps/rev.) could be utilized for moderate eccentricity cases for accurate orbit computations during long-term integrations.

From the application point of view, the package was utilized to study the long-term behaviour of 900 km height near-circular sun-synchronous satellite orbit of PSLV mission. The mean orbital elements were generated for 220 days time (nearly 3078 revolutions). The conversion of the osculating orbital elements to mean orbital elements was done through Chebotarev's (1964) first-order short-periodic variations due to J_2 . Numerical integration was done up to J_{24} terms. The long-periodic terms in eccentricity and inclination were found to have a period of 129.9 days. The extrema of mean eccentricity and inclination were found to occur very near to + 90 degrees of mean argument of perigee.

A particular canonical form of the KS differential Equations is with all 10 elements constant. The equations can be used for elliptic, parabolic and hyperbolic motion. They are found to provide accurate orbit predictions numerically as well as analytically.

4.4.1 Equations of motion

$$\ddot{\bar{x}} + \frac{\mu}{r^3} \bar{x} = -\frac{\partial V}{\partial \bar{x}} + \bar{P},$$

\bar{x} – position vector of the particle

V – perturbing potential

\bar{P} – remaining perturbing forces

Canonical Equation of motion

$$\dot{x}_i = \frac{\partial H}{\partial P_i}, \quad \dot{p}_i = -\frac{\partial H}{\partial x_i} + P_i \quad (i = 1, 2, 3) \quad (4.20)$$

$$p_i = \frac{\partial T}{\partial \dot{x}_i}, \quad T = \frac{1}{2}(\dot{x}_1^2 + \dot{x}_2^2 + \dot{x}_3^2),$$

$$p_1 = \dot{x}_1, \quad p_2 = \dot{x}_2, \quad p_3 = \dot{x}_3$$

Unperturbed Hamiltonian is:

$$H = \frac{1}{2}(p_1^2 + p_2^2 + p_3^2) - \frac{\mu}{r} + V. \quad (4.21)$$

New independent variable is

$$\frac{dt}{ds} = \mu(x_k, p_k). \quad (4.22)$$

Homogeneous Hamiltonian is

$$H_p = H + p_0,$$

p_0 is $-h$, negative of total energy.

Canonical form is preserved if (4.23)

$$\bar{H}_h = H_h \mu = \left[\frac{1}{2}(p_1^2 + p_2^2 + p_3^2) - \frac{\mu}{r} + V \right] \mu, \quad (4.24)$$

New functions $x_k(s)$, $p_k(s)$ are determined from the equations

$$\frac{dx_j}{ds} = \frac{\partial H_h}{\partial p_j}, \quad \frac{dp_j}{ds} = -\frac{\partial H_h}{\partial x_j}, \quad (j = 0, 1, 2, 3) \quad (4.25)$$

At $t=0$, $s = 0$

4.4.2 Canonical KS-Transformation

$$\mu = r$$

$$\bar{H}_h = \frac{1}{2}(p_1^2 + p_2^2 + p_3^2)r + rp_0 + rV - \mu \quad (4.26)$$

Let

$$\Lambda(\bar{x}) = \begin{pmatrix} \bar{x}_1 & -\bar{x}_2 & -\bar{x}_3 & \bar{x}_4 \\ \bar{x}_2 & \bar{x}_1 & -\bar{x}_4 & -\bar{x}_3 \\ \bar{x}_3 & \bar{x}_4 & \bar{x}_1 & \bar{x}_2 \end{pmatrix}, \quad (4.27)$$

The KS-transformation can be written as

$$\begin{pmatrix} x_1 \\ x_2 \\ x_3 \end{pmatrix} = \Lambda(\bar{x}) \begin{pmatrix} \bar{x}_1 \\ \bar{x}_2 \\ \bar{x}_3 \\ \bar{x}_4 \end{pmatrix}, \quad x_0 = \bar{x}_0. \quad (4.28)$$

P-transformation can be written as

$$\begin{pmatrix} p_1 \\ p_2 \\ p_3 \end{pmatrix} = \frac{1}{2(\bar{x}_1^2 + \bar{x}_1^2 + \bar{x}_1^2 + \bar{x}_1^2)} \Lambda(\bar{x}) \begin{pmatrix} \bar{p}_1 \\ \bar{p}_2 \\ \bar{p}_3 \\ \bar{p}_4 \end{pmatrix}, \quad p_0 = \bar{p}_0. \quad (4.29)$$

$$\bar{H} = \frac{1}{2}|\bar{w}|^2 + \frac{1}{2}w_0|\bar{u}|^2 + \frac{1}{4}|\bar{u}|^2 V - \frac{\mu}{4}, \quad (4.30)$$

The equations of motion are

$$\frac{du_{\bar{k}}}{ds} = \frac{\partial H}{\partial w_{\bar{k}}}, \quad \frac{dw_{\bar{k}}}{ds} = -\frac{\partial H}{\partial u_{\bar{k}}}, \quad (k = 0, 1, 2, 3, 4), \quad (4.31)$$

which are the equations of a harmonic oscillator.

The bilinear relation is

$$u_4 w_1 - u_3 w_2 + u_2 w_3 - u_1 w_4 = 0, \quad (4.32)$$

$$|\bar{u}|^2 = u_1^2 + u_2^2 + u_3^2 + u_4^2, \quad |\bar{w}|^2 = w_1^2 + w_2^2 + w_3^2 + w_4^2. \quad (4.33)$$

On any solution, the value of $p_0=2w_0$ is the negative of physical energy and the value of Hamiltonian H is zero.

The separation of Jacobi's equation corresponding to unperturbed Hamiltonian can be achieved through the canonical transformation

$$w_k = \frac{\partial S}{\partial u_k}, \quad \beta_k = \frac{\partial S}{\partial \alpha_k}, \quad (k=0,1,2,3,4) \quad (4.34)$$

having the generating function

$$S = \sum_{k=1}^4 \int [2\alpha_k - \alpha_0 u_k^2]^{1/2} du_k + \alpha_0 u_0, \quad (4.35)$$

and the transformed unperturbed Hamiltonian becomes

$$H = \alpha_1 + \alpha_2 + \alpha_3 + \alpha_4, \quad (4.36)$$

The corresponding perturbed Hamiltonian is

$$H = \alpha_1 + \alpha_2 + \alpha_3 + \alpha_4 + \frac{1}{2\alpha_0} \sum_{k=1}^4 \alpha_k \sin^2 \sqrt{\alpha_0} \beta_k V(\alpha_0, \dots, \alpha_4, \beta_0, \dots, \beta_4) - \frac{\mu}{4}. \quad (4.37)$$

The generating function

$$S = \frac{1}{\sqrt{w_0} \sin(\sqrt{w_0} s)} + \sum_{k=1}^4 \left[\frac{1}{2} (w_k^2 + \beta_k^2) \cos(\sqrt{w_0} s) - w_k \beta_k \right] - w_0 \beta_0, \quad (4.38)$$

with the generated canonical transformation

$$u_k = -\frac{\partial S}{\partial w_k}, \quad \alpha_k = -\frac{\partial S}{\partial \beta_k}, \quad (k=0,1,2,3,4) \quad (4.39)$$

transforms the above Hamiltonian

$$\bar{H} = H + \frac{\partial S}{\partial s} = \frac{1}{4} \left[\sum_{k=1}^4 u_k^2(\alpha_j, \beta_j) \right] V(\alpha_j, \beta_j) - \frac{\mu}{4}, \quad (4.40)$$

and the equations of motion are

$$\frac{d\beta_k}{ds} = \frac{\partial \bar{H}}{\partial \alpha_k}, \quad \frac{d\alpha_k}{ds} = -\frac{\partial \bar{H}}{\partial \beta_k}, \quad (k=0,1,2,3,4) \quad (4.41)$$

It follows that all 10 elements are constant in unperturbed motion in (4.41).

4.4.3 Perturbations and Numerical Results

In this study (Sharma and Raj, 1988), we assumed that the only force acting on an artificial satellite is those due to the Earth's gravitational field with axial symmetry; in which case, we have

$$V = \frac{K^2}{r} \sum_{n=2}^{\infty} J_n \left(\frac{R}{r} \right)^n P_n(\cos \nu), \quad \cos \nu = \frac{x_3}{r}, \quad (4.42)$$

where R is the equatorial radius, r the distance of the particle from the central body. J_n 's are dimensionless constants known as zonal harmonics and P_n are Legendre polynomials of degree n. With respect to V in (4.42), we developed an orbit computation package through the uniformly regular KS canonical Equations (4.41). For the economic computation of V and $\nabla V / x$ with respect to Legendre polynomial of any degree n, we have utilized the recurrence formulas of Legendre's polynomials

$$nP_n(x) = (2n - 1)xP_{n-1}(x) - (n - 1)P_{n-2}(x), \quad (4.43)$$

Having starting values

$$P_0(x) = 1, \quad P_1(x) = x; \quad P'_n(x) = xP'_{n-1}(x) + nP_{n-1}(x), \quad (4.44)$$

with

$$P'_0(x) = 0. \quad (4.45)$$

4.4.4 Checks during Numerical Integration

The bilinear relations

$$\alpha_4\beta_1 - \alpha_3\beta_2 + \alpha_2\beta_3 - \alpha_1\beta_4 = 0 \quad (4.46)$$

and

$$u_4w_1 - u_3w_2 + u_2w_3 - u_1w_4 = 0, \quad (4.47)$$

satisfied by the canonical variables α_i, β_i and u_i, w_i ($i = 1, 2, 3, 4$) are used as checks for numerical integration accuracies of the Equations (4.41) with respect to the force model given by (4.42).

4.4.5 Sun-Synchronous Orbit

From the application point of view, we utilized the orbit computation package to generate mean orbital elements of 900 km near-circular Sun-synchronous orbit for 220 days time (nearly 3078 revolutions). Its initial osculating orbital elements chosen for the study along with mean elements are given in Table 4.2. The conversion of the osculating orbital elements to mean orbital elements is done through Chebotarev's (1964) first-order short-periodic variations due to J2 (Sharma, 1990). It was noticed a meter level accuracy in the osculating semi-major axis computation with 36 steps/rev. after 60 revolutions. The mean orbital elements for this case were generated after integrating Equations (4.41) with J2 to J24 terms up to 220 days time (nearly 3078 revolutions). It was noted that the mean semi-major axis (a_m) remains nearly constant, while the mean right ascension of ascending node (Ω_m) varies almost linearly during the 220 days time. The variation of mean eccentricity (e_m), argument of perigee (ω_m) and inclination (i_m) are depicted in Figure 4.4 up to 220 days time. It was noticed from the Figure 4.4 that the eccentricity and the inclination have long-periodic terms of period 129.9 days and occur almost at the same time. A slight increase in the peak values of i_m was also noted. The extrema of these variations occur when the argument of perigee is near to + 90 degrees. The argument of perigee varies rapidly near the minimum of e_m and i_m . Variation of e_m and ω_m , with terms up to J2 and J6 was also shown in Figure 4.6 to show the effect of higher zonal harmonic terms. It was noticed that the terms J3 to J24 have very significant effect on e_m , ω_m , and i_m . Effect of J7 to J24 was also noticed on e_m . The figure also depicted that J2 has no long-periodic effect on e_m .

Table 4.2: Orbital parameters of Sun-synchronous Orbit

Parameter	Osculating	Mean
a (km)	7282.7	7277.6969
e	0.00063	0.000717
i (deg.)	99.033	99.091146
Ω (deg.)	290.033	290.0376
ω (deg.)	207.844	180.014
M (deg.)	0.0	27.744

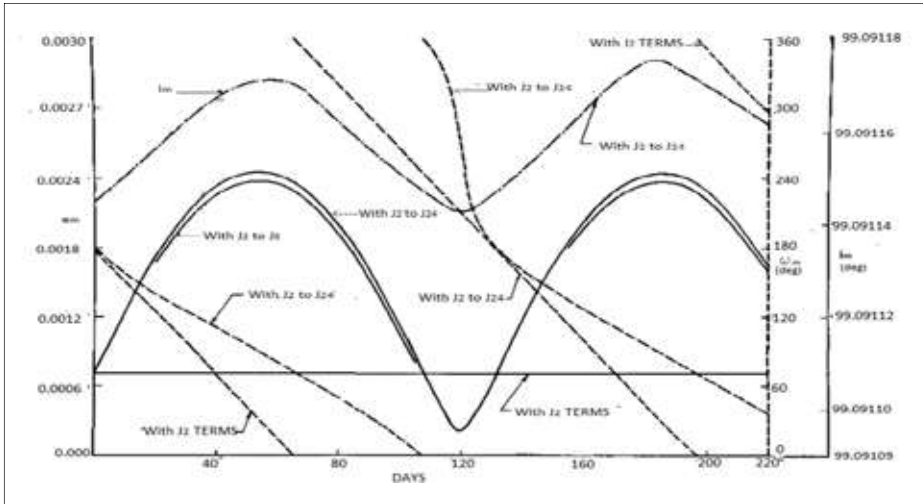


Figure 4.6: Variation of mean eccentricity (e_m), argument of perigee (w_m) and inclination (i_m)

4.5

Analytical approach using KS elements to short-term orbit predictions including J_2 , J_3 and J_4

KS elements equations were utilized to generate non-singular short-term orbit theories with Earth's zonal harmonic terms J_2 , J_3 and J_4 . Due to symmetry in the KS element equations (4.1) and (4.4) and the angular frequency ω being constant, only two of the ten equations were integrated analytically. The series expansions included terms of fourth power in eccentricity for J_2 and of third power for J_3 and J_4 (Sharma, 1989, 1993b). Further, these equations were used to generate non-singular analytical theory for the short-term motion in closed form in eccentricity for J_2 (Sharma, 1997a). The theory worked well for small to high eccentricity orbits during a revolution, which was further improved by using King-Hele's (1958) expression for the radial distance ' r ' which included the effect of J_2 (Saji et al., 2017).

4.6

Analytical short-term orbit predictions with J_2 , J_3 , J_4 in terms of K-S uniformly regular canonical elements

In Raj and Sharma (2003), a new non-singular analytical theory with respect to the Earth's zonal harmonic terms J_2 , J_3 , J_4 was developed for short-periodic motion, by analytically integrating the uniformly regular KS canonical equations. It showed an improvement over the analytical solution in terms of the KS elements. The analytical theory with respect to J_2 was further simplified by Smibi et al. (2017) by analytically integrating the uniformly regular KS canonical equations of motion using the

generalized eccentric anomaly 'E' as the independent variable in place of 's'. The integrals became much simpler in terms E than earlier obtained in Raj and Sharma (2003) in terms of the independent variable's'.

4.7

Contraction of Satellite Orbits using KS Elements with Air Drag for Low Eccentricity Orbits

A number of new non-singular analytical theories for the motion of near-Earth satellite orbits with the air drag effect were developed in terms of the KS elements for small eccentricity orbits, utilizing different analytical atmospheric density models (oblate atmosphere; Sharma, 1991, 1992; oblate diurnal atmosphere; Sharma, 1997b; Nair and Sharma, 2003). Due to symmetry of the KS element equations, only one of the eight equations was integrated analytically to obtain the state vector at the end of each revolution.

4.8

Generation of Non-singular Analytical Theories for the Contraction of High Eccentricity Satellite Orbits under the Influence of Air Drag

The KS elements equations were utilized to generate non-singular analytical theories for the contraction of high eccentricity satellite orbits under the influence of air drag using different analytical density models (spherically symmetrical atmospheric model; Sharma, 1998; oblate exponential atmospheric model; Sharma, 1999; oblate atmospheric model with variation of density scale height with altitude; Sharma and Raj, 2009, 2010). The decay rates of semi-major axis and eccentricity with the oblate atmosphere were found to be lower than those obtained with spherically symmetrical atmosphere (Sharma, 1998). The results were presented in the 32nd COSPAR assembly, held in Nagoya, Japan during July 1998 (Sharma, 1999).

4.9

Non-singular Analytical Theories for the Motion of Near-Earth Satellite Orbits with Air Drag in terms of Uniformly Regular KS Canonical Elements for Small Eccentricity Orbits

A number of new non-singular analytical theories for the motion of near-Earth satellite orbits with the air drag effect were developed in terms of uniformly regular KS canonical elements for small eccentricity orbits, utilizing different analytical atmospheric density models (oblate atmosphere; Sharma and Raj, 2005; symmetrically spherical atmosphere; Raj and Sharma, 2006; oblate diurnally varying atmosphere; Raj and Sharma, 2007; oblate atmosphere with density scale height

variation with altitude; Raj and Sharma, 2009a, Sharma and Raj, 2009; diurnally varying oblate atmosphere with altitude-dependent scale height; Raj and Sharma, 2009b).

For long-term debris environment projection model named 'KSCPROP' described in chapter 2 (Liou, Anil Kumar et al., 2013) was utilized to carry out computations for 200 years, revolution by revolution, using the non-singular, fourth-order analytical theory for the motion of near-Earth satellite orbits. The air drag effects were generated in terms of uniformly regular KS canonical elements using a diurnally-varying oblate atmosphere with variation in density scale height dependent on altitude (Raj and Sharma, 2009b).

4.10 Orbit Propagation using Semi-Analytical Theory and its Applications in Space Debris Field

OPSAT software used for lifetime estimation of space objects was developed by Dutt and Anil Kumar (2017). It used semi-analytical equations provided by Chao and Platt (1991) for orbit propagation. The averaged equations of motion included J2 and J3 and atmospheric drag. The equations were integrated with a step size of one or a multiple of orbit period. The integrations, which give the averaged drag effects on semi-major axis 'a' and eccentricity 'e' with respect to mean anomaly M from 0 to 2π , were carried out with respect to the true anomaly f. It uses BFGS Quasi-Newton algorithm to minimize least square error on apogee and perigee altitudes of a given TLE set to estimate ballistic coefficient (BC). This BC is used for future orbit prediction. It has been used for identification of potential candidate for active debris removal (ADR) and future projection of space debris environment with ADR.

Broad features of the Orbit lifetime estimation process is provided in Figure 4.7. OPSAT can be utilized for short- as well as long-term orbit predictions using TLE data.

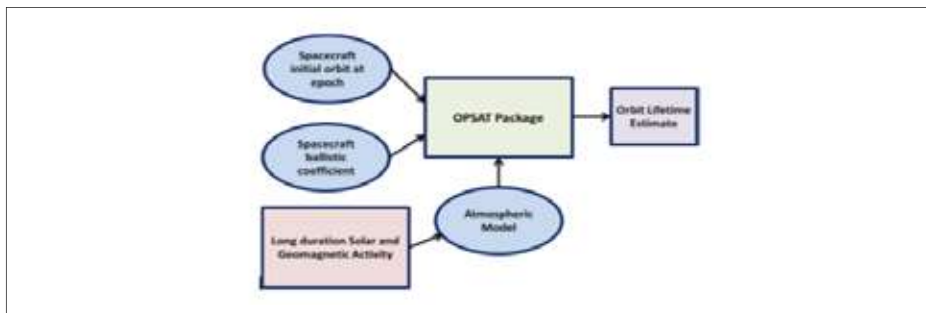


Figure 4.7: Broad Features of the Orbit Lifetime Estimation Process

Table 4.3: BC Estimation of Phobos-Grunt with different TLE sets and re-entry prediction (Re-entry epoch: 15th Jan 2012 17:45 UTC)

S. No.	TLE epoch of matching set	Estimated BC (kg/m ²)	Predicted re-entry date	Error (days)
1.	09-Jan to 12-Jan 2012	274.63	16-1-2012 1:40:55.3	1
2.	06-Jan to 09-Jan 2012	268.98	16-1-2012 0:24:0.5	1
3.	31-Dec 2011-06-Jan 2012	270.90	16-1-2012 6:35:22.3	1
4.	21-Nov-28-Dec 2011	251.12	12-1-2012 9:43:28.8	3
5.	09-Nov-24-Nov 2011	294.17	5-1-2012 5:46:34.6	10
6.	09-Nov-09-Dec 2011	296.05	5-1-2012 16:11:5.7	10

Table 4.4: BC Estimation of SFERA with different TLE sets and re-entry prediction (Re-entry epoch date: 24th Nov 2012)

S. No.	Matched data TLE epoch	Estimated BC (kg/m ²)	Predicted re-entry date	Error (days)
1.	15-20 Nov 2012	16.35	24-11-2012 21:6:58.9	0
2.	5-18 Nov 2012	17.74	25-11-2012 18:34:22.2	1
3.	11-23 Oct 2012	16.85	25-11-2012 14:5:9.5	1
4.	22-Sep-04-Oct 2012	15.3	20-11-2012 16:22:31.2	4

OPSAT is evaluated for short-term and long-term orbit predictions. For short-term orbit prediction 2-4 months TLE data of Phobos-Grunt (37872) and SFERA (38751) is used. The re-entry epoch is known for these satellites. Different sets of TLEs are used for ballistic coefficient (BC) estimation and the estimated BC is used for propagation. The predicted re-entry date is matched with the actual re-entry date. An error of about 10 days is observed when the matching TLE set is 2-3 months away from the re-entry date while 0-1 day error when matching TLE set is 4-5 days away from re-entry date. Tables 4.3 and 4.4 give the analysis details for re-entry prediction of Phobos-Grunt and SFERA, respectively.

For long-term evaluation, Transit 1B (7.5 years data), Cosmos 1939 (5 years data) and Tiantuo-1 (2.5 years data) are used. Tiantuo-1 (Figure 4.8), Cosmos 1939 (Figure 4.9) and Transit 1B (Figure 4.10) had re-entered on 31-10-2014, 29-10-2014 and 03-10-1967, respectively. The predicted re-entry date of Tiantuo-1 is same as the actual date, while there is 1 day difference between predicted and actual re-entry date of Cosmos 1939.

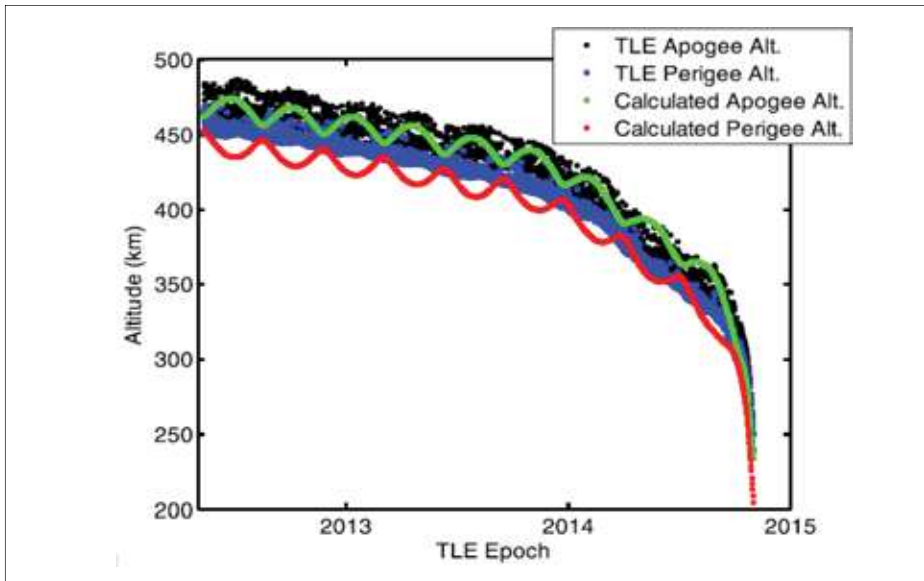


Figure 4.8: Perigee-Apogee profile of Tiantuo-1 ($BC = 67 \text{ kg/m}^2$)

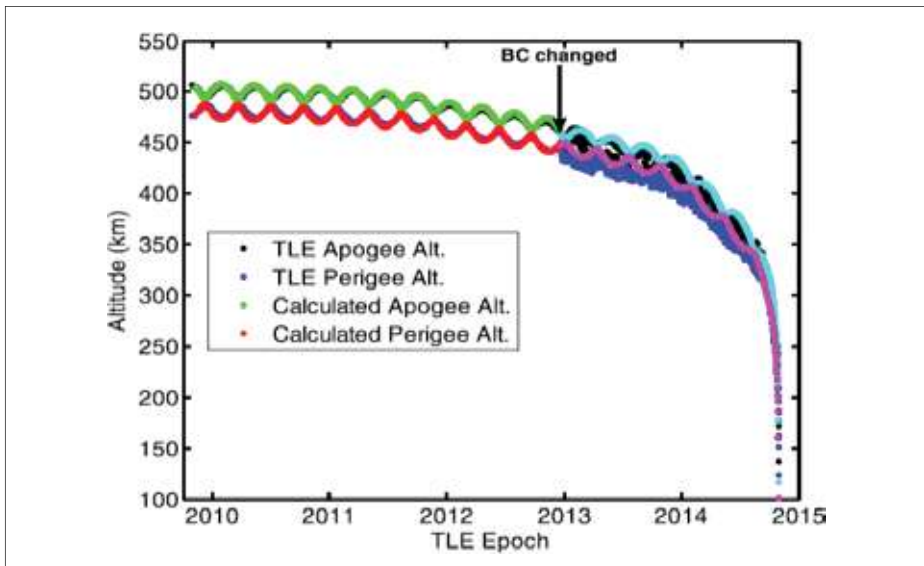


Figure 4.9: Perigee-Apogee profile of Cosmos 1939 ($BC 60 \text{ kg/m}^2$ in initial phase and later 55 kg/m^2)

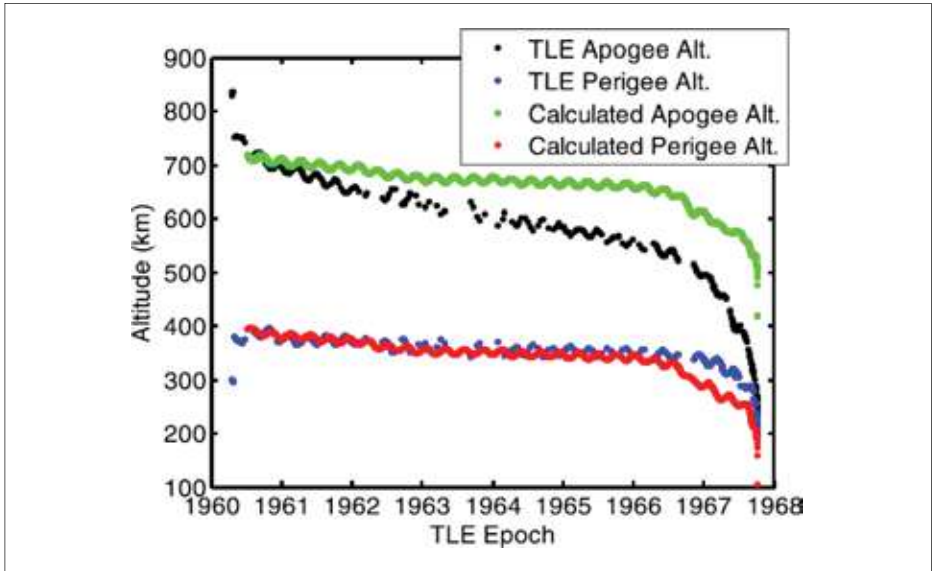


Figure 4.10: Perigee-Apogee profile of Transit-1B ($BC = 135 \text{ kg/m}^2$)



SDSSARS IN ISRO

Space Debris and Space Situational
Awareness Research Studies



CHAPTER 5

Modelling of the Space Debris Environment

5.1 Introduction

From the time of the launch of Sputnik 1 in 1957, the man-made space objects have steadily increased. Now the objects are tracked by a number of space agencies. The objects travel in different directions, at different altitudes, on different planes. Table 5.1 provides space objects on-orbit and decayed or beyond Earth orbit for different countries and others. To display the distribution statistics, 01 May 2022 U.S. Satellite Catalogue was categorized by their nominal variables (Anz-Meador et al. 2022).

Table 5.1: On-orbit or decayed-and-beyond-Earth-Orbit of Space objects Distribution

on-orbit	US	CIS	France	PRC	India	Japan	ESRO/ ESA	Other	Total
Payloads	4413	1467	80	636	104	196	83	1664	8643
rocket bodies	613	957	155	194	39	54	7	42	2061
mission-related debris	751	795	151	336	6	38	14	17	2108
breakup debris	3450	4935	202	3311	70	11	28	55	12062
anomalous debris	316	221	7	4	0	1	12	2	563
Total	9543	8375	595	4481	219	300	144	1780	25437

Decayed or beyond Earth orbit	US	CIS	France	PRC	India	Japan	ESRO/ESA	Other	Total
Payloads	1497	2054	11	103	15	84	32	153	3949
rocket bodies	811	2582	80	209	25	74	6	16	3803
mission-related debris	1044	5854	175	315	14	141	10	110	7663
breakup debris	3598	5698	492	940	432	130	13	62	11365
anomalous debris	186W	129	6	3	2	6	2	4	338
Total	7136	16317	764	1570	488	435	63	345	27118
							GRAND TOTAL		52555

5.2 Satellite Breakups

Figure 5.1 shows the number of breakups by year since 1961 to 2022. 1981 had maximum number of breakups of 10.

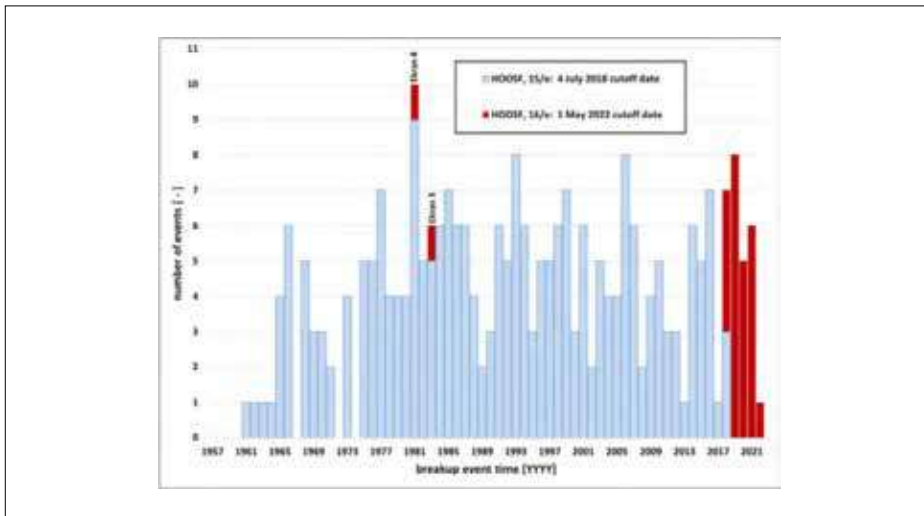


Figure 5.1: Number of breakups by year since 1961. Breakups after 18 July 2018 are shown in red. (Anz-Meador et al., 2022)

Ananthasayanam et al. (2002) developed the Stochastic IMPressionistic Low Earth (SIMPLE) engineering model for the space debris. Using the database provided by the Two Line Elements of the objects from 1999 to 2002 catalogued in NORAD, Ananthasayanam et al. (2003) presented detailed characterization of the eccentricities and ballistic coefficients of space debris in altitude and perigee bins using SIMPLE model. It was shown that in LEO (altitude less than 2000 km), the characteristics of the debris with eccentricity less than 0.2 could be specified in terms of suitable probability distributions. The number of objects in the altitude and perigee height bins in the model could be represented in terms of a mixture of Laplace distributions, and the eccentricity and ballistic coefficient of the objects were based on suitable lognormal distributions. The model further provided a statistical description of the debris objects with respect to five inclination bands. The paper brought out the details of further analysis regarding the characterization of the eccentricity and the ballistic coefficient in SIMPLE model across the altitude and perigee bins. In order to further demonstrate the stability and consistency of the estimated parameters, location, scale, mean and standard deviation values, a moving window of bin size 100 km and a window shift of 50 km was considered with respect to the altitude and the four parameters were estimated for the eccentricity distribution for the years 1999 to 2002. Comparison of the individual bin estimates to that of the moving window estimates were provided in Figures 5.2 and 5.3 and they showed that the estimates were consistent across the years and independent of moving window size and shift.

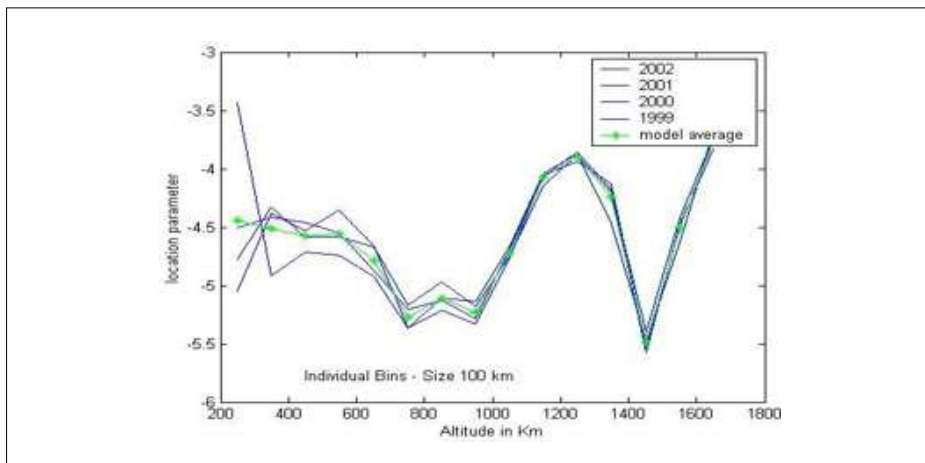


Figure 5.2: Variation of Location Parameter for Eccentricity in Individual Altitude bins

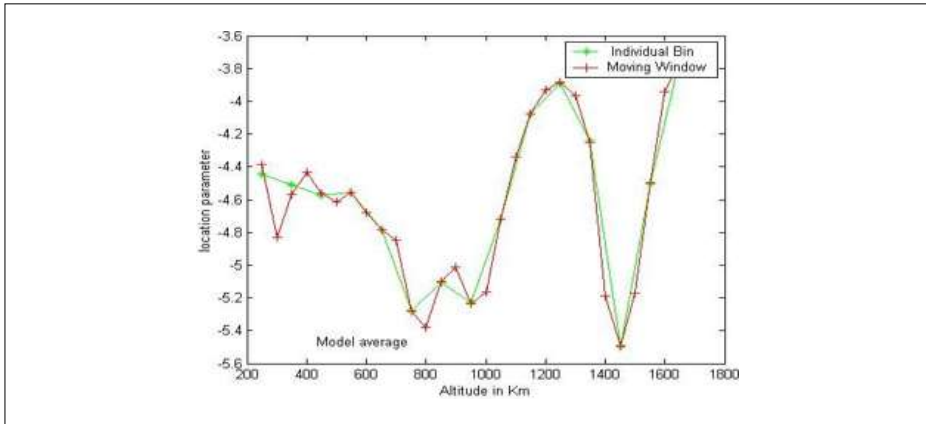


Figure 5.3: Comparison of model values of Location Parameter for Eccentricity in moving window Altitude bins and individual Altitude bins

The match had been very good for altitude above 1000 km and some mismatch were observed between the fits below 1000 km across the years. That could be attributed to the effect of drag in low altitudes and be viewed as short-term effects. The characterization provided to help in a proper assessment of the space debris environment in LEO. A Monte Carlo simulation of the orbital parameters, namely perigee height, altitude and eccentricity, based on the SIMPLE characterization could be used to obtain the closest approach, in a statistical sense, to a target object.

As the catalogued data consisted of only the objects of size greater than 10 cm to obtain the risk assessment due to other un-catalogued objects, statistical simulation of small objects was essential. That was a potential area of application of SIMPLE structure as the statistical simulation of the complete LEO debris environment was possible by expanding the SIMPLE scenario.

Also, SIMPLE structure gave insight into the evolution of the space debris scenario. It brought out the equilibrium nature of source and sink of the space debris through the parameters specifying the lognormality of the eccentricity and ballistic coefficient and Laplace nature to altitudes and perigee height. It showed that the distribution nature of the orbital parameters did not vary across the time and the variation was only in numerical values of parameters, and was minor for altitude or perigee heights and eccentricity, which described the distribution. The processes like explosions or collisions or increased launch activity in a certain region in LEO such as constellations, changed the equilibrium between source and sink, but that state of non-equilibrium will be dissipated into background debris environment and will be brought back again to the statistical equilibrium as represented by SIMPLE structure.

The debris flux and hence the spatial density described by SIMPLE model could be combined with any of the collision probability assessment tools, such as Poisson density approach, and hence obtain the probability of collision either with a target object or between the debris objects.

Efforts were taken to further model the parameters across the bins. An adequate polynomial fit for the model parameter values across the altitude bins was generated. The nature of the eccentricity and ballistic coefficient in each of the altitude bins and perigee height bins were analyzed for appropriate distribution fitting and it turned out that once again the nature of these parameters followed a lognormal distribution. Finally, a brief recipe of the application areas of the overall SIMPLE model was also provided.

5.4 A New Stochastic Impressionistic Low Earth Model of Space Debris Scenario

With reference to the space debris, Ananthasayanam et al. (2006b) provided in detail the insight of the SIMPLE model into the physical process by characterizing the distribution of the number density 'n', eccentricity 'e', and the ballistic coefficient 'B' of objects over whole of the LEO region for all inclinations put together and also separately. The other called 'local' model characterized the distribution of 'e' and 'B' of the debris across suitable local altitude and perigee bins useful for mission analysis and risk assessment for spacecraft designers interested in specific altitude or perigee height bins and inclination bands. The number density 'n' in all the gross models could be represented in terms of a mixture of Laplace distributions. The SIMPLE model captured closely all the peak fragment densities without loss of accuracy at other altitudes. The distribution of 'e' and the 'B' in each and every gross and local model could be represented by suitable lognormal distributions. Qualitatively the parameters of the 'n' and 'e' distributions in the gross and the local models exhibited statistically quasi-equilibrium state (though quantitatively the fragment density was varying all over) across the time period from 1999 to 2002 and hence an average was recommended as the model value. Since, the parameters of 'B' showed large variations or trend in their values derived from the TLE data sets, the latest year 2002 value was suggested as a reference in the model.

The approach provided the statistical distributions of the orbital characteristics of the environment and was limited to large objects, which were catalogued in USSPACECOM two line element (TLE) sets from 1999 to 2002 used in the analysis. In line with the general concept of LEO and near-circular orbits, the catalogued objects with altitude less than 2000 km and eccentricity < 0.2 were used. Such objects constituted about 75% of the catalogued objects. In fact, that region was most used by the satellite missions. The number of objects in that region across the years 1999 to 2002 varied around 6000.

Two kinds of models namely, global and local models in space each providing different in- sight and useful in orbital debris studies were used. The distributions in terms of the altitude and the perigee height in global model helped simulation studies to have better accuracy in defining the low earth near-circular orbital debris scenario. From Figure 5.4 (a) it could be seen that there was debris accumulation around some particular altitudes around 750 km, 1000 km and also at about 1500 km in LEO due to the greater launch activity and the later breakup creating debris clouds around the breakup point.

It had been reported earlier that out of the on-orbit breakups up to 2002, most of them of about 175 had occurred in that region of LEO. The marginal probability density functions $f(n, h, t)$, $f(n, hp, t)$, $f(n, e, t)$ and $f(n, B, t)$ are considered, where 't' ranges from the year 1999 to 2002 and subsequently had been able to derive whenever appropriate suitable time averaged marginal distributions for the purpose of the model were required. The distribution of the orbital elements namely altitude, perigee height, eccentricity and the ballistic coefficient values for one set of data in each of the years (the first available set in the month of January) were analysed to arrive at their characteristic probability distributions.

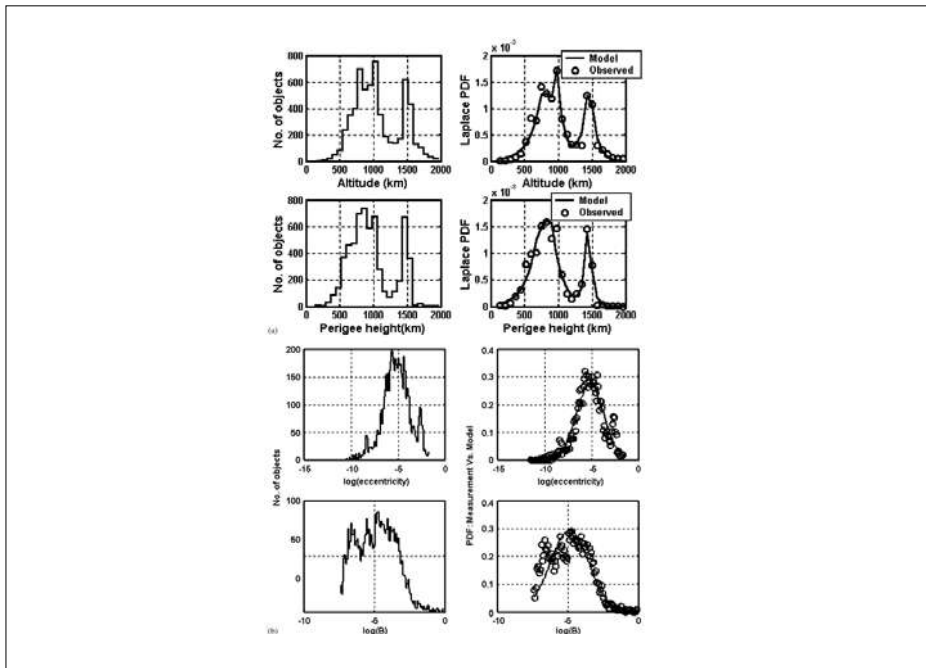


Figure 5.4: (a) Number density distributions in altitude and perigee for the year 2002 and (b) eccentricity and B distributions of the debris objects for the year 2002

The altitude of non-circular debris varied from time to time. To provide the probabilistic description of the orbital debris the distribution of the argument of the perigee, and the right ascension of the ascending node was necessary. Those were assumed to follow uniform distribution as used in other established models. Thus, the probability distribution of the number density was taken to be uniform across the altitude swept by the debris.

After analyzing many data sets all of which had a weight between 0.66 and 0.73, both the weight parameters were fixed in the model at 0.7 and it was noticed that the worked out location and scale parameters did not deteriorate the fit. It brought out the fact that the location of the first peak and its dispersion on both sides could be considered as constants. It means that there was some kind of quasi-equilibrium state maintained in that region of LEO as far as the catalogued objects are concerned though the number of debris themselves are changing. That phenomenon might be attributed to various reasons including, the source mechanisms such as launch activities, breakup of objects in space and rain down effect and also to sink mechanisms such as decay of objects due to drag effects and solar activity variation effects in the atmosphere. While the second scale parameters were qualitatively the same across the years the third scale parameter defining the dispersion of the third peak around 1450 km shows some slightly increasing trend perhaps due to the much less drag decay but not significant enough for the present quasi-equilibrium modelling.

The parameters for an averaged model fit over the 4-year period namely 1999–2002 with tertiary mixture of Laplace distributions were found to be (790, 975, 1470, 160, 85, 95, 0.7, and 0.7), respectively, for three locations, three scales and two weights. The marginal distributions for the number density of fragments with perigee heights for each of the years were considered. A three-component mixture of Laplace distributions was used to fit the model density with perigee height. It was noted that the parameters did not vary significantly across the years. The bottom of Figure 5.4 (a) showed once again the goodness of fit of the Laplace distribution for the perigee height. As pointed out by the figures, the peaks of the number density of debris in the altitudes and the perigee heights being different a separate study for the perigee height was justified. The parameters for the averaged model fit for the perigee height with tertiary mixture of Laplace distributions were obtained as (710, 870, 1450, 180, 140, 50, 0.5, and 0.8). First three were locations, next three were scales and last two were weights. Eccentricity values for all the years showed a clear left skewing and a high concentration close to the neighbourhood of zero. This nature pointed to a log-normal distribution fit for the eccentricity. Table 5.2 provided the parameters for the eccentricity in the data for various years. It also provided the sample mean and standard deviation of the eccentricity across the period 1999–2002. Figure 5.4 (b) showed a closer look at the goodness of fit of the model.

Table 5.2: Parameters of the lognormal distribution for the eccentricity of catalogued debris objects

Data year	Location parameter		Scale parameter		Statistics	
	Estimate μ	95% confidence limit	Estimate β	95% confidence limit	Mean	Sigma
2002	-5.15	(-5.19, -5.12)	1.46	(1.44, 1.49)	0.0151	0.0248
2001	-5.12	(-5.16, -5.09)	1.16	(1.44, 1.49)	0.0155	0.0246
2000	-5.10	(-5.14, -5.06)	1.48	(1.45, 1.50)	0.0159	0.0251
1999	-5.03	(-5.07, -4.99)	1.43	(1.41, 1.46)	0.0165	0.0257

Five inclination bands (0, 36), (36, 61), (61, 73), (73, 91) and (91, 180) in degrees were considered. It was observed that in terms of the altitude the number of tracked objects in all the inclination bands followed a mixture of Laplace distributions with eight parameters except for the third band (610, 730) as shown in Figure 5.5. For the third band a single Laplace distribution with just two parameters alone was sufficient. It was noted that the parameters corresponding to the different bands did not vary significantly across the years.

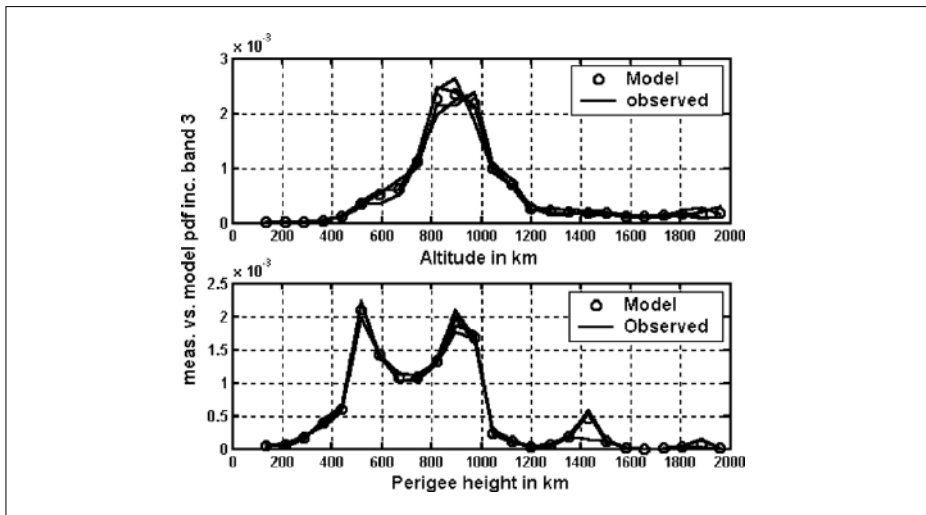


Figure 5.5: Comparison of number density of debris from measurements and model distributions in inclination band (61°, 73°)

Though in general there was quantitatively increasing number of space debris the structure of the SIMPLE model brought out the qualitative quasi-equilibrium structure of the conglomeration of the debris due to the source mechanisms like launches, breakups, rain down effect and sink mechanisms such as decay due to drag. The characterization provided by the SIMPLE model gave an insight through the probability distributions about the orbital debris environment in LEO. A Monte Carlo simulation of the debris using the parameters in the SIMPLE model could be used to obtain the closest approach, in a statistical sense, to a target object at a given time. After propagating the debris in time in an appropriate environment the varying distance of closest approach and the changing collision risk to the target could be studied. Utilizing the number density distributions from the SIMPLE model estimate the spatial number density of debris per km³ in any given appropriate volume of space could be done. Debris flux denoting the number of debris per m² per year could also be worked out. Those helped in the estimation of probability of collisions of the debris with target objects. As the catalogued data consisted of only objects of large size, to obtain the risk assessment due to other uncatalogued objects, statistical simulation of small debris was essential. A statistical simulation of the complete LEO debris environment was possible by expanding the SIMPLE scenario. The suggestion that was made was that one should look for insightful probability distributions for extending the model to uncatalogued debris of smaller sizes. Such a study could be based on laboratory studies of collisions or explosions that generate debris of all sizes.

5.5 Regularized Luni-Solar Gravity Dynamics on Resident Space Objects

Resident space objects population in highly elliptical orbits are significantly affected by luni-solar gravity. Sellamuthu and Sharma (2021) using regularization developed an analytical orbit theory with luni-solar gravity effects as third-body perturbations in terms of Kustaanheimo–Stiefel (KS) regular elements. Numerical tests with different cases resulted in good accuracy for both short- and long-term orbit propagations. The analytical theory was tested with the observed orbital parameters of a few objects in highly elliptical orbits. The analytical evolution of osculating perigee altitude was found to be concurrent with observed data. Solar perturbation, when compared with lunar perturbation, was established to be dominant over such orbits. Extensive numerical comparison tests of the analytical solution (LSANAL) with the numerically integrated solution (LSNUM) using varying step-sizes and initial conditions revealed high accuracy in position and velocity. The tests revealed that LSANAL was stable for relatively long-term predictions. For both short- and long-term computations, the error evolution was found to be oscillatory owing to the fundamental specificity of the KS space. The relative percentage and absolute errors in position and velocity

were found to be higher in lunar perturbation than in solar perturbation. LANSAL captured the full osculation of the luni-solar perturbations and the evolution of the orbit was analogous to the observed TLEs. The short-periodic oscillation in perigee altitude for the selected cases was found to be between 100 and 500 km for solar perturbation and up to 100 km for lunar perturbation. The sensitivity of the initial conditions on the actual orbital evolution reflected upon the analytical solution accuracy. Two cases A and B are chosen for illustrating the comparison for osculating perigee altitude (hp) computed from KANSAL and TLEs, respectively. In case A, hp increases with time elapsed and in case B, it decreases with time.

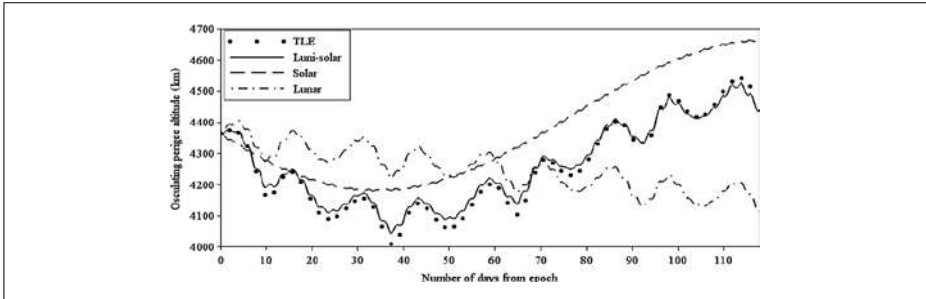


Figure 5.6: Comparison between observed and predicted osculating perigee altitude for Transtage 10 of Titan III C launch vehicle (Case A-NORAD ID: 2770)

The case A with NORAD ID 2770, had mass of 3103 kg. Its initial aosc, eos and ios were 66181.3916 km, 0.837702 and 32.979886 degrees, respectively, at launch epoch of 28 April 1967. The initial osculating perigee altitude (hp) was 4362.972 km. As it is seen in Figure 5.6, even though lunar gravity is decreasing hp, solar gravity is increasing hp, but the osculating perigee altitude computed from the analytical solution with luni-solar gravity matched well with the osculating perigee altitude computed from the TLEs.

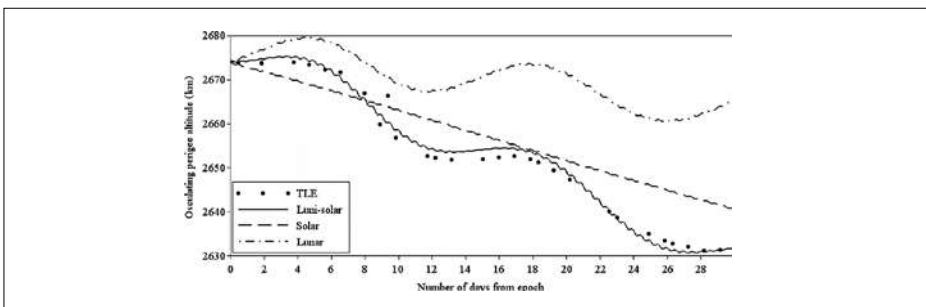


Figure 5.7: Comparison between observed and predicted osculating perigee altitude for H-2A Rocket Body (NORAD ID: 41037)

In Case B, which is a H-2A rocket body which was launched by Japan on 24 November 2015 with osculating perigee and apogee altitudes of 2736 and 35609 km, respectively and inclination of 19.02 degrees, the osculating perigee altitude (h_p) decreases slowly quasi-periodically due to lunar gravity as seen in Figure 5.7. It decreases linearly relatively more due to solar gravity. As seen in the Figure 5.7, a comparison made for 30 days between the observed and the computed osculating perigee altitude (h_p) with lunar and solar perturbations is shown to decrease h_p further. It matches quite well with the observed values of h_p computed from TLEs for 30 days duration.



SDSSARS IN ISRO

Space Debris and Space Situational
Awareness Research Studies



CHAPTER 6

Conjunction Analysis and Modeling

6.1 Introduction

The number of space debris objects in the low Earth orbits, and the breakups in 2007 of Fengyun-1C of intentional collision (ASAT), 2009 of Cosmos 2251 of accidental collision with Iridium 33 and 2021 Kosmos 1408 of Intentional collision (ASAT) have added more risk to the satellites in this region. It was necessary to study the risk of conjunctions in these orbits to plan a future course of action regarding the control and mitigation of space debris objects.

6.2 Statistical Conjunction analysis and Modeling of Low-Earth Orbit Catalogued Objects

A statistical approach to obtain the number of conjunctions in a prescribed altitude bin considering various inclination bands was presented by Anil Kumar and Reddy (2009). The low Earth orbits, which are affected the most by the accumulation of space debris objects, were analyzed with special emphasis on sun synchronous orbits. The study was based on the catalogued objects from the two line element sets. It was observed that, after the major breakup in 2007, the number of conjunctions in the sun synchronous orbital region was highly significant. The second part of the study concentrated on the modeling aspects of spatial density and brought out a stochastic model based on a mixture of Laplace distributions. It was noted from the model that the fragmentation events in low Earth orbit during 2007 had redefined the pattern of spatial density distribution in the region below 1100 km.

A modified version of the Laplace distribution introducing one more parameter, called area parameter, was considered for the modeling. The modified modeling function with the area parameter 'a' is of the form:

$$f(x) = \frac{a}{2s} \exp\left(\frac{-|x - m|}{s}\right)$$

'm' is location parameter and 's' is scale parameter in the modified Laplace distribution.

Figures 6.1, 6.2 and 6.3 showed the match between the observed and modeled spatial density with modified Laplace distribution model for August 2007 data for inclinations of 0 to 180 degrees, 98-99 degrees and 95-105 degrees, respectively. It was noted that the matching in all the three cases was good. Figure 6.4 showed the match between the observed and modeled spatial density with modified Laplace distribution model for December 2006 data for inclination of 95-105 degrees. It might be noted that there was a substantial shift in the second peak after the breakup in 2007. It was concluded that the major breakup during 2007 had redefined the pattern of spatial density in the LEO region.

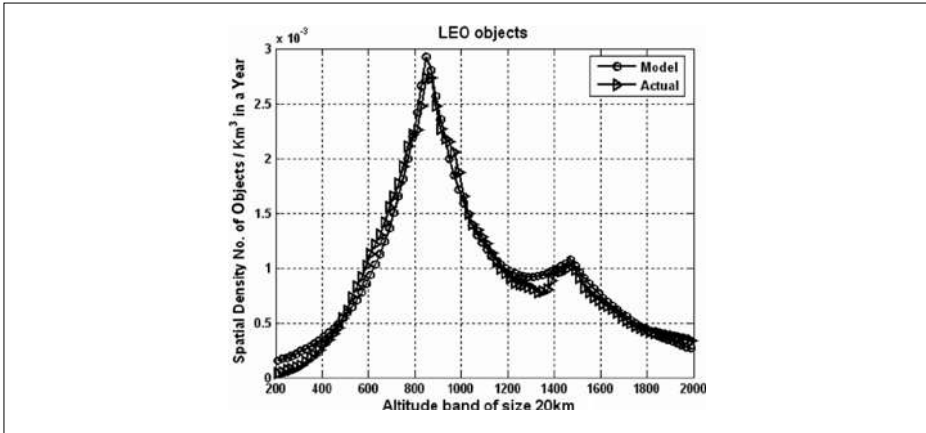


Figure 6.1: Fit of binary mixture of the modified Laplace distribution for the Spatial density for the August 2007 data for inclinations from 0-180 degrees

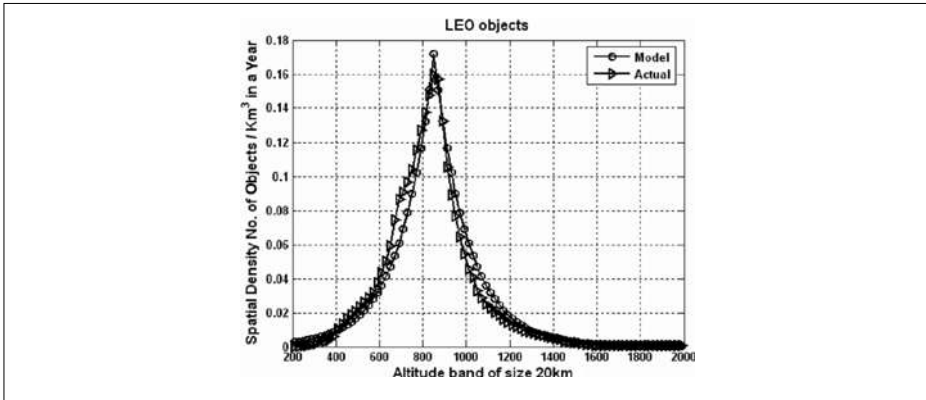


Figure 6.2: Fit of binary mixture of the modified Laplace distribution for the Spatial density for the August 2007 data for inclinations of 98-99 degrees

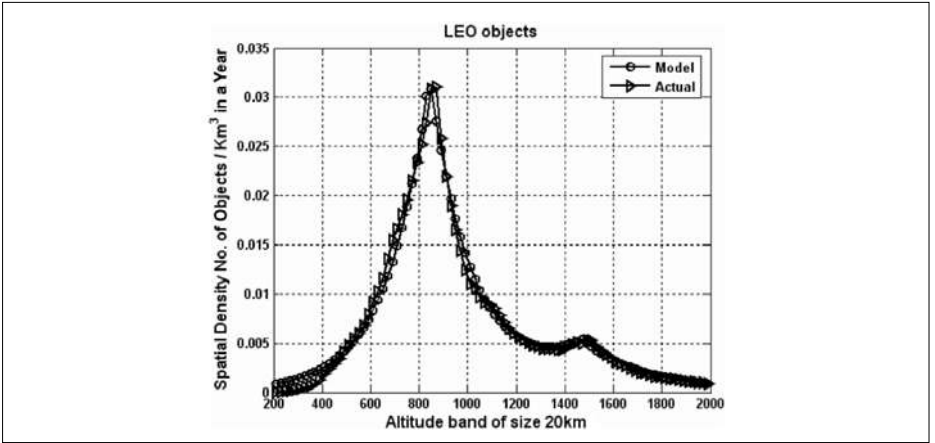


Figure 6.3: Fit of binary mixture of the modified Laplace distribution for the Spatial density for the August 2007 data for inclinations of 95-105 degrees

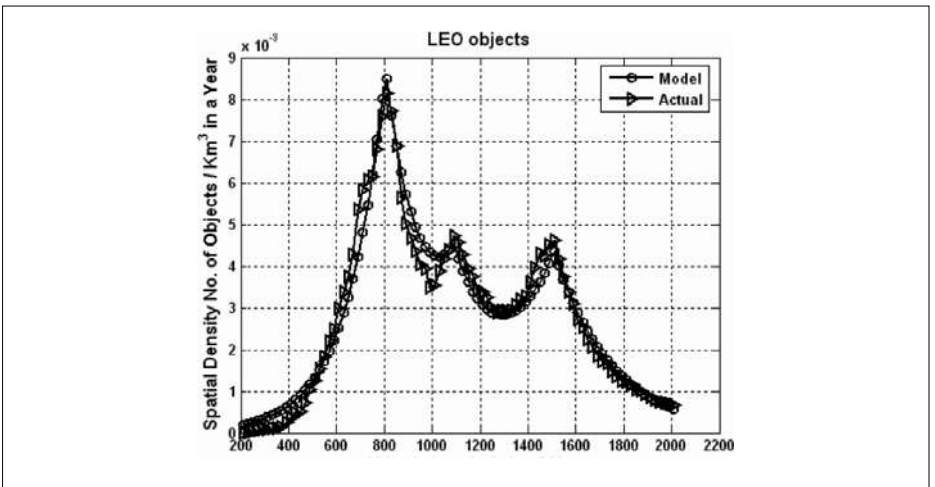


Figure 6.4: Fit of binary mixture of the modified Laplace distribution for the Spatial density for the December 2006 data for inclinations of 95-105 degrees

The events that occurred after 2007 such as Chinese anti-satellite test, explosion of Briz-M upper stage, break up of Cosmos-2421 and collision of Cosmos-2251 with Iridium-33 satellites had changed the spatial density patterns appreciably in low earth orbits. This has increased the risk of collision between active satellites and debris created by them.

Reddy et al. (2011) presented an algorithmic procedure for automatically estimating exact model parameters corresponding to the peak location and number of peaks using wavelets that will speed up the parameter estimation process for the models with peaks and was found to be useful in finding exact location parameters of peaked distributions such as mixtures of Laplace distribution. The proposed methodology was applied to April 2010 TLE data. A new peak position at 765 km was observed in all inclinations from 0 to 180 degrees, attributing to the new collisions and explosions that occurred during August 2007 to April 2010, as shown in Figures 6.5 to 6.7.

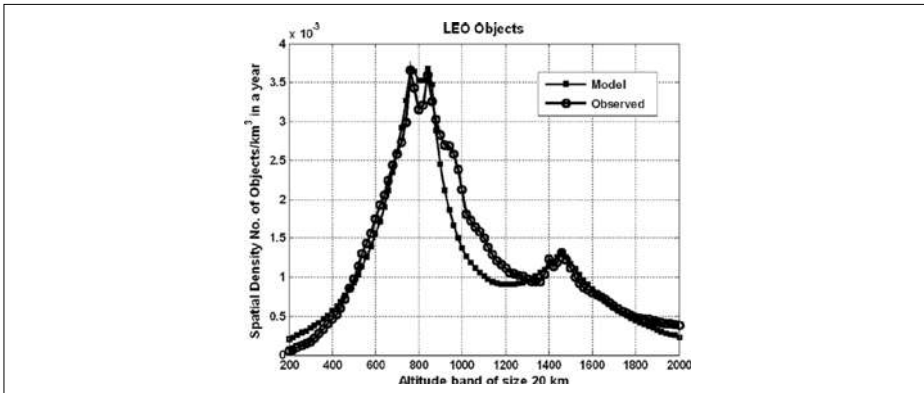


Figure 6.5: Fit of tertiary mixture of the modified Laplace distribution for the Spatial density for the April 2010 data for inclinations from 0–180 degrees

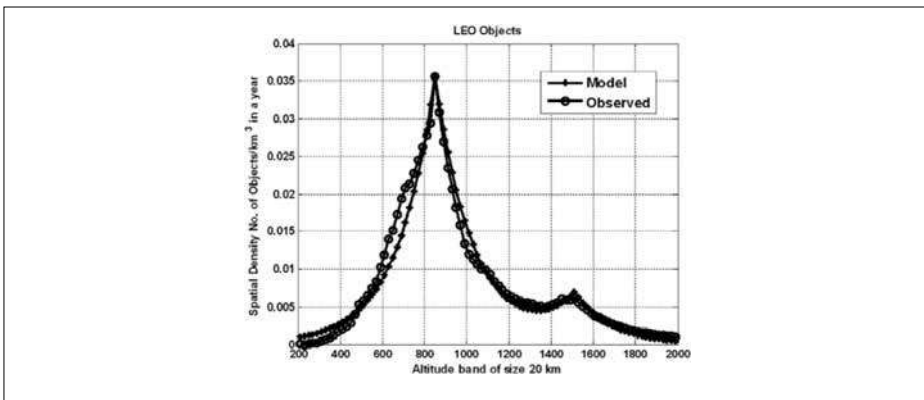


Figure 6.6: Fit of tertiary mixture of the modified Laplace distribution for the Spatial density for the April 2010 data for inclinations from 95–105 degrees

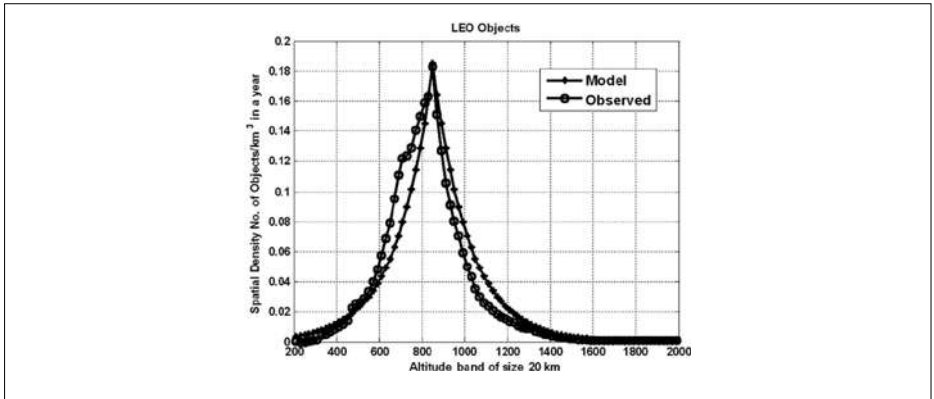


Figure 6.7: Fit of tertiary mixture of the modified Laplace distribution for the Spatial density for the April 2010 data for inclinations from 98–99 degrees

6.4 Analytical methods for pre-filtering of close approaches between space objects

Raj and Mutyalarao (2013) carried out a study related to the pre-filtering of close approaches between the space objects using the analytical techniques. The methodology was found effective in reducing the number of objects for simulation. A numerical experimentation was performed with a model consisting of 23544 LEO-crossing simulated objects. The first object was chosen as primary and other 23543 objects were chosen as secondaries. A separation distance of 100 meters was considered. After applying the filtering techniques, 8579 objects were pre-filtered by perigee-apogee pre-filter and 14675 objects by geometrical pre-filter. So, total numbers of objects pre-filtered were 23254. Hence, the job became much easier with only 289 secondaries to be considered for long-term conjunction analysis.

6.5 Collision Avoidance Analysis for ISRO Launch Vehicles

Gupta et al. (2014a) carried out the close approaches to launch vehicle during its ascent and satellite in its first orbit using close approach tool of STK. Several pre-filters were used to reduce computational time. The computation was carried out for entire launch window in very small intervals.

COLA analysis for a LEO mission is illustrated using the PSLV-C54 mission as an example. This mission launched EOS-06 satellite as its primary payload along with 8 other piggy-back satellites the nominal lift-off time was 26th Nov 202 06:26:00 UTC.

A launch window of 10 minutes was subjected to COLA analysis. Figure 6.8 shows the time instances not-cleared for launch because at least one of the objects being launched was violating the COLA probability threshold. In this mission the nominal liftoff time was cleared because none of the launched objects violated the COLA thresholds for the nominal lift-off time.

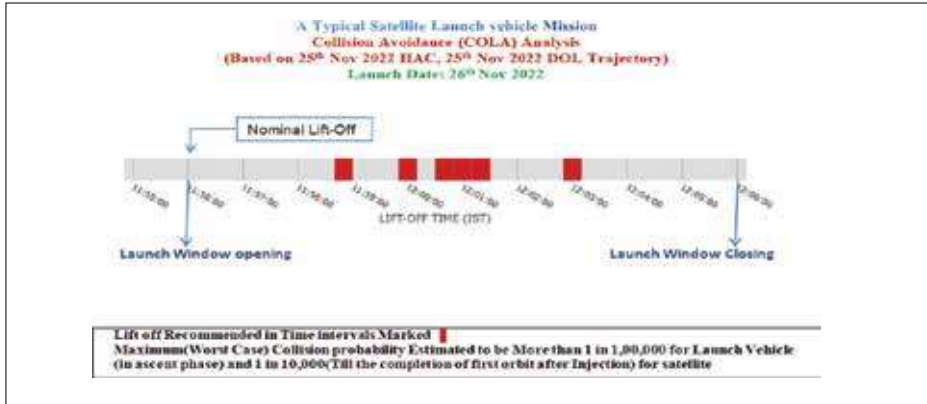


Figure 6.8: COLA analysis for a typical LEO mission on the launch day

Table 6.1: Close conjunction objects within launch window (only 2 piggy-back satellites are included for brevity)

Threat Object	NORAD ID	Min. Dist. (km)	Collision Probability	Lift-Off Time (IST) 26.11.2022	TIME FROM LIFT-OFF
Threat objects with satellite EOS-06					
THOR ABLESTAR DEB	15783	0.296	1.78E-04	11:55:29.418	4436.835
FENGYUN 1C DEB	30898	0.231	2.57E-04	11:58:49.339	1990.052
FENGYUN 1C DEB	30437	0.363	1.18E-04	12:01:19.007	3452.830
COSMOS 2251 DEB	36000	0.069	3.22E-03	12:03:02.417	6544.401
Threat objects with piggy-back satellite-1					
SL-24 DEB	27611	0.099	6.71E-04	11:55:25.115	11204.086
FENGYUN 1C DEB	30898	0.164	1.10E-04	11:58:49.314	1990.063
STARLINK-2460	48120	0.110	6.92E-04	12:00:26.240	5609.724
ARIANE 3 DEB	27740	0.450	1.51E-04	12:03:57.278	6421.647
STARLINK-1462	45770	0.095	9.30E-04	12:05:10.728	5612.562
STARLINK-2468	48127	0.202	2.06E-04	12:05:54.530	5611.931

Threat Object	NORAD ID	Min. Dist. (km)	Collision Probability	Lift-Off Time (IST) 26.11.2022	TIME FROM LIFT-OFF
Threat objects with piggy-back satellite-2					
SL-24 DEB	27611	0.047	2.95E-03	11:55:25.177	11204.026
FENGYUN 1C DEB	30898	0.164	1.10E-04	11:58:49.314	1990.063
STARLINK-2460	48120	0.110	6.92E-04	12:00:26.240	5609.724
ARIANE 3 DEB	27740	0.450	1.51E-04	12:03:57.278	6421.647
STARLINK-1462	45770	0.095	9.30E-04	12:05:10.728	5612.562
STARLINK-2468	48127	0.202	2.06E-04	12:05:54.530	5611.931

6.6 Space Object Proximity Analysis for Indian LEO Satellites

The Indian remote sensing satellites are operating in low Earth orbit region which is heavily populated. The current debris population poses a risk of collision to IRS (Indian Remote Sensing) satellites which are exposed to this environment. In this regard, space object proximity analysis is carried out to assess threats to Indian low Earth satellites from the space objects. Gupta et al. (2014b) outlined the elements of space object proximity analysis (SOPA) carried out for Indian low Earth satellites on daily basis and conjunctions with close approach distance less than 1 km are monitored. In case where maximum collision probability of conjunctions exceeds the threshold limit, collision avoidance manoeuvre strategy is formed and is provided to satellite team. Some of the cases where Indian satellites are maneuvered to avoid close conjunctions are discussed.

6.6.1 SOPA Methodology and Analysis Tool

SOPA is carried out with integrated software comprise of commercial tool STK and interface modules developed in MATLAB to automate the procedure. The interface modules facilitate input/output processing, automatically feed input and fetch output to STK and to compute collision probability of all conjunctions with close approach distance less than 5 km. State vectors / ephemeris of LEO/GEO satellites are received daily through mail/ftp links. TLEs and SP ephemerides of RSOs are downloaded from space-track and for the analysis. The state vectors are propagated through a numerical propagator while the TLEs of resident space objects are propagated using SGP4 theory. Close approaches during next 7 days are computed using close approach tool of STK. The conjunctions with close approach distance less than 5 km are extracted and maximum collision probability is computed. A formatted report is sent to team concerned. Figure 6.9 shows the flow chart for SOPA analysis.

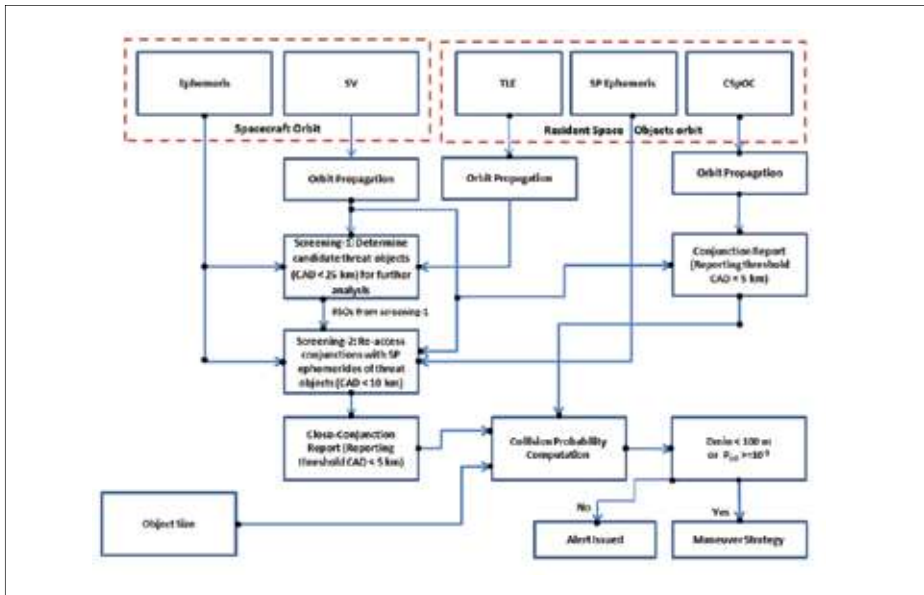


Figure 6.9: SOPA flow chart

6.6.2 Satellite Orbit Propagation

Satellite state vectors are propagated for seven days using numerical propagator (HPOP-High Precision Orbit Propagator) of STK. The details of the force model considered in propagation are provided in Table 6.2.

Table 6.2: Details of Force Model

S. No	Force Model	Details
1.	Earth Gravity	WGS84_EGM96, 36 x 36
2.	Drag Force	Atmospheric Model: Jacchia-Roberts Solar and geomagnetic flux: Flux/AP value from space weather file Area to mass ratio of satellite
3.	Third Body Perturbation	Sun and Moon
4.	Solar radiation Pressure	Cr=1.5; Area to mass ratio of satellite

The close approaches for the satellites in the analysis are computed using close approach tool of STK. Close conjunctions are computed between IRS satellites and resident space objects. Several pre-filters are used to reduce computational time. The basic idea behind close approach processing is to first eliminate population as possible via geometric properties, which takes considerably less time than fully propagating these satellites and then computing close approaches. The final determination of the existence of close approaches is always done by sampling the ephemeris of the candidate and reference objects. The pre-filters available as part of Close Approach processing in STK are out of date pre-filter, apogee/perigee pre-filter, orbit path pre-filter and time pre-filter. These filters are computationally inexpensive methods for limiting the number of objects and the periods of time for which brute force searching is needed. The proper use of the pre-filters reduces the amount of time needed for close approach processing. After all pre-filters are applied, the range filter is used to determine the final list of close approach objects specified ranges are listed along with conjunction epoch.

6.6.3 Operational Examples

IRS Satellites have been maneuvered several times for mitigating high-risk close conjunctions. Based on SOPA analysis, collision avoidance maneuvers were carried out 14 times for LEO Satellites in the year 2022. Details of these maneuvers are listed in Table 6.3. The collision avoidance maneuver was executed between 1.2 to 16.2 hours before the TCA. Most of the maneuvers were executed at least 6 hours before TCA. Only one maneuver required normalization maneuver to maintain satellite ground track after CAM. All other mitigation maneuvers were optimized to serve as regular ground track maintenance maneuvers as well.

Table 6.3: Details of Collision Avoidance Maneuvers for LEO spacecraft carried out in 2022

#	Satellite	Threat Object (NORAD ID)	Conjunction Epoch(UTC)	Close approach Distance (km)	Maneuver Epoch	Maneuver ΔV (m/s)
1	CARTOSAT 2B	IRIDIUM 33 DEB (35739)	17-Jan-22 08:01:59	0.123	17-01-2022 06:48:00	-0.1
2	CARTOSAT 2E	COSMOS 1674 (15944)	24-Jan-22 21:49:30	0.121	24-01-2022 12:46:00	0.03

#	Satellite	Threat Object (NORAD ID)	Conjunction Epoch(UTC)	Close approach Distance (km)	Maneuver Epoch	Maneuver ΔV (m/s)
3	CARTOSAT 2E	COSMOS 1408 DEB (49539)	23-Mar-22 04:18:18	0.08	22-03-2022 15:09:00	0.11
4	CARTOSAT 2A	FENGUN IC DEB (37013)	28-Mar-22 13:40:39	0.091	28-03-2022 11:37:00	0.04
5	ASTROSAT 1	FENGUN IC DEB (30596)	01-Apr-22 19:54:34	0.05	01-04-2022 08:48:03	0.043
6	MEGHATROPIQUES 1	UNKNOWN (81259)	05-Apr-22 01:10:40	0.067	04-04-2022 13:11:00	0.05
7	SARAL	COSMOS 407 (5174)	18-Apr-22 19:28:28	0.157	18-04-2022 11:17:01	0.028
8	IRS-P6	COSMOS 1900 DEB (43499)	08-May-22 18:49:19	0.062	08-05-2022 13:06:00	0.016
9	EOS-04	ASTROCAST (48952)	21-Jun-22 20:05:41	0.005	21-06-2022 13:50:23	0.01
10	EOS-1	SL-14 R/B (10096)	26-Jul-22 01:18:50	0.131	25-07-2022 16:20:00	0.07
11	RESOURCESAT 2B	CSI(49261)	18-Aug-22 13:26:46	0.096	18-08-2022 10:15:00	0.07
12	CARTOSAT 3	COSMOS 1707 (16326)	08-Sep-22 00:48:58	0.108	07-09-2022 08:35:00	0.02
13	RESOURCESAT 2A	DMSP 5D-2F13 DEB (42259)	15-Sep-22 01:38:23	0.052	14-09-2022 13:18:00	0.015
14	SARAL	FENGUN IC DEB (30949)	21-Sep-22 16:47:58	0.052	21-09-2022 11:45:23	0.06

6.7

On-Orbit Collision Probability in LEO Using SIMPLE Model

Anil Kumar et al. (2003b) dealt with the application of SIMPLE model in predicting the probability of collision of large objects with respect to a target body in LEO based on Poisson probability distribution and kinetic theory of gases. They also discussed the application of SIMPLE Model in the analysis of closest approach based on MC

technique and extreme value distributions. SIMPLE Model provides the spatial density with respect to altitude for objects below 2000 km and eccentricity less than 0.2, through a tertiary mixture of Laplace distributions, which is characterized by 8 parameters, namely, three location, three scale and two weight, for the whole inclination band as well as five separate inclination bands, namely, (0, 36), (36, 61), (61, 73), (73, 91) and (91, 180).

Based on the assumption that the probability of more than one collision is negligible and by applying the arguments to a confined volume in space, the collision rate between a specified object and all other objects in a given volume can be found for an interval of time. Hence the probability depends on the object's cross-sectional area (A), average spatial density of all other object (S), the average relative velocity (V) between the target object and other objects under consideration and the time (T). This paper provides the comparison of the present estimates of collision probability for different target orbits with the collision probability predictions using the NASA DAS Version 1.53 Model. It was noted that the results are well compared as seen from Table 6.4.

Table 6.4: Comparison of collision probability prediction between SIMPLE and DAS

Description	DAS prediction	SIMPLE prediction
Case-1: 500 Km circular, 1m ² and 1 year	1.192 e -6	0.81 e-6
Case-2: 700 X 400 km elliptic, 1m ² and 1 year	1.609 e -6	1.27 e -6
Case-3: 1185 X 835 Km elliptic, 11 m ² and 10 year	5.4 e-4	3.2 e-4

6.8

A Proposed Reference Collision Probability Estimation Model of the Space Debris Scenario

probability of target spacecraft with space debris and classified them into various levels (including the proposed reference model) based on the sophistication and usage in practice. The proposed reference model is neither too simple nor complex in terms of the scenario or the calculation and is based on the closed form expressions for the decay time of an object in circular orbit due to atmospheric drag alone. Utilizing the simple expression for the decay time of a debris fragment from an altitude (H) to a target altitude (H₀) the limiting ballistic coefficient 'B' could be estimated. Then during a specified time period of say one year it is now simple to formulate a three-dimensional table of (H₀, H, B). Next in order to assess whether a debris object has a chance for collision the required ballistic coefficient for a target

altitude is calculated from the look up table. If the ballistic coefficient of the debris object is more than the calculated value, the object will sweep through the target altitude within a year; otherwise, it does not pose a threat to the target. This process can be continued for all the debris objects and an estimate of the number of objects reaching or sweeping through the target altitude in a year can be made. From this information the probability of collision in a year due to the debris cloud, or the debris scenario in any model can be obtained. A comparison of the estimated probabilities using the present approach with those from other models is also presented. This reference collision probability is very useful for comparison with the results from more sophisticated atmospheric environment models accounting for the solar flux F10.7 and magnetic index Ap and other perturbations as well as orbital characteristics.

6.8.1 Comparison of the Present Results with Other Models

Comparison of the collision probability obtained through the present approach with that of obtained from “ORDEM96” and “MASTER2000” was made. Only TLE background was considered for “MASTER2000” application and the epoch considered was the same as that of the TLE sets used for the present approach validation. For “ORDEM96” application the objects of size above 8 cm were considered. The collision probabilities were estimated based on a 10 km bin size for altitudes. Table 6.5 provides a comparison between different models. It may be noted from Table 6.5 that the results are comparable, and match is good in lower altitudes. The differences in the collision probabilities can be attributed to the fact that any two models would not provide exactly matching results due to the differences in the underlying assumptions on probability distributions, source models and terms and evolution models. Essentially this is due to the differences in the specification of the sample space. However, most estimates are well within one order of magnitude. It may be noted that the present model and the Poisson model provide conservative values of the collision probabilities which are quantitatively higher than MASTER and ORDEM predictions as the inclination was not taken into account.

Table 6.5: Comparisons of Collision Probabilities at different Target Altitudes

Sl. No	Tar	Tar	Collision Probability				
	Alt.	Incl.	Pres.	Poiss.	MC	MAS	ORD
	In km	In deg	Mod*	Mod*	Ext. value	TER 2000	EM 96
1.	500	28.5	5.8e-7	6.4e-7	2.8e-7	3.9e-7	3.9e-7
2.	600	28.5	2.8e-6	2.7e-6	1.8e-6	8.8e-7	9.6e-7
3.	700	28.5	2.5e-6	2.6e-6	3.1e-6	8.8e-7	2.1e-6

*Inclination is not included.

6.9 Selection of optimal collision avoidance manoeuvre by evolutionary algorithms

Bandyopadhyay et al. (2004c) described the methodology for the selection of optimal collision avoidance manoeuvre strategy for an orbiting spacecraft. Since, any orbital manoeuvre required certain amount of precious on-board propellant it was highly desirable to find out an optimal strategy for collision avoidance manoeuvre. The problem of optimal avoidance manoeuvre was a constrained optimization problem with four parameters, namely, imparted velocities in three orthogonal directions and the time of application of impulse. The minimization of collision probability was performed by an optimization code based on genetic algorithms. The methodology was successfully tested with a typical representative set of resident space objects.

6.9.1 Input Data Set for Space Debris Proximity Analysis

For the analysis a typical representative set of resident space objects was taken. The distributions of about 8300 objects according to their respective semi-major axis, eccentricity, inclination, argument of perigee, right ascension of ascending node and true anomaly are presented in Figure 6.10. The detection of close approaches to the spacecraft of interest during a day is an important subset of the overall problem. The maximum collision probability for a single close conjunction event is given as

$$P_{col} = \frac{4}{\pi e} \left(\frac{R_s}{R_{min}} \right)^2$$

Here, R , and R_{\min} are effective collision radius and minimum approach distance, respectively. The spacecraft of interest has the following osculating elements at the starting time for the analysis

Semi-major axis (a)	=	6987.507324 km
Eccentricity (e)	=	0.005758
Inclination (i)	=	67.860298 ⁰
Argument of Perigee (ω)	=	312.023285 ⁰
Right Ascension of Ascending Node (Ω)	=	101.23300 ⁰
True Anomaly (θ)	=	48.088917 ⁰

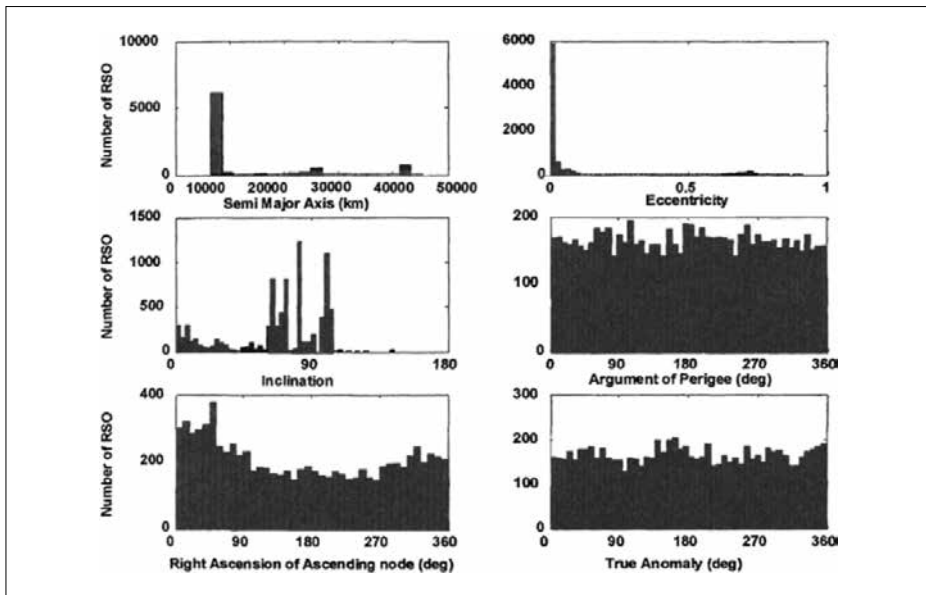


Figure 6.10: Distribution of Resident Space Objects (RSO)

For the present analysis, a very low order orbital propagation model has been adopted. The model accounts for the oblateness of the Earth (J_2 effect) through changes in argument of perigee (ω), right ascension of ascending node (Ω) and mean anomaly (M). The drag has been neglected in the present analysis. It is assumed that osculating orbital elements of the spacecraft of interest as well as those of other resident space objects are available at the starting point of the analysis. The simplest way to predict a close conjunction event is to move forward in time along the trajectory of two spacecrafts and to compute the distance between these two at some regular intervals. Based on this information, the exact minimum approach distance and time can be easily evaluated by any one-dimensional gradient-based

optimization scheme. The conjunction event detection algorithm also uses apogee-perigee filter in order to eliminate resident space objects which cannot come closer than a minimum specified miss distance. The mathematical formulation of various filters is described by Hoots et al. (1984). The maximum probabilities of collision with other resident space objects are computed for duration of one day assuming collision radius of 10 m. The approach window is defined as time span wherein spacecraft of interest and a resident space object remain within 25 km. The results are presented in a Table 6.6.

Table 6.6: Close Conjunction Events with Resident Space Objects without Any Collision Avoidance Manoeuvre

Collision Event	RSO Identification	Minimum Approach Distance (km)	Maximum Collision Probability	Approach Window Entry Time (s)
1	1	20.38	1.12784×10^{-7}	11498.8
2	1120	18.55	1.36144×10^{-7}	4771.19
3	1216	13.21	2.68448×10^{-7}	42296.1
4	2238	20.09	1.16064×10^{-7}	46761
5	3338	22.39	0.93440×10^{-7}	36004.1
6	3338	21.97	0.97056×10^{-7}	38930.1
7	3535	9.47	5.22352×10^{-7}	56607.6
8	3675	23.75	0.83056×10^{-7}	68325.6
9	3739	23.14	1.52432×10^{-7}	56261
10	4288	17.53	1.06128×10^{-7}	18301
11	4646	21.01	1.06128×10^{-7}	5220.52
12	5554	20.66	1.09744×10^{-7}	20720.3
13	5766	22.04	0.96432×10^{-7}	49377.4
14	6537	18.67	1.34384×10^{-7}	59706.1
15	6654	10.36	4.36464×10^{-7}	62561.7
16	6686	21.91	0.97584×10^{-7}	9851.42
17	7116	17.25	1.57424×10^{-7}	49055.7
Total			28.07424×10^{-7}	

If, it is required to reduce cumulative collision probability from the level of 28.07424×10^{-7} , evasive manoeuvre has to be carried out.

6.9.2 Optimal Collision Avoidance Manoeuvre Strategy

When the cumulative collision probability is unacceptably high, evasive manoeuvre is undertaken. The problem of optimal avoidance manoeuvre is treated as a constrained optimization problem with four parameters, namely, imparted velocities in three orthogonal directions ($\Delta V\theta$, ΔVn , ΔVr) and the time of application of impulse (tf). The objective function is the cumulative collision probability for a specified

duration. The changes in the orbital elements of the spacecraft of interest, upon application of impulse, are computed by Lagrange's planetary equations.

The secular changes in the orbital elements of the spacecraft of interest that take place between the starting time of analysis and that of the application of impulse, are computed by including the secular effects of J2 on ω , Ω and M . The cumulative maximum collision probability was minimized using optimization techniques based on genetic algorithm under constraints on ΔV and t_f . The optimal collision avoidance strategy is presented through a flowchart in Figure 6.11.

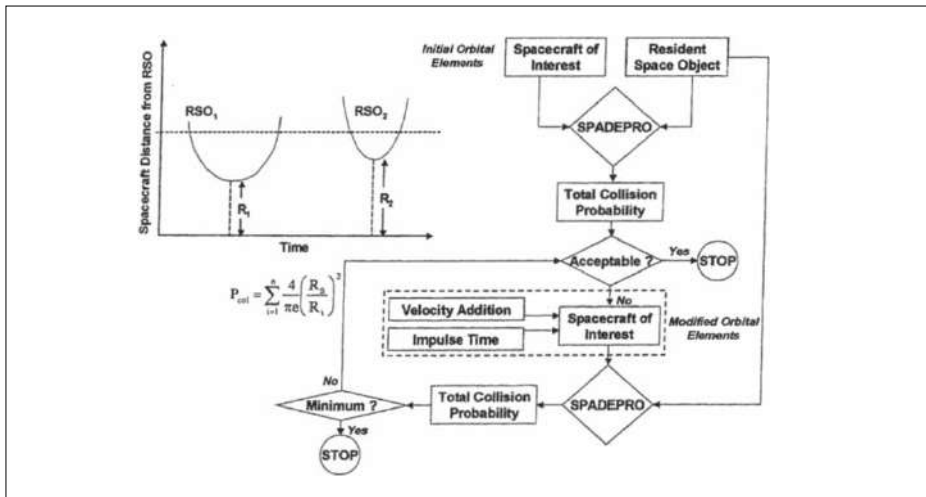


Figure 6.11: The Strategy for Optimal Collision Avoidance Maneuver

In the first case, the cumulative maximum collision probability was minimized under the assumption that velocity addition in any direction was not more than 20 m/s. To determine the bound on the time of application of impulse, results presented in the Table 6.6 were analyzed. It was found out that an object came within 25 km after 4771.19 s from the starting point. So it was decided to impart velocities before that potential collision event could occur. The strategy also ensured considerable reduction in search space. The optimizer based on genetic algorithm was initiated with a population of 30 and was allowed to run for 25 generations. The minimum value of cumulative maximum collision probability was found to be 6.36961×10^{-7} . The velocities imparted in transverse, radial and normal directions were 17.503 m/s, 7.888 m/s and -7.891 m/s, respectively. For this case, the impulse had to be applied at 1611.724003 s after the starting point. The results were presented in Table 6.7.

Table 6.7: Collision Avoidance Manoeuvre to Achieve Minimum Cumulative Collision probability (Case 1)

Collision Event	RSO Identification	Minimum Approach Distance (km)	Maximum Collision Probability	Approach Window Entry Time (s)
1	3535	16.45	1.7280×10^{-7}	50839.1
2	3675	24.67	0.7696×10^{-7}	56749.7
3	3828	21.75	0.9888×10^{-7}	14818.7
4	4958	22.42	0.9312×10^{-7}	51317.6
5	7401	15.49	1.9520×10^{-7}	83261.5
Total			6.3696×10^{-7}	

To investigate further, the projection of objective function was taken on the time line near the optimum value. The values of cumulative maximum collision probability were computed with the converged values of velocity additions required but at different points of time around the minimum. In Figure 6.12, the cumulative maximum collision probability was plotted against the time of application of impulse. It was seen that multiple minima existed and in some points collision probability changed very sharply with the choice of time of application of impulse. In that scenario, an evolutionary algorithm was expected to perform better than a traditional algorithm in finding a minimum.

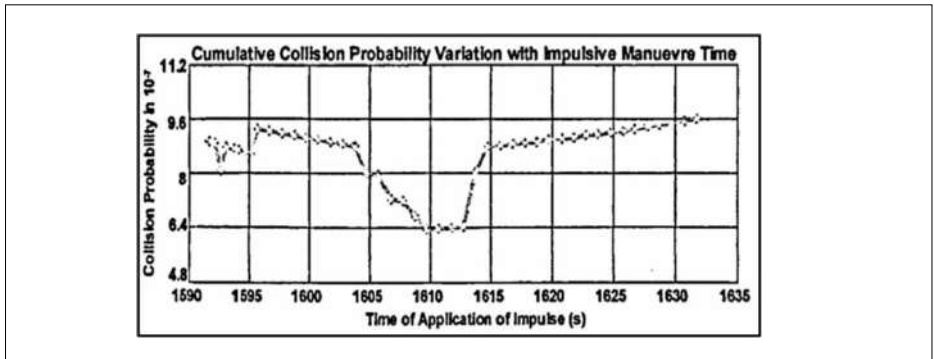


Figure 6.12: Variation of Cumulative Collision Probability with the Time of Application of Impulse

In the second case, total $(AV)^2$ was minimized subjected to a constraint on cumulative maximum collision probability. It is required that cumulative maximum collision probability must be less than equal to 16×10^{-7} . Here, the optimizer based on genetic algorithm was initiated with a population of 30 and was allowed to run for generations. The minimum value of the magnitude of AV was found to be 11.7 14 m/s. The velocities imparted in transverse, radial and normal directions were 0.475 m/s, -11.21 m/s and -0.039 m/s, respectively.

Next, minimum $(AV)^2$ values required to achieve different levels of cumulative maximum collision probability were computed. It was found out that minimum $(AV)^2$ values increase as the required cumulative maximum collision probability values are lowered. The variation in minimum $(AV)^2$ to achieve a specified collision probability was plotted in Figure 6.13.

For this case, the impulse had to be applied at 1729.95 1 165 s after the starting point. The results are presented in a Table 6.8.

Table 6.8: Collision Avoidance Manoeuvre to Achieve Specified Cumulative Collision Probability (Case 2)

Collision Event	RSO Identification	Minimum Approach Distance (km)	Maximum Collision Probability	Approach Window Entry Time (s)
1	3535	16.45	1.7280×10^{-7}	50839.1
2	3675	24.67	0.7696×10^{-7}	56749.7
3	3828	21.75	0.9888×10^{-7}	14818.7
4	4958	22.42	0.9312×10^{-7}	51317.6
5	7401	15.49	1.9520×10^{-7}	83261.5
Total			6.3696×10^{-7}	

The convergence characteristics of optimization scheme for Case 1 and Case 2 are presented below in Figure 6.13.

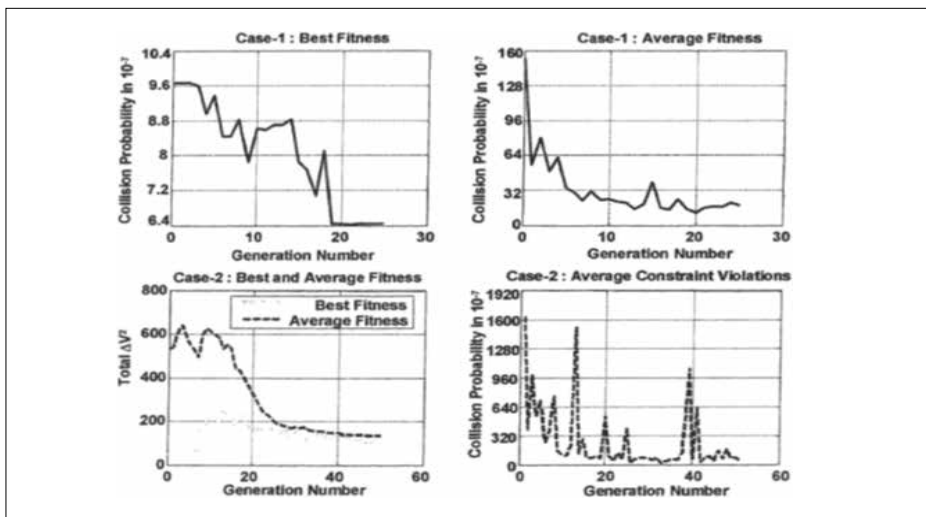


Figure 6.13: Convergence of Genetic Algorithm in Case 1 and Case 2

Next, minimum $(AV)^2$ values required to achieve different levels of cumulative maximum collision probability was computed. It was found that minimum $(AV)^2$ values increase as the required cumulative maximum collision probability values were lowered. The variation in minimum $(AV)^2$ to achieve a specified collision probability was plotted in Figure 6.14.

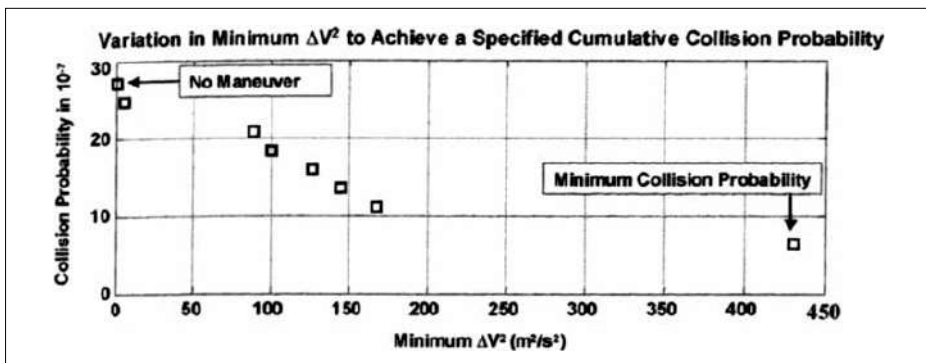


Figure 6.14: Relation between Minimum $(\Delta V)^2$ and Cumulative Maximum Collision Probability

6.10 Recent Collision Avoidance Maneuver Detection and Design

A study on the utility of Space Object Proximity Analysis (SOPA) was presented by Shahjahan et al. (2017). SOPA had been carried out daily using Satellite Tool Kit (STK) to determine threats to IRS satellites from other resident space objects. The analysis of the conjunction was carried out daily using the state vectors of IRS satellites provided by FDO/ISTRAC and the TLE's of the resident space objects for next 7 days. JSpOC (Joint Space Operation Centre) also rendered alerts of possible close conjunction of IRS satellites which were analyzed regularly using SOPA methodology. In case of any critical close conjunction, extensive analysis was carried out and need for CAM (Collision Avoidance Maneuver) of the satellite to avoid the conjunction was assessed.

Maneuver strategy was formulated based on visibility/pass of satellite over tracking stations, fuel availability and time left for conjunction. In order to avoid the conjunction, a small delta velocity (Δv) was given to the satellite well before the time of conjunction which increased the close approach distance. The maneuver could be performed only when the satellite was visible over one of the tracking stations. Thus, the first step to form maneuver strategy was to compute visibility of the satellite over the tracking stations. The visibility was computed and the time of pass of the satellite before conjunction time was chosen for the maneuver. For the selected

pass, Δv was computed which could increase the close approach distance by more than 1 km. It was also ensured that the satellite did not have close approach with any other object in next 7 days after the maneuver. If the maneuver is planned well ahead of the conjunction time, the Δv required would be less. Typically, only 0.01 m/s Δv maneuver was sufficient enough to increase the distance more than 1 km if the maneuver was done at least one day prior to the conjunction.

The change in orbit of satellite due to collision avoidance maneuver was usually followed by orbit normalization maneuver to meet the satellite operational constraints. Orbit normalization maneuver was carried out after the conjunction time was passed. All close conjunctions in next 7 days after orbit normalization maneuver were analyzed and it was ensured that there was no critical conjunction.

In many cases IRS satellites were maneuvered to avoid close conjunctions. During the fourth quarter of 2017, four satellites were maneuvered owing to the risk of collision identified in The SOPA analysis. Details of these maneuvers were listed in Table 6.9. In all the four conjunctions, two maneuvers were carried out on the day of conjunction. Other two maneuvers were carried out before the day of conjunction. In the case of Resourcesat-2A, normalization maneuver was carried out to normalize the orbital constraints.

Table 6.9: Details of Collision Avoidance Maneuvers Carried out during fourth quarter of 2017

Satellite	Threat object	Conjunction Epoch(UTC)	Close approach distance (km)	Maneuver Epoch(UTC)	Maneuver ΔV (m/s)	Maneuver Δa (km)
Resourcesat-2	SL-16 R/B (19120)	23 Sep2017 18:53:03.130	0.177 (1.33e-003)	23 Sep 2017 08:42:20.00	0.0050	0.010
Resourcesat-2A	Fengyun-1C Deb (30201)	14 Nov 2017 21:53:41.369	0.072 (1.41e-003)	14 Nov2017 12:48:00.000	0.01 m/s	0.019
Saral	TANSUO 4 (37931)	3 Dec 2017 04:00:26.937	0.034 (7.69e-003)	02 Dec 2017 12:40:33.777	0.0210 m/s	0.0404
Cartosat-2	Gravity Probe B (28230)	5 Dec 2017 06:31:13.692	0.048 (1.84e-003)	4 Dec 2017 18:36:33.918	0.0420 m/s	0.078

SOPA team notified a conjunction between Resourcesat-2and SL-16 R/B with close approach distance of 177 m with collision probability of 1.33e-03 on 23 September

2017 18:53:03.130 UTC which was within the SOPA threshold. ISTRAC was requested to plan collision avoidance maneuver. In order to avoid the probable collision, maneuver of Resourcesat-2 was planned on 23 Sep 2017 08:42:20 UTC as per the communication with ISTRAC. Detailed analysis was carried out with the details provided by ISTRAC. Table 6.10 provided the close approach distance and collision probability for different ΔV for Resourcesat-2 maneuver planned on 23 Sep 2017 08:42:20 UTC.

A collision avoidance maneuver with highest ΔV (0.0050 m/s) was suggested in this case. Analysis was repeated with latest state vectors of Resourcesat-2 on 23 September 2017 to confirm the collision avoidance maneuver requirement. The close approach distance was increased by 0.418 km, which was beyond the SOPA threshold, hence maneuver was deferred.

Table 6.10: Maneuver Strategy for Resourcesat-2 on 23 September 2017

Delta V (m/s)	Close approach distance (km)	Collision probability	Other threat object in next 7 days
0.0033	0.329	3.85e-04	DELTA 1 DEB(13562) 0.602 km on 25 Sep 2017 12:13:34.925UTC FENGYUN 1C DEB(31847) 0.510 km on 28 Sep 2017 12:50:08.827UTC
0.0050	0.421	2.36e-04	DELTA 1 DEB-13562 0.906 km on 25 Sep 2017 12:13:35.013UTC

JSpOC issued alert on conjunction between Resourcesat-2A and Fengyun-1C debris with close approach distance of 72 m with collision probability of 1.41e-03 on 14 November 2017 21:53:41.369 UTC. The close approach distance and collision probability values for conjunction of Resourcesat-2A with Fengyun-1C debris computed using latest state vector of R2A (14 Nov 2017) and state vector of threat object provided by JSpOC are 58 m and 2.18e-03, respectively, which is within SOPA threshold. FDO/ISTRAC was requested to provide maneuver plan for Resourcesat-2A satellite. Collision avoidance maneuver (CAM) was planned on 14 November 2017 12:48:00.000 UTC with delta V of 0.01 m/s (change in SMA in km = 0.019). SOPA analysis was carried out by considering the state vector of Resourcesat-2A

satellite after the planned Collision Avoidance Maneuver with mid-point epoch of Orbit maneuver as the orbit time epoch. The post orbits maneuver distance of this conjunction is 257 m (with max. collision probability $1.11e-04$) was noticed, which was out of SOPA threshold and no other objects had close conjunctions within 1 km for the next 7 days. As the ground track of this satellite was not within the mission specification Normalization maneuver was planned on 16 November 2017 17:14:01UTC. Based on SOPA analysis, maneuver was cleared and was executed by ISTRAC.

A close conjunction alert between SARAL satellite and TANSUO 4 was notified by SOPA team and the same was confirmed by JSpOC on 2 Dec 2017. A close approach distance of 34 m (Max collision probability of $7.69e-003$) at 04:00:26.937 UTC on 3 Dec 2017 was noticed. Since the close approach distance and maximum collision probability values were within SOPA threshold values an alert notification was issued to FDO, ISTRAC for carrying out the Orbit Maneuver for SARAL satellite. Subsequently, an orbit maneuver was planned for SARAL on 2 Dec 2017 12:40:33.777 UTC with $\Delta v = 0.0210$ m/s ($\Delta a = 0.0404$ km). SOPA analyses with Post Maneuver Predicted State vector of SARAL cleared the OM plan. The post orbits maneuver distance of 722 m (with Max. Collision probability $1.71e-005$) was noticed with TANSUO 4body, which was out of SOPA threshold and no other objects had close conjunctions within 1 km for the next 7 days. This maneuver was carried out on 2 Dec 2017 12.40:33.77 UTC and the post maneuver state vector confirmed the analyses.

SOPA team issued a conjunction alert between CARTOSAT-2 satellite and Gravity Probe B (NORAD No. 28230) to FDO, ISTRAC on 4 Dec 2017. The close approach distance of 148 m between them at 06:31:13.692 UTC on 5 Dec 2017 was noticed. Since the threat object RCS was very large (~ 19.6 m²), the Max. Collision probability ($1.84e-003$) was within SOPA threshold values. An orbit maneuver with $\Delta v = 0.0420$ m/s ($\Delta a = 0.078$ km), was planned for CARTOSAT-2 at 18:36:33.918 UTC on 4 Dec 2017. For the post orbit maneuver, the close approach distance of 608 m (with Max Collision probability of $8.73e-005$) was computed and no other catalogued objects are within 1 km close approach for the next 7 days. Maneuver was cleared by SOPA team to mitigate the close approach.

6.11 Modeling of sunspot numbers

Solar activity prediction had been an important activity of the space science community. Solar flux causes the upper atmosphere density variation and in turn it affects directly the orbital lifetime of the near-Earth satellites. Accurate predictions of the maximum sunspot number and other characteristics of solar cycle are useful inputs for space mission planning, orbital assessments and re-entry time prediction

of risk objects. The sunspot number cycle prediction is a very difficult task owing to high frequency contents, noise contamination, high dispersion levels, and high variability both in the phase and amplitude. In several independent research papers, Sabarinath, Anil Kumar and Beena had presented significant amount of research work on this important topic. Some of the research papers are summarized below:

Sabarinath and Anil Kumar (2008) presented a new approach for describing the shape of 11-year sunspot cycles by considering the monthly averaged values and brought out a prediction model based on the analysis of 22 sunspot cycles from the year 1749 onward. It was found that the shape of the sunspot cycles with monthly averaged values could be described by a functional form of modified binary mixture of Laplace density functions, modified suitably by introducing two additional parameters in the standard functional form. The six parameters, namely two locations, two scales, and two area parameters, characterized the model. The nature of the estimated parameters for the sunspot cycles from 1749 onward had been analyzed and finally arrived at a sufficient set of the parameters for the proposed model. It was seen that the model picked the sunspot peaks more closely than any other model without losing the match at other places at the same time. The goodness of fit for the proposed model was also computed with the Hathaway –Wilson – Reichmann χ measure, which showed, on average, that the fitted model passed within 0.47 standard deviations of the actual averaged monthly sunspot numbers.

Sabarinath and Anil Kumar (2011) presented a stochastic prediction model for the sunspot number cycle. The model was based on a modified binary mixture of Laplace distribution functions and the moving average on the model parameters. A six-parameter modified binary mixture of Laplace distribution function was used for modeling the shape of a generic sunspot number cycle. The model parameters were estimated for all the 23 sunspot number cycles independently and the primary prediction model parameters were derived using a moving average stochastic model. Two correction factors termed as hump factors were introduced to get final predictions. The two different hump factors were derived from the observed sunspot numbers and the estimated model parameters for the modified binary mixture of Laplace distribution function. The hump factors could be applied one at time over the primary prediction model to get final prediction of a sunspot number cycle. The model was used to predict the characteristics of the sunspot number cycle 24. The methodology was validated using the previous sunspot number cycles, which showed the adequacy and the applicability of the prediction model. The statistics of the variations of sunspot numbers at the high solar activity period was used to provide the lower and upper bound for the predictions using the model.

Sabarinath and Anil Kumar (2013) presented Box-Cox transformation and applied to model the sunspot number cycle time series. All the past 23 cycles were modeled

and the sunspot number cycle 24 was predicted using the extrapolation of the estimated model coefficient of the past cycles. The prediction method was validated by predicting the cycles 20 to 23. The model for each cycle was developed by transforming each of the sunspot number cycle using the Box-Cox transformation for a non-zero λ parameter. The parameter λ is estimated in the maximum likelihood sense. Then a cubic polynomial was fitted to the transformed sunspot cycle by suitably adjusting the λ value. Then the inverse Box-Cox transform of the fitted cubic polynomial model was taken as the final model of the sunspot cycle. This model is a function of the transformation parameter λ and the four polynomial coefficients. All the five parameters were estimated through the least square error minimization technique.

Sabarinath and Anil Kumar (2018) presented the sunspot cycle prediction by a hybrid model which employed multivariate regression technique and the binary mixture of Laplace distribution (BMLD) function. The Expectation Maximization (EM) algorithm was applied to the multivariate regression analysis to obtain a robust prediction of the sunspot cycle. Sunspot cycle 24 had been predicted using this technique. Multivariate regression model had been derived based on the available cycles 1 to 23. This model could predict cycle 24 as an average of previous cycles. Prediction from this model had been refined to capture the cycle characteristics such as bimodal peak at the high solar activity period by incorporating a predicted peak sunspot number from the BMLD model. This revised prediction had shown more accuracy in forecasting the major discrete features of sunspot cycle like maximum amplitude, the Gnevyshev gap, time duration from peak-to-peak amplitude, and the epoch of peak amplitude. The refined prediction showed that cycle 24 will be having peak amplitude of 78 with an uncertainty of ± 25 . Moreover, the present forecast says that, cycle 24 will be having double peak with a strong second peak compared to the first peak. This hypothesis was found to be true with the realized data of cycle 24. Further, this technique has been validated by predicting sunspot cycles 22 and 23. A preliminary level prediction of sunspot cycle 25 has also been carried out using the technique presented here. Present study predicts that, cycle 25 also will be a modest cycle like the present cycle 24, and the peak amplitude may vary in a band of 75–95. By combining the multiple regression models and BMLD model we could predict the cycle 24 more accurately. These predicted sunspot cycle profile can be used for predicting the solar flux intensity, and it can be directly used in satellite orbital lifetime prediction tools.

Sabarinath et al. (2020) presented a new model, which was derived from the well-known Maxwell-Boltzmann probability distribution function. A modification had been carried out by introducing a new parameter, called area parameter to model sunspot number cycle using Maxwell-Boltzmann probability distribution function.

This parameter removed the normality condition possessed by probability density function, and fitted an arbitrary sunspot cycle of any magnitude. The new model had been fitted in the actual monthly averaged sunspot cycles and it is found that, the Hathaway, Wilson and Reichmann measure, the goodness of fit is high. The estimated parameters of the sunspot number cycles 1 to 24 have been presented in this paper. A Monte Carlo based simple random search is used for nonlinear parameter estimation. The Prediction has been carried out for the next sunspot number cycle 25 through a model by averaging of recent cycle's model parameters. This prediction can be used for simulating a more realistic sunspot cycle profile. Through extensive Monte Carlo simulations, a large number of sunspot cycle profiles could be generated and these can be used in the studies of the orbital dynamics.

Beena et al. (2021) proposed a model which could unify many of the shape models existing in the literature and showed that the shape of the sunspot number cycle could be described as a product of a polynomial and a negative exponential function. The proposed model had certain free parameters, which were needed to be estimated from the observed sunspot number data. Since all the models reviewed in this paper are a product of a polynomial and a negative exponential along with a number of parameters, it was seen that all these models could be derived from a modified generalized Gamma probability density function by transforming certain parameters and fixing certain parameters. The parameters of the model from the revised monthly averaged sunspot numbers available in the SIDC website were estimated. A preliminary level prediction had also been attempted to forecast the characteristics of sunspot number cycle 25.



SDSSARS IN ISRO

Space Debris and Space Situational
Awareness Research Studies



CHAPTER 7

Space Debris Mitigation and Risk Estimation

7.1 Introduction

The prime objective of the Indian Space Research Organization (ISRO) had been to develop space technology and its application to various national tasks. Since 1969, when it was set up, ISRO had established space systems like the INSAT for telecommunication, television broadcasting and meteorological services, and the Indian Remote Sensing Satellites (IRS) for resources monitoring and management. ISRO had developed the satellite launch vehicles PSLV, GSLV and GSLV MK3 to place these satellites in the required orbits. The primary aim of ISRO's programme is to promote development and application of space science and technology to assist in all-round development of the nation. In the 1980s, ISRO initiated a major revolution in India's communication sector. The Indian national satellite (INSAT) System is one of the largest in the Asia-Pacific region today. The INSAT System provides a variety of communication services in S-band, C-band, Extended C-band and Ku band. It also provides meteorological images through very high resolution Radiometer and CCD cameras. INSAT system serves many other important sectors of the Indian economy. Today, India has also the largest constellation of Remote Sensing Satellites (IRS), which is providing services both at the national and global levels. Great emphasis is placed on the operational use of remote sensing applications in the fields of water resources, agriculture, soil and land degradation, mineral and groundwater exploration, geomorphological mapping, coastal and ocean resources monitoring, environment, ecology and forest mapping, land-use and land-cover mapping. Unfortunately, over a period of time, international space initiatives have left behind a plethora of space objects that no longer serve any useful functions, but pose risk to space operations. Thus, space debris becomes an important subject for all space faring nations in particular and humanity in general. The milestones in the space debris mitigation measures in India are described in Adimurthy and Ganeshan (2006).

The space debris activities in ISRO have been addressed in the design and operational phases of its launch vehicle and satellite programs. In the design of PSLV final stage, which uses earth storable liquid propellants, a propellant venting system has been designed. ISRO's launch vehicle, GSLV, also employs passivation of the Cryogenic Upper Stage at the end of its useful mission. The ISRO's communication satellites in Geo-synchronous orbit (GSO) are designed with adequate propellant margins for re-orbiting to a higher orbit at the end of their useful life. The strategy is implemented on a case-by-case basis consistent with national service requirements. The propulsion systems, by design, are built as integrated systems with the spacecraft bus and payload. The propulsion system is not separated in orbit. Also, these are liquid propulsion systems and the ejecta do not contain any solid particles. In the operational phase, the last stage of PSLV has been passivated beginning with PSLV-C4, which was successfully launched on 12th September 2002. The options considered for implementation of passivation are presented here. The pressure measurements during the flight were telemetered indicating the successful implementation of passivation of the stage. With the implementation of this passivation, the possibility of on orbit fragmentation has been minimized in all the future flights of PSLV. India's launch vehicles, PSLV and GSLV, and the satellites IRS, INSAT and GSAT series are designed in such a way that no operational debris is created in the launch and deployment phases of the mission.

At the end of mission, the GEO satellites are planned to be re-orbited in accordance with the IADC guidelines. Also, the batteries are safed in order to prevent an orbit explosion. An example of the GSO satellite re-orbiting was presented in Parameswaran (2003). The analysis of close approaches of space debris with active ISRO spacecraft was carried out on a routine basis at the operational centers. ISRO developed the models and software to predict the close approach of any of the debris to the functional satellites as described by Bandyopadhyay et al. (2004a). The software are being regularly used during the control and management of the orbiting spacecraft, and are especially useful during the relocation of the geo-stationary satellites from one orbital slot to another orbital slot. The analysis software can also be used for planning the launch window. The planned lift-off time of PSLV-C4 launch vehicle in September 2002 was modified by a few minutes to avoid possible close approach by some of the existing space debris. In the area of analytical modeling related to fragmentation, a number of approaches were developed to study the evolution of break up fragments (Ganeshan et al., 1988; Ganeshan and Ananthasayanam, 1996, 1997; Ganeshan et al., 2001; Ananthasayanam et al. 2002, 2003; Anil Kumar et al. 2002, 2003 and Sharma et al. 2004a). Further modeling of fragmentation and subsequent decay of space objects in LEO and Geostationary Transfer orbit (GTO) were made by

Anil Kumar and Subba Rao (2002) and Bandyopadhyay et al. (2004a). In the area of protection, hypervelocity impacts, a study was made using finite element techniques by Mathew (2003). As a member of the UN Committee on the Peaceful Uses of Outer Space (UNCOPUOS), and through ISRO's membership in the Inter-Agency Space Debris Coordination Committee (IADC), India is contributing significantly to the international efforts and activities in the field of space debris. This commitment is amply reflected in its earlier hosting of the 21st and 28th IADC Meetings in Bangalore and Thiruvananthapuram during March 2003 and March 2010, respectively.

7.3 Passivation of upper stages

On-orbit explosions of spacecraft and upper stages create a substantial portion of the space debris. More than 40% of the catalogued space debris originated from such explosions. These breakups are caused by a wide variety of causes: battery failure, over-pressurization and/or ignition of fuels, accidental collisions, deliberate detonation, etc. Over 260 cases of on-orbit fragmentations are reported so far. Glimpses of some major breakup events are given in Table 7.1 (Anz-Meador et al., 2022).

Table 7.1: Top debris creation events

Object	Year	Pieces	Reason
Fengyun-1C	2007	3,549	Intentional collision (ASAT)
Kosmos 2251	2009	1,716	Accidental collision with Iridium 33
Kosmos 1408	2021	1,562	Intentional collision (ASAT)
STEP 2 Rocket Body	1996	756	Residual propellant explosion
Iridium 33	2009	659	Accidental collision with Kosmos 2251
Kosmos 2421	2008	511	Disintegrated
SPOT 1 Rocket Body	1986	506	Residual propellant explosion
Parus	1981	482	Battery explosion
OV2-1 Rocket Body	1965	473	Engine explosion

Analyses of accidental fragmentation for both spacecraft and upper stages have shown that vehicle passivation, i.e. removal of all forms of stored energy, would

eliminate most such events. Effective measures include the expulsion of residual propellants by burning or venting, the discharge of batteries, the release of pressurized fluids, safing of unused destruct devices, etc. Though studies on passivation of upper stage were initiated much earlier, the breakup of PSLV-C3 R/B has accelerated the implementation of passivation scheme in the upper stage of PSLV from C4 mission onwards. Passivation of the upper stage is successfully implemented in the stage design to avoid any explosions after its useful purpose is completed. The following options were considered for passivation of PS4:

- Venting the trapped propellants and subsequently the pressurant through the main engines in a sequential manner by opening the main engine valves.
- Consuming the total propellants by restarting the main engines.
- Consuming the propellants by firing the reaction control thrusters meant for attitude stabilization.
- Venting the propellants through an additional branching in the feed lines of each propellant using separate pyro valves added in the circuit.
- Venting the pressurant gas from the propellant tank and gas bottles along with the propellant vapors in the tanks through an additional branching in the pressurization lines of each tank using separate pyro valves added in the circuit.

The last option considered was selected for the passivation of PS4 stage due to its simplicity and safety to the separated spacecraft. In course of the design of the passivation system the following specific problem areas were addressed to and required corrective measures were incorporated in the design:

- Buckling of tank common bulkhead during passivation. MON-3 compartment is vented first to have a positive pressure in MMH tank.
- To avoid exhaust plume interaction with the structure, location of the vent nozzles was selected to eliminate the interaction zone between the exhaust plume and the structure.
- To avoid contamination of the spacecraft, sufficient time gap is given before initiating passivation after spacecraft separation.
- Propellant freezing during passivation. Experiments with MON-3 gas in high altitude test facility indicate no freezing of propellants. Thermal analysis also corroborates this.

Pressure measurements telemetered during the flight of PSLV-C4 substantiated the successful implementation of the passivation scheme. ISRO's launch vehicle, GSLV, also employs passivation of the cryogenic upper stage at the end of useful mission. A detailed analysis was made on the fragmentation of the PSLV-C3 Upper Stage, which took place before the implementation of passivation. The pre-fragmentation orbit of the rocket body was 550 km×675 km, with an inclination of 97.9°. 371 catalogued fragments were generated in this explosion. By 1st October 2023, 317 fragments had

decayed and only 54 have remained in orbit. A pictorial representation of the decay till 1st October 2023 is shown in Figure 7.1. Different deterministic and stochastic models, developed in ISRO, for fragmentation events, are reported in (Ganeshan et al., 1988; Ganeshan and Ananthasayanam, 1996, 1997; Ganeshan et al., 2001; Ananthasayanam et al. 2002, 2003; Anil Kumar et al. 2002, 2003 and Sharma et al. 2004).

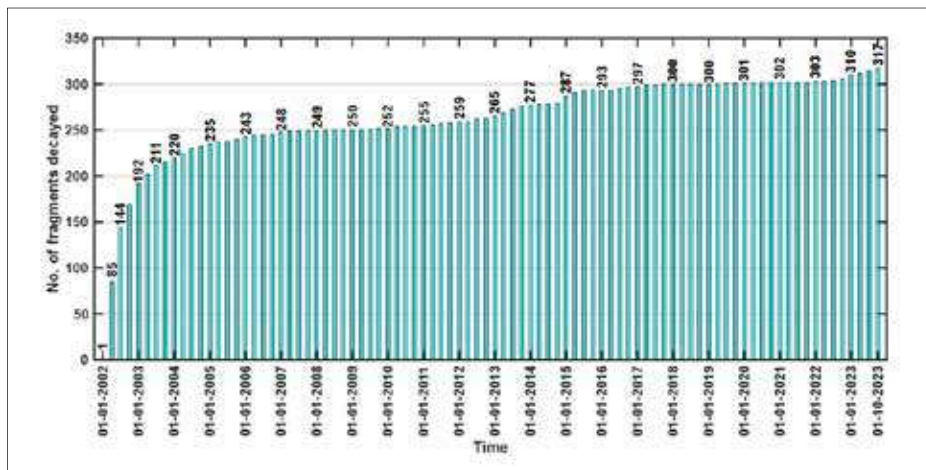


Figure 7.1: Cumulative decay of PSLV-C3 debris fragments

7.4 End-of-mission re-orbiting from GSO

ISRO's communication satellites in GSO are designed with margins for re-orbiting to a higher orbit at the end of their useful life. The strategy is implemented on a case-by-case basis consistent with National service requirements. The re-orbiting and decommissioning operation of INSAT-2C are briefly described here. The operations are planned and executed by the Master

Control Facility (MCF) at Hassan (Parameswaran, 2003). INSAT-2C was launched on December 6, 1995 and had been collocated with INSAT-2B at 93.5° until March 01, 2002. The spacecraft was repositioned to 48°E longitude successfully on April 05, 2002 for operational reasons. Subsequently, INSAT-2C had fulfilled all its mission goals and a decision was taken for decommissioning INSAT-2C.

The decommissioning of INSAT-2C was planned along the lines of International Guidelines of Space Debris management by targeting apogee and perigee heights above GSO. The maneuvers had to be planned and executed having observed the

propellant-depleted condition. The micro-pulsing maneuver operations were started on June 10, 2003 and continued until July 25, 2003 to obtain a drift rate of 1.71°/rev westward drift rate. In this process, orbital perigee height was increased to 127 km above GSO and Apogee height was increased to 150 km above GSO. As per the IADC guidelines, at the end of useful mission life, spacecraft should be disposed off to the graveyard orbit with minimum perigee height above GSO given by

Perigee height (km) $\geq 235 + 1000 \times \text{reflectivity coefficient} \times (\text{area/mass})$.

For the case of INSAT-2C, the above requirement translates to 281.4 km above GSO. The initial Perigee height was 30 km below GSO and Apogee height was 30 km above GSO. It was decided to raise the perigee first to reach the level of observed apogee height and further maneuvers to alternate between perigee and apogee rising suitably. Increasing the orbital height results in a westward drift. Necessary operational procedures were worked out to effect the delta-velocity change to the orbit. In particular, the following operational procedures were observed:

- Prior to the start of activities, all communication receivers and transponders were switched OFF to avoid any interference to any other spacecraft while drifting.
- With the new orbital elements, critical evaluation of close approach to any other listed spacecrafts was carried out. While crossing nearby spacecrafts, duration of pulsing was limited to minimum, or not done to ensure mutual safety.
- As part of final passivation, spacecraft Ni-Cd batteries were disconnected from Main Busses and the charge arrays from solar panels were also disconnected. Self-discharge is expected to finally deplete the batteries of the stored energy.
- At the end of operations, all the unused thermal loads were also switched OFF, which were earlier kept ON for thermal balance.
- All the propulsion valves were kept closed and it was also ensured that the system was empty.
- The telemetry transmitters were switched OFF so that there was no RF emission from the spacecraft.

The maneuver operations were started on June 10, 2003. The maneuvers were continued for nearly 44 days to achieve a drift rate of 1.71°/day. The details of the pulsing duration and orbit achieved each day are illustrated in the Figs. 7.2 and 7.3, respectively. On average, thrusters were fired daily for 600 s with a number of pulses of 130 ms duration.

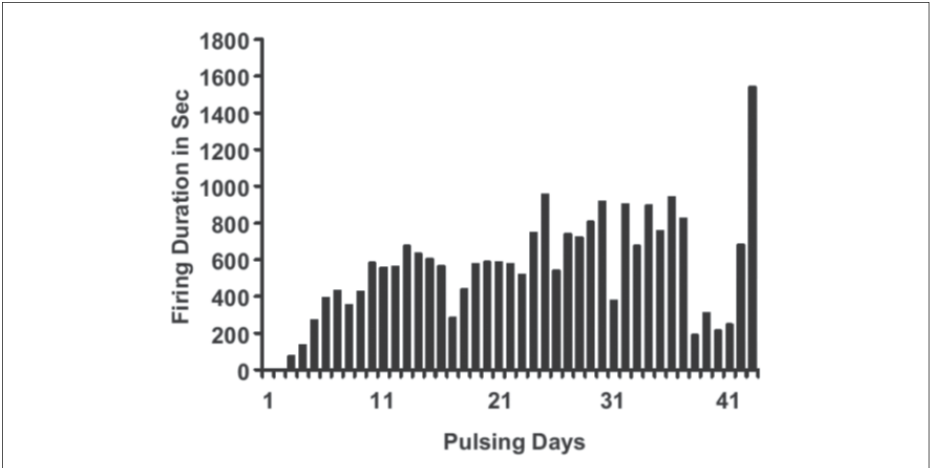


Figure 7.2: Firing pulse durations for INSAT-2C relocation

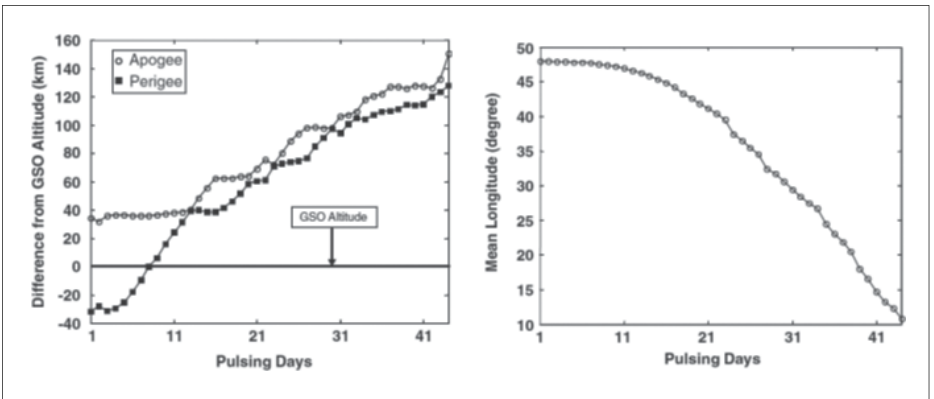


Figure 7.3: Changes in INSAT-2C position during relocation operation

INSAT-2C was successfully decommissioned after its useful mission life on July 30, 2003. Though the target perigee height of 281 km above GSO could not be achieved due to propulsion and visibility constraints, the achieved apogee height of 150 km and perigee height of 127 km above GSO were commensurate with the system constraints. Maximum efforts were taken so that interference to other satellites was avoided during the 44 days of operation. The spacecraft was also passivated at the final stage.

There is a need to protect a launch vehicle in its ascent phase, as well as the spacecraft upon injection from any risk owing to debris collision, even though such risk is small. One of the methodologies developed is that of SPACeDEbrisPROximity (SPADEPRO) analysis, which is required for COLLision Avoidance or COLA studies. SPADEPRO refers to assessment of collision risk between catalogued resident space objects and a launch vehicle or a satellite of interest. The detection of close approaches to satellites/launch vehicles during the launch and early post-deployment phase of their lifetimes is an important subset of the overall problem. Potential collisions during this period can usually be avoided by adjusting the time of launch within a specified launch window. The basic philosophy of the Space Debris Proximity Analysis hinges on three facets, namely,

- computation of collision probability between spacecraft of interest and other resident space objects,
- assessment of acceptable collision probability,
- choice of appropriate interval for space debris proximity analysis.

For the computation of the collision probability between a spacecraft of interest and other resident space objects, necessary inputs are:

- threshold for minimum conjunction distance,
- combined trajectory dispersion,
- effective collision radius.

The minimum conjunction distance between the spacecraft of interest and other resident space objects within a specified time span is computed in a deterministic sense. This is computationally expensive since trajectories of all the catalogued objects need to be checked vis-à-vis that of the spacecraft of interest. So, before this process can proceed, in order to avoid unnecessary computational burden and produce a fast assessment, four filters can be used: an orbital separation filter, an apogee-perigee filter, a time filter, and an epoch filter. The application of the filters drastically reduced the number of catalogued objects to be considered in the proximity analysis. The combined trajectory dispersion for the spacecraft of interest and a particular catalogued object is to be determined for carrying out the space debris proximity analysis. For the spacecraft of interest, trajectory dispersions are obtained through Monte Carlo analysis and for a particular catalogued object, approximate trajectory dispersion values can be fixed by considering the age of the orbital information of the object and the type of orbit it represents. The procedural details are given in Bandyopadhyay et al. (2004a). A typical result of the SPADEPRO analysis will be given in terms of identification of time intervals during which the risks of collision with

debris is above an acceptable level. The launch of the spacecraft can be postponed by a few minutes to avoid these high-risk intervals. Such a methodology has been successfully implemented during the satellite launches of the Indian Space Research Organization, for example the PSLV-C4 launch was postponed by a few minutes on 12th September 2002. Interestingly, one of the debris pieces that led to this brief postponement is a fragment of PSLV-C3 rocket body.

7.6 Minimization of GTO lifetime

Many spent upper stages are separated and left in the GTO, which is a highly eccentric orbit with the perigee normally at low altitudes (180–800 km) and the apogee near the geostationary altitude of around 36,000 km. The evolution of objects in GTOs is determined by a complex interplay of atmospheric drag and luni-solar gravity. These orbits are characterized by periodic changes in perigee altitudes caused by gravitational perturbations of the Sun and the Moon. The initial orientation of the orbit just after the launch with respect to the Sun and the Moon predominantly determines the subsequent histories of the orbital evolution. The launch time plays an important role. The combined influence of the luni-solar perturbations and drag can result in lifetime variations from a few months to several decades. The desired effect from the space debris point of view is a short lifetime. Unfortunately, one cannot always use this natural phenomenon to limit the orbital lifetime, as the launch time of a geostationary satellite is dictated by many other factors like thermal aspects and eclipse time related to the spacecraft design. However, through appropriate choice of the initial perigee altitude and launch time, the lifetime in GTO can be significantly reduced. This feature was demonstrated both in the case of GSLV-D1 upper stage as well as that of GSLV-D2. The predicted history for the orbital evolution of the GSLV-D1 spent third stage is presented in Figure 7.4. The uncertainties in the drag-related parameters are taken into consideration in generating a dispersion band on the time for decay. The apogee and perigee histories for orbiting third stage of GSLV-D1 were obtained using monthly averages of actual solar activity indexF10.7 from April 2001. In this study, using the NPOE software with numerical integration of the GTOs, the Earth's gravitational potential up to J6,6, luni-solar point mass gravitation with Sun and Moon positions computed from JPL DE405ephemeris and MSIS90 atmospheric model were used. Here one interesting point is to note a cross-over point in apogee profile occurring around 530 days of the orbital life. In the case of lower drag, the decay occurs owing to sharper decrease in perigee altitude after 530 days due to sharper decrease in perigee from the influence of luni-solar gravity. It can be seen that for the curves with higher drag the lifetimes are longer. Because of higher drag the apogee altitude decreases faster which results in attenuation of luni-solar gravity effects. In cases with higher drag the perigee remains at a relatively higher level as compared to those of cases with lower drag.

During this period, following the cross-over point, the perigee altitude then continues to fall marginally. The evolution of the spent upper stage of GSLV-D1 was studied and it was predicted that the reentry is expected to take place around December 2002/ January 2003 (Sharma et al. 2004a). The actual decay took place on January 18, 2003.

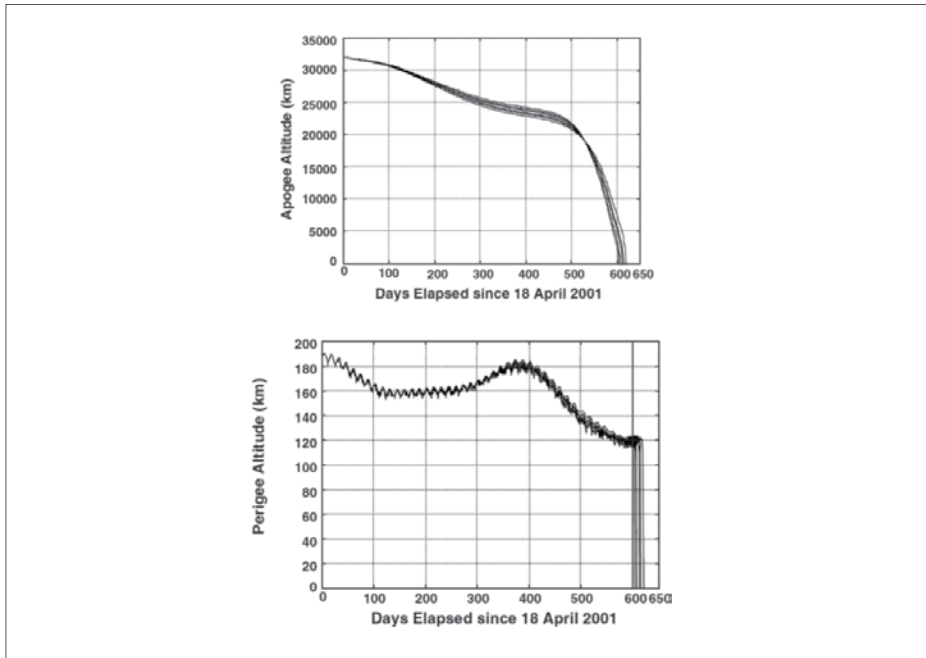


Figure 7.4: Orbital evolution of GSLV-D1 rocket body

7.7 Estimation of On-Ground Risk due to Uncontrolled Re-entries from Eccentric Orbits

Estimation of casualty expectancy associated with a reentry event is important for long-term risk assessment (Bandyopadhyay and Kumar, 2004). The decay process, from highly elliptic orbits like GTO or Molniya, re-entry is governed by either predominantly hi-solar gravity effect with drag playing a very marginal role or by a combination of atmospheric drag and luni-solar perturbations. Often, full circularization of orbit prior to re-entry remains incomplete. This kind of scenario also arises when an intermediate stage of a launch vehicle is deliberately left in a low perigee eccentric orbit as a part of overall mission. Here the following method is proposed to compute impact probability as a function of orbital inclination, argument of perigee and eccentricity at the last perigee passage prior to re-entry.

The method is used to perform parametric study to assess the on-ground risk posed by an object making uncontrolled re-entry from eccentric orbits. This method can also be utilized to provide more realistic near-term risk assessment of on-ground risk.

The method is presented in the form of an algorithm below:

- For a given latitude, Φ , the nodal longitude (the longitude measured with respect to the line of nodes), λ , is given as

$$\lambda = \sin^{-1} \left(\frac{\tan \phi}{\tan i} \right)$$

- The true anomaly, θ , for argument of perigee, ω , is computed as

$$\theta = \tan^{-1} \left(\frac{\tan \lambda}{\cos i} \right) - \omega$$

- The time of flight, t , from perigee for eccentricity, e and time period, T , is evaluated as

$$t(\theta) = \frac{T}{2\pi} \left[\tan^{-1} \left(\sqrt{\frac{1-e}{1+e}} \tan \left(\frac{\theta}{2} \right) \right) - \frac{e\sqrt{1-e^2} \sin \theta}{1+e \cos \theta} \right]$$

- The impact probability between two latitudes Φ_1 and Φ_2 is given as

$$P_i(\phi_1, \phi_2) = \frac{t(\theta_2) - t(\theta_1)}{T}$$

Once the impact probability is known, the total casualty expectancy is estimated using

$$C_A = \sum P(\phi) \cdot \rho_p(\phi) \cdot A_C,$$

$\rho_p(\Phi)$ is the population density expressed in terms of latitude bins and A_C is the casualty area.

7.7.1 Application of the proposed method in long-term risk assessment

The proposed method was applied to two orbits with the same inclination of 200 but with different eccentricities. One of the orbits was a circular orbit. The elliptic orbit had argument of perigee and eccentricity of 2700 and 0.05 respectively. The variations in impact probability and casualty expectancy with latitude were plotted in Figure 7.5. It was seen that for the circular orbit, the variation in impact probability about the equator is symmetric whereas for the eccentric orbit there was a distinct asymmetry.

The asymmetry was more in the case of extreme latitudes. This difference was translated to two different casualty expectancy figures. The study showed that for any inclination there will be maximum and minimum casualty expectancy figures. These numbers could be taken as the dispersions in casualty expectancy obtained with the assumption of circular orbit. Next, for an upper limit of 0.05 on eccentricity casualty expectancy was computed for all the inclinations. This plot was very important since it allowed mission planner to get an idea of casualty expectancy bands at different orbital inclinations. The plot was given in Figure 7.6.

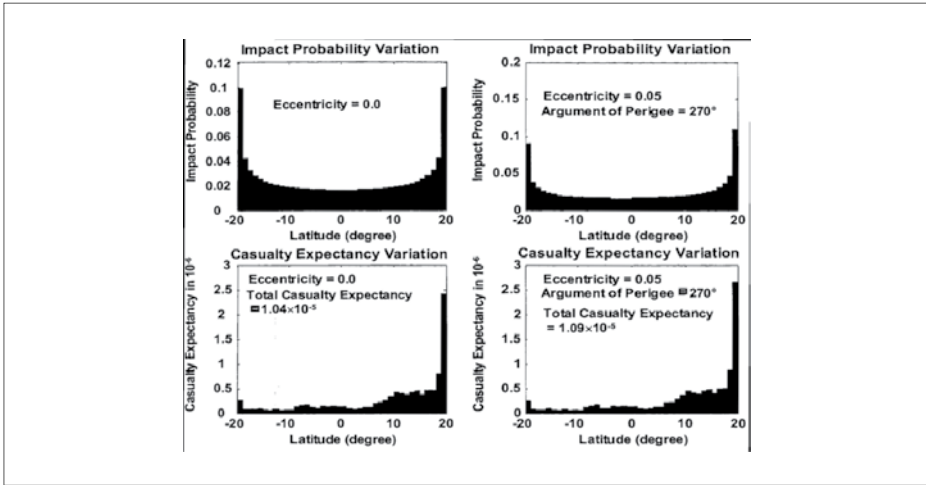


Figure 7.5: The Impact Probability and Casualty Expectancy Variations for Circular and Elliptic Orbits

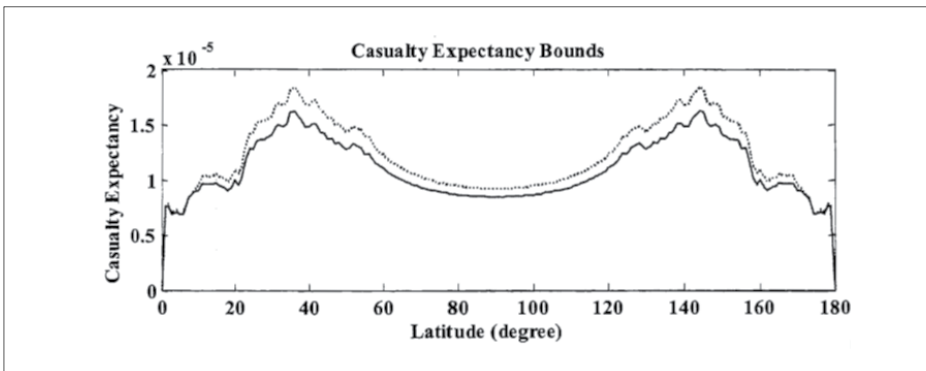


Figure 7.5: The Impact Probability and Casualty Expectancy Variations for Circular and Elliptic Orbits

7.8 Active Debris Removal

Active Debris Removal (ADR) is necessary to stabilize the growth of space debris. Also it is important that the newly launched objects comply with post-mission disposal guidelines – especially orbital decay in less than 25 years. If this is not done, then most of the required ADR effort would go to compensate for the non-compliance of new objects. The IADC mitigation measures will reduce the growth, but long-term proliferation is still expected, even with full mitigation compliance, and even if all launch activities is halted. This is an indication that the population of large and massive objects has reached a critical concentration in LEO.

Furthermore, an IADC study with six different models (Liou, Anil Kumar et al, 2013) show that in an almost perfect scenario with 90% compliance with the mitigation guidelines and with no explosions on orbit, the population suffers a steady increase, and a collision could be expected every 5–9 years. All these studies clearly indicate that the population of large and massive objects has reached a critical density in LEO, and that mitigation alone is not sufficient. It is necessary to introduce a program of active debris removal, in order to reduce the number of large and massive (mostly physically intact) objects.

7.8.1 Identification of Space Debris from SSO for Active Debris Removal

As a preliminary analysis towards identification of candidate objects which have greater potential of generation of space debris in future, Dutt and Anil Kumar (2014) had selected the Sun synchronous Orbit (SSO) region. It was noted that SSO region in LEO was most useful and was one of the most populated regions. In order to access the potential of a resident space object (RSO) to create more fragments in future the following criteria was considered.

- Size of RSO: In most of the cases, the size of an RSO is unknown. It can be estimated from RSO's radar cross section (RCS) history. We have a collection of about 2½ years Satellite Situation Report (SSR) files downloaded from **www.space-track.org**, which contain the RCS of all RSOs. From the RCS history the maximum RCS is obtained, and used for categorizing these objects.
- Mass of an RSO goes as an input to break-up model to determine the no. of fragments can be generated after a collision/fragmentation. If density is assumed to be the same for all RSOs then mass will be a function of size of RSO. Hence in the preliminary analysis, it can be ignored.
- Lifetime of an RSO: Longer an object remains in the orbit, more chances it has for collision.

- Orbital Flux at a given altitude and inclination gives an idea of how much populated that region is. It can be determined by statistical methods also. Apart from objects in the given altitude and inclination of an RSO, other objects also cross its orbit and might cause a collision. So, it is important to get an estimate no. of objects crossing the orbit of an RSO. This can be obtained from the space object catalogue and with the help of conjunction pre-filters like apogee-perigee filter and orbit path filter.

The following assumptions were made in the analysis:

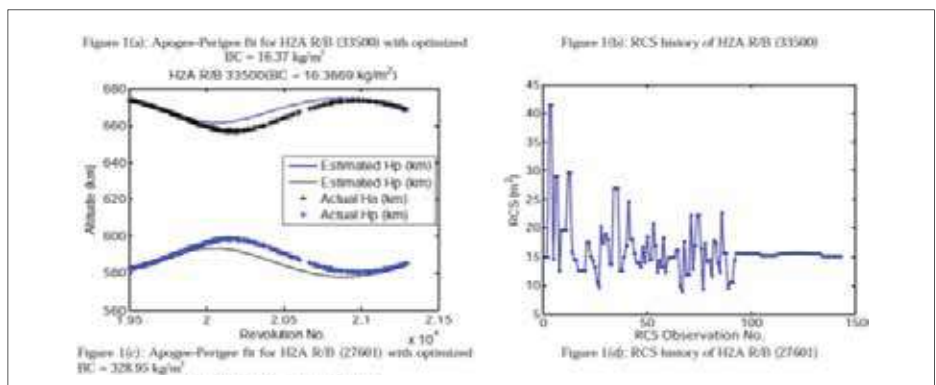
- Size of an RSO is proportional to RCS and hence only the maximum value of RCS was considered.
- All space objects were assumed to have uniform density and hence mass was taken to be proportional to size (RCS).
- The analysis was carried out with the space object scenario as by Jan 2013.
- For lifetime computations, ballistic coefficient (BC) was calculated using a set of Two Line Elements (TLE).
- During propagation it was assumed that the BC remains unchanged.
- Error due to TLE inaccuracy was not considered.
- It was also assumed that the objects surviving the apogee perigee and orbit path filter will cross the orbit of a space object sometime in future. An error bar of 30 km was put on the filters.
- Only catalogued data (size > 10 cm) was considered.

The SSO objects were first sorted on the basis of maximum RCS value and 20 such objects were identified. Their orbital lifetime estimation was done using OPSAT (Orbit Propagation using Semi-Analytical Theory) developed in-house and lifetime tool of STK. Further, to determine the no. of objects crossing the orbit of an RSO, all catalogued TLEs are evaluated using the perigee apogee and orbit-path filter using STK's conjunction analysis tool. An error of 30 km was considered, that is, whenever an object qualifies these two filters within 30 km range, it is assumed that it will cross the given orbit, sometime in future. Moreover, since these objects are in similar orbital regime, orbital flux mostly remains same for all of them. On the basis of these three criteria, Table 7.2 is generated. Table 7.2 gives the details of identified RSOs in descending order of their maximum RCS value. It gives the name of the object, its NORAD Catalogue Number or Satellite Number (it is a unique identifier assigned by North American Aerospace Defense Command or NORAD to each Earth orbiting artificial satellite or object in their satellite catalogue SATCAT), its maximum RCS value, estimated BC (obtained from OPSAT), Decay date/Lifetime estimate

(obtained from STK, by using the estimated BC) and number of conjunction objects (gives an estimate of orbital flux at the object's altitude). The TLE set of RADARSAT-2 (NORAD#32382) and RADARSAT (NORAD# 23710) appear in a random fashion and so could not be used for BC estimation. Also, BC of H2A R/B (NORAD# 24279) and YOGAN 15 (NORAD#38354) could not be estimated because their apogee altitude is above 1000 km. BC estimation and RCS history for some of these objects (in Table 7.2) are shown in Figure 7.7.

Table 7.2: List of Candidates from SSO selected on the basis of RCS

S.No.	Name of RSO	NORAD No.	Max. RCS	Estimated BC (kg/m ²)	Decay date/ Lifetime estimate	No. of conjunction objects
1.	Meteor M	35865	188.151	66.3385	>150 yrs	4062
2.	CZ-2C R/B	39000	48.3069	84.3809	13-04-2020 - 7 yrs	1608
3.	H2A R/B	33500	45.0453	16.3669	31-03-2021 - 8 yrs	1915
4.	RADARSAT-2	32382	42.361	No pattern seen in TLE set		
5.	Envisat	27386	41.9168	42.8545	>150 yrs	3771
6.	H-2A R/B	27601	39.8347	328.95	>150 yrs	4401
7.	ADEOS 2	27597	39.2465	21.037	>150 yrs	3953
8.	JAS 2	24277	39.1163	77.1727	>150 yrs	3934
9.	H2A R/B	24279	35.4174	Apogee altitude above 1000 km		
10.	OKEAN O	25860	35.4174	46.6582	>150 yrs	1972
11.	YOGAN 15	38354	34.1095	Apogee altitude above 1000 km		
12.	COBE	20322	32.8953	100	>150 yrs	3416
13.	ARIANE R/B	28499	30.92	7.2497	19-02-2020 - 7 yrs	2252
14.	RADARSAT	23710	30.664	No pattern seen in TLE set		
15.	ERS 1	21574	30.0875	1825.2	>150 yrs	3887
16.	ARIANE 40 R/B	21610	29.8753	18.6574	>150 yrs	3659
17.	COSMOS 2441	33272	29.764	100	>150 yrs	2970
18.	SL 16 R/B	25400	29.483	95.7728	>150 yrs	4050
19.	CZ-2D R/B	36597	29.2387	54.5356	>150 yrs	1795
20.	H2A R/B	28932	29.0537	950.56	>150 yrs	1969



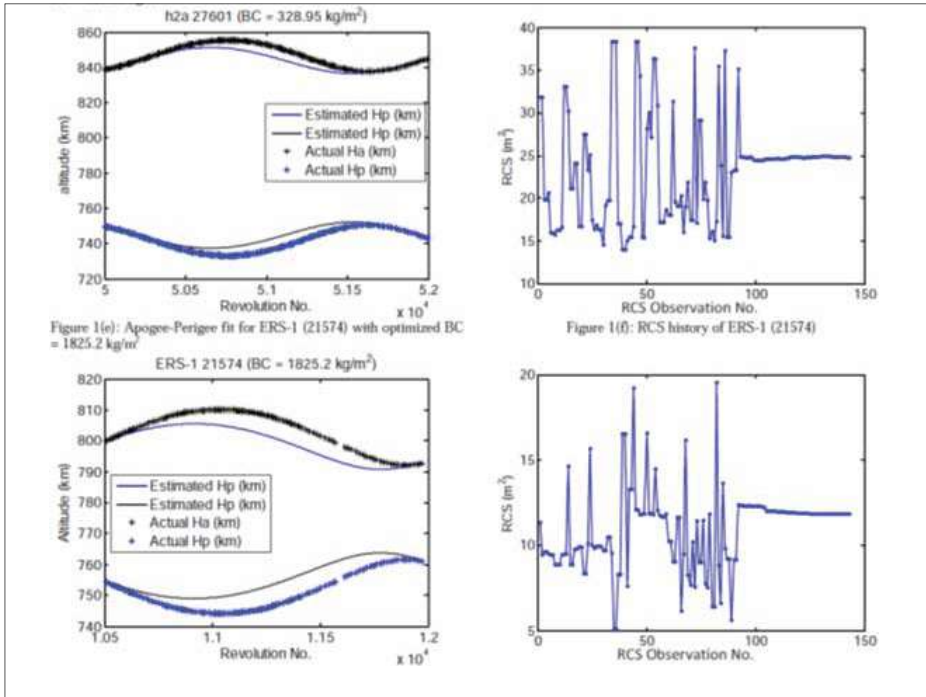


Figure 1(e): Apogee-Perigee fit for ERS-1 (21574) with optimized BC = 1825.2 kg/m³

Figure 1(f): RCS history of ERS-1 (21574)

Figure 7.7: BC Estimation and RCS History of some of the Identified Objects

Implementation of space debris mitigation measures are highly essential since some of them has the potential to damage an active satellite, leading to loss of mission, or loss of life in the case of manned spacecraft. For manned flight orbits, space debris mitigation measures are very much necessary due to crew safety implications. Mitigation guidelines have been developed by IADC, reflecting the fundamental mitigation elements of a series of existing practices, standards, codes and handbooks developed by a number of national and international organizations. The Committee on the Peaceful Uses of Outer Space acknowledges the benefit of the qualitative guidelines, which are accepted by the global space community. Many member states and international organizations voluntarily take measures, through national mechanisms or through their own applicable mechanisms, to ensure that these guidelines are implemented, to the greatest extent feasible, through space debris mitigation practices and procedures. These guidelines are applicable to mission planning and the operation of newly designed spacecraft and orbital stages and, if possible, to existing ones. They are not legally binding under international law.

The following guidelines should be considered for the mission planning, design, manufacture and operational (launch, mission and disposal) phases of spacecraft and launch vehicle orbital stages (United Nations, 2010):

- Limit debris released during normal operations;
- Minimize the potential for break-ups during operational phases;
- Limit the probability of accidental collision in orbit;
- Avoid intentional destruction and other harmful activities;
- Minimize potential for post-mission break-ups resulting from stored energy;
- Limit the long-term presence of spacecraft and launch vehicle orbital stages in the low-Earth orbit (LEO) region after the end of their mission;
- Limit the long-term interference of spacecraft and launch vehicle orbital stages with the geosynchronous Earth orbit (GEO) region after the end of their mission.

In the near future, it may become imperative for the space-faring nations to selectively implement Active Debris Removal (ADR) to effectively contain the evolutionary growth of space debris. Several simulation and technology-development studies are seriously taken up at this juncture.

7.9

Requirements of Shielding from Space Debris for Human Space Missions

For human space flight missions, crew safety is of paramount importance in the entire segment of the mission, which includes ascent phase, on-orbit phase, de-boost and descent phase. Nowadays spacecrafts are threatened by the increasing probabilities of micro-meteoroid and orbital debris (MMOD) impact damage, which can potentially degrade performance, shortens the service life, or result in catastrophic accidents. In view of the micro-meteoroid and orbital debris population in LEO, it is important to assess the threat from space debris; and also provide the necessary shielding requirements for the Crew Modules (CM) and Service Modules (SM). This requires the assimilation analysis from a large amount of structural, thermal, material, and aerodynamics studies, involving intensive theoretical and numerical analysis and hypersonic testing.

A typical summary is given below, while detailed theoretical, numerical and testing studies are pursued in all the relevant integrated domains:

- Shoulder area of thermal protection system (TPS) must be protected to prevent unpredicted heat in leak during re-entry. Until separation of service module, this critical exposed surface is not protected. Hence, a protection shield is recommended. This extension ensures not only the safety of crew, but also of the high-pressure life support system gas bottles inside the annular region.

- In the boat tail region, Nextel and Kevlar cloths mounted half way between the outer shell and inner pressurized compartment are proposed for shielding the inner pressurized compartment.
- Based on Skylab, Apollo, Space shuttle experience, viewport glass is most vulnerable and life threatening and hence prevention of windows pointing towards velocity vector directions in all circumstances is to be avoided. It is also recommended to bring down the number of windows to essential minimum. Earth viewing orientation of viewports is most preferred one.
- Apex cover protection is also found essential because it houses the main parachutes that are packed in cloth bags. Hence, any damage to the apex cover may damage the parachute.
- Damage of top hatch cover is life threatening as crew are housed just under the top hatch. A classical Whipple shield with thin aluminium plates separated at a stand-off distance can be proposed for top hatch. Whipple shields have been widely applied to protect space modules from MMOD. The conventional Whipple shield consists of a thin front bumper followed at a standoff distance from the rear wall. Aluminium alloys are recognized as a conventional bumper material of Whipple shield for its high strength-to-weight ratio. However, with the rapid development of space exploration activities, high-performance shielding materials will be required. To achieve this objective, MMOD test specimen shields based on innovative materials, such as advanced C/SiC, have been developed. Hyper Velocity Impact test of MMOD specimen with Aluminium AA2014 bumper & C/SiC bumper were conducted at 3 km/s and 5 km/s. These studies are presented by Vijay et al. (2021).
- It is essential to assess the ability of thermal protection system (TPS) in the boat tail region to withstand the thermal loads on impact. For this, hypervelocity impact tests must be carried out for the boat tail TPS configuration at various angles of impact. The impacted specimen shall then be subjected to aerothermal heating to assess the thermal performance.
- The major exposed areas of Service Module like solar array and thermal radiators are equally vulnerable for MMOD impact. Experience encountered by International Space Station and re-entered Space Shuttle, Long Duration Exposure Facility (LDEF), Solar panel of Hubble Space Telescope (HST) and Eureka states that design of solar array shall consider its survivability under MMOD impact in terms of short circuit protection and isolation.
- With multiple liquid engines and their associated control valves and plumbing requires apart from thermal shielding, a complimentary MMOD impact protection. From experience of others, use of Nextel and Kevlar fabrics behind the thermal protection may ensure the required safety of propulsion bay. It does not comply to the reliability requirement of hypergolic fuel and oxidizer storage

and supply system. Hence, additional protection shielding to fuel oxidizer tanks and plumbing must be ensured.

- It is also necessary to embed certain impact monitoring sensors in solar array drive, thermal radiator, extension shield of TPS to acquire any possible impact data to be compared with ground experimental data. To get confirmation on estimated debris flux data, it is desirable to extensively instrument the Orbital Module of unmanned flights with sensors for measuring parameters like shock, strain etc. and execute the mission for longer duration. Number of MMOD impacts on Crew Module and Service Module can be measured and obtained real time through telemetered data.



SDSSARS IN ISRO

Space Debris and Space Situational
Awareness Research Studies



CHAPTER 8

Re-entry Prediction Studies

8.1 Re-entry of Space Objects

Re-entry of space objects is sometimes a dangerous issue. When objects in space, like satellites or rocket stages, reach the end of their useful life, they need to be disposed of somehow. Intentional disposal will be costly, requires lots of efforts and proper functioning of systems and subsystems of the object to be disposed. The most common option for debris is to let them re-enter the atmosphere, where they will either burn up or break up during re-entry. However, this can pose a threat if the object doesn't completely burn up or break up, and pieces of it reach the ground. There have been a number of incidents where space debris has fallen to Earth, sometimes causing damage or even injury.

Uncontrolled re-entry is when a space object is coming back to Earth without being actively controlled by ground operators. In other words, it's essentially "falling" back to Earth. This can be dangerous for a number of reasons such as

- The object is moving very fast when it hits the atmosphere, creating a lot of friction and heat. This can cause it to break up or even explode, leading to aero thermal fragmentation.
- Even if the object doesn't explode, it can still cause damage when it hits the ground. For example, the Soviet satellite Cosmos 954 scattered radioactive debris across Canada in 1978 after an uncontrolled re-entry.
- Even small pieces of debris can cause damage if they hit a populated area or an important structure.

Predicting re-entry time and location is extremely important for a few reasons. First, it allows authorities to warn people in the area regarding re-entry of big objects to take necessary safety measures or evacuate if necessary. Second, it can help to minimize the damage caused by the reentering object. Third, predicting re-entry time and location can help researchers learn more about the physics of atmospheric re-entry, which can help improve our ability to design safer and more efficient spacecraft.

Accuracy in predicting re-entry time and location depends on many factors. The factors include (i) the accuracy of the data used to predict re-entry, including the object's orbit, atmospheric conditions, and the object's mass and shape, (ii) The capabilities of the software and models used to make the predictions and (iii) The amount of time available to make the prediction. The closer the object is to re-entry, the more accurate the prediction can be. In general, re-entry predictions can be made, but there's always some uncertainty involved. In some cases, the margin of error can be as large as a few hundred kilometers.

8.2 IADC Re-entry Test Campaigns

The risk potential of re-entries was recognized at the occasion of Cosmos 954 (Jan. 1978), Skylab (July 1979), and Salyut 7 (Feb. 1991). An initial, limited IADC (Inter-Agency Space Debris Coordination Committee) data exchange was realized for the Cosmos 398 re-entry (Dec. 1995); a more formalized data exchange was later implemented for the re-entry of the Chinese FSW-1-5 capsule (March 1996). In 1997 plans were adopted to develop a web-based IADC Re-Entry Events Database to facilitate the exchange of information on a re-entry object, on its orbit, and on its predicted re-entry time and location; this data base is hosted by the European Space Operations Centre of ESA; it is operational since 1998 (Klinkrad, 2010). The 13 IADC member agencies are: – ASI (Agenzia Spaziale Italiana) – CNES (Centre National d'Etudes Spatiales) – CNSA (China National Space Administration) – CSA (Canadian Space Agency) – DLR (German Aerospace Center) – ESA (European Space Agency) – ISRO (Indian Space Research Organisation) – JAXA (Japan Aerospace Exploration Agency) – KARI (Korea Aerospace Research Institute) – NASA (National Aeronautics and Space Administration) – ROSCOSMOS (State Space Corporation "ROSCOSMOS") – SSAU (State Space Agency of Ukraine) – UKSA (United Kingdom Space Agency).

The re-entry risk object qualification criterion was that the object or parts of it may survive to cause potential significant damage, or the entry event may cause radioactive contamination (Klinkrad, 2009).

The IADC runs annual re-entry prediction campaigns to test and improve the accuracy of re-entry predictions. These campaigns bring together experts from different space agencies and organizations to collaborate on re-entry predictions and data sharing. The campaigns are intended to simulate real-world scenarios of high-risk reentries and to test the effectiveness of the re-entry prediction models and communication protocols used by the IADC. The campaigns also allow participants to share best practices and identify areas for improvement in the prediction and response to

reentries. The IADC has been conducting these campaigns since 1998 and has made significant progress in improving the accuracy and timeliness of re-entry predictions.

The past IADC re-entry prediction campaigns till 2016 were (Pardini and Anselmo, 2017): Inspektor (1998), GFZ-1 (1999), Soyuz stage (2000), Vostok stage (2002), Cosmos 389 (2003), Cosmos 2332 (2005), Coronas F (2005), Cosmos 1025 (2007), Delta-2 R/B (2007), EAS (2008), Molniya 3-39 (2009), Vostok US (2010), UARS (2011), ROSAT (2011), Phobos-Grunt (2012), GOCE (2013), Cosmos 1939 (2014), CZ-2D (2015), CZ-2C (2016) and AVUM (2016).

28 campaigns have been conducted since 1998, including: 2021-01 Starlink-26 satellite (2019-029F, #44240), re-entered 10-Apr-2021 12:27 UTC. 2021-02 CZ-5B rocket body (2021-035B, #48275), re-entered 09-May-2021 02:14 UTC (Metz, 2021). In the IADC Re-entry Test Campaign 2022/2, Starlink-24 Satellite (2019-029D, # 44238) was estimated to have re-entered the Earth's atmosphere on 24 Oct 2022 UTC 05:50 \pm 56 minutes. In the IADC Re-entry Campaign of 2023 with Starlink-1065 as Test Object, the declared date of re-entry was 19:55:00 UTC, 20 April 2023.

8.3 Orbital Lifetime of Decaying Objects

The accurate estimation of the orbital lifetime of decaying objects is of considerable importance for prediction of risk object re-entry time and proper planning of mitigation strategies and hazard assessment. The database for the orbital lifetime prediction or re-entry time of large debris objects is the set of Two Line Elements provided by agencies like USSPACECOM. Anil Kumar et al. (2003c, 2007) presented the highlights of the implementation strategies adopted for the online re-entry prediction using Kalman filter approach with constant gains. The states considered for the analysis was the semi-major axis, eccentricity and ballistic coefficient. The measurements used for the analysis are the apogee height and perigee height which are equivalent to semi-major axis and eccentricity. A very simple model for the orbit propagation, which considered only the atmospheric drag effect for the Low Earth orbit, and a mean standard atmosphere USSA 1976 were utilized in the study. The basic feature of the approach was that the model and measurement errors could be accounted in terms of adjusting the Kalman gains that are chosen based on suitable cost function. Also, details are provided of the validation results of the approach utilizing three re-entries of debris objects, namely US Sat No. 25947, SROSS-C2 Satellite and Cosmos 1043 Rocket Body. These objects re-entered the Earth's atmosphere on 4th March 2000, 12th July 2001 and 19th January, respectively. Figure 8.1 provides the observed and estimated values of apogee and perigee heights with the constant gain approach for Sat25947.

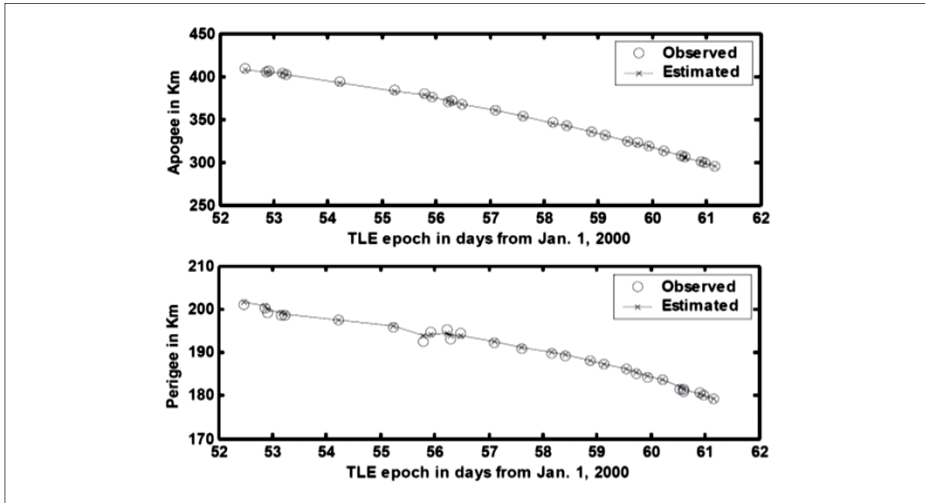


Figure 8.1: Sat25947 re-entry prediction: Observed and estimated values of Apogee and Perigee heights with the constant gain approach

The evolution of objects in geostationary transfer orbit (GTO) is determined by a complex interplay of atmospheric drag and luni-solar gravity. These orbits are characterized by periodic changes in perigee altitudes caused by gravitational perturbations of the Sun and the Moon. Sharma et al. (2004a) and Adimurthy (2006b) investigated the basic physics of the luni-solar perturbations in GTO and their interaction with drag perturbation. A detailed analysis was made to study the influence of launch time on the orbital lifetime. The study revealed that even minute changes in the launch time could result in very large changes in the lifetime. The analysis was applied to the orbital evolution of the orbiting upper stage of the first development flight of the Indian Geo Stationary Satellite Launch Vehicle GSLV-D1, which took place on 18 April 2001. On the basis of the two-line element sets already available, the future evolution of the spent upper stage of GSLV-D1 was studied and it was predicted that the re-entry might take place around 600 days after the launch. The re-entry took place on 18th January 2003 after 639 days.

8.3.1 Characteristics of Decay from GTO

The GTO is a highly eccentric orbit with the perigee normally at low altitude (180–650 km) and the apogee near geo-stationary altitudes. The combined influence of the luni-solar perturbations and drag can result in lifetime variations from a few months to several decades. The desired effect from the space debris point of view is a short lifetime. The long-term evolution of objects in GTO can fall into two broad categories,

namely, decay predominantly by luni-solar gravity effect and decay by combination of atmospheric drag and luni-solar perturbations. The atmospheric drag generates a retarding force on the satellite and in that sense it is unidirectional in its effect by reducing apogee and perigee altitudes. On the other hand, the effects of the Sun and the Moon on the satellite are more complex and can result in either increase or decrease in the perigee altitude. In view of this, it will be interesting to understand the basic physics of the luni-solar perturbations. range, the orbit contracts under the effect of drag resulting in significant reduction in apogee altitude. Subsequently, the perigee altitude may increase under the influence of luni-solar perturbations and may not lead to any immediate decay.

8.3.2 The Effect of Third Body Perturbations on GTO

In the presence of a third body, a space object experiences a net differential perturbing acceleration outward from the Earth whenever it is collinear with the Earth and the perturbing body. However, when the object is perpendicular to the Earth and the perturbing body, it experiences a perturbing acceleration towards the Earth. The cumulative effect of this disturbing acceleration on the variation of perigee altitude is illustrated in Figure 8.2 for solar gravity. The change of perigee altitude during the course of a day essentially depends on the Sun azimuth angle with respect to the spacecraft orbital plane. The rate of perigee variation is zero at the Sun azimuth angles of 0° , 90° , 180° , 270° and 360° , irrespective of the apogee altitude. However, the higher the apogee altitude, the larger is the variation of perigee during a day, for a particular Sun azimuth angle.

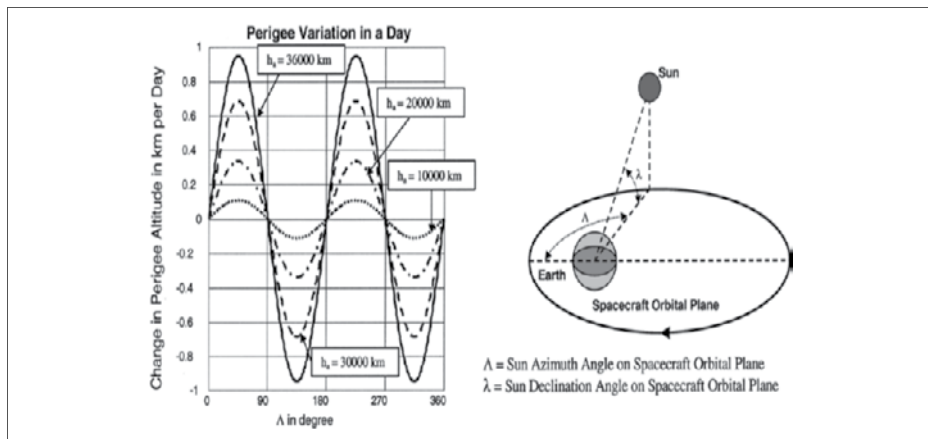


Figure 8.2: Perigee altitude variation during a day for different apogee altitudes with the variation of Sun azimuth angle on spacecraft orbital plane. Nominal perigee altitude is taken as 150 km

8.3.3 Effect of Launch Time on Lifetime

For highly eccentric orbits like a GTO, the lifetime strongly depends on two parameters, namely, the initial right ascension of ascending node of the spacecraft and the solar longitude, both of which define Sun azimuth angle on spacecraft orbital plane. These two parameters are functions of time. The data presented in Figure 8.3 is generated corresponding to 18th October 2001, for an orbit with the following parameters: Perigee height = 177 km, apogee height = 31,950 km, argument of perigee = 177.4940, inclination = 19.2530. There are several interesting observations, which can be made from Figure 8.3. The first is that there are intervals of launch time when the lifetime of the resulting orbit is very small. The more striking observation is that there are zones in which a very small change in launch time can result in significant changes in the lifetime.

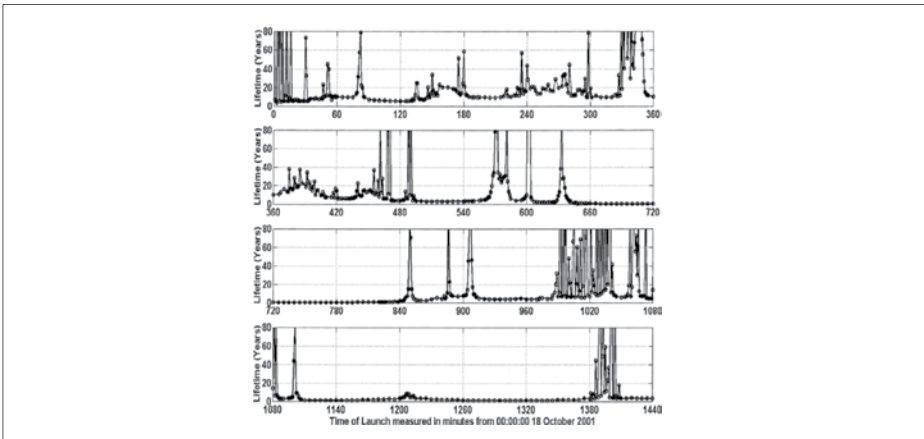


Figure 8.3: Typical dependence of orbital lifetime on the time of launch during a day

Typical cases are illustrated in Figure 8.4 with launch at 00:03:00 UTC (Case 1) and 00:04:00 UTC (Case 2) on 18th October 2001. It may be noted that the lifetime for Case 1 is only 1367 days but the lifetime for Case 2 is several decades. The bifurcation occurs around 1075 days after the launch. When Λ for Case 2 crosses 1800, Λ for Case 1 is still around 1670, which is short of 1800. The rate of variation of perigee for Case 1 is negative, whereas for the Case 2 it is positive, as seen from Figure 8.4. At the same time, in this case, the rate of change of apsidal line due to Earth's oblateness (J_2) effect, approximately matches with that of the solar longitude leading to constant Sun azimuth angle below 1800 on spacecraft orbital plane, which results in a resonance. This resonance leads to a fairly constant Λ for a very long time. As a result, the perigee altitude for Case 2 increases to a high value, where the influence due

to drag is lower. Hence, the lifetime for Case 2 is very high. In contrast, the perigee for Case 1 continuously decreases from the bifurcation point and results in orbital decay due to high drag, ending the life in 1367 days. It is observed that this kind of resonance occurs when the apogee altitudes are between 13,000 and 16,000 km. This is important, since at these altitudes the required rate of movement of apsidal line is around 10 per day, which matches with that of the Sun. Variation of Sun azimuth angle (Λ -dot) at various inclinations is depicted in Figure 8.5 for various apogee altitudes with respect to perigee altitude of 150 km.

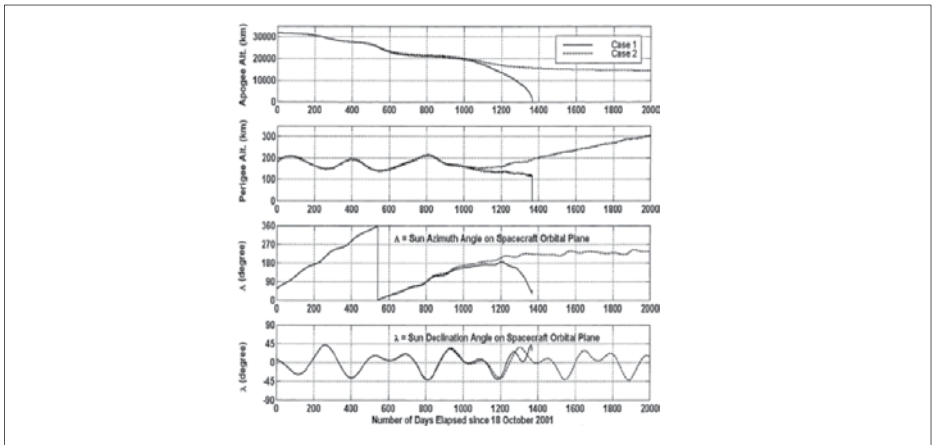


Figure 8.4: Illustration of a bifurcation in neighboring orbital evolution patterns

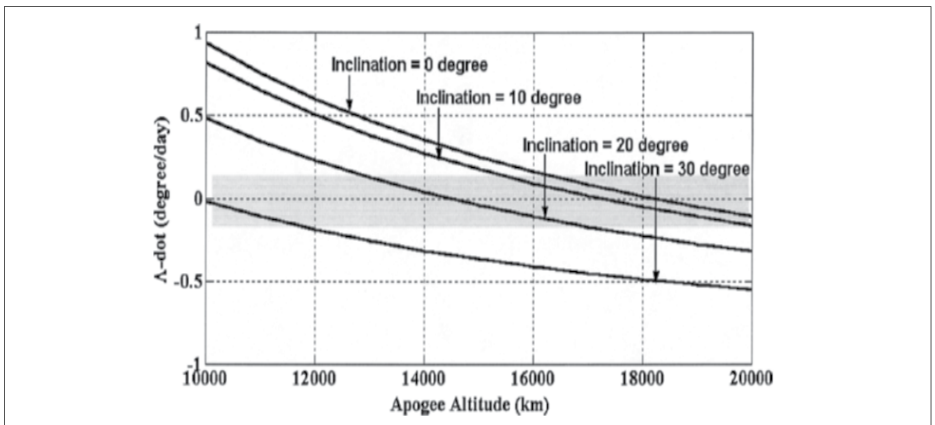


Figure 8.5: Variation of Λ -dot with apogee altitude at various inclinations. The bifurcation at a given apogee altitude can occur in neighboring orbital evolution patterns when the Λ -dot is very small, as indicated with the shaded area (Perigee altitude of 150 km is assumed)

8.3.4 Decay of the Spent Orbiting Stage of GSLV-D1

The predicted history for the orbital evolution of the spent third stage is presented in Figure 8.6. The uncertainties in the drag related parameters are taken into consideration in generating a dispersion band on the time for decay.

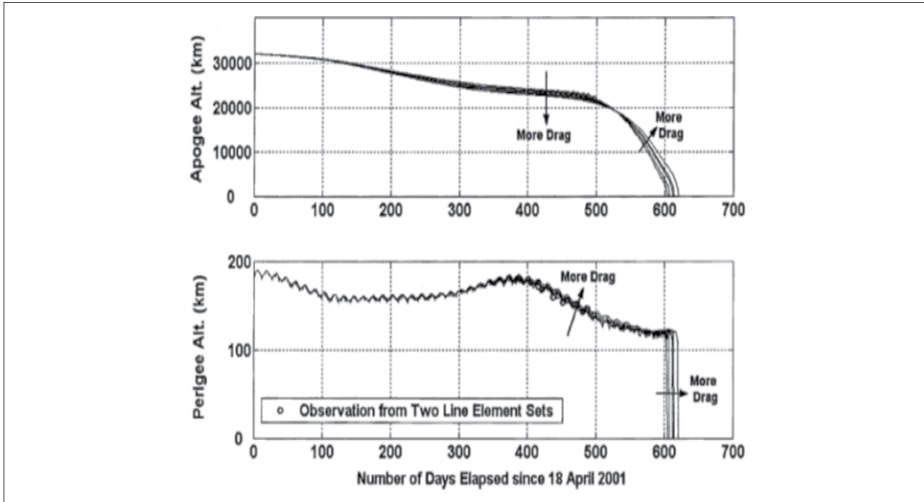


Figure 8.6: Orbital evolution of the spent orbiting stage of GSLV-D1

The apogee and perigee histories for orbiting third stage of GSLV-D1 have been obtained using monthly averages of actual solar activity index F10.7 from April 2001. Typical value for the ballistic coefficient is 110 kg/m^2 and dispersions on this value are considered consistent with the observed TLE. In this study, using NPOE software with numerical integration of the orbits, the Earth's gravitational potential up to J6,6, luni-solar point mass gravitation with the Sun and the Moon positions computed from JPL DE405 ephemeris, and MSIS90 atmospheric model are used. Here one interesting point is to note a cross over point in apogee profile occurring around 530 days of the orbital life. In the case of lower drag, the decay occurs owing to sharper decrease in perigee altitude after 530 days due to sharper decrease in perigee from the influence of luni-solar gravity. It can be seen that for the curves with higher drag the lifetimes are longer. Because of higher drag the apogee altitude decreases faster which results in attenuation of luni-solar gravity effects. In cases with higher drag the perigee remains at a relatively higher level as compared to the cases with lower drag. During the period following the cross over point, the perigee altitude continues to fall marginally. The details of the methodology used in this study were presented in Bandyopadhyay et al. (2001).

8.3.5 Re-entry time Estimation of GSLV-F01/CS and More

Mutyalarao and Sharma (2010) carried out the re-entry time of the cryogenic stage of the Indian Geostationary Satellite Launch Vehicle GSLV-F01/CS as an optimal estimation problem. The RSM with GA was applied to determine the optimal estimates of ballistic coefficient (B) and eccentricity (e). The investigation employed TLEs, determined 165 days before the re-entry epoch, 24 November 2007, 19:30 [Greenwich Mean Time (GMT)]. The decay location was characterized by longitude of 5°N , and latitude of 2°E , and an orbital inclination of 19.3° . An accurate re-entry time prediction of the cryogenic stage was made seven days before its re-entry. The methodology selected offered an improvement over least squares method. The study also showed that the object must have tumbled during the last day in the orbit.

It may be noted in Figs. 8.7 and 8.8 that there is a good comparison between the observed and the predicted values of the mean apogee by the RSM with GA method than the least square method. Towards the end of the orbital life, RSM with GA method provides better estimates of the re-entry times than the least square method.

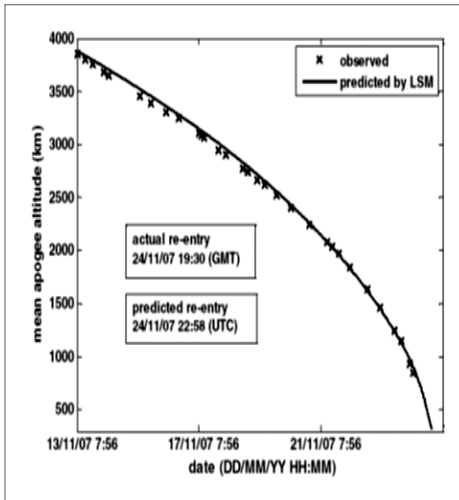


Figure 8.7: Orbital evolution of the spent orbiting stage of GSLV-D1

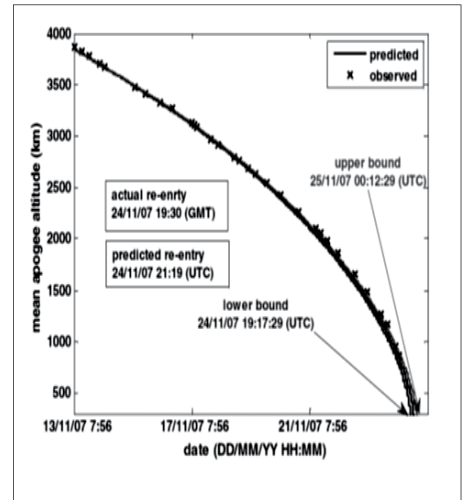


Figure 8.8: Comparison between the observed and predicted mean apogee altitudes using RSM with GA method

Mutyalarao and Sharma (2011) studied the re-entry time of the cryogenic stage of the Indian geo-synchronous launch vehicle, GSLV-F04/CS (#32051), which was decaying since 2 September 2007 from initial orbit with eccentricity equal to 0.706. Two parameters, initial eccentricity and ballistic coefficient, were chosen for optimal estimation. It is known that the errors are more in eccentricity for the observations based on two line elements (TLEs). These two parameters were computed with response surface method using a genetic algorithm for the selected eight different zones, based on rough linear variation of the mean apogee altitude during 200 days of orbit evolution. The study showed that the GSLV-F04/CS will re-enter between 5th December 2010 and 7th January 2011. The details of re-entry are provided in Table 8.1. However, it was known later that the re-entry took place on 8th February 2011. The methodology was also applied to study the re-entry of six decayed objects (cryogenic stages of GSLV and Molniya satellites). Good agreement was noticed between the actual and the predicted re-entry times. The absolute percentage error in re-entry prediction time for all the six objects shown in Table 8.2 was found to be less than 7%.

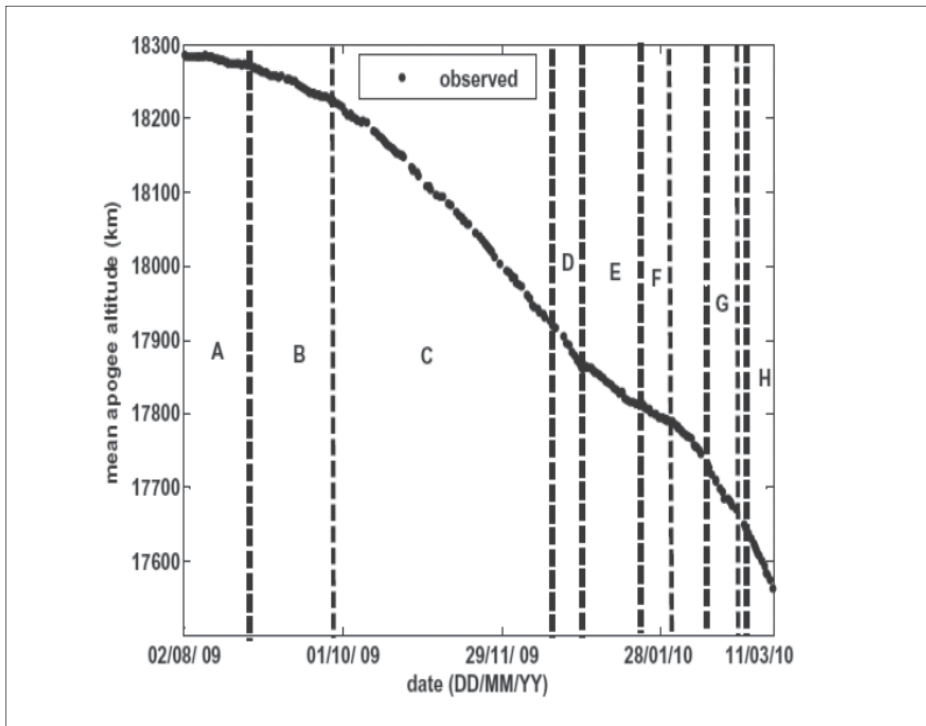


Figure 8.9: Variation of mean apogee altitude of GSLV-F04/CS (NORAD No. 32051) with each zone label mentioned

Table 8.1: Predicted reentry time in zones A to H

Zone label	TLEs considered (UTC)		Computed values		Initial ballistic coefficient (kg/m ²)	Predicted reentry time (UTC) ^a	Time interval ^b (days)
	From	To	Initial osculating eccentricity (e)				
	A	02/08/09 15:45:30	25/08/09 08:30:40	0.57928426			
B	25/08/09 08:30:40	29/09/09 06:40:57	0.57889926	129.2699591	05/12/10 16:30:00	490.0309	
C	29/09/09 06:40:57	20/12/09 13:44:30	0.57794232	59.49630780	07/01/11 09:30:00	522.73	
D	20/12/09 13:44:30	31/12/09 05:08:49	0.57520681	49.57082347	30/12/10 22:04:00	515.2628	
E	31/12/09 05:08:49	19/01/10 14:37:04	0.57467718	89.22781823	02/01/11 19:48:00	518.1684	
F	19/01/10 14:37:04	07/02/10 12:31:01	0.57435027	135.4438362	23/12/10 16:27:00	508.0288	
G	12/02/10 13:32:46	21/02/10 12:42:04	0.57327266	81.43612833	19/12/10 04:22:00	503.5253	
H	01/03/10 14:15:09	11/03/10 03:30:13	0.5718824	92.28161084	22/12/10 08:35:00	506.7010	

^a UTC Coordinated Universal Time: day(DD)/month(MM)/year(YY) hour(HH): minutes(MM): seconds(SS).

^b Time intervals calculated as the number of days between the re-entry prediction and the first TLE epoch of zone A.

Table 8.2: Comparison between actual and predicted reentry times of some decayed objects

Zone label		TLEs considered (UTC)		Computed values		Initial ballistic coefficient (B)	Predicted re-entry time (UTC)	% Error	
From	To	Initial osculating eccentricity (e)							
<i>GSLV DII/CS (NORAD No. 26746) actual re-entry: 18/01/03 05:31 UTC</i>									
I	22/12/02 17:45:30	31/12/02 17:47:19	0.37468978			93.13786894	17/01/03 02:25	-6.46	
<i>GSLV D2/CS (NORAD No. 27808) actual re-entry: 24/02/05 17:24 UTC</i>									
II	19/01/05 17:13:34	29/01/05 09:59:57	0.39534279			97.99438216	23/02/05 02:43	-6.13	
<i>GSLV-FII/CS (NORAD No. 28418) actual re-entry: 24/11/07 19:300 UTC</i>									
IIIa	15/07/07 23:17:41	12/08/07 01:24:46	0.5390412			72.146125132	25/11/07 07:17	0.47	
IIIb	06/10/07 05:41:37	14/10/07 11:15:18	0.40580561			81.87754181	24/11/07 23:59	0.45	
<i>Mohiniya3-34(NORAD No. 19713) re-entry: 27/05/07 07:17 UTC</i>									
IV	17/05/07 03:39:08	20/05/07 19:15:36	0.55847152			168.26991032	27/05/07 07:39	0.24	
<i>Mohiniya3-46(NORAD No. 23211) re-entry: 10/02/09 13:18 UTC</i>									
V	30/01/09 14:49:33	02/02/09 16:00:38	0.47445539			42.75788298	10/02/09 07:38	-2.99	
<i>Mohiniya3-39(NORAD No. 20813) re-entry: 08/07/09 22:49 UTC</i>									
VI	29/06/09 05:21:12	4/07/09 03:05:12	0.54609431			1250.87636707	08/07/09 17:31	-4.58	
Root-sum-square (RSS) of (%) error								10.4741	

[§]percentage error = $\frac{(\text{predicted re-entry time} - \text{actual re-entry time})}{(\text{actual re-entry time} - \text{time of the latest TLE epoch used})} \times 100$.

Re-entry time Estimation of the upper stage of GSLV-D5

Fletcher and Sharma (2014) predicted the re-entry time of the upper stage (Norad No. 39499) of the Indian geosynchronous satellite launch vehicle, GSLV-D5, which inserted the satellite GSAT-14 into a GTO on January 05, 2014, with mean perigee and apogee altitudes of 170 km and 35975 km. Four intervals A to D of near linear variation of the mean apogee altitude observed were used in predicting the orbital lifetime. For these four intervals, optimal values of the initial osculating eccentricity and ballistic coefficient for matching the mean apogee altitudes were estimated with the response surface methodology using a genetic algorithm. It was found that the orbital lifetime from these four time spans was between 144 and 148 days as shown in Table 8.3. The actual life time was found to be 154 days with re-entry date of 8th June 2014.

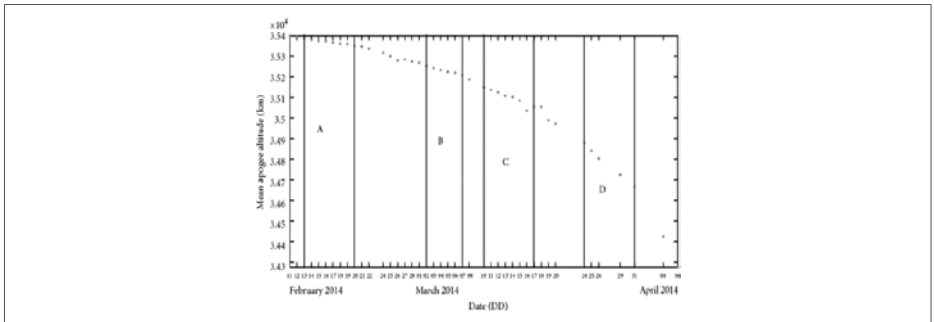


Figure 8.10: Variation of observed mean apogee altitude of GSLV R/B

Table 8.3: Computed values of initial osculating eccentricity and ballistic coefficient and re-entry time for each zone using RSM and GA

Zone label	TLEs considered (UTC)		Computed values		Predicted reentry time (mm-dd-yyyy)	Time interval ^a (days)
	From	To	Initial osculating eccentricity (<i>e</i>)	Initial ballistic coefficient (<i>B</i>)		
A	February 13, 2014, 15:24	February 20, 2014, 13:05	0.72796	84.4065933	June 1, 2014	147
B	March 2, 2014, 10:45	March 7, 2014, 04:11	0.72789621	85.8965302	June 1, 2014	147
C	March 10, 2014, 14:32	March 17, 2014, 21:07	0.72761744	81.6301346	June 2, 2014	148
D	March 24, 2014, 06:31	March 31, 2014, 01:15	0.72680628	76.4813202	May 29, 2014	144

^aTime interval is the number of days between the predicted reentry time and the first TLE epoch of zone A.

Re-entry time Estimation of GSLV -D5/CUS, Phobos-Grunt and ROSAT

Mutyalarao and Raj (2015) studied the re-entry time predictions of the three decayed space objects; namely spent cryogenic stage of the Indian geo-synchronous launch vehicle, GSLV -D5/CUS, Phobos-Grunt and ROSAT. Two parameters, eccentricity and ballistic coefficient, were considered for optimal estimation of initial state of the space objects orbits. These two parameters were computed based on the response surface method using genetic algorithm for the selected different time zones. The time zones were arrived in terms of near linear variation of the mean semi-major axis values. The study showed a good agreement between the actual and the predicted re-entry times.

Re-entry Prediction of Cryogenic Spent Stage of GSLV–D5 (GSLV-D5/CUS)

GSLV-D5 mission accomplished on 5th January 2014, injected GSAT-14 satellite into GTO, powered by an indigenous Cryogenic Upper Stage (CUS). The spent upper stage (GSLVD5/CUS), had mean perigee and apogee altitudes of 181.03 km and 35630.974 km, respectively on 05 Jan 2014 16:29:18.242 UTC. Table 8.4 provides the TLE time intervals along with the re-entry predictions obtained using RSM with GA and percentage error. The percentage error is found to be very less with the last prediction.

Table 8.4: Computed values of parameters with predicted re-entry time of GSLV-D5/CUS (Re-entry epoch: 8 June 2014 01:31 UTC a)

Time interval considered (UTC)		Estimated initial parameters		Predicted re-entry (UTC)	Time interval ^b (days)	Mean deviation ^c (days)	Percentage error ^d
From	To	Osculating eccentricity (e)	Ballistic coefficient (B)				
11 Mar 2014 1:07:11	19 Mar 2014 03:54:23	0.727652	454.095	31 May 2014 22:21	81.8846	-3.4597	-8.8157
24 Mar 2014 6:31:49	08 Apr 2014 09:56:50	0.726888	499.981	28 May 2014 18:10	78.7103	-6.6340	-16.9933
29 May 2014 3:49:25	02 Jun 2014 02:12:38	0.478968	578.947	06 Jun 2014 04:51	87.1554	1.8111	-31.1687
03 Jun 2014 15:03:34	05 Jun 2014 05:18:32	0.367956	536.585	09 Jun 2014 00:06	89.9575	4.6132	33.1096
07 Jun 2014 09:02:02	07 Jun 2014 18:51:11	0.173660	517.647	08 Jun 2014 01:27	89.0138	3.6694	-1.0004

^aUTC : day(DD)/month(MM)/year(YYYY) hour(HH):minutes(MM):seconds(SS).
^bTime interval is calculated as the number of days between the first TLE epoch (i.e., 11 Mar 2014 1:07:11) and the predicted re-entry epoch.
^cMean Deviation is calculated as deviation of time interval from the average of all time intervals.
^dpercentage error=[(predicted re-entry epoch – re-entry epoch)/(re-entry epoch – latest TLE epoch in the time interval)] x 100.

For the spent upper-stage rocket and defunct spacecraft bodies re-entering the Earth's atmosphere, the extent of aero-thermal degradation depends on the rate of energy dissipated during flight and on the thermal characteristics of the material. It is well known that the re-entry trajectory and the aerodynamic heating are significantly influenced by the aerodynamic drag. Deependran (2014) and Balakrishnan and Kurian (2014) carried out a study involving the measurement of rarefied drag and of material degradation under simulated re-entry heating. The rarefied drag coefficient was experimentally determined by direct pressure measurements in a rarefied wind tunnel. From the ensuing re-entry trajectory, the aerodynamic heating was estimated. The material thermal response and the physical nature of degradation were studied experimentally through transient heat flux simulations. Results of the experiments were compared with numerical results of transient heat flux simulations.

Various space facing materials were considered for study and the sensitivity of the thickness on degradation was brought out. It was found that aluminum alloys and carbon fiber reinforced plastics have the potential for early degradation, whereas columbium and similar high-temperature alloys would possibly survive the re-entry heating environments.

Sharma and Anil Kumar (2005) proposed a new technique for the re-entry prediction using Kalman filter approach with constant gains that are based on a minimization of a suitable cost function derived out of estimated lifetime at different epochs of Two Line Elements (TLE) sets and the measurements such as positional and velocity components. Prediction of the orbital lifetime and the propagation of the osculating orbital elements were carried out by utilizing the software based on KS element equations. The constant gains were estimated by minimizing the suitable objective function. The states considered were the position and velocity components of the object derived from TLEs and ballistic coefficient ($B = CD A/m$). The constant Kalman gains chosen as above are able to account for the modeling and measurement errors. The main contribution in the study is the fusion of two objective functions, based on least square error between the predicted states and measurements, and the variation in the predicted re-entry at different TLE epochs. Comparisons of the present approach with some of the known re-entry predictions are provided. In the case of the re-entry of Cosmos 2332 Satellite, a total of 54 TLEs available from 17th Jan. to 28th Jan. 2005, obtained by request from www.celestrack.com, were utilized for testing the algorithm. The actual re-entry reported was 28th Jan. 2005,

16:37 hours (UTC). Table 8.5 provides the re-entries from different epochs. It might be noted that the predicted re-entries were found to be all along quite close to the actual re-entry time, with quite less uncertainties bands on the predictions.

Table 8.5: Prediction of Re-entry of COSMOS 2332 Satellite

SI No.	Prediction Epoch	Predicted Reentry	Uncertainty in Hrs	
			Lower Bound	Upper Bound
1	2005/01/28 15:02	2005/01/28 16:17	-0.4500	0.5000
2	2005/01/28 14:29	2005/01/28 16:17	-0.8500	0.8500
3	2005/01/28 10:40	2005/01/28 16:00	-1.2000	1.3000
4	2005/01/28 07:29	2005/01/28 16 24	-1.3000	1.7500
5	2005/01/28 05:45	2005/01/28 16 18	-1.3000	1.9000
6	2005/01/28 01:23	2005/01/28 17 11	-1.2500	1.8700
7	2005/01/27 15:08	2005/01/28 16 50	-2.0000	2.2500
8	2005/01/27 13:40	2005/01/28 15 53	-2.2200	2.4500
9	2005/01/27 10:44	2005/01/28 16 41	-2.5600	2.6600
10	2005/01/27 07:48	2005/01/28 17:05	-2.9000	3.3300
11	2005/01/27 00:28	2005/01/28 17:02	-2.7500	3.3300
12	2005/01/26 21:32	2005/01/28 19:01	-3.0000	4.1000
13	2005/01/26 20:04	2005/01/28 17:21	-4.4100	5.0000
14	2005/01/26 11:15	2005/01/28 15:31	-4.1000	4.5000
15	2005/01/25 20:32	2005/01/28 15:50	-4.9900	5.8800
16	2005/01/25 11:42	2005/01/28 15:37	-4.7700	5.4000
17	2005/01/25 01:23	2005/01/28 15:50	-4.9900	5.8500
18	2005/01/24 20:58	2005/01/28 16:22	-6.0000	7.5000
19	2005/01/24 16:32	2005/01/28 15:01	-6.4300	8.0200
20	2005/01/24 15:04	2005/01/28 13:48	-6.6600	8.3300
21	2005/01/24 12:07	2005/01/28 11:31	-7.5500	9.0000
22	2005/01/24 01:47	2005/01/28 11:40	-10.0000	11.1100
23	2005/01/23 19:52	2005/01/28 10:36	-12.1000	13.7900
24	2005/01/23 18:24	2005/01/28 09:25	-13.5500	14.0000
25	2005/01/23 13:58	2005/01/28 09:21	-16.0000	16.7800
26	2005/01/23 03:37	2005/01/28 13:50	-16.6600	17.6300
27	2005/01/22 20:13	2005/01/28 13:18	-19.0000	18.9900
28	2005/01/22 12:50	2005/01/28 13:44	-19.7500	21.0000
29	2005/01/20 20:50	2005/01/28 14:37	-20.5500	23.2500
30	2005/01/20 13:25	2005/01/28 15:31	-22.0000	23.7800
31	2005/01/20 04:31	2005/01/28 16:00	-24.0000	25.0000
32	2005/01/19 22:35	2005/01/28 15:40	-25.0000	26.2500
33	2005/01/19 19:37	2005/01/28 15:15	-25.0000	27.5000
34	2005/01/19 13:41	2005/01/28 11:59	-26.5900	27.5500
35	2005/01/19 03:18	2005/01/28 11:26	-26.7600	28.0000
36	2005/01/18 21:21	2005/01/28 09:11	-28.2500	29.4500
37	2005/01/18 13:56	2005/01/28 09:10	-28.2500	30.8900
38	2005/01/18 05:01	2005/01/29 02:40	-29.9900	33.9200
39	2005/01/17 23:04	2005/01/29 00:57	-32.0700	37.9000
40	2005/01/17 20:06	2005/01/29 04:46	-33.0000	40.0000

Anil Kumar and Subba Rao (2002) proposed a procedure for estimating the ballistic coefficient by utilizing the genetic algorithm, by improving the orbital life time (OLT) prediction accuracy from an initial set of two line elements of risk objects and developed software 'BALEST'. This was achieved by minimizing the variance of the OLT predictions. Predictions were carried out using a simple and fast propagator based on mean atmospheric models. In this approach the short-periodic variations in the ballistic coefficient get averaged out while data noise also gets smoothed out and the uncertainties in predicting atmospheric variations gets absorbed to the ballistic coefficient estimation. The aim of this ballistic coefficient is only to improve the OLT prediction accuracy, not necessarily to improve the ballistic coefficient estimates. The precision of this approach has been verified over considerable number of simulations based on numerical integration. Further, the performance of method with the decay of some re-entered debris objects. SROSS-C2 (USSPACECOM Id 23099 U) and third stage of SOYUZ 1 IA5 1 1U Launcher (US SPACECOM Id. 25947) is studied. Figure 8.11 provides the online re-entry prediction times from different epochs. It may be noted that from the last 15 epochs the re-entry predictions are quite good.

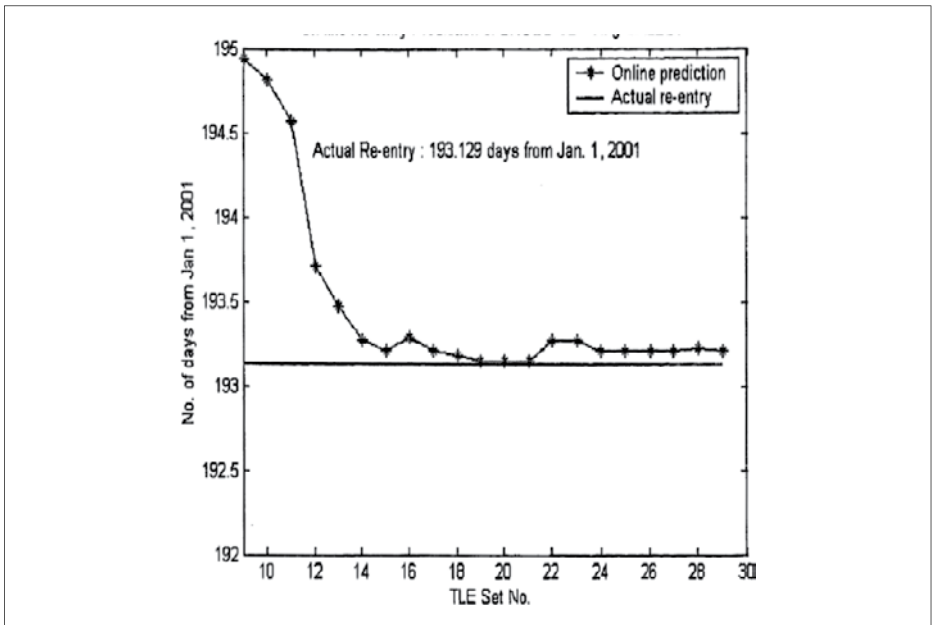


Figure 8.11: SROSS-C2 re-entry times using BALEST– Online predictions

Sharma et al. (2004b) proposed a procedure for estimating the ballistic coefficient, thereby improving the orbital life time (OLT) prediction accuracy, from an initial set of orbit determination data via minimization of the variance of the OLT predictions using the orbit prediction code KSNUM. The basic feature of the approach was that the model and measurement errors are accountable in terms of adjusting the ballistic coefficient and hence the estimated BC is not the actual ballistic coefficient but an effective ballistic coefficient. Variance minimization is achieved through the application of a simple version of the Genetic Algorithm. It is demonstrated that the inaccuracies or deficiencies in the inputs, like F10.7 and A_p values, are absorbed in the estimated BC. Details of the re-entry predictions with respect to the 4th and 5th IADC re-entry campaigns, related to COSMOS 1043 rocket body and COSMOS 389 satellite, which re-entered the Earth's atmosphere on 19 January 2002 and 24 November 2003, respectively, are described. The re-entry results of US Sat No. 25947 and SROSS-C2 Satellite, which re-entered the Earth's atmosphere on 4th March 2000 and 12th July 2001, are also provided. The predicted re-entries were found to be all along quite close to the actual re-entry time, with quite less uncertainties bands on the predictions. A comparison with the re-entry predictions made by the other agencies brings out the efficiency and soundness of the present procedure.

The software 'KSGEN' developed in VSSC and described by Sharma et al. (2004 b) was utilized for the re-entry predictions in the IADC re-entry campaigns. This software is an integrated package of 'KSNUM' and Genetic algorithm. Effective ballistic coefficient BC is estimated with respect to the state vectors from different epochs that minimize the dispersions in the re-entry times from the state vectors under consideration. KSNUM integrates numerically the KS element equations by including the perturbing forces due to Earth's flattening (J_2 to J_6) and air drag (analytical oblate diurnal atmosphere), with the fourth-order Runge-Kutta-Gill method using Jacchia 1977 atmospheric density model.

The software required suitable values of solar flux (F10.7), magnetic index (A_p) and interval for ballistic coefficient variation. F10.7 values utilized at the epoch are based on an average of the 81 days just prior to the epoch TLE and for further propagation the software used either predicted or estimated values in day-by-day basis. Similarly, the A_p values were also updated based on the predicted and estimated values. The limits for ballistic coefficients were taken as 70 and 85, which were found to be sufficient enough after test runs of 'KSGEN'. The TLEs were converted by SatSpy software to position and velocity components for the numerical integration and propagation by 'KSGEN'. The execution of the program provided the best ballistic coefficient estimated, which minimized the predicted re-entry time variations with

respect to each set of TLE data, together with the mean prediction and dispersions on the predictions at the TLEs utilized. It also provided the prediction of the re-entry for the latest available TLE. The mean prediction from the sufficient number of TLE sets was considered as the re-entry prediction for the latest epoch. In all our prediction exercises, we assumed that the object re-enters the Earth's atmosphere when it reaches an altitude of 90 km above the Earth.

8.8 Orbital lifetime estimation of upper stages with different inclinations

Bandyopadhyay et al. (2006) carried out a study on the orbital lifetime estimation of upper stages with different inclinations through response surface technique. The combined influence of the luni-solar perturbations and drag on lifetime variations plays an important role. In order to extract information on the lifetime from orbital data, the estimation of area to mass ratio, initial perigee altitude and ballistic coefficient is performed. In this context, it is noticed that when an object undergoes orbital resonance, bifurcation between the observed and predicted trajectories takes place. However, in some scenarios, simulation of apogee and perigee altitude profiles can still be performed to estimate relevant parameters. To capture only secular changes in apogee and perigee altitudes, osculating elements can be converted to their respective mean values by utilizing a suitable theory. Furthermore, a study on the re-entry of the object is examined closely by estimating different ballistic coefficients to match the position at different epochs. The non-uniform change in the ballistic coefficient provided an indication of possible chaotic motion.

8.9 Presence of Chaotic Motion

The estimation of initial ballistic coefficient, $B (= m/CDA)$ was made during the study from different TLE epochs from 03-Januaray-2001, 18:16:09 (UTC) to the last TLE epoch 31-May-2002, 16:40:02(UTC). The estimation of initial ballistic coefficient plays an important role in minimizing the cost function that involves mean perigee and apogee values. Six TLE epochs between January 2001 and May 2002, provided in Table 8.9 were utilized for detailed study. Table 8.9 provides the estimated values of ballistic coefficient (B). A numerical propagator NPOE (Numerical Prediction of Orbital Events), was used for this purpose. Orbit propagation was carried out with NPOE using the force model which included 36×36 Earth gravity model of GEM10B, atmospheric drag perturbations, lunar and solar gravity effects. MSIS90 density model with the monthly averaged values of solar flux (F10.7) and geomagnetic activity (A_p) obtained from www.dxlc.com/solar website was utilized to compute the drag force.

A detailed study, using NPOE was carried out with the last 3 days TLEs (15 epochs) to estimate the ballistic coefficient from one epoch to match the location of the next epoch. The results were presented in Table 8.10. They provided a reasonably good match between computed and observed values of latitude, longitude, altitude, mean perigee and mean apogee heights. It may be noticed that for first 3 epochs the ballistic coefficient (kg/m^2) varied between 51.5 and 98.8. For the next 8 epochs, it was between 65 and 176.4. Since the mean perigee altitude did not vary significantly for these 8 epochs, so m/CD will not change appreciably, therefore the effective area of rocket body must have decreased near perigee, where drag force is the maximum and was mainly responsible for the orbital decay. Further, the value of ballistic coefficient decreased to 57.8, then increased to 98 and finally decreased to 62.1, which provided the last observed orbital parameters. It suggested that during the third day before the day of re-entry, the rocket body had toppled and had different effective areas near perigee passage during each orbit. It suggested that the motion must have been chaotic.

Table 8.6: Computed values of initial ballistic coefficients (B) (Match TLE 28-May-2002, 10:51:54 (UTC))

S.No	TLE Epoch (UTC) (DD/MM/YY)	ballistic coefficient (kg/m^2)
1	03/01/2001, 18:16:09	95.5
2	03/03/2001, 12:16:56	153.5
3	03/10/2001, 15:58:56	26
4	03/01/2002, 04:05:34	75.3
5	03/04/2002, 16:10:15	124.94
6	28/05/2002, 04:52:17	96.8

Table 8.7: Computed values of initial ballistic coefficients (B) (Match TLE 28-May-2002, 10:51:54 (UTC))

S.No	TLE Epoch From – To (UTC)	latitude (deg) Observed [Computed]	longitude (deg) Observed [Computed]
1	28-May-2002, 04:52:17 to 28-May-2002, 10:51:54	0.020 [0.019]	27.238 [27.225]
2	28-May-2002, 10:51:54 to 28-May-2002, 17:50:28	-0.021 [-0.018]	280.169 [279.504]
3	28-May-/2002, 17:50:28 to 28-May-2002, 23:02:19	0.013 [-0.030]	200.856 [200.397]
4	28-May-2002, 23:02:19 to 29-May-2002, 04:12:11	0.007 [0.006]	121.772 [121.817]

Table 8.7: Computed values of initial ballistic coefficients (B) (Match TLE 28-May-2002, 10:51:54 (UTC))

5	29-May-2002, 04:12:11 to 29-May-2002, 05:24:17	-2.109 [-2.109]	11.573 [11.390]
6	29-May-2002, 05:24:17 to 29-May-2002, 07:37:28	-0.015 [-0.015]	68.840 [68.803]
7	29-May-2002, 07:37:28 to 29-May-2002, 10:55:01	-0.734 [-0.745]	358.125 [358.140]
8	29-May-2002, 10:55:01 to 29-May-2002, 21:10:49	0.061 [0.009]	223.011 [221.682]
9	29-May-2002, 21:10:49 to 30-May-2002, 03:50:51	0.002 [-0.002]	119.296 [119.184]
10	30-May-2002, 03:50:51 to 30-May-2002, 10:15:50	-1.248 [-1.266]	344.618 [344.001]
11	30-May-2002, 10:15:50 to 30-May-2002, 18:45:35	0.985 [0.997]	279.110 [278.898]
12	30-May-2002, 18:45:35 to 30-May-2002, 20:13:36	-0.017 [-0.010]	227.903 [227.843]
13	30-May-2002, 20:13:36 to 31-May-2002, 04:13:04	0.005 [-0.040]	105.352 [104.527]
14	31-May-2002, 04:13:37 to 31-May-2002, 16:39:55	0.0785 [0.0783]	275.849 [275.843]
15	31-May-2002, 16:39:55 to 31-May-2002, 16:40:02	275.905 [276.241]	663.715 [661.469]

S.No	mean perigee (km) Observed [Computed]	mean apogee (km) Observed [Computed]	altitude (km) Observed [Computed]	B (kg/m ²)
1	125.598 [119.386]	1917.376 [1917.344]	1811.901 [1808.851]	98.8
2	121.752 [125.806]	1849.955 [1849.944]	1772.348 [1782.477]	51.5
3	122.988 [121.866]	1784.626 [1784.625]	1729.762 [1728.804]	66.7
4	124.137 [114.497]	1718.705 [1718.757]	1680.926 [1679.791]	176.4
5	119.568 [123.904]	1702.200 [1702.321]	1011.282 [1011.102]	65.0
6	121.535 [120.290]	1680.194 [1680.135]	1653.342 [1653.716]	74.98
7	1629.830 [1630.323]	1640.737 [1640.677]	121.825 [120.560]	90.1
8	1502.140 [1504.540]	1509.748 [1509.673]	115.452 [122.047]	66.7
9	1404.430 [1404.552]	1405.182 [1405.233]	122.150 [121.125]	67.5

Table 8.7: Computed values of initial ballistic coefficients (B) (Match TLE 28-May-2002, 10:51:54 (UTC))

10	1169.663 [1167.111]	1315.150249 [1315.1939]	119.701 [121.465]	67.1
11	1112.434 [1112.462]	1153.880 [1154.935]	122.963 [119.656]	66.8
12	1126.557 [1125.8008]	1131.698 [1131.663]	120.541 [122.987]	60.1
13	945.072 [944.154]	956.502 [956.688]	114.000 [119.672]	57.8
14	660.678 [660.308]	679.495 [679.150]	82.998 [82.466]	61.30
15	99.998 [98.001]	275.905 [276.241]	680.184 [679.494]	62.1

(UTC-Coordinate Time Reference Frame)

8.10

Orbit life time prediction using KS elements equations and genetic algorithm

Sharma et al. (2009b) discussed an integrated procedure for orbit life time prediction combining the KS elements and genetic algorithm (GA). The orbit prediction was carried out by numerically integrating the KS element equations. In this methodology, the ballistic coefficient is estimated from a set of observed orbital parameters in terms of the Two Line Elements (TLE) by minimizing the variance of the predicted re-entry time from different TLE using GA. Software, KSGEN, systematically developed in-house using KS elements and genetic algorithm was utilized for predicting the re-entry time of the risk objects. This software had been effectively used for the prediction of the re-entry time in the past seven re-entry exercise campaigns conducted by the Inter Agency Space Debris Coordination Committee (IADC). The predicted re- entry time matched quite well with the actual re-entry time for all the seven IADC re-entry campaigns. A detailed analysis was carried out with two case studies.

Two objects were considered, SROSS C2 satellite and SL-12 Rocket Body, which re-entered or decayed on 12th July 2001 and 3rd March 2009, respectively. The re-entry prediction of SROSS C2 satellite was carried out with a total of 14 TLE's available for the last five days (from 8th July 2001). From the latest TLE epoch of 12th July 2001, 00:38:01, the prediction was made as 12th July 2001, 4 hours 43 minutes against the actual re-entry time of 4 hours 37 minutes. The difference of 6 minutes was noted. The details of all the 14 predictions made from different TLE's with their percentage error, upper and lower bounds are provided in Table 8.8.

The percentage errors are computed by the following formula.

$$\%error = (TCOM-TREF)*100/(TREF-TIN)$$

where, TCOM is the time of actual re-entry, TREF is the predicted time of re-entry, TREF is the time corresponding to the initial TLE propagated. Maximum % error of 7.1 was noted.

Table 8.8: Re-entry prediction results for SROSS satellite

TLE epoch	Prediction	Lower bound	Upper bound	Difference in minutes	% error
12/07/2001 00:38:01	12/07/2001 4:43	12/07/2001 4:40	12/07/2001 4:56	5.8	2.4
11/07/2001 22:05:35	12/07/2001 4:48	12/07/2001 4:33	12/07/2001 5:18	10.1	2.7
11/07/2001 21:43:13	12/07/2001 5:20	12/07/2001 4:30	12/07/2001 5:42	24.5	5.9
11/07/2001 12:57:07	12/07/2001 4:58	12/07/2001 4:27	12/07/2001 5:49	20.2	2.1
11/07/2001 05:37:27	12/07/2001 5:9	12/07/2001 4:23	12/07/2001 6:5	31.7	2.3
11/07/2001 02:41:21	12/07/2001 5:6	12/07/2001 4:13	12/07/2001 7:3	28.8	1.9
10/07/2001 17:52:20	12/07/2001 5:29	12/07/2001 4:10	12/07/2001 7:13	51.8	2.5
10/07/2001 13:27:29	12/07/2001 5:24	12/07/2001 3:50	12/07/2001 9:23	46.1	2.0
10/07/2001 04:37:20	12/07/2001 8:2	12/07/2001 3:41	12/07/2001 9:43	204.5	7.1
09/07/2001 16:49:34	12/07/2001 8:16	12/07/2001 3:44	12/07/2001 9:53	218.9	6.1
09/07/2001 10:55:22	12/07/2001 8:48	12/07/2001 3:56	12/07/2001 12:28	226.1	5.7
09/07/2001 05:00:57	12/07/2001 8:38	12/07/2001 3:23	12/07/2001 14:25	240.5	5.6
08/07/2001 21:37:38	12/07/2001 9:20	12/07/2001 2:28	12/07/2001 14:19	265.0	5.6
08/07/2001 11:16:33	12/07/2001 8:22	12/07/2001 5:38	12/07/2001 14:25	259.2	4.8

The re-entry prediction of SL-12 rocket body was carried out with a total of 13 TLEs available for the last three days (from 1st March 2009). From the latest TLE epoch of 3rd March 2009 at 16:54:51, the prediction was made as 03rd March 2009 at 17hours 25 minutes against the actual re-entry time of 03rd March 2009, 17hours 30 minutes. The difference of 5 minutes was noted. The details of all the 13 predictions made from different TLE's with their percentage error, upper and lower bounds were provided in Table 8.9. Maximum % error of 12.4 was noted, where the difference was only 4.3 minutes. For other predictions, % error was less than 10.

Table 8.9: Re-entry prediction results of SL3-rocket body

TLE epoch	Prediction	Lower bound	Upper bound	Difference in minutes	% error
03/03/2009 16:54:51	03/03/2009 17:25	03/03/2009 17:21	03/03/2009 17:31	4.3	-12.4
03/03/2009 15:27:54	03/03/2009 17:18	03/03/2009 17:13	03/03/2009 17:34	11.5	-9.5
03/03/2009 14:00:53	03/03/2009 17:10	03/03/2009 16:56	03/03/2009 18:11	18.7	-9.0
03/03/2009 11:06:41	03/03/2009 17:22	03/03/2009 16:49	03/03/2009 18:48	7.2	-1.9
03/03/2009 03:49:31	03/03/2009 17:30	03/03/2009 14:26	03/03/2009 19:14	25.9	-3.2
02/03/2009 20:31:15	03/03/2009 16:55	03/03/2009 14:31	03/03/2009 20:29	34.6	-2.7
02/03/2009 17:35:50	03/03/2009 16:32	03/03/2009 13:39	03/03/2009 19:45	57.6	-4.0
02/03/2009 11:44:46	03/03/2009 16:40	03/03/2009 13:36	03/03/2009 19:56	49.0	-2.7
02/03/2009 02:57:39	03/03/2009 16:19	03/03/2009 13:27	03/03/2009 20:12	70.6	-3.1
01/03/2009 21:05:55	03/03/2009 16:40	03/03/2009 13:48	03/03/2009 20:13	85.0	-3.2
01/03/2009 16:42:01	03/03/2009 15:30	03/03/2009 12:30	03/03/2009 19:39	113.8	-3.9
01/03/2009 10:49:55	03/03/2009 15:14	03/03/2009 12:50	03/03/2009 19:17	138.2	-4.2
01/03/2009 04:57:40	03/03/2009 15:21	03/03/2009 12:00	03/03/2009 19:13	128.2	-3.5

8.11

Re-entry Prediction of Phobos-Grunt and ROSAT satellites

Mutyalarao and Raj (2012) presented a methodology to predict the re-entry time of decaying space objects from low-Earth-orbit through an optimization technique. Two parameters, initial eccentricity and ballistic coefficient were chosen for optimal estimation. It is known that the errors are more for these two parameters based on TLEs. These two parameters are computed with response surface method (RSM) using genetic algorithm (GA) for the selected time intervals. The methodology was verified by calculating the re-entry time of the decayed objects Phobos-Grunt and ROSAT satellites from different epochs.

Mutyalarao and Raj (2014a) made a study to predict the re-entry time of re-entered cryogenic upper stage of GSLV-D5 rocket using response surface method with genetic algorithm. The orbital lifetime estimation of the spent CUS was analyzed by downloading its TLEs of the last 5 days before its re-entry. High Precision Orbit Propagator (HPOP) of STK software was utilized for propagating the orbit with required perturbative forces. Table 8.10 provides the re-entry times of GSLV-D5/CUS from 5 different epochs. As per the website www.space-track.org information on 8th June 2014, the rocket body re-entered at 0.0 hours (UTC).

Table 8.10: Re-entry prediction GSLV-D5/CUS

Sl. No.	TLE time interval		Predicted Re-entry (UTC)
	From	To	
1	11 Mar 2014 1:07:10.990	19 Mar 2014 03:54:22.776	31 May 2014 22:21
2	24 Mar 2014 6:31:48.568	08 Apr 2014 09:56:50.267	28 May 2014 18:10
3	29 May 2014 3:49:24.608	02 Jun 2014 02:12:38.346	06 Jun 2014 04:51
4	03 Jun 2014 15:03:33.603	05 Jun 2014 05:18:32.358	09 Jun 2014 00:06
5	07 Jun 2014 09:02:01.686	07 Jun 2014 18:51:10.832	08 Jun 2014 01:27

8.12

Re-entry Prediction with response surface method using genetic algorithm and Lifetime optimization with STK

Anil Kumar et al. (2014) discussed three novel models namely response surface method with genetic algorithm, optimization with Satellite Tool Kit (STK) and Lifetime optimization with STK. These models will predict the re-entry time of decaying space objects from low-Earth-orbit (eccentricity < 0.2) through an optimization technique. Each of these models is unique in methodology and objective function. Finally, the usefulness of the presented models is demonstrated by presenting re-entry prediction of some decayed satellites.

Using the estimated values of e and B with RSM and GA and keeping all other orbital elements unchanged, the re-entry time was calculated using HPOP. The space object was assumed to have re-entered the atmosphere as soon as it came down to a mean perigee altitude of 10 km, and the re-entry time was referred to this re-entry condition. The force model included terms up to J36, 36 of the Earth's gravity model based on World Geodetic System dating from 1984 (WGS84), atmospheric drag and lunar and solar gravity effects.

Table 8.11 provided the final TLE epochs of selected TLE time intervals, estimated values of B, e, predicted re-entry time and predicted re-entry time along with percentage error [= (predicted re-entry time – actual re-entry time) / (actual re-entry time – time of first TLE epoch used) 100] of each prediction.

Table 8.11: Computed values of parameters with predicted re-entry time of Phobos-Grunt satellite (Re-entry epoch: 15 Jan 2012 17:45:00 UTC^a)

TLE epoch (UTC)	Osculating eccentricity e	Ballistic coefficient B (kg/m²)	Predicted reentry time (UTC)	% error^d
6 Dec 2011 19:32:05	0.00639	287.8781	11 Jan 2012 23:46:00	-9.39
4 Jan 2012 03:12:34	0.00320	322.4260	14 Jan 2012 17:52:00	-8.57
5 Jan 2012 05:45:35	0.00325	325.6454	16 Jan 2012 10:34:00	6.67
8 Jan 2012 00:03:21	0.00304	339.6691	15 Jan 2012 10:07:00	-4.11
14 Jan 2012 05:42:41	0.00268	375.2657	15 Jan 2012 17:27:00	-0.83

^aUTC : day(DD)/month(MM)/year(YYYY) hour(HH):minutes(MM):seconds(SS);
^dpercentage error=[(predicted reentry epoch – reentry epoch)/(reentry epoch – latest TLE epoch in the time interval)] x 100

Table 8.12: Computed values of parameters with predicted re-entry time of ROSAT satellite
(Re-entry epoch: 23 Oct 2011 01:57:00 UTC)

TLE epoch (UTC)	Osculating eccentricity e	Ballistic coefficient B (kg/m²)	Predicted reentry time (UTC)	% error
2 Oct 2011 21:48:19	0.00123	112.3500	24 Oct 2011 10:58:00	6.82
2 Oct 2011 21:48:19	0.00172	111.1011	24 Oct 2011 01:20:00	4.83
11 Oct 2011 20:41:10	0.00142	101.3880	23 Oct 2011 10:12:00	3.06
13 Oct 2011 21:46:17	0.00158	102.5641	23 Oct 2011 05:49:00	1.76
14 Oct 2011 06:41:15	0.00158	103.1992	23 Oct 2011 03:58:00	0.95

Table 8.12 provided the final TLE epochs of selected TLE time intervals, estimated values of B, e, predicted re-entry time along with percentage error for each prediction. It was noted that the absolute value of percentage error in all the predictions was less than 6.9 percent. The final prediction is 23rd October 2011 03: 58:00, which is close to the actual re-entry time.

8.13 STK OPTIM

Optimization with Satellite Tool Kit (STK OPTIM) is an innovative approach to estimate the essential ballistic parameter (EBP) of the risk object from a span of TLEs and hence to predict re-entry time of the object. The technique uses High precision orbit propagator (HPOP) of the software STK integrated with an optimization technique to arrive at the best re-entry time prediction. Among the latest available TLEs in a short span of time, three TLEs are chosen, first at beginning, other at middle and third at last part of the time span. These TLEs are propagated with a range of ballistic parameters. The trajectories are then matched with the observed values obtained from TLEs to estimate EBP. A multi objective function, considering the errors on apogee and perigee predictions with the observed, is minimized to arrive at the EBP. Three measures, namely, least square error, weighted least square error considering the expected remaining life as weights, and normalized non-dimensioned errors on apogee and perigee are employed as the objective function. Here in this methodology

three types of cost functions are used for optimization to arrive at EBP. They are multi objective functions taking into account (i) least square error on semi-major axis, apogee and perigee height (ii) weighted least square error on semi-major axis, apogee and perigee height with weights being considered depends on time span left between the predicted re-entry time to TLE epoch at which prediction is made and (iii) non-dimensioned normalized least square errors, normalized with respect to the initial orbital value with respect to semi-major axis, apogee and perigee height.

8.14 Re-entry Time Prediction of Phobos-Grunt

For Phobos-Grunt, four predictions were made from TLEs available on last four days (12th to 14th Jan 2012) of re-entry. TLEs were taken from space-track site. For first prediction, a TLE on 12 Jan 2012 was chosen and the state available from it was propagated using HPOP for different ballistic parameters ranging from 340 to 400 which provided different trajectory profiles.

Observed values of semi-major axis, apogee and perigee were obtained using 15 TLEs on the same day. The above mentioned three objective functions were minimized in least square sense through a random search technique (RST). The estimated EBP for this case was 371.0686. The life time was calculated using this EBP with last TLE used in the analysis. Table 8.13 provides the estimated EBP and the predicted re-entry time along with the percentage error in prediction. It can be observed that the percentage error for all the four cases is less than 6 %. The last prediction predicted using TLE at epoch 15 Jan 2012 16: 36:03.905 UTC has difference of only 9 minutes from actual re-entry time of Phobos-Grunt (15 Jan 2012 17:45 UTC).

Table 8.13: Re-entry predictions of Phobos-Grunt

S. No	EBP (kg/m ²)	TLE Epoch (UTC)	Predicted Reentry (UTC)	% Error
1	371.0686	12 Jan 2012 22:58:44.604	15 Jan 2012 15:23:00.000	3.54 %
2	375.3719	13 Jan 2012 20:54:53.035	15 Jan 2012 16:47:04.000	2.15 %
3	369.5749	14 Jan 2012 23:10:33.775	15 Jan 2012 16:38:24.000	5.98 %
4	379.7508	15 Jan 2012 16:36:03.905	15 Jan 2012 17:54:15.142	1.34 %

It can be seen in Table 8.14 that the percentage error for ROSAT for all four cases is less than 3.4 %. For the last prediction the difference in predicted re-entry time and actual re-entry time (23 Oct 2012, 01:57 UTC) is only 12 minutes.

Table 8.14: Re-entry predictions for ROSAT

S. No	EBP (kg/m ²)	TLE Epoch (UTC)	Predicted Reentry (UTC)	% Error
1	104.9459	19 Oct 2011 21:29:35.563	23 Oct 2011 03:20:00	1.81 %
2	104.5043	20 Oct 2011 19:36:13.233	23 Oct 2011 02:25:00	0.86 %
3	104.1217	21 Oct 2011 13:34:01.000	23 Oct 2011 01:38:00	0.87 %
4	117.3970	22 Oct 2011 20:00:09.499	23 Oct 2011 02:09:00	3.36 %

8.15 STK LTOptim

In this method Lifetime Optimization using Satellite Tool Kit (STK LTOptim), a set of TLEs is selected and is propagated using HPOP propagator with a range of ballistic coefficients. For each TLE, lifetime is calculated corresponding to each ballistic coefficient in the range. The best ballistic coefficient which gives the minimum dispersion on lifetime predictions from number of TLEs is estimated with an optimization technique. The lifetime is then calculated using this optimized ballistic coefficient using latest TLE. The re-entry time as per ESA for GOCE satellite was 11 Nov 2013 02:30 UTC. Table 8.15 provides the re-entry predictions made using STK LTOptim.

Table 8.15: Re-entry predictions for GOCE made using STK LTOptim

Latest TLE epoch (UTC)	No: of TLE used	Estimated Area to mass ratio (Cd*A)	Predicted reentry epoch(UTC)
26 Oct 2013 12:14:47	08	0.0036	5 Nov 2013 19:40
30 Oct 2013 19:46: 00	10	0.0036	6 Nov 2013 01:25
03 Nov 2013 20:48:16	12	0.0036	7 Nov 2013 10:51
04 Nov 2013 20:54:55	11	0.0032	7 Nov 2013 17:00
07 Nov 2013 21:56:48	12	0.0034	11 Nov 2013 02:00

8.16 Prediction of Orbital Lifetime of Space Objects in GTO as a Function of Launch Time

Mutyalarao and Raj (2014b) made a study on the prediction of orbital lifetime of space objects in GTO as a function of launch time. Numerical simulation of orbital lifetime of spent stage was discussed. Spent cryogenic stage of the launch vehicle GSLV-F04 was chosen for studying the effect of launch time on orbital lifetime. Lifetime tool of Satellite-Tool-Kit (STK) was utilized for orbit propagation. The study results showed the presence of time zones where the orbital lifetime was of several decades.

8.17 Comparison of Three Methods for Re-entry Prediction for Low Eccentricity Orbits

Anil Kumar et al. (2017) discussed three novel models namely Response Surface Method with genetic algorithm, Optimization with Satellite Tool Kit (STK) and Lifetime optimization with STK for re-entry prediction. These models will predict the re-entry time of decaying space objects from low-Earth orbit (eccentricity < 0.2) through an optimization technique. Each of these models is unique in methodology and objective function. Finally the usefulness of the presented models is demonstrated by presenting re-entry prediction of CZ-2C rocket body. The results obtained from these models were presented in Table 8.16. Percentage errors were provided for RSM-GA and STK LTOptim methods in Tables 8.17 and 8.18. The error for last prediction is found to be minimum with RSM-GA method.

Table 8.16: Prediction of re-entry time of CZ-2C rocket with RSM-GA method

(reentry epoch: 27 June 2016 19:11 UTC ^{a)})			
S.No	TLE Epoch (UTC)	Predicted Re-entry Epoch (UTC)	Percentage error ^d
1	16 Jun 16 19:15:43.415	27 Jun 16 19:14	0.0235
2	20 Jun 16 03:30:09.898	27 Jun 16 08:44	-5.6821
3	20 Jun 16 19:49:15.216	27 Jun 16 09:25	-5.8269
4	21 Jun 16 21:01:12.949	27 Jun 16 19:25	0.1756
5	23 Jun 16 01:09:11.147	28 Jun 16 02:44	6.6315
6	23 Jun 16 23:20:07.908	27 Jun 16 17:36	0.0181
7	25 Jun 16 09:16:53.823	27 Jun 16 18:35	-1.0193

^aUTC : day(DD)/month(MM)/year(YY)
hour(HH):minutes(MM):seconds(SS); ^dpercentage
error=[(predicted reentry epoch – actual reentry epoch)/(actual reentry epoch – latest TLE epoch in the time interval)] x 100

Table 8.17: Re-entry predictions with STKOptim method

Analysis date	EBP (kg/m ²)	Pivot TLE epoch (UTC)	Re-entry prediction (UTC)
21 Jun 16	29.326	19 Jun 16 18:51:23 (15) [#]	27 Jun 16 10:31:00
22 Jun 16	29.516	20 Jun 16 21:18:14 (8)	27 Jun 16 16:54:00
23 Jun 16	31.786	21 Jun 16 03:14:06 (10)	28 Jun 16 03:04:00
24 Jun 16	32.467	22 Jun 16 04:25:37 (10)	28 Jun 16 04:19:00
25 Jun 16	29.325	23 Jun 16 20:22:46 (10)	27 Jun 16 17:30:00
26 Jun 16	29.325	24 Jun 16 15:34:56 (10)	27 Jun 16 18:25:00
26 Jun 16	31.348	24 Jun 16 20:00:35 (8)	27 Jun 16 20:03:00
26 Jun 16	30.303	24 Jun 16 20:00:35 (9)	27 Jun 16 18:57:00
27 Jun 16	29.709	24 Jun 16 20:00:35 (10)	27 Jun 16 19:39:00
27 Jun 16	29.516	24 Jun 16 20:00:35 (10)	27 Jun 16 18:17:00
27 Jun 16	29.709	25 Jun 16 01:54:37 (10)	27 Jun 16 18:11:00
27 Jun 16	30.921	26 Jun 16 01:28:49 (7)	27 Jun 16 18:27:00

#: Numbers in parenthesis' represents No. of TLE used for prediction

Table 8.18: Re-entry predictions for CZ-2C using STK LTOptim method

S No	Latest TLE epoch (UTC)	Predicted re-entry time (UTC)	Percentage Error
1	16 Jun 16 19:15:43	27 Jun 16 11:54	-2.7597
2	19 Jun 16 20:04:56	27 Jun 16 11:36	-3.9682
3	20 Jun 16 19:49:15	27 Jun 16 11:55	-4.3419
4	21 Jun 16 21:01:13	27 Jun 16 19:01	-0.1172
5	23 Jun 16 01:09:11	27 Jun 16 23:39	3.9171
6	26 Jun 16 08:49:53	27 Jun 16 16:56	-6.5499
7	26 Jun 16 16:10:36	27 Jun 16 18:41	-1.8514

All these predictions uses 10 number of TLEs prior to latest TLE epoch

8.18 Re-entry time prediction for CUS of GSLV-F09 mission

Mutyalarao and Anil Kumar (2018) studied the re-entry time prediction for CUS of GSLV-F09 mission. CUS was inserted into GTO on 5 May 2017 and it re-entered on 10 Oct 2017. Optimal estimation of two initial parameters namely osculating eccentricity and ballistic coefficient was considered based on linear variation of mean apogee altitude. Optimal estimation of these two parameters was done using response surface method with genetic algorithm. Accurate prediction of re-entry time with decay location was carried out one day before its re-entry. The final re-entry time announced by NASA was 10 Oct 2017 03:37: 00 UTC (± 40 minutes). Good agreement was noticed between predicted and actual re-entry time as seen from Table 8.19.

Table 8.19: Re-entry prediction time computed for GSLV-F09/CUS rocket using RSM with GA in each time interval

S.No.	TLE time interval (UTC ^a)		Predicted Re-entry time (UTC)
	From	End	
1	12 May 2017 16:26:28.272	17 Jun 2017 11:31:27.921	21 Oct 2017 21:54:00 (±1 month)
2	23 Jul 2017 17:48:07.365	10 Sep 2017 02:37:05.661	13 Oct 2017 14:43:00 (±4 days)
3	1 Oct 2017 08:49:24.066	3 Oct 2017 14:20:48.041	8 Oct 2017 08:34:00 (±3 days)
4	4 Oct 2017 16:17:47.634	7 Oct 2017 20:34:05.938	10 Oct 2017 10:36:00 (±27 hrs)
5	7 Oct 2017 16:34:51.335	9 Oct 2017 01:57:46.725	10 Oct 2017 03:58:00 (±3 hrs)
6	8 Oct 2017 09:44:12.976	9 Oct 2017 13:51:48.834	10 Oct 2017 03:30:00 (±2 hrs)

^a Co-ordinated universal time

8.19 Re-entry predictions of space objects from highly elliptical orbits using KS Elements

Sellamuthu and Sharma (2018) used Kustaanheimo-Stiefel (KS) regularization method to obtain linear differential equations of a harmonic oscillator with constant frequency and extended to perturbed motion. A regularized numerical orbit propagator (KSROP), with constant step-size, in terms of KS regular elements was developed. The Sun and the Moon ephemeris was computed using Plataforma Solar de Almería and a series expansion algorithm, respectively. An oblate atmospheric model using density scale height varying with altitude for drag and zonal harmonic terms up to J6 for oblateness effects, were considered. In this study, re-entry prediction of HEO RSO was treated as an optimal estimation problem. Two-line element sets of few RSO was used with SGP4/SDP4 theory to obtain initial osculating orbital elements. Optimal estimates of B and e were found using response surface methodology with genetic algorithm. KSROP was used to propagate the optimal initial parameters. Re-entry times were predicted with low error (<6%) when compared with actual data. Figure 8.12 describes the re-entry time methodology. Figure 8.13 shows the five selected zones for estimation of eccentricity (e) and ballistic coefficient (BC). Table 8.20 provides the details related to the number of TLE used in each zone and the estimated eccentricity and BC for each zone. Table 8.21 provides the relative percentage error, which is maximum for fifth zone. Its value is 5.78.

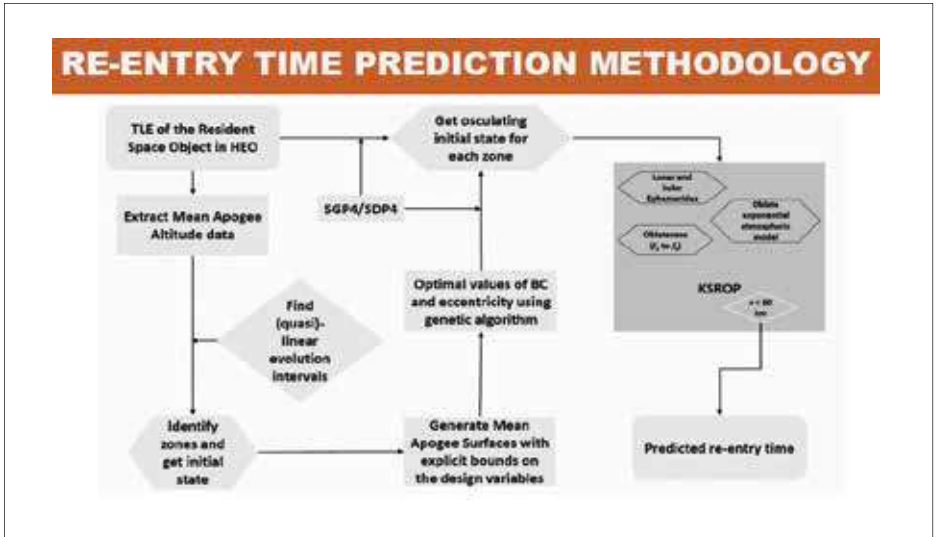


Figure 8.12: Re-entry prediction methodology

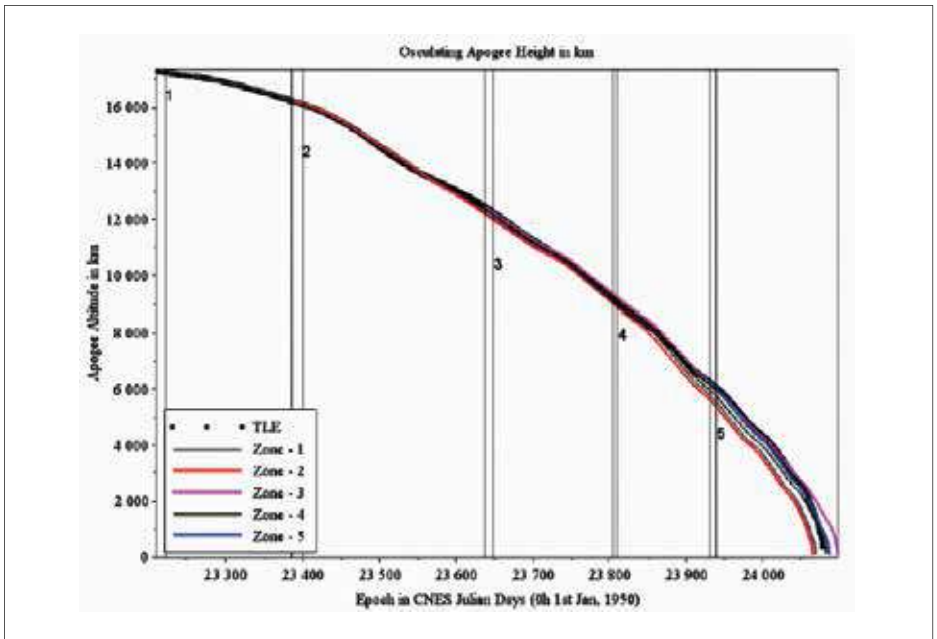


Figure 8.13: Five zones for finding ballistic coefficient and eccentricity (Case 2)

8.20 Re-entry predictions of Space Objects from Low Eccentric Orbits

Lawrence and Sharma (2019) studied the re-entry predictions of the space objects from the low eccentric orbit. An object re-enters the Earth’s atmosphere with a high orbital velocity. Due to the aerodynamic heating the object tends to break into multiple fragments which later pose a great risk hazard to the population. A satellite was considered as the space object for which the re-entry prediction is made. This prediction was made with a package where the trajectory path, the time of re-entry and the survival rate of the fragments was done. The prediction was made using DRAMA 2.0—ESA’s Debris Risk Assessment and Mitigation Analysis Tool suite, MATLAB and Numerical Prediction of Orbital Events software (NPOE). The predicted re-entry time of OSIRIS 3U was found to be on 7th March 2019, 7:25 (UTC), whereas the actual re-entry time was on 7th March 2019, 7:03 (UTC). The trajectory path found was 51.5699 deg. (Lat), –86.5738 deg. (Long.) with an altitude of 168.643 km. The actual trajectory was 51.76 deg. (Lat), –89.01 deg. (Long.) with an altitude of 143.5 km.

Table 8.20: Eccentricity and ballistic coefficient (BC) used for 5 intervals

Zone	No. of TLE	Initial & Final TLE Epoch		Eccentricity	BC (kg/m ²)
1	34	2013-07-19	2013-07-31	0.5647780358	84.391
2	27	2014-01-10	2014-01-25	0.5502844178	72.39898
3	23	2014-09-20	2014-09-29	0.4843383016	57.01749
4	18	2015-03-04	2015-03-11	0.4099154005	74.01749
5	21	2015-07-10	2015-07-18	0.3177805245	84.70306

8.21 Re-entry time prediction of Molniya orbit objects

Sellamuthu et al. (2019) studied the re-entry of Molniya orbits which are highly elliptical orbits (HEOs), with a period of ~12 hours, and are critically inclined (63.4°) with the swath covering the high latitudinal regions of the Earth. Despite the availability of high fidelity orbit propagators, the uncertainty in the initial parameters can lead to an inaccurate prediction. The re-entry time prediction of Molniya satellites was carried out as an optimal estimation problem. For carrying out optimal re-entry

estimation of Molniya satellites, eccentricity and ballistic coefficient were treated as uncertain parameters. Optimal estimate of these design variables was determined by using response surface method (RSM) and genetic algorithm (GA). Using Numerical Prediction of Orbital Events (NPOE) software, the numerical propagation was carried out with realistic perturbation model. By use of this method, accurate re-entry time of six Molniya satellites were predicted with errors less than 5% when compared with the actual data. Table 8.22 provides the launch log of the selected Molniya satellites. Table 8.23 provides optimal solutions for Molniya satellites re-entry time prediction. Figure 8.14 provides optimal and non-optimal apogee altitude solution compared with TLE data for case 4.

Table 8.21: Predicted re-entry decay and percentage errors for 5 predictions

NORAD ID	Zone	No. of days to actual decay from initial TLE epoch	Predicted Decay epoch	Actual Decay Epoch	Rel. % Error
37151	1	859	2015-11-25	2015-12-04	1.052
	2	680	2015-11-21		-1.92
	3	459	2015-12-23		4.42
	4	278	2015-12-08		1.497
	5	158	2015-12-12		5.78

8.22

Assessment of three in-house developed re-entry prediction methods

Dutt et al. (2020) presented three in-house developed re-entry prediction methods namely, RSM- GA, STKOptim and STKLOptim. All the three methods used a set of TLEs of re-entering object as input. They optimized the ballistic coefficient (BC) to reduce the error function and this optimized BC was used for propagation of latest TLE to predict the re-entry time epoch. All the three methods have different objective functions and use High Precision Orbit Propagator (HPOP) from System Tool Kit (STK) for orbit propagation. RSM-GA uses response surface methodology (RSM) to estimate the osculating eccentricity and ballistic coefficient at the initial epoch by minimizing the error between the observed and predicted mean apogee altitude in the specified time interval with the help of genetic algorithm (GA). STKOptim estimates essential ballistic parameter of the risk object from a span of TLEs and uses it for re-entry time prediction. STKLOptim minimizes the dispersions in TLE lifetime to obtain re-entry time estimate. The effectiveness and applicability of these methods are presented here through case studies of recently decayed objects namely, Electron Rocket Body (#43166) and PSLV-C39/IRNSS-1H composite rocket body (#42928).

Table 8.22: Launch log of selected Molniya satellites

Case	NORAD ID	Launch epoch
1	11007	August 22, 1978
2	22729	August 4, 1993
3	24273	August 14, 1996
4	26867	July 20, 2001
5	28163	February 18, 2004

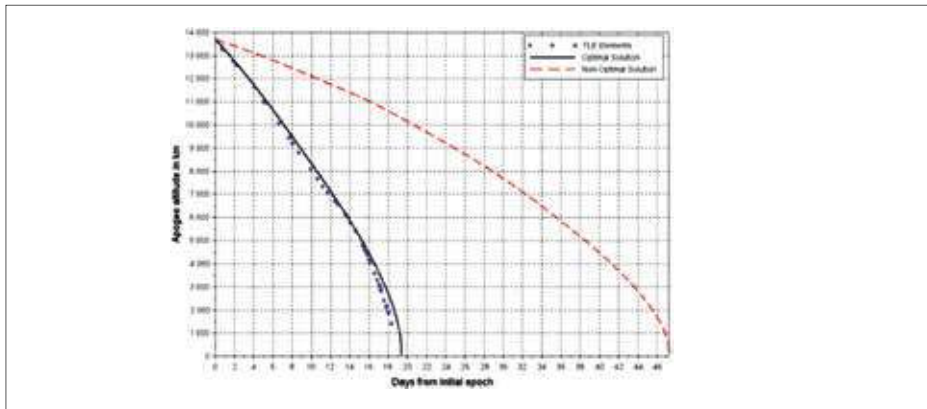


Figure 8.13: Five zones for finding ballistic coefficient and eccentricity (Case 2)

Table 8.23: Optimal solutions for Molniya satellites re-entry time prediction

Case	Zone	Decay Epoch (mm-dd-yyyy)		Relative error (%)
		Predicted	Actual	
1	1	08-09-2015	08-10-	0.9122
	2	08-09-2015	2015	0.7760
	3	08-12-2015		1.6107
2	1	12-26-2013	12-30-	2.2514
	2	12-30-2013	2013	0.5864
	3	12-28-2013		2.2508
3	1	04-11-2012	04-06-	2.8885
	2	04-05-2012	2012	1.2565
	3	04-06-2012		0.2190
5	1	04-07-2016	04-14-	4.3508
	2	04-15-2016	2016	0.4068
	3	04-12-2016		2.0951

8.23 Regularized analytical orbit theory with solar radiation pressure

Sellamuthu et al. (2020) derived a new non-averaged non-singular solution for describing the orbital motion around the Earth under the influence of solar radiation pressure (SRP), using Kustaanheimo-Stiefel (KS) regularization technique. Despite the increase in the dimensionality of the system, there exists symmetry in the KS space. Just three out of the ten equations are solved completely, while only initial conditions are changed for the rest, to produce the dynamics. Performance evaluation of the theoretical solution was carried out with the KS numerical orbit propagator under the assumption of a cannon-ball SRP model for the object. Different high area-to-mass ratio objects from high altitude orbits were considered for analyzing the accuracy of the solution.

8.24 Assessment of four in-house re-entry prediction algorithms

Dutt et al. (2021c) utilized four in-house developed re-entry prediction algorithms namely, RSM- GA, STKOptim, STKLT Optim and ABPro to study the re-entry predictions of Starlink-26 (COSPAR ID 2019-029F or NORAD ID 44240) and CZ-5B (COSPAR ID 2021-035B or NORAD ID 48275) during the IADC re-entry test campaigns 2021/1 and 2021/2, respectively. Both the re-entry campaigns were unique; the life of Starlink-26 kept increasing during the initial phase of re-entry campaign while there was no convergence till the end for the re-entry prediction of CZ-5B rocket body. The effectiveness and applicability of these algorithms were studied based on percentage error. This will be helpful for decision making on automation of switching between these algorithms for re-entry prediction during various phases (short term) of the re-entry campaign. The study focused on the overall and time-based performance of the four methods. Six more re-entered objects are selected (three GTO objects and 3 LEO objects) from various orbits and their re-entry time prediction was done using the four methods in different time instances before re-entry. Predictions were compared between the methods at all the time instances in terms of percentage error. The study helped in fixing the algorithm for re-entry time assessment of any object, in GTO or LEO, during any time phase. Table 8.24 provides the re- entry estimation of the three PSLV R/Bs (LEO objects) during different time zones. As seen from Table 8.24, the average percentage error with the last available TLE with the three methods: RSM-GA, STKOptim and STKLT Optim are up to 2.0, which is quite good.

Table 8.24: Re-entry estimation of the three PSLV R/Bs (LEO objects) during different time zones

Object Name	Prediction by RSM GA	Prediction by STKOptim	Prediction by STKLOptim	Prediction by ABPro
Prediction before six month				
PSLVC40 R/B (43129)	02 Mar 2019 02:34(20.0)	14 Jan 2019 22:30(1.1)	-	26 Mar 2019 13:04(31.8)
PSLVC38 R/B (42796)	17 Jun 2018 01:45(17.3)	23 Jun 2018 09:28(14.7)	-	5 Sep 2018 19:07(20.2)
PSLVC10 R/B (32477)	18 Jun 2020 05:47(64.7)	6 Aug 2020 09:51(87.9)	-	28 Apr 2020 07:55(43.0)
Average percentage Error	34.1	34.6	-	31.7
Prediction before one month				
PSLVC40 R/B (43129)	19 Jan 2019 21:41(7.7)	21 Jan 2019 02:16(12.0)	21 Jan 2019 05:55(12.5)	21 Jan 2019 22:31(14.7)
PSLVC38 R/B (42796)	29 Jul 2018 19:32(15.6)	26 Jul 2018 04:53(5.0)	27 Jul 2018 23:40(10.8)	26 Jul 2018 06:17(5.2)
PSLVC10 R/B (32477)	31 Jan 2020 00:36(17.2)	30 Jan 2020 07:14(18.0)	30 Jan 2020 16:04(18.9)	29 Jan 2020 15:07(16.2)
Average percentage Error	13.5	11.7	14.1	12.0
Prediction before one week				
PSLVC40 R/B (43129)	17 Jan 2019 12:40(2.2)	17 Jan 2019 14:14(3.7)	17 Jan 2019 12:42(2.9)	17 Jan 2019 17:55(5.8)
PSLVC38 R/B (42796)	24 Jul 2018 23:53(3.2)	24 Jul 2018 23:13(3.8)	25 Jul 2018 00:31(4.5)	24 Jul 2018 23:13(3.8)
PSLVC10 R/B (32477)	23 Jan 2020 03:10(1.8)	23 Jan 2020 05:29(1.4)	23 Jan 2020 04:43(1.8)	23 Jan 2020 09:42(0.9)
Average percentage Error	2.4	3.0	3.1	3.5
Prediction before one day				
PSLVC40 R/B (43129)	17 Jan 2019 08:05(0.84)	17 Jan 2019 07:57(3.4)	17 Jan 2019 08:03(4.5)	17 Jan 2019 07:59(3.8)
PSLVC38 R/B (42796)	24 Jul 2018 17:51(2.2)	24 Jul 2018 17:40(8.0)	24 Jul 2018 18:16(11.1)	24 Jul 2018 18:21(11.5)
PSLVC10 R/B (32477)	23 Jan 2020 13:46(6.7)	23 Jan 2020 13:09(13.3)	23 Jan 2020 13:35(14.4)	23 Jan 2020 11:52(9.9)
Average percentage Error	3.3	8.2	10.0	8.4
Prediction with last TLE				
PSLVC40 R/B (43129)	17 Jan 2019 07:38(0.05)	17 Jan 2019 07:39(0)	17 Jan 2019 07:38(0.55)	17 Jan 2019 07:35(2.2)
PSLVC38 R/B (42796)	24 Jul 2018 19:12(4.1)	24 Jul 2018 19:51(4.9)	24 Jul 2018 19:03(3.9)	24 Jul 2018 19:19(4.2)
PSLVC10 R/B (32477)	23 Jan 2020 08:22(0.74)	23 Jan 2020 07:56(0.93)	23 Jan 2020 08:08(0.31)	23 Jan 2020 07:22(4.5)
Average percentage Error	1.62	2.0	1.58	3.6

8.25 Non-linear optimization algorithms on weighted least-square based method for re-entry predictions

Dutt et al. (2021b) made an assessment of non-linear optimization algorithms on weighted least-square based method for re-entry predictions. An integrated model based on weighted least-square error-function minimization to estimate an essential

ballistic parameter (EBP) was implemented and had been found to work well for re-entry predictions. The process required manual intervention due to reasons namely, (i) wide search range, (ii) outlier removal, (iii) lack of good initial guess, (iv) presence of invalid ballistic parameters in the search range, and (v) variation in EBP during the re-entry exercise. The implementation of optimization logic for EBP estimation to reduce user-interference and automatize the complete re-entry prediction procedure was presented (proposed scheme). This is based on assessment of optimization algorithms, for re-entry prediction of different space objects, subjected to their sensitivity to initial guess, convergence and number of function evaluations. Some failure cases were also presented and methodology implemented to overcome these failure cases were discussed here.

Table 8.25: Comparison of optimization methods for EBP estimation using STKOptim method

Optimisation Algorithm	Success Rate	Average no. of function evaluations	Average Execution time (min)
SQP	22%	60	1.6 - 2.3
Nelder-Mead simplex algorithm	100%	64	1.7 - 2.1
BFGS	72%	40	1.1 - 2.0
GA	100%	3268	80 - 130
Proposed scheme	100%	30	1.0 - 2.0

The comparison of above mentioned optimization algorithms was presented in Table 8.25, in terms of their success rate (convergence), average number of function evaluations and average execution time. Overall the proposed scheme was found to be better.

8.26

Assessment of in-house algorithms on re-entry time prediction of uncontrolled space objects

Four in-house developed re-entry prediction methodologies: RSMGA, STKOptim, STKLTOptim, and ABPro are discussed and their performance based on percentage error are presented (Dutt et al., 2023). Two test cases namely (i) Starlink-26 and (ii) CZ 5B rocket body, which were test objects for IADC re-entry test campaigns 2021/1 and 2021/2 are selected for the short-term prediction analysis. Re-entry time estimation for Starlink-26 and CZ-5B using the four methods are depicted in Figures 8.15 and 8.16, respectively. Table 8.26 provides average percentage error during campaign for Starlink-26 and CZ-5B using the four methods.

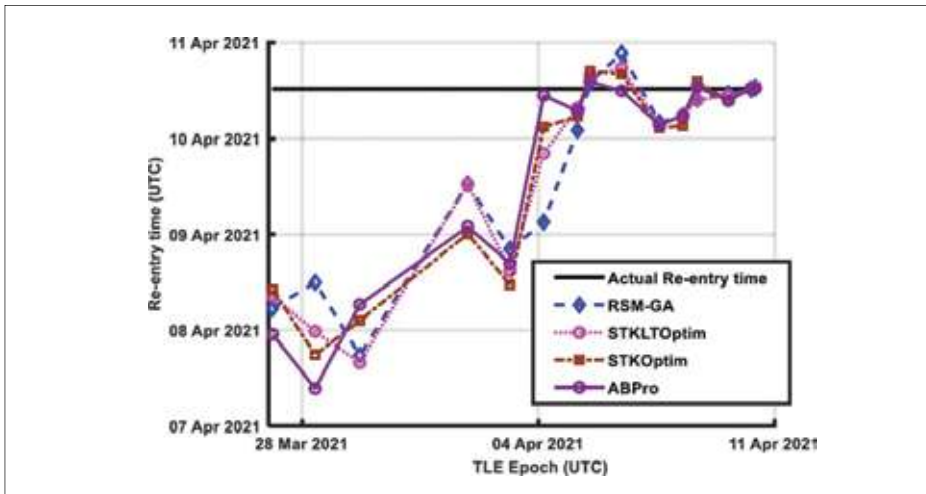


Figure 8.15: Re-entry time estimation for Starlink-26 using four methods

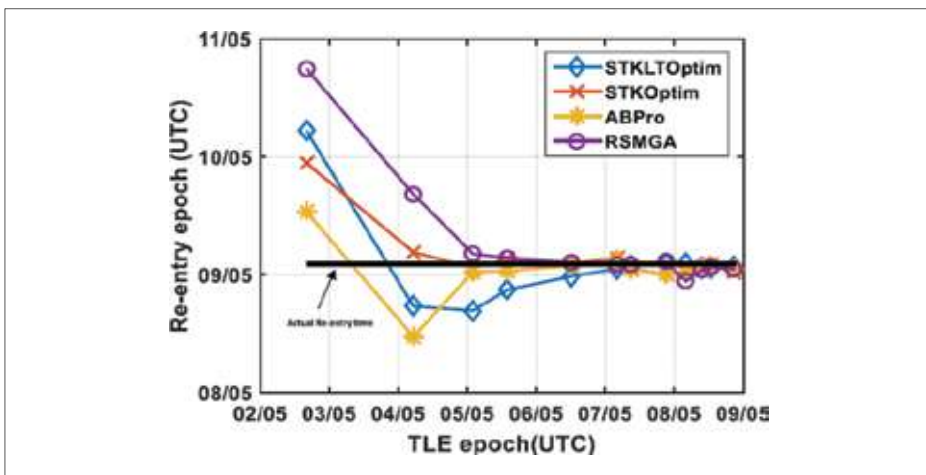


Figure 8.16: Re-entry time estimation for CZ-5B using four methods

Table 8.26: Average percentage error during campaign for Starlink-26 and CZ-5B using four methods.

Method	Starlink-26	CZ-5B
RSMGA	11.8	7.49
STKOptim	12.35	6.11
STKLTOptim	11.49	5.68
ABPro	10.71	5.84

The analysis shows that ABPro and STKLTOptim can be used for short-term re-entry analysis. Time-based evaluation (long term) is done with the four methods using three GTO and three LEO objects. More specifically, for GTO objects, ABPro gives less error for the prediction with the last TLE, and RSMGA gives less error for the six-month earlier predictions, STKOptim gives less error during the intermediate predictions. For LEO objects, STKLTOptim gives less error for the predictions with the last TLE and ABPro gives less error for the six-month earlier predictions, STKOptim and RSMGA give less error during the intermediate predictions.

8.27

8.27 Summarized Results of the IADC Re-entry Campaigns Obtained by ISRO

ISRO has been an active participant in the IADC re-entry exercises since 2000, and this chapter provides the details about ISRO's participation in these campaigns.

8.27.1 IADC Re-entry Prediction of Campaign 2003#1 - COSMOS 389 Satellite

The Cosmos 389 (1970-1 13A) was a Soviet ELINT (Electronic and Signals Intelligence) satellite launched on 18 December 1970 into an initial orbit of 642 km x 687 km at 8.12 degrees inclination with an on orbit dry mass of ~ 2500 kg. The satellite had a cylindrical shape of ~1.5 m diameter and ~ 5 m length, with solar arrays of ~ 5 m span.

For this re-entry campaign, seven different agencies (two from ISRO, one from ISAC and other from VSSC) participated. Others are Johnson - USA; Klinkrad - Germany; Ivanov - Russia; Pardini - Italy; Nonaka - Japan. Ganeshan - INDIA communicated the re-entry predictions to IADC, made by ISAC and VSSC using 'KSGEN' software (Sharma et al., 2004b). It was learnt that the actual re-entry occurred on 24th Nov. 2003 at 22:

36 hrs (UTC). Table 8.27 provides all the re-entry predictions made by VSSC. It may be noted that the three of the 12 predictions were not uploaded to the official site as shown in the Table 8.27. Percentage errors on re-entry predictions made by VSSC are provided in Table 8.28, which are less than 6 % except in case 9, which was not uploaded to IADC Website.

Table 8.27: COSMOS 389 satellite re-entry predictions made using 'KSGEN' (Actual re-entry time ≈ 24th November 2003, 22:36 hrs. UTC)

Sl. No	Last TLE Epoch Utilised (UTC)	Re-entry Prediction (UTC)	Uncertainty (hrs)	
1	2003/11/12 23:10	2003/11/24 07:25	-9.00000	+9.00000
2	2003/11/14 14:05	2003/11/24 11:50	-9.00000	+9.00000
3	2003/11/16 18:22	2003/11/25 06:30	-9.00000	+9.00000
4	2003/11/17 05:01	2003/11/24 16:16	-20.00000	+22.50000
5	2003/11/18 12:25	2003/11/24 17:12	-14.50000	+21.50000
6	2003/11/19 13:26	2003/11/24 20:40	-11.50000	+19.50000
7	2003/11/20 17:42	2003/11/25 04:34	-11.50000	+19.00000
8	2003/11/21 20:23	2003/11/24 21:48	-11.00000	+14.00000
9*	2003/11/22 05:16	2003/11/24 16:50	-4.00000	+7.50000
10*	2003/11/23 21:36	2003/11/24 21:40	-3.00000	+3.00000
11*	2003/11/24 04:28	2003/11/24 23:05	-2.00000	+2.50000
12	2003/11/24 12:01	2003/11/24 23:14	-1.50000	+1.83333

* Predictions are not uploaded to IADC Website

Table 8.28: Percentage errors on re-entry predictions made by VSSC (Actual re-entry time ≈ 24th November 2003, 22:36 hrs. UTC)

Sl No.	Prediction Epoch (UTC)		Predicted Re-entry (UTC)		Error (%)
1	12 /11/2003	23 : 10	24 /11/2003	07 : 25	05.28
2	14 /11/2003	14 : 05	24 /11/2003	11 : 50	04.33
3	16 /11/2003	18 : 22	25 /11/2003	06 : 30	04.03
4	17 /11/2003	05 : 01	24 /11/2003	16 : 16	03.42
5	18 /11/2003	12 : 25	24 /11/2003	17 : 12	03.50
6	19 /11/2003	13 : 26	24 /11/2003	20 : 40	01.50
7	20 /11/2003	17 : 42	25 /11/2003	04 : 34	05.92
8	21 /11/2003	20 : 23	24 /11/2003	21 : 48	01.08
9*	22 /11/2003	05 : 16	24 /11/2003	16 : 50	08.83
10*	23 /11/2003	21 : 36	24 /11/2003	21 : 40	03.73
11*	24 /11/2003	04 : 28	24 /11/2003	23 : 05	02.67
12	24 /11/2003	12 : 01	24 /11/2003	23 : 14	05.98

* The predictions which have not entered in the IADC website

Table 8.29 provides the percentage errors on re-entry predictions made by different Agencies. It may be noted that the ISRO had the minimum % error of 5.59 with 9 predictions. Next was Pardini from ASI with 6.11 % error with 9 predictions.

Table 8.29: Percentage errors on re-entry predictions made by Different Agencies (Actual re-entry time \approx 24th November 2003, 22:36 hrs. UTC)

Reproduced from IADC/SG/2004-01, Steering Group IADC, Issue 0.1 dated 08 April 2004

P. o. C	IADC Member	From Total predictions		From Predictions of last 48 Hours	
		Inputs (No. Predictions)	% Error	Inputs (No. Predictions)	% Error
Pardini	(ASI)	20	07.98	09	06.11
Klinkrud	(ESA)	18	08.21	10	08.65
Ganeshan*	(ISRO)	22	05.24	09	05.69
Nonaka	(JAXA)	09	14.39	03	20.18
Johnson	(NASA)	05	98.12	04	122.35
Ivanov	(RASA)	16	08.17	07	11.00

* The predictions contains those made by KSGEN and ISAC together

8.27.2 IADC Re-entry Test Campaign 2005/1: Re-entry of Cosmos 2332 Satellite

Software “KSGEN” was utilized for the re-entry predictions. During the last 7 days, ISRO (VSSC) made 19 re-entry predictions with average percentage error of 4.61, which was third best among the participating agencies. With the last available TLE at 15:02 UTC on 28th Jan 2005, ISRO (VSSC) made the closest re-entry prediction with re-entry time of 16:31 UTC with uncertainties of -18 and +28.8 minutes against the actual re-entry time of 16:37 UTC, a difference of -6 minutes (Sharma et al., 2005a).

8.27.3 IADC Re-entry Campaign 2005/2: Re-entry of Coronas-F Satellite

Software “KSGEN” was utilized for the re-entry predictions. ISRO (VSSC) made 13 re-entry predictions with average percentage error of 7.38. ISRO (ISAC) made 8 re-entry predictions with average percentage error of 6.66. Overall ISRO with 21 re-entry predictions had average percentage error of 7.11, which was best among all the participating agencies (Sharma et al., 2005b).

8.27.4 IADC Re-entry Campaign 2008/1: Re-entry of Early Ammonia Servicer

Software “KSGEN” and NPOE” were utilized for the re-entry predictions. During the last 48 hours of the re-entry time, 11 predictions were made by ISRO (VSSC). Average percentage error was found to be 7.18 (Sharma et al., 2008).

8.27.5 IADC Re-entry Campaign 2009/1: Re-entry of Molniya 3-39 Satellite

Response surface method with genetic algorithm was used. ISRO made the third closest re-entry prediction of 22:43 (UTC) with uncertainties of 15 minutes against the actual re-entry time of 22:49 (UTC), a difference of 6 minutes with respect to the last available TLE at 21:48 (UTC) on 8th July 2009. Only ISRO made the re-entry prediction with the last available TLE. The maximum error in the last 5 re-entry predictions made by ISRO during the last 6 hours was only 9 minutes (Sharma et al. 2009a).

8.27.6 IADC Re-entry Campaign 2010/1: Re-entry of Vostok SL-3/A-1 Third Stage

Software “KSGEN” and “NPOE” were utilized for the re-entry predictions. The average % error in the 14 re-entry predictions made by ISRO (VSSC) during the entire campaign was found to be 2.31 % and was best among the 11 participants. The average % error during the last 12 hours for ISRO (VSSC) re-entry predictions was only 1.29 and was the best among all the participants. The final prediction error made by ISRO (VSSC) using the TLE more than 5 hours before the declared re-entry time of 16h 54m of 30th April 2010 was only 6 minutes and was second lowest among all the participants. The lowest error was 4 minutes (Sharma et al., 2010).

8.27.7 IADC Re-entry Campaign 2011/2: Re-entry time of Roentgen Satellite (ROSAT)

Software “KSGEN” and “STK” were utilized for the re-entry predictions. 16 re-entry predictions were made by ISRO (VSSC) during the entire campaign from 10th Oct. to 23rd Oct. 2011. The latest prediction made by ISRO (VSSC) with the TLE corresponding to 22nd Oct. 2011 (22:54 UTC) was 14 minutes away from the declared re-entry time of 23rd Oct. 2011 (01: 57 UTC). The average prediction error was 2.71 % (Mutyalarao et al., 2011).

8.27.8 IADC Re-entry Test Campaign 2012/1: Re-entry Analysis of Phobos-Grunt

17 re-entry predictions were made by ISRO (VSSC) during the campaign from 3rd Jan to 15th Jan 2012. The latest re-entry prediction made by ISRO (VSSC) was only 8 minutes away - early (15th Jan 2012-17:37 UTC) from the declared re-entry time of 15th Jan 2012 (17:45 UTC). The average percentage error for the 17 predictions was found to be about 5 % (Gupta et al., 2012).

8.27.9 IADC Re-entry Test Campaign 2013/1: Re-entry of GOCE Satellite (#34602)

Software “KSGEN”, “DRSM with GA”, “STK OPTIM” and “STK LTOptim” were utilized for the re-entry predictions. 23 re-entry predictions were made by ISRO (VSSC). The last re-entry prediction made by ISRO (VSSC) was 32 minutes away from the declared re-entry time (APMD IADC Team, 2014a).

8.27.10 IADC Re-entry Test Campaign 2014/1: Re-entry of Cosmos 1939 Satellite (#19045)

11 re-entry time predictions were made by ISRO (VSSC). The last prediction made by ISRO (VSSC) was on 29th Oct 2014, 15:14 UTC, which was only 34 seconds away (early) from the declared re-entry time of 29th Oct 2014, 15:14:34 UTC. Over all ISRO re-entry predictions compared very well with the other agencies. The average percentage error for the 6 re-entry predictions made during the last 72 hours was 4.95, which was third best among all the agencies (APMD IADC Team, 2014b).

8.27.11 IADC Re-entry Test Campaign 2016/1: Re-entry of CZ-2C Rocket Body (#39000)

Software “KSGEN”, “Response Surface Method (RSM) and GA”, “STKOPTIM” and “STKLOptim” were utilized for the re-entry predictions. There was a difference of 20 minutes (early) in the last re-entry prediction made by ISRO (VSSC). The predicted re-entry time was on 27th June 2016, 18:51 UTC. The actual re-entry time was on 27th June 2016, 19:11 UTC. Overall 14 re-entry predictions were made with average percentage error of 4.16, which was third best among the participating agencies (Mutyalarao et al., 2016a).

8.27.12 IADC Re-entry Test Campaign 2016/2: Re-entry of VEGA AVUM Rocket Body (#38086)

Software “KSGEN”, “RSM and GA”, “STKOPTIM” and “STKLOptim” were utilized for the re-entry predictions. Over all 16 re-entry predictions were made by ISRO (VSSC) with average percentage error of 4.77, which was second best among the participating agencies. During the last 72 hours, 7 re-entry predictions were made with average percentage error of 3.38. During the last 24 hours, 4 re-entry predictions were made with average percentage error of 0.89, which was best among the participants those made 4 and above re-entry predictions. The last prediction made by ISRO (VSSC) was 2nd Nov 2016, 04:55 UTC, which was only 6 minutes away (late) from the declared re-entry time of 2nd Nov 2016, 04:49 UTC (Mutyalarao et al., 2016b).

8.27.13 IADC Re-entry Test Campaign 2017/1: Re-entry of CZ-3B Rocket Body (#38253)

Software “KSGEN”, “RSM and GA”, “STKOPTIM” and “STKLTOptim” were utilized for the re-entry predictions. Overall ISRO (VSSC) made 8 re-entry predictions with average percentage error of 3.6, which was third best among all the participating agencies. During the last 48 hours, the average percentage error was 3.28, which was second best among all the participating agencies (Mutyalarao et al., 2017).

8.27.14 IADC Re-entry Test Campaign 2018/1: Re-entry of Tiangong-1 (#37820) Chinese Experimental Space Station

“RSM and GA”, “STKOPTIM” and “STKLTOptim” were utilized for the re-entry predictions. Overall 11 re-entry predictions were made by ISRO (VSSC) with average percentage error of 11.75. For the last 48 hours, the average percentage error was 7.74. The final re-entry prediction made by ISRO (VSSC) was 18 minutes away (2nd April 2018, 00:41: 00 UTC) from the declared re-entry time of 2nd April 2018, 00:23: 00 UTC. The final percentage error on final prediction of 3.08 by ISRO (VSSC) stood first among all the 11 participating agencies (IADC Re-entry Campaign Team, 2018).

8.27.15 IADC Re-entry Test Campaign 2019/1: Re-entry of Electron Rocket Body (#43166)

“RSM and GA”, “STKOPTIM” and “STKLTOptim” were utilized for the re-entry predictions. The last re-entry prediction made by ISRO (VSSC) was 3rd March 2019, 12:04 UTC, which was 5 minutes away from the actual re-entry time of 3rd March 2019, 11:59 UTC \pm 1 min (Nandhu et al., 2019).

8.27.16 IADC Re-entry Test Campaign 2021/1: Re-entry of Starlink-26 Spent Stage (#44240)

“RSM and GA”, “STKOPTIM”, “STKLTOptim” and “ABPro in STK” were utilized for the re- entry predictions. Overall 15 re-entry predictions were made by ISRO (VSSC) with average percentage error of 11.27, which was second best among all the participating agencies. The average percentage error for ISRO (VSSC) for last 2 days re-entry predictions was 5.84, which was best among all the participating agencies. The second last re-entry prediction made by ISRO (VSSC) was on 10th April 2021, 12:29 UTC, which was 2 minutes away from the declared time of 10th April 2021, 12:27 UTC (IADC Re-entry Campaign Team, 2021).

8.27.17 IADC Re-entry Test Campaign 2021/2: Re-entry of CZ-5B rocket body (2021-035B, #48275)

The re-entry prediction results with the latest available TLE are given in Table 8.30. It re-entered on 09-May-2021 02:14 UTC. There was difference of 28 minutes 18 seconds between the actual and the nominal re-entry time (Mutyarao et al., 2021).

Table 8.30: Re-entry Prediction of CZ-5B Rocket Body

Latest TLE Epoch (UTC)	Nominal re-entry time (UTC)	Lower bound (UTC)	Upper bound (UTC)
08 May 2021 12:31:57.456	09-May-2021 01:45:42	08-May-2021 23:34	09-May-2021 05:19

8.27.18 IADC Re-entry Test Campaign 2022/2: Re-entry of Starlink-24 Satellite (2019-029D, # 44238)

The IADC annual re-entry campaign of 2022 with Starlink 24(NORAD-id 44238) as the test object commenced on 13 Oct 2022 and ended on 24 Oct 2022. The object was estimated to have re-entered the Earth's atmosphere on 24 Oct 2022 UTC 05:50 ± 56 minutes (satellitemap.space@starlink_map). ISRO submitted 10 predictions between 18 Oct 2022 and 24 Oct 2022 shown in Figure 8.17.

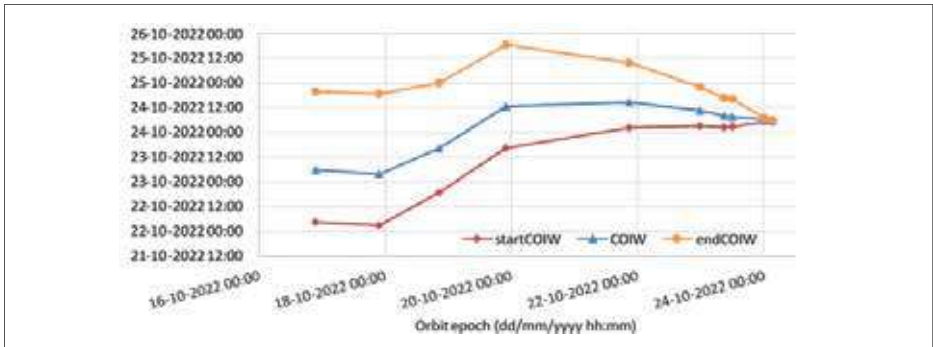


Figure 8.17: Re-entry predictions by ISRO (COIW: Centre of Impact Window)

Only 4 agencies, namely ESA, DLR, NASA, and ISRO made their predictions based on the last available TLE (Epoch 02:45:44 UTC on 24 Oct 2022), which are 05:33:23 UTC; 05:53:40 UTC; 05:01:00 UTC and 05:39:00 UTC of 24 Oct 2024, respectively (Mukherjee, 2022).

8.27.19 IADC Annual Re-entry Test Campaign of 2023 with Starlink-1065 (# 44770)

At the time of IADC re-entry campaign on 3rd April 2023, the satellite was in 355 km x 366 km orbit. Out of the thirteen member agencies, eight agencies including ISRO participated in the campaign. APMD team of VSSC and SSOM team of ISTRAC participated in the campaign. ISRO submitted 7 predictions between 7th and 20th April 2023. The annual re-entry campaign came to an end on 21st April 2023. The declared date of re-entry into the Earth's atmosphere is 19:55:00 UTC, 20 April 2023. Table 8.31 provides the final predictions made by various agencies. ISRO had a relative error % of -3.2 (Mukherjee, 2023).

Table 8.31: Final predictions by various agencies

Originator	Uploaded Time	Orbit Epoch	Centre of Impact Window	Relative error %
ESA	2023-04-20T20:27:10	2023-04-20T13:14:45	2023-04-20T19:56:40	-0.4
CNSA	2023-04-20T13:38:59	2023-04-20T07:13:44	2023-04-20T19:51:17	0.5
NASA	2023-04-20T18:57:15	2023-04-20T13:14:46	2023-04-20T20:02:00	-1.7
KARI	2023-04-20T17:55:15	2023-04-20T13:14:45	2023-04-20T19:44:45	2.6
ISRO	2023-04-20T19:15:42	2023-04-20T13:14:46	2023-04-20T20:08:00	-3.2
UKSA	2023-04-20T19:36:27	2023-04-20T13:14:45	2023-04-20T19:31:07	6.0
DLR	2023-04-20T12:41:39	2023-04-20T07:13:44	2023-04-20T23:31:15	-28.4

Relative error (%) is calculated as: $100 \times (\text{declared re-entry epoch} - \text{last predicted epoch}) / (\text{declared re-entry epoch} - \text{Orbit Epoch used in last prediction})$. Date format yyyy-mm-ddThh:mm:ss



SDSSARS IN ISRO

Space Debris and Space Situational
Awareness Research Studies



CHAPTER 9

Future Concerns on Space Debris Environment and Best Practices for Space Sustainability

9.1 Introduction

Space debris poses growing risks to the safety and sustainability of operations in outer space. Historically fragmentation/break-up has been the major contributor to the growth of space debris population, but several studies show that future debris population will be driven by on-orbit collisions. If the business-as-usual approach is continued, eventually triggering of Kessler's syndrome would hinder future space activities. It is well-recognized by all space-faring entities that collective efforts are imperative to find a solution to this complex issue. Space debris mitigation measures have evolved as part of such efforts. However, so far, they have been adhered to by space-faring entities as voluntary, non-binding instruments and have partly been adopted in national policies by some of the space-faring nations. Furthermore, as the scope of space activities expand and diversify rapidly, newer challenges arise for the safety of spaceflight, especially due to the proliferation of large constellations and increasing preference towards small satellites. In this chapter we consolidate such challenges along with the future directions to tackle this growing menace, which can help improve our ability to design safer and more efficient spacecraft.

9.2 Future Concerns and Challenges

9.2.1 Space Object Observation

Space situational awareness (SSA), which involves continual monitoring of the space assets, their activities, and the prediction of their impact on the space environment, is an integral and indispensable part of safe and sustainable space operations. As more and more satellites are being launched, it is imperative to have SSA capability commensurate with the increase in object population to safeguard operational space assets. A full-fledged SSA capability demands a widely distributed network of

sensors (radars and optical telescopes) across the globe for a complete and repeated coverage of all space objects.

At present, the US operates the largest network of sensors and USSPACECOM maintains the most comprehensive catalogue of space objects. The catalogue is available free-of-cost in public domain and serves as the primary source of data for most space-faring entities for close approach risk assessment for their space assets. The SSA services offered by USSPACECOM also include issuance of close approach alerts on a regular basis. However, the users of these services have no control over when orbital data of objects of their own interest or an updated conjunction alert of a particularly high interest event would be available. Such uncertainty in timeline of data availability adds to operational difficulties. There are occasions where collision avoidance manoeuvres for conjunctions on subsequent analyses with updated data have been found to be beyond critical threshold. In such cases, setting up of own facilities which can track specific objects of own interest more intently and frequently is desirable. Such independence would also equip one for unforeseen situations where the free SSA services could be discontinued.

An alternate approach would be to have a geographically well distributed network of SSA sensors within one's own territory and to complement the data obtained from this network with the data collected by other networks of SSA sensors across the globe. In either case, acquisition of observational data with global coverage from complementary sensors entails collaboration and coordination with multiple agencies through suitable data sharing mechanisms. Such collaborations can either be bilateral or multilateral, and therefore, are essentially influenced by geopolitical relationships between the States.

At present, majority of SSA sensors are concentrated in the northern hemisphere of the Earth. Furthermore, the existing systems have limitations in terms of tracking smaller objects, including cubesats and nanosats. Some of the legacy SSA systems originally meant for tracking missiles, are also not suited to track objects in certain orbits. Upgrade or replacement of these sensors can be a major challenge.

9.2.2 Data Processing and Analyses

- To determine the likelihood of a collision, operators often combine their own higher-accuracy tracking data with less accurate, externally accessible data. The collision risks are assessed differently as a result of these data of varying quality.

With several SSA service providers, including commercial ones, it is not easy for a new entrant in space arena to compare and to assess veracity of their data and benchmark the accuracy of their conjunction assessment services.

- SSA data can be from multiple, sometimes disparate sources and of different grades of accuracy. Considering the requirements of “fusion” of such data, handling of a huge volume of conjunction alerts, and complex decision making, high performance computing and storage requirements would be essential for data processing and analysis, and for applying the appropriate concepts of data analytics. As of now, the idea of fully autonomous collision avoidance as an end-to-end solution seems to be highly complex and not viable, mainly due to the human element involved in inter-operator coordination. Though it is expected that such a system may be realisable in near future with advanced technology (usage of AI and ML), considerable efforts and testing will be involved in its implementation.
- One collision avoidance manoeuvre to resolve conjunction with one spacecraft may lead to conjunction risks with several other spacecraft. Resolution of multiple conjunctions involving multiple active satellites will be challenging, even with transparent sharing and exchange of data. One future possibility is to automate the collision avoidance manoeuvres completely with AI tools when large number of uncertainties are involved.
- At present, different operators adopt different methodologies for risk estimation and also, different criteria and thresholds for identifying critical conjunctions. As a result, in some cases, a conjunction between two operational satellites may be deemed critical to one of the operators while it may be beyond the actionable threshold of the other. In such cases, accurate observational data is essential to make informed decisions to mitigate the risk of collision.
- For space actors intending to develop capabilities in the areas of SSA and space debris research, there will always be a trade-off between developing the software in-house and using readily available, proven commercial software. The former provides better insight, customizability and control, but has a longer development cycle while the latter can be very expensive.
- Orbit determination and trajectory prediction is challenging for objects having low thrust manoeuvre capabilities and/or exhibiting irregular manoeuvring pattern as traditional flight dynamics-based analyses would yield incorrect prediction of their orbit evolution. This limitation can be overcome by using operator shared ephemerides and to some extent, ML approaches in case the satellite has definite, reasonably predictable pattern of manoeuvring.

Challenges arising due to small satellites and large constellations

The present trend in the space industry is towards miniaturization, resilience, and responsiveness. Small satellites like cubesats, nanosats and picosats have emerged as preferred options, enabling affordable access to space for many non-traditional actors, including universities and other academic institutions. Similarly, large constellations of satellites offer undeniably attractive advantages over the heavier, custom-built conventional satellites in terms of better coverage of the region of interest, reduced latency, and better resilience to failures. The constellations being proposed and deployed at present are at least an order of magnitude larger in size than their predecessors, with the number of satellites within a constellation typically ranging from a few hundred to several thousand. Satellites in these constellations typically have shorter life spans and require periodic replenishment for service continuation.

9.3.1 Lack of trackability and identifiability of small satellites

Their deployment being typically through ride-share as a secondary payload, small satellites are often launched in batches, and injected with very less gap (few seconds) between separation timings. Their small size further compounds the problem of tracking as well as identifying and distinguishing the satellites from each other immediately after injection.

9.3.2 Lack of manoeuvrability of small satellites

CubeSats and nanosats usually do not carry on-board propulsion and hence, are devoid of manoeuvring capability while continuing to pose significant collision risk to larger operational assets. As a result, the onus of collision avoidance falls single handedly on owner/operator of the manoeuvrable satellites.

Lack of contact details of operators for coordination constellations

One of the foremost difficulties faced while dealing with on-orbit conjunctions with small satellites is the lack of information to contact their operators for coordination, particularly since some of these satellites tend to be in orbit only for a short time. The actual dimension, manoeuvrability status of satellites not be known a priori, consequently, one has to make a conservative collision risk estimate. In some cases, the satellites may not even be registered in their respective national registries. This

is especially the case with States that lack adequate regulatory and administrative provisions for this purpose. Such situations pose major challenges while conducting collision avoidance procedures.

9.5 Lack of reliability

CubeSats and nanosats are often mass-produced using COTS components and are more prone to on-orbit failures. Even with their relatively shorter orbital life-time, the defunct objects would pose short-term collision risks to operational assets.

9.6 Extensive coordination needs

It is apparent that LEO will be hosting not just one, but multiple large constellations simultaneously. Unlike space debris, which are non-maneuvrable objects, the trajectory of manoeuvrable spacecraft, especially those equipped with ion thrusters, cannot be predicted by the straight-forward application of conventional flight dynamics. Hence, the exchange of operational ephemeris is essential for any meaningful decision-making on collision avoidance.

At present there are only a handful of operational large constellations; their operators have so far readily cooperated by transparent sharing of data and information to resolve the conjunction situations. In future, mitigating collision risk would entail close coordination and negotiations with multiple operators from different nations.

9.7 Increased operational complexity and penalties for collision avoidance

With the proliferation of multiple large constellations in outer space, the number of conjunction warnings and the number of collision avoidance manoeuvres to be performed are likely to increase proportionally. The likelihood of one collision avoidance manoeuvre with respect to one spacecraft resulting into conjunction risks with several other spacecraft cannot be ruled out. Multiple critically close conjunctions occurring in very short time intervals (in a day or less) may be inevitable, and would add to operational complexities. Collision avoidance manoeuvres incur significant penalties in terms of service disruption, fuel consumption, additional operational overhead, including orbit restitution requirements, and associated cost, etc. Thus, the consequent operational burden and cost may be difficult to be borne by emergent space actors, especially for those from developing countries, and may prove to be an impediment for them to embark into space ventures.

Unavailability of safe lift-off timings within launch window

As per the recommendations on limiting orbital life-time, the satellites of large constellations are initially deployed at 350 km to undergo testing and qualification. They are also de-orbited at end-of-life below this altitude. Hence cumulatively they also contribute to a sizable population of objects in VLEO. As a result, a launch vehicle has to necessarily transit through multiple, crowded shells of large constellations, and encounters with the satellites in constellations are inevitable. Furthermore, some of the constellations consisting of thousands of satellites are planned to be deployed around the 320-350 km altitude. All human spaceflight missions have to traverse this orbital regime during their forward as well as return journey. Hence, proliferation of large constellations would affect the availability of conjunction-free liftoff timings within a launch window significantly and pose additional challenges to safety of crewed missions.

At present there are only a handful of operational large constellations; their operators have so far readily cooperated by transparent sharing of data and information to resolve the conjunction situations. In future, mitigating collision risk would entail close coordination and negotiations with multiple operators from different nations. Such level of cooperation will be extremely challenging as it is likely to be dictated by prevailing geopolitical relations.

Increased threat of space debris

Most of the satellites in large constellations are proposed to be placed in Low Earth Orbit, and their average operational lifetime is typically between 5-6 years. The currently deployed satellites in the large constellations have manoeuvring capability and have provisions to be actively de-orbited at the end-of-mission. However, for satellites belonging to constellation, the resilience of the overall system is given preference. Even though the failed satellites have limited life-time, the sheer number of satellites deployed in multiple large constellations is likely to result in a non-trivial number of failed satellites adding to the already dense population of space debris in LEO.

It may be noted that a few of the constellations are proposed to be deployed above 1000 km. In general, objects placed in orbits below 600 km are expected re-enter the Earth's atmosphere within 25 years as they experience higher drag forces. However, defunct objects placed above 1000 km altitude tend to remain in space for hundreds of years, making these altitude bands more collision prone.

The large constellation satellites are de-orbited at end of life to a lower orbit (typically 300 km) to drastically reduce their post mission life. While this is highly desirable from sustainability point of view, there can be a virtual graveyard shell of satellites at VLEO if there are numerous constellations. At present (as of Nov 2023) about 10 satellites of large constellations are found to re-enter the atmosphere per month. With multiple large constellations the re-entries will also increase rapidly. Even if the satellites are made of demisable components to limit ground casualty risks, the cumulative effect due to ablation of materials due to re-entry heating is likely to have significant impact on environment in the long run.

9.10 Impact on ground based optical observation

Satellites in lower altitudes, when illuminated by sunlight, appear as streaks in the night-sky, interfering with the images of objects of interest. These streaks significantly degrade the data quality of ground-based optical telescopes used for space object tracking and monitoring. Sometimes there can be irrecoverable loss of data of an object of interest for ground-based observation.

9.11 Potential Debris Issue Beyond Earth

At present, space beyond the Earth is inhabited by only a few operational spacecraft, the population is concentrated near Mars, the Moon, and the Sun-Earth Lagrange's points. Even with a handful of spacecraft, the greater uncertainty associated with the orbital knowledge and the potentially chaotic dynamics make collision risk assessment a necessity for the safety of operations. Learning from the experiences of operating in Earth orbits which is plagued by unprecedented and ever-increasing congestion, it is desirable to have specific forward-looking guidelines and best practices in place to address the future accumulation of debris object and mechanisms for space traffic coordination.

9.12 Others

- The sharing of data amongst satellite operators or even taking specific actions to evaluate the risk of collisions is not currently mandated. There is no centralised approach to collision avoidance and it is entirely up to the spacecraft operators to determine whether or not to conduct an evasive manoeuvre.

- Owing to competition in market, operators may be often compelled to make decisions that favour their economic interests over the sustainability of the space environment.
- Currently, there are no internationally accepted space debris mitigation guidelines applicable for large constellations and small satellites. Even the regulatory policies at national levels are only focused on disclosure of compliance with these guidelines and satellite operators are encouraged but not strictly required to implement these guidelines in their missions.

9.13 Space weather

Space weather events, such as solar storms and flares lead to geomagnetic storms and influence atmospheric drag, which in turn affect orbital evolution of space objects as well as the orientation and instrument performance of spacecraft. Any severe event has a drastic effect on the orbit of a space object, the deviation between the actual orbit and the predicted orbit may exceed the margins of safety in some cases. As the orbital regimes get more crowded, accurate prediction of imminent space weather events will be crucial to minimise the error in the prediction of the orbital evolution for the safety of spaceflight and to initiate pre-emptive actions to protect on-board sensitive instruments.

9.14 Way forward

- It is desirable to select an operational orbit sufficiently away from already crowded orbital regimes through suitable assessment of collision risks.
- Depending on the altitudes at which they orbit, defunct spacecraft and debris fragments tend to remain in space for a long time. Given the higher rate of failures associated with small satellites, there is a need to put in place specific guidelines to minimise the presence of the derelict satellites in crowded orbital regimes.
- To minimise the risk of on-orbit collisions, it is necessary that all satellites are trackable and identifiable to assess this threat. Most of the small satellites lack manoeuvring capability. For such satellites, installing on-board active and/or passive tracking components on the satellites improve orbit determination and prediction and should be a requirement for ensuring safe operations.
- A specific requirement for all space actors, including commercial and non-traditional actors like universities and other private institutions, to share orbital data and employ more comprehensive tracking technologies would aid in reducing the threat of collisions considerably. Especially while operating at

specific altitudes, in the vicinity of manned missions, spacecraft should have manoeuvring capabilities and reliable communication.

- In the absence of a space traffic management system, a central entity facilitating data sharing and providing updates on orbital flight plans would help in its confidence and a common understanding among all space actors over conducting manoeuvres in a crowded region. Additionally, use of standardized communication protocols would enable effective and timely communication, and would help in streamlining procedures for conjunction assessment and collision avoidance.
- While the IADC debris mitigation guidelines recommend a 25-year limit for orbital lifetime of objects in LEO, given the large number of spacecraft and the associated high probability of collisions anticipated in the near future, shorter post-mission orbital lifetimes should be considered to reduce the risk of collision to operational assets.
- Widespread implementation of guidelines, standards and best practices for space traffic management is necessary to ensure safe and responsible space operations. Furthermore, voluntary best practices need to be supplemented with formal regulatory mechanisms that would ensure safety of operations. It is therefore important for all Member States to develop and adopt necessary measures to regulate satellite launches, their operations and ensure compliance with existing international debris mitigation standards at a domestic level.
- In particular, all operators should adopt measures to obtain timely and actionable alerts to safeguard their assets from any impending hazard.
- An internationally accepted limit has to be evolved on the number of satellite licenses that each State can issue to its entities.
- It needs to be impressed upon all space actors that the penalties for adopting space debris mitigation measure are eventually superseded by the reward of continued service of the space assets yielding revenue, science throughput, and delivering societal benefits.
- Rocket launches and satellite re-entries release particles and gases into the atmosphere that can have adverse effects. Mitigation lies in limiting the development and use of rocket engines that produce certain harmful emissions and adopting environment friendly, demisable components to address re-entry risks.
- Satellite operators need to mitigate the adverse effects due to satellite streaks by darkening their satellites. Astronomers are using tools to avoid or filter out light reflections or radio transmissions from images/signals, similar tools are required to process space debris observational data.
- Given the monumental increase in the number of objects in future and to circumvent the aforementioned image corruption by large constellations, the ground-based sensors need to be complemented with space-based sensors to circumvent some of the aforementioned issues.

- For mitigating accumulation of debris in LEO, the following best practices recommended
 - Satellites should be de-orbited on a fixed schedule with proper replacement planned beforehand.
 - Life extension of a satellite should be subject to PMD capability assessment
 - Controlled re-entry should be attempted wherever feasibility exists
 - Design for Demise-principles to be adopted for minimising the ground casualty risks due to surviving parts of re-entering objects

9.15 Conclusion

While space-based activities are immensely beneficial also leads to increased space debris because the presence of defunct objects in outer space significantly increases the chances of collisions in crowded orbital regimes. Due to their high velocity (of the order of 7-10 km/s), space debris on accidental collision can damage or destroy satellites resulting in loss of commercial services, scientific observational data, and even threaten national security. Cumulatively, the number of defunct objects arising out of multiple large constellations and deployment of numerous small satellites may not be trivial. The main concern is the presence of large number of objects in orbit, whether functional or defunct, inherently increases the chances of collisions in crowded orbital regimes. Fragments generated from one collision/fragmentation event might trigger other fragmentation events leading to a cascading effect known as Kessler's syndrome. This will render space unusable for future applications. Remediation lies in incorporating our understanding of space debris during mission design, strict adherence to guidelines during operational phase, and post mission disposal / active debris removal at the end of mission.

As the number of active satellites continues to grow sharply and are projected to outnumber the debris population, Space Traffic Management (STM) concepts must be incorporated to prevent on-orbit collisions. Therefore, enhanced coordination, cooperation and collaboration among space-faring entities become imperative to safeguard space assets. However, unlike air traffic, such an STM system is unlikely to emerge in the near future through consensus among all nations due to the prevalent geopolitical quagmire. Furthermore, studies indicate that stabilising the existing object population in the heavily congested LEO region requires removal of at least 5 large objects per year through ADR. However, ADR is yet to reach a sufficiently high level of technological maturity and is limited to demonstration missions. In addition, several challenges remain to be addressed on the legal, economic, and technology fronts. As of today, widespread implementation of existing best practices for mitigating space debris is the only available option way for preserving outer space for sustainable utilisation.

Implementing space debris measures undeniably incur additional cost and effort, but such measures also ensure the operational safety of a space-based platform, allowing its sustained utilization. Incorporating space debris mitigation measures in the early stages of design phases is recommended for cost-effectiveness. Improving compliance with the mitigation guidelines hinges on raising awareness among the emerging space actors on the extent of threats posed by space debris and debunking the “Big Sky Theory”. It is also important to recognise space situational awareness to be an essential and integral part of ensuring the safety of space operations. In particular, space object tracking and monitoring capabilities need to be commensurate with the increase in object population for a realistic assessment of risks posed by space debris.

Cooperation and collaboration amongst space faring entities for data sharing, utilising common pool of database /knowledge base contributed by multiple stakeholders is essential for efficient operational management and informed decision making to contain the space debris environment. Ultimately the future challenges require novel approach and innovative solutions where public private partnership would play a significant role.



SDSSARS IN ISRO

Space Debris and Space Situational
Awareness Research Studies



References

1. Adimurthy, V. (2001), "Space Debris Scenario", *Proceedings of the Workshop on Space Debris Software Tools*, VSSC/AERO/SP/001/2001, Vikram Sarabhai Space Centre, Thiruvananthapuram, 42-71.
2. Adimurthy, V. (2006a), "Space Debris: Magnitude of the problem and Engineering Solutions to its Mitigation", *Current Trends in Engineering Practice*, Published by INAE/AICTE, Ed. C.V. Ramakrishnan, ISBN: 81-7319-689-3, Narosa Publishing House, New Delhi, 437-453.
3. Adimurthy, V. (2006b), "Re-entry of objects from objects from geostationary transfer orbits", *Current Trends in Engineering Practice*, Published by INAE/AICTE, Ed. C.V. Ramakrishnan, ISBN: 81-7319-689-3, Narosa Publishing House, New Delhi, 454-466.
4. Adimurthy, V. and Ganeshan, A. S. (2006), "Space debris mitigation measures in India", *Acta Astronautica*, 58, 168-174.
5. Agarwal, A., Mukherjee B. and Kandari, A., (2022), "Post Mission De-orbiting of Cartosat-2", *Advances in Space Research*, 70, 1312-1324.
6. Ananthasayanam, M. R., Anil Kumar, A. K. and Subba Rao, P. V. (2002), "A New Stochastic Impressionistic Low Earth (SIMPLE) Model of the Space Debris Scenario", 34th COSPAR Scientific Assembly, Second World Space Congress, 10-19 October, 2002, Houston, Texas, USA, COSPAR 02-A-01772. Also, Fluid Mechanics Report, 2002 FM 5, Dept. of Aerospace Engineering, Indian Institute of Science, Bangalore.
7. Ananthasayanam, M. R., Anil Kumar, A. K., Subba Rao, P.V. and Adimurthy, V. (2003), "Characterization of Eccentricity and Ballistic Coefficient of Space Debris in Altitude and Perigee Bins", 54th International Astronautical Congress, 3 Oct 2003, Bremen, Germany. IAC-03-IAA.5. P .04.
8. Ananthasayanam, M. R., Anil Kumar, A. K. and Subba Rao, P. V. (2006a), "New Approach for the Evolution and Expansion of Space Debris Scenario", *Journal of Spacecraft and Rockets*, 43, 1271-1282.



9. Ananthasayanam, M. R., Anil Kumar, A. K. and Subba Rao, P. V. (2006b), "A New Stochastic Impressionistic Low Earth Model of the Space Debris Scenario", *Acta Astronautica*, 59, 547–559.
10. Anil Kumar, A. K. (2004), "New Perspectives for Analyzing the Breakup, Environment, Evolution, Collision Risk and Reentry of Space Debris Objects", Ph.D. Thesis, Department of Aerospace Engineering, *Indian Institute of Science*, February 2004.
11. Anil Kumar, A. K. (2022), "India's efforts in Space Debris Management", *UNOOSA Scientific and Technical Subcommittee*, https://www.unoosa.org/documents/pdf/copuos/stsc/2022/19_INDIA_Item8_India's_efforts_in_Space_Debris_Management.ptdf
12. Anil Kumar, A. K., Ananthasayanam, M. R., and Subba Rao, P. V. (2002a), "A New Modeling Approach for Orbital Breakup in Space", 34th COSPAR *Scientific Assembly, Second World Space Congress*, 10-19 October 2002, Houston, Texas, USA, COSPAR02-A01843, 2002.
13. Anil Kumar, A. K. and Subba Rao, P. V. (2002b), "Re-entry prediction accuracy improvement using Genetic Algorithm", 34th COSPAR *Scientific Assembly, Second World Space Congress*, held 10-19 October, 2002 in Houston, TX, USA, COSPAR 02-A01372, 2002.
14. Anil Kumar, A. K., Ananthasayanam, M. R. and Subba Rao, P.V. (2003a), "Simulation of Some Historical On-Orbit Breakups Using ASSEMBLE Model", *AIAA-2003-572, 41st Aerospace Science Meeting and Exhibit (Atmospheric Environment)*, 6-9 January 2003, Reno, Nevada.
15. Anil Kumar, A. K., Ananthasayanam, M. R., Subba Rao, P. V., and Adimurthy, V. (2003b), "On-Orbit Collision Probability in LEO Using SIMPLE Model", *IAC-03-IAA5.2.09, IAF Conference*, Bremen, October 2003.
16. Anil Kumar, A. K., Ananthasayanam, M. R. and Subba Rao, P.V. (2003c), "Prediction of Re-entry of Space Debris Objects: Constant Gain Kalman Filter Approach", *AIAA Atmospheric Flight Mechanics Conference and Exhibit*, 11 -14 August 2003, Austin, Texas, USA, AIAA-2003-5393, 2003.

17. Anil Kumar, A. K., Ananthasayanam, M. R., and Subba Rao, P.V. (2004), "A Proposed Reference Collision Probability Estimation Model of the Space Debris Scenario", *55th International Astronautical Congress*, 4- 8 October 2004, Vancouver, British Columbia, Canada, IAC-04-IAA.5.12.5.05.
18. Anil Kumar, A. K., Ananthasayanam, M. R., and Subba Rao, P. V. (2005a), "A posterior semi-stochastic low-Earth debris on-orbit breakup simulation model", *Acta Astronautica*, 57, 733-746.
19. Anil Kumar, A.K., Ananthasayanam, M.R., Subba Rao, P. V. and Adimurthy, V. (2005b), "Statistical Analysis of the Orbital Characteristics of the Geo Debris Environment", *Proceedings of the 4th European Conference on Space Debris (ESASP-587)*, Darmstadt, Germany, 2005.
20. Anil Kumar, A. K., Ananthasayanam, M. R. and Subba Rao, P.V. (2007), "A constant gain Kalman filter approach for the prediction of re-entry of risk objects", *Acta Astronautica*, 61, 831 – 839.
21. Anil Kumar, A.K. and Reddy, D. S. (2009), "Statistical Conjunction analysis and Modeling of low-earth-orbit catalogued objects", *J. Spacecraft Rockets*, 46, 160-167.
22. Anil Kumar, A. K., Raj, M. X. J., Mutyalarao, M., Gupta, S. and Kumari, T. R. S. (2014), "Models for Re-entry Time Prediction of Risk Objects", *National Conference on Space Debris Management and Mitigation Techniques*, ASI-SDMMT.
23. Anil Kumar, A. K., Raj, M. X. J., Mutyalarao, M., Dutt, P., Bhanumathy, P. B., Kumari, T. R. S. and Selvan, A. (2017), "Performance of prediction models on re-entry time prediction of CZ-2C rocket body", *First International Conference on Recent Advances in Aerospace Engineering*, ICRAAE 2017.
24. Anz-Meador, P. and Shoots, D. (2015), "Orbital Debris Quarterly News", *NASA*, Volume 19, April 2015.
25. Anz-Meador, P., Opiela, J. and Liou, J. (2022), "History of On-orbit Satellite Fragmentations", *NASA/TP-20220019160*, December 2022.



26. Anz Meador, P., Opiela J., and Liou, J.-C. (2023), "*History of On-orbit Satellite Fragmentations*," Orbital Debris Program Office. 2023
27. APMD IADC Team (2014a), "16th IADC Re-entry Test Campaign 2013/1: Re-entry of GOCE Satellite", *VSSC/APMD/IADC/SP/011/2014*: 20-01-2014.
28. APMD IADC Team (2014b), "17th IADC Re-entry Test Campaign 2014/1: Re-entry of COSMOS 1939 Satellite", *VSSC/APMD/IADC/SP/739/2014*: 23-12-2014.
29. Balakrishnan, D. and Kurian, J. (2014), "Material Thermal Degradation under Re-entry Aerodynamic Heating", *Journal of Spacecraft and Rockets*, 51, 1319-1328.
30. Bandyopadhyay, P., Sharma, R.K. and Adimurthy, V. (2001), "The Orbiting Third Stage of GSLV-D1 as Space Debris", *Proceedings of the Workshop on Space Debris Software Tools*, VSSC/AERO/TR-001/2001, Vikram Sarabhai Space Centre, Thiruvananthapuram, 86-98.
31. Bandyopadhyay, P. and Kumar, K. (2004), "Estimation of On-Ground Risk due to Uncontrolled Re-entries from Eccentric Orbits", *55th International Astronautical Congress*, 2004, Vancouver. IAC-04-IAA.5.12.2.10.
32. Bandyopadhyay, P., Sharma, R. K. and Adimurthy, V. (2004a), "Space debris proximity analysis in powered and orbital phases during satellite launch", *Advances in Space Research*, 34, 1125–1129.
33. Bandyopadhyay, P., Sharma, R. K. and Adimurthy, V. (2004b), "A method of calculating fragment velocity additions for the analysis of the breakup of a launch vehicle upper stage", *Advances in Space Research*, 34, 1246–1250.
34. Bandyopadhyay, P., Adimurthy, V., Deb, K. and Kumar, K. (2004c), "Selection of optimal collision avoidance manoeuvre by evolutionary algorithms", *55th International Astronautical Congress*, 4- 8 October 2004, Vancouver, British Columbia, Canada, IAC-04-IAA.5.12.5.07.
35. Bandyopadhyay, P., Sharma R. K., Mutyalarao, M. and Adimurthy, V. (2006), "Lifetime Estimation of Upper Stages Re-entering from GTO with different inclinations", IAC-06-B6.2.11, *57th International Astronautical Congress (IAC)*, Valencia, 2006.

36. Beena, G.P., Sabarinath, A. and Anil Kumar, A.K. (2021), "A unified shape model for sunspot number cycles", *Ratio Mathematica*, 41, 119-136.
37. Bhatnagar, K. B. and Taqvi, Z. A. (1977), "Perturbations of the Elements of Near-Circular Earth Satellite Orbits", *Proceedings of the Indian National Science Academy*, 43, 432-451.
38. Chao, C.C. and Platt, M.H. (1991), "An accurate and efficient tool for orbit lifetime Predictions", Paper No. 91-134, *AAS/AIAA Space Flight Mechanics Meeting*, Houston, Texas February 1991.
39. Chebotarev, G. A. (1964), "Motion of an artificial earth satellite in an orbit of small eccentricity", *AIAA J.*, 2, 203-208.
40. COSPAR/ CIRA (1972), "*COSPAR International Reference Atmosphere (CIRA) 1972*", Akademie-Verlag, Berlin, 1972.
41. Cowardin, H. and Johnson, A. (Editors), (December 2022), "*Orbital Debris Quarterly News*", NASA, Vol. 26, Issue 4, December 2022.
42. Cowardin, H. and Johnson, A. (Editors), (March 2023), "*Orbital Debris Quarterly News*", NASA, Vol. 27, Issue 1, March 2023.
43. Cowardin, H. and Johnson, A. (Editors), (June 2023), "*Orbital Debris Quarterly News*", NASA, Vol. 27, Issue 2, June 2023.
44. Culp, R. D. And McKnight, D. S. (1985), "Distinguishing Between Collision-Induced and Explosion Induced Satellite Breakup Through Debris Analysis", *AAS/ AIAA Astrodynamics Specialist Conference, Vail, Colorado*, August 1985.
45. Deependran, B. (2014), "Studies on Material Degradation under Re-Entry Conditions", Ph.D. Thesis, Department of Aerospace Engineering, Indian Institute of Technology, Madras, June 2014.
46. Dutt, P. and Anil Kumar, A. K. (2014), "Identification of Space Debris from SSO for Active Debris Removal", *ASI National Conference on Space Debris Management and Mitigation Techniques (SDMMT-2014)*.



47. Dutt, P. and Anil Kumar, A. K. (2017), "Orbit Propagation using Semi-Analytical Theory and its Applications in Space Debris Field", *Astrophysics and Space Science*, 362, Article No. 35.
48. Dutt, P., Mutyalarao, M., Bhanumathy, P., Kumari T.R.S., Negi, D., Anil Kumar, A. K., Kumar, A., Ashok, V. and Deniel, D.A. (2020), "Assessment of in-house developed re-entry prediction methods", *IAA-UT Space Traffic Management Conference STM 2020*, Paper No. IAA-UT-STM-03-04, 19-20 February 2020, Austin, TX, USA.
49. Dutt, P., Raja, J., Negi, D., Mukherjee, B., Anilkumar, A. K., Kumar, A. and Ashok, V. (2021a), "Impact of Upcoming Large Satellite Constellations on Launch Vehicle Collision Avoidance", *Stardust-R, Global Virtual Workshop II: Space Traffic Management and Resilient Space Environment*, 13-17 September 2021.
50. Dutt, P., Negi, D., Kumar, A., and Ashok, V. (2021b), "Assessment of Nonlinear Optimization Algorithms on Weighted Least-Square-Based Method for Re-Entry Prediction". In: Pradeep Pratap, et al. (Eds.) *Advances in Multidisciplinary Analysis and Optimization*. 7-9 Oct 2021, IIT Madras; Also, NCMDAO 2021. *Lecture Notes in Mechanical Engineering*. Springer, Singapore.
51. Dutt, P., Mutyalarao, M., Bhanumathy, P., Kumari T.R. S., Negi, D., Anil Kumar, A. K., Kumar, A. and Ashok, V. (2021c), "Assessment of in-house re-entry prediction algorithms", *Stardust-R Global Virtual Workshop II: Space Traffic Management and Resilient Space Environment*, 13-17 Sep 2021.
52. Dutt, P., Mutyalarao, M., Bhanumathy, P., Kumari T.R.S., Negi, D., Anil Kumar, A. K., Kumar, A. and Ashok, V. (2023), "Assessment of in-house algorithms on re-entry time prediction of uncontrolled space objects", *Advances in Space Research*, 72, 2535–2551.
53. ESA (2023), "Space debris by the numbers", ESOC, Darmstadt, Germany, June 2023, https://www.esa.int/Space_Safety/Space_Debris/Space_debris_by_the_numbers
54. Fletcher, J. and Sharma, R. K. (2014), "Lifetime estimation of the upper stage of GSAT-14 in Geostationary transfer orbit", *International Scholarly Research Notices* 2014, Article ID864953.

55. Foust, J. (2022), "Majority of tracked Russian ASAT debris has deorbited", *SPACENEWS*, September 29, 2022.
56. Ganeshan, A. S., Rathnakara, S. C., Gopinath, N. S. and Padmanabhan, P. (1988), "Collision probability of spacecraft with manmade debris", *IAA 88-552*, 143–154.
57. Ganeshan, A. S. and Ananthasayanam, M. R. (1996), "Modeling the Low Earth Space Debris Distribution with Limited Data", *IAA-96-6.3.05, Space Safety and Rescue*, AAS vol. 95.
58. Ganeshan, A. S. and Ananthasayanam, M. R. (1997), "Simulation and modelling of orbital debris environment by equivalent breakups", *Advances in Space Research*, 19, 309–312.
59. Ganeshan, A. S., Nirmala, S., Rathnakara, S. C. and Ananthasayanam, M. R. (2001), "Ballistic Parameter Estimation for the Equivalent Break-up Model", *IAA-01-IAA.6.5.02*, 2001.
60. Gooding, R. H. (1981), "On the generation of satellite position (and velocity) by a mixed analytical-numerical procedure", *Advances in Space Research*, 1, 83-93.
61. Gregersen, E. (2023), "Space debris", *Encyclopedia Britannica*, 18 Mar. 2023, <https://www.britannica.com/technology/space-debris>.
62. Gupta, S., Mutyalarao, M., Saini, H., Sabarinath, A., Raj, M. X. J. and Anil Kumar, A. K. (2012), "15th IADC Re-entry Test Campaign 2012/1: Re-entry Analysis of Phobos-Grunt", *Vikram Sarabhai Space Centre, VSSC/APMD/IADC/SP/480/2012: 16-01-2012*.
63. Gupta, S., Dutt, P. and Anil Kumar, A. K. (2014a), "Collision Avoidance Analysis for ISRO Launch Vehicles", *National Conference on Space Debris Management and Mitigation Techniques*, SDMMT-2014.
64. Gupta, S., Dutt, P., Bandyopadhyay, P., Mutyalarao, M. and Kumari, S. (2014b), "Space Object Proximity Analysis for Indian LEO Satellites", 2014, *National Conference on Space Debris Management and Mitigation Techniques*, ASI-SDMMT.
65. Gupta, S., and Anil Kumar, A. K. (2015), "Integrated Model for Prediction of Reentry Time of Risk Objects", *Journal of Spacecraft and Rockets*, 52, 295 - 299.



66. Hoots, F. R., Crawford, L. L., and Roehrich, R. L. (1984), "An analytic method to determine future close approaches between satellites", *Celestial Mechanics*, 33,143-158.
67. <http://www.winger.demon.co.uk/satevo/>.
68. https://www.isro.gov.in/mission_PSLV_C3.html?timeline=timeline.
69. <https://www.drdo.gov.in,mission-shakti>.
70. IADC Re-entry Campaign Team (2018), "IADC Re-entry Test Campaign 2018/1: Re-entry of Tiangong-1 (37820) Chinese Experimental Space Station", *Vikram Sarabhai Space Centre, VSSC/APMD/TM/IADC/SP/66/2018: 11-06-2018*.
71. IADC Re-entry Campaign Team (2021), "IADC Re-entry Test Campaign 2021/1: Re-entry starlink-26 spent stage (#44240)", *Vikram Sarabhai Space Centre, VSSC/APMD/TM/IADC/SP/049/2021: 07-05-2021*.
72. Inter-Agency Space Debris Coordination Committee
<https://www.iadc-home.org>
73. IADC Working Group 4. (2021), "Support to the IADC Space Debris Mitigation Guidelines", Inter-Agency Space Debris Coordination Committee. IADC-04-06 Rev. 5.8.
74. Inter-Agency Space Debris Coordination Committee. (2021), "IADC Space Debris Mitigation Guidelines", *Inter-Agency Space Debris Coordination Committee IADC-02-01 Rev. 3. IADC*.
75. ISRO Home, (2023), "Megha-Tropiques-1 (MT1) Controlled Re-entry Successful and impacted on the Pacific Ocean", March 07, 2023, *Indian Space Research Organisation*, <https://www.isro.gov.in/index.html>.
76. ISRO Home (2023), "Indian Space Situational Assessment for the year 2022– Highlights", April 03,2023, Indian Space Research Organisation, https://www.isro.gov.in/Indian_Space_Situational_Assessment_2022.html.

77. ISRO Home/Archives (2023), "Successful post mission disposal of INSAT-4B Satellite", April 26, 2023, *Indian Space Research Organisation*, <https://www.isro.gov.in/INSATSuccess.html>.
78. ISRO Press Release (2023), "Controlled Re-entry Experiment of Megha-Tropiques-1", March 05, 2023, *Indian Space Research Organisation*, <https://www.isro.gov.in/mt1-reentry-successful.html>.
79. ISRO Press Release (2023), "Megha-Tropiques-1 (MT1) Controlled Re-entry Successful and impacted on the Pacific Ocean", March 07, 2023, *Indian Space Research Organisation*, <https://www.isro.gov.in/mt1-reentry-successful.html>.
80. ISRO Press Release (2023), "Dedication of ISRO System for Safe & Sustainable Operations Management (IS4OM) to the Nation", 14 Sept 2023, *Indian Space Research Organisation*, <https://www.isro.gov.in/IS4OM.html>.
81. Jacchia, L. G. (1977), "Thermospheric temperature, density, and composition: New models", SAO Special Report 375, NASA-CR-153049.
82. Jehn, R. (1996), "Modelling Debris Clouds", Shaker Verlag, Aachen, Germany.
83. Johnson, Nicholas L. (2009), NASA, "The Collision of Iridium 33 and Cosmos 2251: The Shape of Things to Come", 60th International Astronautical Congress, Daejeon, Republic of Korea, 16 October 2009.
84. Kelso, T. S. (1985), "CELESTRAK", since 1985.
85. Kelso, T S (2016), CelesTrak [@TSKelso] (October 21, 2016).
86. Kessler, D. J. and Cour Palais, B. G. (1978), "Collision frequency of artificial satellites: The creation of a debris belt", *Journal of Geophysical Research: Space Physics* 83 (A6): 2637-2646.
87. King-Hele, D. G. (1958), "The effect of the Earth's oblateness on the orbit of a near satellite", *Proceedings of the Royal Society of London. Series A: Mathematical, Physical*, 247, 49-70.
88. King-Hele, D. G. and Scott, D. W. (1969), "The effect of atmospheric rotation on a satellite orbit, when scale height varies with height", *Planetary and Space Science*, 17, 217-232.



89. Klinkrad, H. (2006), "*Space Debris: Models and Risk Analysis*", Springer Science & Business Media.
90. Klinkrad, H. (2009), "*IADC Re-Entry Prediction Campaigns*", UNCOPUOS STSC, Feb 2009.
91. Klinkrad, H. (2010), "*An ESA View of the IADC* ", European Space Agency, 27th October 2010.
92. Lawrence, C. S. and Sharma, R. K. (2019), "Re-Entry of Space Objects from Low Eccentricity Orbits", *International Journal of Astronomy and Astrophysics*, 9, 200-216.
93. Lincoln, V. (Ed.) (1980-1981), "*Solar Geophysical Data Prompt Reports*", *The NOAA National Geophysical Data Center*, USA.
94. Liou, J. C. and Shoot, D. (2009), "*Orbital Debris Quarterly News*", NASA, Volume 13: April 1, 2009.
95. Liou, J. C., Anilkumar, A. K., Bastida Virgili, B., Hanada, T., Krag, H., Lewis, H., Raj, M, X. J., Rao, M. M., Rossi, A. and Sharma, R. K. (2013), "*Stability of the Future LEO Environment – An IADC Comparison Study*", *6th European Conference on Space Debris*, ESA, Darmstadt, Germany, 22-25 April 2013 (ESA SP-723, August 2013).
96. Mathew, S. P. (2003), "*Design and analysis of space debris shield for spacecrafts*", M.Tech. Thesis, *Cochin University of Science of Technology*, July 2003.
97. Metz, M. (2021), "*IADC activities overview and latest updates of IADC documents*" DLR Space Agency Technical Presentation, *64th session of the UN COPUOS*, 25th August-3rd September 2021.
98. Mukherjee, B. (2022), "*IADC Annual Re-entry Campaign of 2022 with Starlink-24 as Test Object - Final note*", SSOM/1.6/2022/19, 25 October 2022.
99. Mukherjee, B. (2023), "*IADC Annual Re-entry Campaign of 2023 with Starlink-1065 as Test Object*", ISTRAC/SSOM/TR/09/2023, 29 April 2023.

100. Mutyalarao, M. and Sharma, R. K. (2010), "Optimal re-entry time estimation of an upper stage from geostationary transfer orbit", *Journal of Spacecraft and Rockets*, 47, 686-690.
101. Mutyalarao, M. and Sharma, R. K. (2011), "On prediction of re-entry time of an upper stage from GTO", *Advances in Space Research*, 47, 1877-1884.
102. Mutyalarao, M., Dutt, P., Gupta, S., Sabarinath, A., Saini, H., Raj, M. X. J. and Anil Kumar, A. K. (2011), "14th IADC Re-entry Campaign 2011/2: Re-entry time of Rontgen Satellite (ROSAT)", *Vikram Sarabhai Space Centre, VSSC/APMD/IADC/SP/470/2011: 16-11-2011*.
103. Mutyalarao, M. and Raj, M. X. J. (2012), "Optimal re-entry prediction of space objects from low Earth parking orbits using RSM with GA", *39th COSPAR Scientific Assembly*. 14-22 July, 2012, Mysore, India.
104. Mutyalarao, M. and Raj, M. X. J. (2014a), "Prediction of re-entry time of an upper stage from geostationary transfer orbit using RSM with GA", *Proceedings of 59th Congress of ISTAM*, 59-istam-fm-fp-183, 2014.
105. Mutyalarao, M. and Raj, M. X. J. (2014b), "Orbital lifetime of GTO objects with respect to launch time", *2014 National Conference on Space Debris Management and Mitigation Techniques*, ASI-SDMMT.
106. Mutyalarao, M. and Raj, M. X. J. (2015), "Performance of Response surface method using genetic algorithm on re-entry time prediction problem", *Canadian Journal of Basic and Applied Sciences*, 3, 182-194.
107. Mutyalarao, M., Dutt, P., Bhanumathy, P., Saritha Kumari, T. R., Selvam, A. and Raj, M. X. J. (2016a), "IADC Re-entry Test Campaign 2016/1: Re-entry of CZ-2C Rocket Body (#39000)", *Vikram Sarabhai Space Centre, VSSC/APMD/IADC/SP/890/2016: 28-08-2016*.
108. Mutyalarao, M., Dutt, P., Bhanumathy, P., Selvam, A., Raj, M. X. J. and Anil Kumar, A. K. (2016b), "IADC Re-entry Test Campaign 2016/2: Re-entry of VEGA AVUM rocket body (#38086)", *Vikram Sarabhai Space Centre, VSSC/APMD/TM/IADC/SP/903/2016: 08-11-2016*.



109. Mutyalarao, M., Gupta, S., Bhanumathy, P., Raj, M. X. J. and Anil Kumar, A. K. (2017), "IADC Re-entry Test Campaign 2017/1: Re-entry of CZ-3B rocket body (#38253)", *Vikram Sarabhai Space Centre, VSSC/APMD/TM/IADC/SP/961/2017: 12-10-2017*.
110. Mutyalarao, M. and Anil Kumar, A. K. (2018), "Optimal re-entry time prediction of an uncontrolled spent stage of GSLV", *Proceedings of National Conference on Essence of Mathematics and Engineering Applications (EMEA 17)*, p.11-15, 2018.
111. Mutyalarao, M., Dutt, P., Bhanumathy, P. and Saritha Kumari, T. R. (2021), "Re-entry Prediction of CZ-5B Rocket Body (48275) – Update", *Vikram Sarabhai Space Centre, APMD/COMM/R&D/113(9)/2021, 08 May 2021*.
112. Nair, L. S. and Sharma, R. K. (2003), "Decay of satellite orbits using KS elements in an oblate diurnally varying atmosphere with scale height dependent on altitude", *Advances in Space Research*, 31, 2011-2017.
113. Nandhu Raj, S, Saritha Kumari, T.R., Bhanumathy, P, Dutt, P. and Mutyalarao, M. (2019), "IADC Re-entry Test Campaign 2019/1: Re-entry of Electron Rocket Body (#43166)", *Vikram Sarabhai Space Centre, VSSC/APMD/TM/IADC/SP/009/2019: 12-03-2019*.
114. Parameswaran, S. (2003), "Report on Re-orbiting and Decommissioning of INSAT-2C", Technical Report, *Master Control Facility, ISRO, Hassan, August 2003*.
115. Pardini, C. and Anselmo, L. (2017), "Assessing the Risk and Uncertainty Affecting the Uncontrolled Re-entry of Manmade space Objects", *Proceedings of 7th European Conference on Space Debris, Darmstadt, Germany, 18-21 April 2017*.
116. Portman, S. A. (Ed.), (2002), "NASA, *The Orbital Debris Quarterly News*", January 2002.
117. Prasad, M. Y. S. (2005), "Technical and Legal Issues Surrounding Space Debris—India's Position in the UN", *Space Policy*, 2, 243–249.
118. Raj, M. X. J. and Sharma, R. K. (2003), "Analytical short-term orbit prediction with J2, J3, J4 in terms of K-S uniformly regular canonical elements", *Advances in Space Research*, 31, 2019-2025.

119. Raj, M. X. J. and Sharma, R. K. (2006), "Analytical orbit predictions with air drag using KS uniformly regular canonical elements", *Planetary and Space Science*, 54, 310-316.
120. Raj, M. X. J. and Sharma, R. K. (2007), "Contraction of satellite orbits using KS uniformly regular canonical elements in an oblate diurnally varying atmosphere", *Planetary and Space Science*, 55, 1388-1397.
121. Raj, M. X. J. and Sharma, R. K. (2009a), "Contraction of near-Earth satellite orbits using uniformly regular KS canonical elements in an oblate atmosphere with density scale height variation with altitude", *Planetary and Space Science*, 57, 34-41.
122. Raj, M. X. J. and Sharma, R. K. (2009b), "Prediction of satellite orbits contraction due to diurnally varying oblate atmosphere and altitude-dependent scale height using KS canonical elements", *Planetary and Space Science*, 57, 1312-1320.
123. Raj, M. X. J. and Mutyalarao, M. (2013), "Analytical methods for prefiltering of close approaches between space objects", *International Journal of Engineering, Science and Technology*, 5, 36-44.
124. Reddy, D. S., Reddy, N. G. and Anil Kumar, A. K. (2011), "Modeling spatial density in low Earth orbits using wavelets and random search", *Advances in Space Research*, 48, 1432-1440.
125. Ren, S., Gong, Z., Wu, Q., Song, G., Zhang, Q., Zhang, P., Chen, C., Yan and Cao, Y. (2023), "Satellite breakup behaviors and model under the hypervelocity impact and explosion: A review", *Defence Technology*, 27, 284-307.
126. Reynolds, R. C. (1990), "A Review of Orbital Debris Environment Modeling at NASA/JSC", *AIAA Orbital Debris Conference*; AIAA-90-1355, Baltimore, 1990.
127. Sabarinath, A. and Anil Kumar, A.K. (2008), "Modeling of sunspot numbers by a modified binary mixture of Laplace distribution functions", *Solar Physics*, 250, 183-197.



128. Sabarinath, A. and Anil Kumar, A.K. (2011), "A stochastic prediction model for the sunspot cycles", *Solar Physics*, 273, 255-265.
129. Sabarinath, A. and Anil Kumar, A.K. (2013), "Modeling of Sunspot Cycle using Box-Cox Transformation", *2nd ICACM-International Conference*, GRIET, Hyderabad, August 2013.
130. Sabarinath, A. and Anil Kumar, A.K. (2018), "Sunspot Cycle Prediction Using Multivariate Regression and Binary mixture of Laplace distribution model", *Journal of Earth System Science*, 127: 84, 15 pages.
131. Sabarinath, A., Beena, G.P. and Anil Kumar, A.K. (2020), "Modelling the Shape of Sunspot Cycle Using a Modified Maxwell-Boltzmann Probability Distribution Function", *Ratio Mathematica*, 39, 33-54.
132. Saji, S. S., Sellamuthu, H. and Sharma, R. K. (2017), "On J2 short-term orbit predictions in terms of KS elements", *International Journal of Advanced Astronomy*, 5, 7-11.
133. Sellamuthu, H. and Sharma, R. K. (2018), "Optimal re-entry time prediction of resident space objects from highly elliptical orbits", *42nd COSPAR Scientific Assembly*. 14-22 July 2018, Pasadena, California, USA, Abstract id.PEDAS.1-18-18.
134. Sellamuthu, H., Sharma, R. K., Solomon, B. J., Ravichandran, S. and Khadri, S. P. M. S. (2019), "Optimized re-entry time prediction of Molniya orbit objects", IAC-19-A6.9.10, *70th International Astronautical Congress (IAC)*, Washington D.C., United States, 21-25 October 2019.
135. Sellamuthu, H., Sharma, R. K., Pushparaj, N., Ravichandran, S. and Khadri, S. P. M. S. (2020), "Regularized analytical orbit theory with solar radiation pressure", IAC-20-C1.VP.x60338, *71st International Astronautical Congress (IAC)*, 12-14 October 2020.
136. Sellamuthu, H. and Sharma, R. K. (2021), "Regularized luni-solar gravity dynamics on resident space objects", *Astrodynamics*, 5, 91-108.

137. Shajahan, S., Gupta, S., Mutyalarao, M., Bandyopadhyay, P. and Anil Kumar, A. K. (2017), "Recent Collision Avoidance Manoeuvre Detection and Design", *Proceedings of ISRO Seminar on Computers & Information Technology (ISCIT)*, 2017.
138. Sharma, R. K. (1989), "Analytical approach using KS elements to short-term orbit predictions including J2", *Celestial Mechanics and Dynamical Astronomy*, 46, 321-333.
139. Sharma, R. K. (1990), "On mean elements computation for near-earth orbits", *Indian Journal of Pure and Applied Mathematics*, 21, 468-474.
140. Sharma, R. K. (1991), "Analytical approach using KS elements to near-Earth orbit predictions including drag", *Proceedings of the Royal Society of London. Series A: Mathematical, Physical*, 433, 121-130.
141. Sharma, R. K. (1992), "A third-order theory for the effect of drag on Earth satellite orbits", *Proceedings of the Royal Society of London. Series A: Mathematical, Physical*, 438, 467-475.
142. Sharma, R. K. (1993a), "RS-1 Orbital Decay in an Oblate Diurnal Atmosphere", Technical Report, *Vikram Sarabhai Space Centre, VSSC/TR: 105-93(4)*, December 1993.
143. Sharma, R. K. (1993b), "Analytical short-term orbit predictions with J3 and J4 in terms of KS elements", *Celestial Mechanics and Dynamical Astronomy*, 56, 503-521.
144. Sharma, R. K. (1997a), "Analytical integration of K-S element equations with J2 for short-term orbit predictions", *Planetary and Space Science*, 45, 1481-1486.
145. Sharma, R. K. (1997b), "Contraction of satellite orbits using KS elements in an oblate diurnally varying atmosphere", *Proceedings of the Royal Society of London. Series A: Mathematical, Physical*, 453, 2353-2368.
146. Sharma, R. K. (1998), "Contraction of high eccentricity satellite orbits using KS elements with air drag", *Proceedings of the Royal Society of London. Series A: Mathematical, Physical*, 454, 1681-1689.



147. Sharma, R. K. (1999), "Contraction of high eccentricity satellite orbits using KS elements in an oblate atmosphere", *Advances in Space Research*, 23, 693-698.
148. Sharma, R. K. and Mani, L. (1985), "Study of RS-1 orbital decay with KS differential equations", *Indian Journal of Pure and Applied Mathematics*, 16, 833-842.
149. Sharma, R. K. and Raj, M. X. J. (1988), "Long-term orbit computations with KS uniformly regular canonical elements with oblateness", *Earth, Moon and Planets*, 42, 163-178.
150. Sharma, R. K., and Anil Kumar, A. K. (2005), "Kalman Filter Approach for Re-Entry Predictions of Risk Objects with K-S Element Equations", *56th International Astronautical Congress*, IAC-05-B6.3.05, 2005, Fukuoka, Japan.
151. Sharma, R. K. and Raj, M. X. J. (2005), "Analytical Orbit Predictions with Oblate Atmosphere using K-S Uniformly Regular Canonical Elements", *56th International Astronautical Congress*, October 17-21, 2005, Fukuoka, Japan.
152. Sharma, R. K. and Raj, M. X. J. (2009), "Fourth-order theories for orbit predictions for low- and high-eccentricity orbits in an oblate atmosphere with scale height dependent on altitude", *Acta Astronautica*, 65, 1336-1344.
153. Sharma, R. K. and Raj, M. X. J. (2010), "Analytical approach using KS elements to high eccentricity orbit predictions including drag", *Acta Astronautica*, 66, 864 - 870.
154. Sharma, R. K., Bandyopadhyay, P. and Adimurthy, V. (2004a), "Consideration of lifetime limitations for spent stages", *Advances in Space Research*, 34, 1227-1232.
155. Sharma, R. K., Anil Kumar, A. K. and Raj, M. X. J. (2004b), "An integrated approach for risk object re-entry predictions in terms of KS elements and genetic algorithm", *35th COSPAR Scientific Assembly*, 18 - 25 July 2004, in Paris, France, p. 4146.
156. Sharma, R. K., Anil Kumar, A. K. and Raj, M. X. J. (2005a), "IADC Re-entry Test Campaign 2005/1: Re-entry of COSMOS 2332 Satellite", *ISRO-VSSC-SP-002-0-05, Vikram Sarabhai Space Centre, VSSC/APMD/SP/105/2005: 02-02-2005*.

157. Sharma, R. K., Anil Kumar, A. K. and Raj, M. X. J. (2005b), "IADC Re-entry Test Campaign 2005/2: Re-entry of Coronas-F Satellite", ISRO-VSSC-SP-002-0-05, Vikram Sarabhai Space Centre, VSSC/APMD/SP/105/2005: 02-02-2005.
158. Sharma, R. K., Anil Kumar, A. K., Mutyalarao, M., Sabarinath, A., Raj, M. X. J. and Dutt, P. (2008), "IADC Re-entry Campaign 2008/1: Re-entry of Early Ammonia Servicer", Vikram Sarabhai Space Centre, VSSC/APMD/SP/276/2008: 04-11-2008.
159. Sharma, R. K., Bandyopadhyay, P. and Mutyalarao, M. (2009a), "IADC Re-entry Campaign 2009/1: Re-entry of Molniya 3-39 satellite", Vikram Sarabhai Space Centre, VSSC/APMD/IADC/SP/318/2009: 20-07-2009.
160. Sharma, R. K., Anil Kumar, A. K., Raj, M. X. J. and Sabarinath, A. (2009b), "On Re-Entry Prediction of Near Earth Objects with Genetic Algorithm Using KS Elements", 5th European Conference on Space Debris, Darmstadt, Germany, 30 March – 2 April 2009, ESA SP-672.
161. Sharma, R. K., Anil Kumar, A. K., Mutyalarao, M., Sabarinath, A. and Raj, M. X. J. (2010), "IADC Re-entry Campaign 2010/1: Re-entry of Vostok SL-3/A-1 Third Stage", Vikram Sarabhai Space Centre, VSSC/APMD/SP/351/2010:18-05-2010.
162. Smibi M.J., Sellamuthu, H. and Sharma, R. K. (2017), "An Analytical Theory with Respect to the Earth's Zonal Harmonic Term J₂ in Terms of Eccentric Anomaly for Short-Term Orbit Predictions", *Advances in Astrophysics*, 2, 141-150.
163. Stiefel, E. L. and Kustaanheimo, P. (1965), "Perturbation theory of Kepler motion based on spinor regularization", *J. Reine Angew. Math.*, 218, 204-219.
164. Stiefel, E. L. and Scheifele, G. (1971), "Linear and Regular Celestial Mechanics", Springer, Berlin-Heidelberg, New York.
165. Sundahl, M. J. (2000), "Unidentified orbital debris: The case for a market-share liability regime", *Hastings Int'l & Comp. L. Rev.*, 24, 125.
166. Swinerd, G. G. and Boulton, W. J. (1982), "Contraction of satellite orbits in an oblate atmosphere with a diurnal density variation", *Proceedings of the Royal Society of London. Series A: Mathematical, Physical*, 383, 127-145.



167. UNOOSA (2009), *"Space Debris Mitigation Guidelines of the Committee on the Peaceful Uses of Outer Space"*, 2009, 172.
168. United Nations (2010), *"Space Debris Mitigation Guidelines of the Committee on the Peaceful Uses of Outer Space"*, United Nations Office for Outer Space Affairs, Vienna, 2010.
169. UNOOSA (2023), "Inputs to the Working Group on the Long-term Sustainability of Outer Space Activities: India". https://www.unoosa.org/res/oosadoc/data/documents/2023/aac_105c_12023crp/aac_105c_12023crp_10_0_html/AC105_C1_2023_CRP10E.pdf.
170. Vallado, D. A (2001), *"Fundamental of Astrodynamics and Applications"*, Second Edition, 2001. Microcosm Press, 2001, ISBN-1881883124.
171. Vijay, V. V., Sreejith, K.J., Siva, M. S., Arun Kumar S., Painuly, A., Xavier, S. and Devasia, R. (2021), "Closure Report on the TDP Activity Development of CMC based Micro-Meteoroid & Orbital Debris (MMOD) Shields", ISRO-VSSC-TR-0106-0-21, Vikram Sarabhai Space Centre, Thiruvananthapuram, 2021.

Author Index

Adimurthy V.	13, 20, 121, 144
Agarwal A.	22
Ananthasayanam M.	40, 61, 85, 87, 122, 125
Anil Kumar A.K.	12, 35, 37, 39, 46, 58, 59, 78, 95, 104, 117, 118, 122, 123, 125, 133, 14, 3, 155, 165, 170, 173
Anselmo L.	143
Anz Meador P.	2, 55, 83, 123
Balakrishnan D.	155
Bandyopadhyay P.	13, 35, 56, 107, 122, 123, 128, 130, 148, 159
Beena G. P.	117, 119
Bhatnagar K. B.	66
Boulton W. J.	68
Chao C. C.	78
Chebotarev G. A.,	70, 75
Cowardin H.	7, 53
Cour Palais B. G.	9
Culp R.D.	37
Deependran B.	155
Dutt P.	26, 78, 133, 177, 179, 180, 181
Fletcher J.	153
Foust J.	55
Ganeshan A. S.	121, 122, 125
Gooding R. H.	66
Gregersen E.	34
Gupta S.	13, 99, 101, 186
Hoots F. R.	46, 109
Jacchia L. G.	46, 68, 69, 158
Jehn R.	38, 39
Johnson A.	7, 53
Johnson Nicholas L.	54
Kelso T. S.	55
Kessler D. J.	9
King-Hele D. G.	66, 76
Klinkrad H.	1, 142
Kumar K.	130



SDSSARS IN ISRO

Space Debris and Space Situational
Awareness Research Studies

Kurian J.	155
Kustaanheimo P.	64, 91, 174
Lawrence C. S.	176
Lincoln V.	68
Liou J. C.	46, 78, 133
Mani L.	65, 66
Mathew S. P.	123
McKnight D. S.	37
Metz. M.	143
Mukherjee B.	189, 190
Mutyalarao M.	99, 149, 150, 154, 165, 170, 173, 186, 187
Nair L. S.	77
Nandhu Raj S.	188
Parameswaran S.	122, 125
Pardini C.	143
Platt M.H.	78
Portman S. A.	35
Prasad M. Y. S.	13, 18
Raj M. X. J.	46, 70, 74, 77, 78, 99, 165, 170
Reddy D. S.	95, 98
Ren S.	53
Reynolds R. C.	39
Sabarinath A.	117, 118
Saji S. S.	76
Scheifele G.	46, 64, 70
Scott D. W.	66
Sellamuthu H.	91, 174, 176
Shajahan S.	113
Sharma R. K.	46, 65, 66, 68, 70, 74, 75, 76, 77, 78, 91, 125, 130, 144, 149, 150, 153, 155, 158, 162, 174, 183, 185, 186
Smibi M. J.	76
Stiefel E. L.	46, 64, 70, 91, 174, 179
Subba Rao P. V.	123, 157
Sundahl M. J.	9
Swinerd G. G.	68
Taqvi Z. A.	66
Vallado D.	9
Vijay V. V.	138

Subject Index

Active Debris Removal	2, 29, 46, 50, 78, 133, 137, 202
Assemble Model for debris environment	35-36, 59-60
Atmospheric Re-entry	2, 26-27, 141
Break-up	1-2, 5, 9-10, 18, 24-28, 137, 193-194
Catalogued Population	6-8
Collision Avoidance	11, 12, 16, 99-106
Collision Probability	46, 85-86, 101, 109-116, 128
COLA	16-18, 99, 128
Comparisons of Re-entry Prediction Methods	170-173, 179-183
Conjunction Assessment	13, 95
Controlled re-entry	12, 20, 23, 202
Debris Environmental Modelling	28
Decay from high elliptic orbits	129, 144, 148, 174, 176
Decay of Debris Fragments	124-125
Fragmentation events	3, 58, 95, 124, 200
Future LEO environment	29, 45, 50
GTO Lifetime	19, 129, 145, 155
KS differential equations	64, 70
KS uniformly regular canonical elements	70-74
Long-term orbit computations	46-50, 63-75
Luni-Solar perturbation	2, 91-93, 129-130, 144-145, 159
Manoeuvrability	196-197
Mass distribution	8, 39
Modelling of sun spot numbers	116-119
Oblate diurnal atmosphere	68, 77, 158
On-orbit breakups	29, 59, 88
On-Orbit Collisions	4, 12-13, 193-194
Orbit Propagation	26, 63, 78, 91, 143, 158, 162, 177
Passivation	12-13, 18-19, 24-25, 122-127
Perturbations of Sun-synchronous orbit	6, 20, 75-76
Post Mission Disposal	12, 20-21, 24-25, 133, 200
Re-entry Comparison Studies	183-190



Re-entry Prediction using KS elements and Genetic Algorithm 'KSGEN'	26, 158, 183-190
Re-entry Prediction using Response Surface Method	150, 153-154, 165-174
Re-entry prediction with Kalman Filter	26-27, 143, 155-156
Shield design	27
SIMPLE Model for Debris Environment	39, 61, 85-86, 104
Space Debris Mitigation	10-12, 25-26, 121, 133
Space Debris Proximity Analysis	107-109, 128-129
Spatial density	8, 64-65, 95-99
Uncontrolled re-entry	20, 26-27, 130-132



Indian Space Research Organisation